University of Alberta

Online Measurement and Monitoring of Power System Impedance and Load Model Parameters

by

Seyed Ali Arefifar

A thesis submitted to the Faculty of Graduate Studies and Research
in partial fulfillment of the requirements for the degree of

Doctor of Philosophy
in
Energy Systems

Electrical and Computer Engineering Department

Edmonton, Alberta
Fall 2010

Examining Committee

Wilsun Xu, Electrical and Computer Engineering

Tongwen Chen, Electrical and Computer Engineering

Yasser Abdel-Rady I. Mohamed, Electrical and Computer Engineering

Biao Huang, Chemical and Materials Engineering, University of Alberta

Francisco D. Galiana, Electrical and Computer Engineering, McGill University

Abstract

In power system studies, some parameters cannot be measured directly by using the currently existing power meters. These power system parameters include the power system Thevenin impedance, harmonic impedances, zero sequence impedance, and the load model parameters.

The power system's Thevenin impedance at a load bus is an important parameter for power system planning and operation. The effects of changing the system operation conditions on voltages at the load buses can be easily determined if the power system impedance parameters are known. Moreover, by knowing the Thevenin equivalent parameters, one can calculate the system's voltage stability margin and maximum loadability.

The knowledge of power system harmonic impedances is necessary for harmonic mitigation, determination of harmonic limit compliance, prediction of system resonance, and harmonic propagation studies. Moreover, real-time monitoring of the system's harmonic impedances provides significant improvements to the design and operation of active filters. The system's zero sequence impedance at the substation bus is also important information for power system studies. It is used to calculate the different ground fault levels at substations.

Furthermore, the loads in power systems play a significant role in power system planning, control, and stability analysis. Having reliable and accurate models of the loads is essential for designing automatic control systems and optimizing their configuration. Obtaining such models has been a challenging problem for power system engineers for decades, especially in the current deregulated market environment.

This thesis presents newly developed and verified algorithms for online measurement and monitoring of these power system parameters. The algorithm proposed for monitoring the system's Thevenin, harmonic, and zero sequence impedance parameters, uses the natural variations of the loads connected to the substations. The proposed algorithm for monitoring of load model parameters uses the voltage and current waveforms captured during the operation of the Under Load Tap Change (ULTC) transformers installed in the distribution substations.

The proposed algorithms are applied to several field measurements from different substations. The results show that the algorithms fulfill the requirements for the online measurement and monitoring of power system Thevenin, harmonic and zero sequence impedances as well as the load model parameters.

Acknowledgements

First and Foremost I would like to express my wholehearted gratitude to Allah, the Almighty, for enlightening my path and guiding me through each and every success I have or may reach.

I would like to express my sincere gratitude to my supervisor, Prof. Wilsun Xu, for his inspiring guidance, encouragement and support in the past years while I pursued my Ph.D. degree at the University of Alberta. In the thousands of hours he devoted to my education and research, he showed me how to think like a researcher and educator as well as formulate, test, express, and defend my ideas in a clear and concise manner. His ardor and earnestness for studies are respected and will never be forgotten.

I would also like to sincerely thank the members of my Ph.D. examining committee, Dr. F. D. Galiana, Dr. B. Huang, Dr. T. Chen and Dr. Y. Mohamed for their valuable comments that helped in improving the quality of this thesis.

It is a pleasure to thank my colleagues in the Power Disturbance and Signaling Research Laboratory. I would like to thank all of them specially Dr. Sami Abdulsalam, Enrique Nino, Hooman Erfanian, Iraj Rahimi, Carlos Almeida, Chris Lerohl and Joey Gallant for their cooperation and valuable discussions. I also acknowledge Albert Terhide for all his help and efforts during my laboratory experiments.

I am forever indebted to my parents for all their endless patience, encouragement and love for my entire life. They raised me with a love of science and supported me in all my pursuits. I am also grateful to my siblings who have always loved and supported me.

I owe my deepest gratitude to my beloved wife. Without her encouragement, support and love, this dissertation would have never been completed. I would also like to express my gratitude to the love and support from my parents-in-law.

This thesis was supported by Alberta Ingenuity Fund and iCORE with generous grants, the University of Alberta with the Provost Doctoral Entrance Scholarships, my supervisor and the ECE department with several terms of R.A. and T.A., and the GSA with a PD travel grant. This collection of financial sources made my student life a lot more pleasant, and is highly appreciated.

Lastly, I offer my regards and blessings to all of those who supported me in any respect during the completion of the thesis.

CONTENTS

LIST OF TABLES

LIST OF FIGURES

Chapter 1

Introduction

The state-of-the-art instrumentation and measurement devices are so accurate and improved that they can measure and monitor system parameters with very high accuracy. Through the combination of high-tech measurement devices and fast data-processing units, these power monitors are now able to measure and monitor specific power system parameters that could not be measured previously. These parameters include power system impedance parameters, power system load parameters, harmonic sources, synchronized phasors of voltages and currents, and fault location.

These parameters have several applications in different areas of power system research studies. This thesis proposes a set of new algorithms for the online monitoring and measuring of power system impedance parameters, including the Thevenin impedance, harmonic impedances, and zero sequence impedance parameters, as well as the load model parameters. An introduction to these power system parameters, the measurement scheme, and the thesis contributions and outline are presented in this chapter.

1.1 Power System Impedance Measurement

A supply system can be represented by using the model shown in Figure 1.1. Electric power is usually generated in power plants and is transmitted through high-voltage transmission lines by using high-power transformers and power electronic devices. The flow of power through this equipment causes the voltage to decrease. The amount of voltage reduction depends on the impedance, one of the main characteristics of the devices.

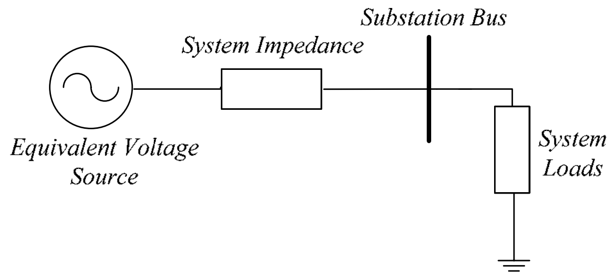

Figure 1.1. Power system as seen at the substation bus

The power system impedance parameters are important issues in power system and power quality studies. In this section, the power system Thevenin impedance parameters, power system harmonic and zero sequence impedance parameters, and their applications in power system research studies are presented.

1.1.1 Power System Thevenin Impedance Parameters

The equivalent circuit parameters of a power supply system such as the short-circuit impedance are important data for both power supply authorities and industrial customers [1]-[7]. The effects of changing the system operation conditions on voltages at the load buses can be easily determined if the power system equivalent circuit parameters are known. These data are used in the following research areas.

1. Model verification and fault level

The fault level at a system's different buses is an important issue for power system studies, especially in the protection fields. The power-flow programs use the system impedance matrix to calculate the fault level at the system's different buses; however, the power system equivalent impedance data can be used to determine the fault level at the system's different buses without knowing the system impedance matrix. Therefore, the system equivalent impedance data can be used to calculate the maximum short circuit current level and to verify the proposed models for power system networks.

2. Power quality improvement

During recent years, the constant increase in the power demanded by loads has not been followed by the adequate development of the electrical network. Therefore, the supply system will likely be subjected to increasing disturbances injected by directly connected loads such as those from arc furnaces and power electronic devices. In such a scenario, the utility impedance will play an important role in the disturbance propagation, and accurate modeling of the supply system will then be necessary to optimize the power quality.

3. Power electronic devices

Power electronic devices are widely used in power systems. In order to fully exploit their capabilities and to reduce the effects of their drawbacks, particularly to limit voltage waveform distortions, the interaction between the power electronic devices and the power system they are connected to should be modeled in detail. The Thevenin equivalent circuits at fundamental and harmonic frequencies usually provide enough information regarding the effects of the changes in the power electronic device operating conditions on the supply voltage waveform [8].

4. Voltage stability margin

It has been proposed that the supply system impedance can be used to help estimate the voltage stability margin and the system's maximum loadability [9].

Several methods with their own advantages and disadvantages have been proposed to track and estimate the power system impedance parameters. Some of these methods are based on the synchronized measurements of waveforms, and others require nonlinear loads to estimate the power system equivalent circuit parameters. These methods involve two different approaches: invasive and non-invasive, which are explained in Chapter Two.

In this thesis, a new non-invasive algorithm based on local measurements of the voltage and current waveforms is proposed to calculate the power system equivalent circuit parameters. Unlike the previous methods, this method involves no restriction on the load model and no requirement to have synchronized measurements. The only information required for the proposed algorithm to calculate the power system equivalent circuit parameters is a few seconds of the waveforms of the voltage and current of the system at the load point, which is usually available.

1.1.2 Power System Harmonic Impedance Parameters

The frequency response of a system at specific buses depends mainly on its impedances at different frequencies [10]-[12]. The knowledge of power system harmonic impedances is important information and has several applications in power system studies. It has a key role in the harmonic disturbance propagation due to the extension and meshed structure of the system [12]. Some other applications are [5], [8], [10]-[30]

- Transient analysis.
- Harmonic mitigation measures.
- Determination of harmonic limit compliance.
- Optimization of the efficiency and minimization of the drawbacks of power electronic devices.
- Design and operation of active filters.
- Prediction of system resonance.

The different methods proposed to calculate the system's harmonic impedances can be classified to two groups: transient-based and steady state-based methods, which are explained in Chapter Three.

In this thesis, a new algorithm is proposed for the online monitoring of the network harmonic impedance parameters and the system's background voltage distortion. The proposed method requires neither an external disturbance source nor synchronized measurement data. For calculations, this method uses the naturally occurring load disturbances connected to the system and overcomes the weaknesses of the existing methods. Implementation issues are addressed in this thesis, and the proposed method is verified through real field measurements from different substations.

1.1.3 Power System Zero Sequence Impedance Parameters

The system's zero sequence impedance seen at a substation bus is important information for power system studies and is used to calculate the different ground fault levels at substations. The system's zero sequence impedance is also important for relay settings and protection studies.

In this thesis, an algorithm is also proposed for the online measurement and monitoring of the zero sequence impedance parameters. The algorithm uses the natural variation of the system's three-phase voltages and currents to calculate the zero sequence impedance parameters. Therefore, the proposed algorithm can be used for online monitoring purposes.

1.2 Power System Load Parameters Measurement

When planning and operating power transmission systems, each substation is modeled as a load point. Therefore, the load in this case represents the collective behavior of all the feeders connected to the substation transformer and the individual loads connected to them. The loads in power systems play an important role in power system planning, control and voltage stability studies [31]-[56]. Power system engineers rely mainly on computer simulation programs to assess a system's dynamic performance for planning and operation studies, and modeling the loads has always been challenging for them. Accurate load modeling enables transmission planners and operators to calculate the true operating boundaries of their systems.

A load model is a mathematical representation of the relationship between a bus voltage (magnitude and frequency) and the power (active and reactive) or current flowing into the bus load. The term "load model" may refer to the equations themselves or the equations plus specific values for the parameters (e.g., coefficients, exponents) of the equations [31]. Improved load models are very important in power system studies. Several studies have shown the significance of the load model's impact on the results of different types of studies. Some of the most important issues are explained in the following [31]-[35].

1. Planning studies

In planning studies, the benefits of improved load modeling depend on the present load model. If the existing load model produces overly pessimistic results, the improved load models will defer or prevent the expense of system modifications and equipment additions. As well, if the existing load model produces overly optimistic results, the improved load models will prevent system inadequacies, which may result in costly operating limitations.

2. Operation and control studies

The load model has a significant impact on operation and control schemes. If the existing load model produces overly pessimistic results, the improved load models will increase the power transfer limits, with resulting economic benefits. Moreover, if the existing load model produces overly optimistic results, the improved load models will prevent system emergencies resulting from optimistic operating limits.

3. Voltage stability analysis

The dynamic properties of power system loads have a major impact on system stability. Different load models will produce different results in voltage stability studies. Simulation results are critically dependent on the choice of the load models. Some previous studies reported in the literature indicated that the parameters of load models had a significant impact on a power system's voltage stability.

4. First-swing transient stability studies

System voltages are normally depressed during the first angular swing following a fault. The power consumed by the loads during this period will affect the generation-load power imbalance and thereby affect the magnitude of the angular excursion and the first swing stability of the system [31].

5. Small-signal stability damping studies

Inter-area modes of oscillation, involving a number of generators widely distributed over the power system, often result in significant variations in voltage and local frequency. In such cases, the load voltage and frequency characteristics may have significant impacts on the damping of the oscillations.

Obtaining detailed and accurate models of power system loads can be a more complicated task than modeling other power system components. The two basic approaches available to model the composite loads in power system studies -- the component-based and the measurement-based approaches -- are explained in Chapter Four.

In this thesis, a newly developed and verified algorithm is proposed for the online measurement and monitoring of load parameters. According to circuit theories, a disturbance coming from the upstream side can be used to estimate the downstream side parameters. Since the load modeling algorithm should be capable of online measurement and monitoring, a disturbance that has a high occurrence frequency and also is large enough is required for the estimation procedure. The natural disturbances in the system are usually very small in terms of magnitude, and their source, either from the system or the load side, is not easily determined; therefore, they are not appropriate for the online measurement of load parameters. One of the disturbances in power system which is large enough and has a high chance of occurring is the transformer tap movement, which has been chosen to estimate the load parameters in this thesis.

Although the concept is simple, it is important to verify if the natural tap movements can indeed yield disturbances with sufficient magnitude and frequency for use in determining the load parameters adequately and continuously. To accomplish the project, the characteristics of the tap movements occurring at the secondary of the transformers in the substations are investigated. For this purpose, an algorithm is developed to detect the tap change and to record the corresponding three-phase voltages and currents by using the Labview program. Based on our experiences, the tap movement has a high chance of occurring and can happen at any loading condition and at any time of the day, seven days a week. This fact is very important and enables us to use the tap changes to monitor the load at any required time during the week. Through the sensitivity analysis of several field measurements data, the final algorithm for the online measurement of the load model parameters has been developed.

1.3 The Measurement Scheme

The most common situation requiring knowledge of supply system impedance, harmonic impedances, zero sequence impedance, and load model parameters is shown in Figure 1.2.

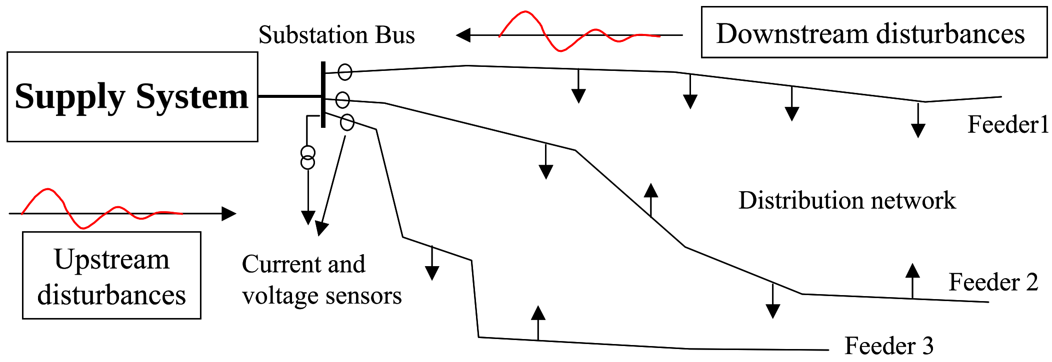

Figure 1.2. The proposed measurement scheme

In this scheme, the supply system includes the generating power plants and the transmission system. The load side includes the distribution feeders and the large number and types of different loads connected to the distribution network, such as fluorescent and incandescent lamps, refrigerators, heaters, compressors, motors, and furnaces. The measurement data are the three-phase waveforms of the voltage and current in a continuous time frame. The measured voltage could be that of the phase-to-phase or phase-to-ground voltages, and the current is the phase current.

This thesis's goal is to determine the system's parameters for each group of loads seen at the substation bus. Although parameters to be estimated are quite different, the same set of measurement data will be used for the parameters' estimations in all cases, and these data are related from the disturbance side perspective. The measurements taken at the substation bus will be used to calculate the power system equivalent circuit parameters, the harmonic impedances, and the zero sequence impedance, as well as the load model parameters. Since the same set of data will be used for all tasks, one of the project's main challenges is to select the measured data appropriate for all purposes. The measurements will be taken in steady state conditions; therefore, the calculated parameters will be subject to change according to the variation of the system and load parameters.

According to electric circuit theories, when a disturbance occurs at the load side, the measurement data can be used for calculating the system side parameters, and when the disturbance occurs at the system side, the load model parameters can be estimated. The disturbance can be any kind of distortion in the voltage or current waveforms, such as continuous variations of the load voltage and current, and step changes caused by transformer taps. Since the probability that variations or disturbances will occur on both the system and load side simultaneously is, practically, very low, it is reasonable to assume that the parameters on the non-disturbance side are constant for the disturbance period.

When the disturbance side is determined, by using the algorithms proposed in this thesis, the measurement data can be used to calculate the system or load side parameters. Therefore, the detection of the disturbance side and the representativeness of the data for online measurement and monitoring are the project's main challenges.

1.4 Thesis Contributions and Outline

The main contributions of this thesis to its research field, and the outline of the thesis are presented in this section.

Chapter Two proposes a new algorithm for the online tracking of power system impedance parameters. The algorithm can be implemented into the power monitors widely available in load-serving substations. The proposed algorithm is independent of load models and does not require synchronized data, so it overcomes the shortcomings of the published methods. Furthermore, a novel algorithm is proposed for disturbance side detection at the substation bus. Practical implementation issues are addressed in this chapter, and the proposed method is verified by using computer simulations, experimental studies, and several field measurements.

In the third chapter, several sensitivity studies are performed. The purpose is to optimize the parameters which are used for the impedance measurement technique. Also, in this chapter, based on the research presented in Chapter Two, an algorithm is proposed for the online monitoring of the network harmonic impedance parameters and the background voltage distortion of the system. Moreover, an algorithm is proposed for the online monitoring of zero sequence impedance parameters. For calculations, the proposed methods, which require neither an external disturbance source nor synchronized measurement data, use the naturally occurring load disturbances connected to the system.

Implementation issues are addressed in this chapter, and the proposed methods are verified through real field measurements from different substations.

Chapter Four discusses the development of a useful practical technique to measure and track the load model parameters at load-serving substations. The idea is to use the natural disturbances caused by the Under Load Tap Changer (ULTC) transformers at the substations to calculate the load model parameters. Our study shows that the tap movement creates a system side voltage step change with a magnitude of approximately one percent. This change creates similar disturbances in the corresponding active power and reactive power consumed by the loads, and the load response to this step change in voltage can be used to determine the load behavior and to estimate the load model parameters. The main focus of this chapter is to calculate the voltage dependent load model parameters. A set of estimation algorithms is developed accordingly. This chapter also presents the implementation of the proposed method and its field experiences.

In Chapter Five, several sensitivity studies are presented to investigate the characteristics of load parameters. The sensitivity studies show that the tap movements occurring in the secondary side of power transformers, existing in load-serving substations, can be used to estimate the load model parameters. A tap change can happen at any time and in any loading condition, and the disturbance magnitude which is a step change in the voltage is large enough for calculating the load model parameters. Therefore, the methodology developed in this research fulfills the requirement for the online measurement of the load model parameters.

Chapter Six concludes the thesis and presents suggestions and recommendations for future studies and improvements in the research field.

Chapter 2

Online Measurement of Power System Impedance Parameters[1]

The Thevenin impedance seen at a load bus is an important parameter for power system planning and operation. This chapter presents a new algorithm to track the impedance parameters online. For impedance estimation, the algorithm uses the natural variations of the loads connected to the substations. It neither depends on the load model nor requires synchronized measurements. The input data, several seconds of voltage and current waveform data, are readily available from substation power monitors. The simulations, experiments and field test results show that the proposed algorithm can be used for the online monitoring of power system impedance parameters.

2.1 Introduction

A power supply system's equivalent circuit parameters such as the short-circuit impedance are important data for both power supply authorities and industrial customers [1-7]. These parameters have several applications: calculating the short-circuit currents, verify models of power system networks, and designing VAr compensators and harmonic filters to avoid creating resonance conditions. In recent years, the equivalent impedance has been used as a parameter for fault and protection calculations. As well, its applications in power electronic device studies are widely adopted in modern power systems. In order to fully exploit their capabilities and to reduce the effects of their drawbacks, particularly to limit voltage waveform distortions, the interaction between the power electronic devices and the power system they are connected to should be modeled

[1] A version of this chapter has been published. S.A. Arefifar and W. Xu, "Online Tracking of Power System Impedance Parameters and Field Experiences," *Power Delivery, IEEE Transactions on*, vol.24, no.4, pp.1781-1788, Oct. 2009.

in detail. The Thevenin equivalent circuits at the fundamental and harmonic frequencies usually provide enough information regarding the effects of the changes in the power electronic device operating conditions on the supply voltage waveform [8]. Moreover, by using the Thevenin equivalent parameters, seen at the load bus, the system's voltage stability margin and maximum loadability can be easily estimated [9].

Reflecting the importance of this issue, two groups of methods have been proposed to calculate the power system impedance parameters: invasive and non-invasive. The invasive approaches impose intentional disturbances on the system and use the voltage and current response for estimations [13], [16], [18], [57]-[59]. These methods must produce a disturbance with enough energy for measurement purposes without affecting the network and the equipment's operation. The invasive methods can be classified in two groups: transient-based and steady state-based methods, which have their own advantages and disadvantages. The transient-based method uses the transient waveforms of the system's voltages and currents for estimations. However, the steady state-based methods use the pre- and post-disturbance waveforms to calculate the power system impedance parameters. Clearly, these methods cannot be used for the real-time measurement of the system impedance parameters.

The non-invasive approaches use the existing load current and voltage variations to identify the network equivalent impedance. These approaches are usually simpler and more applicable than the invasive approaches, since non-invasive methods do not impose any disturbance or waveform distortion on the system and use the existing load current and voltage variations to identify the network equivalent impedance [8], [9], [60]-[62]. In [8] a constrained least square method is proposed to identify the system impedance. This method requires a power electronic device as a load for estimation, but such a device is not always available. The authors in [60] present a signal-processing-based method that needs the load admittance, which is not usually accessible for estimation. For calculations the proposed methods in [9] and [61]-[62] need synchronized measurements among the captured data. These measurements cannot be obtained in practice.

This chapter proposes a new algorithm for the online tracking of power system impedance parameters. The algorithm can be implemented into the power monitors widely available in load-serving substations. The proposed algorithm is independent of load models and does not require synchronized data, so it overcomes the shortcomings of the published methods. Furthermore, practical implementation issues are addressed in this chapter, and the proposed method is verified by using computer simulations, experimental studies, and several field measurements.

2.2 The Proposed Algorithms for Impedance Estimation

The power system as seen at the substation bus can be modeled as the equivalent circuit shown in Figure 2.1.

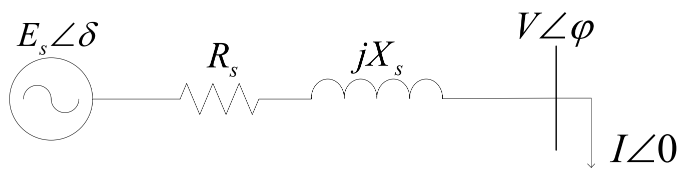

Figure 2.1. Power system model seen at the substation bus

The goal is to calculate the Thevenin equivalent circuit parameters, E_s, R_s and X_s, while the only information available from the system is the local measurement data. These data are the voltage and current waveforms or the RMS values of the fundamental positive sequence components of the voltage, current and the power factor (φ_i). In this section, the proposed algorithms for system impedance estimation are explained. The proposed methods are the three-point and multi-point algorithms.

2.2.1 The Three-Point Method

To explain the algorithm, we assume that the system side, (E_s, R_s and X_s), shown in Figure 2.1, is constant and that the load side has some variations. By neglecting the measurement error and applying KVL, the system equations for a set of measurement data at time t_1 are as follows:

$$E_s\angle\delta_1 = (R_s + jX_s)\times I_1\angle 0 + V_1\angle\varphi_1 . \tag{2.1}$$

Equation (2.1) has seven variables. Three variables are known (V, I and φ), and four variables are unknown (E_s, δ, R_s and X_s). The proposed method in [61] is to use the second set of measurements in another loading condition at time t_2 (t_1 and t_2 can be pre- and post-disturbance times) as follows:

$$E_s \angle \delta_2 = (R_s + jX_s) \times I_2 \angle 0 + V_2 \angle \varphi_2 . \tag{2.2}$$

If we synchronize the instant of the measurements in order to have $\delta_1 = \delta_2$, and subtract (2.1) from (2.2), we will have

$$(R_s + jX_s) \times (I_2 \angle 0 - I_1 \angle 0) = V_1 \angle \varphi_1 - V_2 \angle \varphi_2 . \tag{2.3}$$

Then we can calculate R_s and X_s from (2.4)

$$R_s + jX_s = -\frac{V_1 \angle \varphi_1 - V_2 \angle \varphi_2}{I_1 \angle 0 - I_2 \angle 0} = -\frac{\Delta V}{\Delta I} . \tag{2.4}$$

Using the calculated impedance and (2.1) or (2.2), we can get the solution for E_s. The above method seems to be straightforward. However, one piece of critical information is missing, so that the method is unworkable. Equation (2.4) is based on the assumption that the two sets of phasors refer to the same reference time, namely $\delta_1 = \delta_2$. Such a requirement, i.e., taking two consecutive waveform data that guarantee $\delta_1 = \delta_2$, cannot be met in reality mainly because the power system frequency changes all the time. Therefore, two consecutive shots cannot be synchronized by properly placing the sampling windows.

In order to overcome this problem, a third set of measurements is added to the impedance estimation equations [63]. Assuming that E_s, R_s and X_s are constant during the measurements, for the third set of V, I and φ, at time t_3, we will have the same equation as (2.1) and (2.2):

$$\begin{cases} E_s\angle\delta_1 = (R_s + jX_s)\times I_1\angle 0 + V_1\angle\varphi_1 \\ E_s\angle\delta_2 = (R_s + jX_s)\times I_2\angle 0 + V_2\angle\varphi_2 \\ E_s\angle\delta_3 = (R_s + jX_s)\times I_3\angle 0 + V_3\angle\varphi_3 \end{cases} \cdot \tag{2.5}$$

Separating the real and imaginary parts of (2.5), we will have 6 equations and 6 unknowns which can easily be solved. Equations (2.5) have been solved in [63] by using the iterative Newton-Raphson method. In this chapter, an analytical solution to the above equations is developed to speed up the calculation process and to check the validity of the results. This subject is explained in Section 2.3.1.

2.2.2 The Multi-Point Method

The three-point method is sound theoretically. When it was applied to actual field data, however, several performance problems were encountered. As will be shown in Section 2.4, the method is very sensitive to noise and transients in the voltage and current measurements. To overcome the problem, we propose to extend the three-point method by including six or more measurement points through a least square fitting. For this purpose, (2.5) is rewritten as follows:

$$\begin{bmatrix} E_s\times\cos(\delta_i) \\ E_s\times\sin(\delta_i) \end{bmatrix} = \begin{bmatrix} R_s & 0 \\ 0 & X_s \end{bmatrix} \times \begin{bmatrix} I_i\angle 0 \\ I_i\angle 0 \end{bmatrix} + \begin{bmatrix} Vx_i \\ Vy_i \end{bmatrix} \quad i=1,\ 2,\ 3, \tag{2.6}$$

where Vx_i and Vy_i are the x-component and y-component of the voltage, respectively. For simplifying the equations, we assumed the current phasors as the reference for writing the equations. If we assume that the system side is constant for a set of n measurements, the following equation can be established by extending (2.6) to n-points:

$$\begin{bmatrix} E_s\times\cos(\delta_i) \\ E_s\times\sin(\delta_i) \end{bmatrix} - \begin{bmatrix} R_s & 0 \\ 0 & X_s \end{bmatrix} \times \begin{bmatrix} I_i\angle 0 \\ I_i\angle 0 \end{bmatrix} - \begin{bmatrix} Vx_i \\ Vy_i \end{bmatrix} = \begin{bmatrix} \varepsilon_{xi} \\ \varepsilon_{yi} \end{bmatrix} \quad i=1,\ldots,n, \tag{2.7}$$

where n can have any value greater than three, and ε_{xi} and ε_{yi} are the estimation errors. The goal is to minimize the error for a certain number of measurements. Therefore, we can define the following function and minimize it:

$$f(Z) = \sum_{i=1}^{n} (\varepsilon_{xi}^2 + \varepsilon_{yi}^2), \tag{2.8}$$

where

$$Z = [E_s, R_s, X_s, \delta_i], \qquad i=1,2,\ldots n. \tag{2.9}$$

The vector Z that minimizes the function $f(Z)$ will be the solution to the problem. The minimization can be done by using iterative-based methods. In this chapter, the Gauss-Newton method in MATLAB software has been used for calculations. The Gauss–Newton algorithm, explained in Appendix A, is a method used to solve non-linear least squares problems. It can be seen as a modification of Newton's method for finding the minimum of a function. Unlike Newton's method, the Gauss–Newton algorithm can be used only to minimize a sum of squared function values, but it has the advantage that second derivatives, which can be challenging and time-consuming to compute in real time, are not required. The initial guess for starting the Gauss-Newton algorithm is calculated in Section 2.3.1.

In order to compare the accuracy of the three-point and the multi-point algorithms, some case studies were done to investigate the sensitivity of the two algorithms to the measurement noise. For this purpose, several simulation case studies were prepared, and different random noise levels were added to the measured voltages and currents. The three-point algorithm and the multi-point algorithm using four different numbers of points were applied to calculate the system parameters. To calculate each plotted value in Figure 2.2, 300 cases were run, and the estimation errors were calculated for each case, and then the average was plotted. The error was calculated as follows:

$$Error(\%) = \frac{1}{300} \sum_{i=1}^{300} \frac{\left| Data_{Actual_i} - Data_{Calculated_i} \right|}{Data_{Actual_i}} \times 100 . \tag{2.10}$$

In Figure 2.2, the accuracy of the calculated R_s and X_s is plotted as a function of the signal-to-noise ratio (SNR) for the three- and multi-point algorithms. The SNR is defined as ten times the logarithm of the power ratio of the main signal, to the noise signal. For the simulations in this section, the load was modeled as a variable impedance ($Z_L = 15 + j12$ *ohms*). The system was modeled as shown in Figure 2.1, ($Z_s = 3 + j4$ *ohms* and $E_s = 120$ *Volts*). The system side was assumed to be constant with no variations, and the load was changed randomly with a maximum variation of 5%.

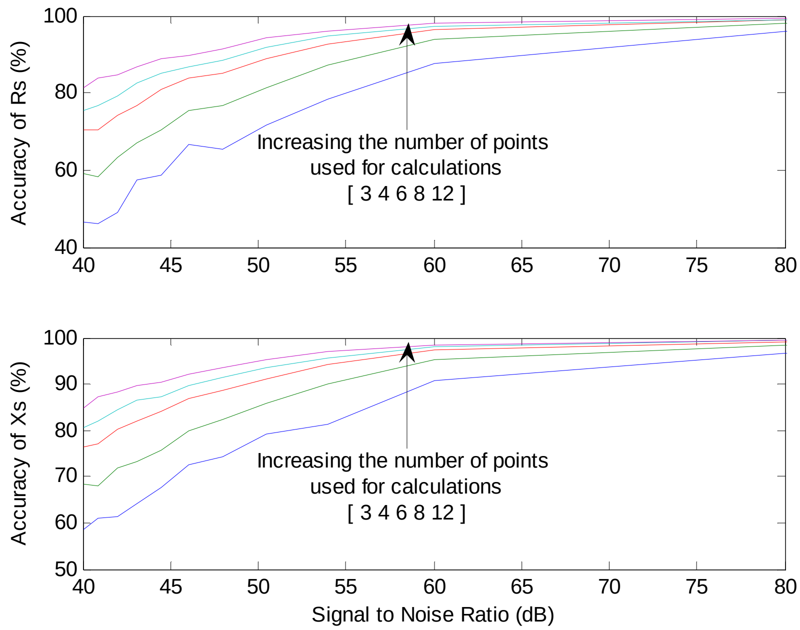

Figure 2.2. Accuracy of the method in noise condition

The simulation results in Figure 2.2 show that increasing the number of points used for calculations reduces the sensitivity of the algorithm to the measurement noise. This result is obtained while all the system side parameters remain constant. For estimation, Equation (2.7) uses a different operating voltage and current for the load. The only required characteristic of the load is its variation for the period of measurement, which in reality usually exists. Therefore, the estimation procedure is not dependent on the load model, and this feature is considered as an advantage of the algorithm.

2.3 Practical Considerations

This section explains some practical problems and their solutions, which should be considered when implementing the algorithm.

2.3.1 Disturbance Side Detection

In the explained multi-point algorithm, it is assumed that the system side parameters remain constant for the period of measurements. In order to estimate the system impedance parameters by using more than three measurements, we need to select the data for which no variation has occurred in the system parameters. The proposed three-point algorithm can certainly determine the disturbance side for the measurements. Defining $V_i = Vx_i + jVy_i$ and taking the square of both sides of (2.5), we can rewrite them as follows:

$$\begin{cases} E_s^{\ 2} = (R_s \times I_1 + Vx_1)^2 + (X_s \times I_1 + Vy_1)^2 \\ E_s^{\ 2} = (R_s \times I_2 + Vx_2)^2 + (X_s \times I_2 + Vy_2)^2 \\ E_s^{\ 2} = (R_s \times I_3 + Vx_3)^2 + (X_s \times I_3 + Vy_3)^2 \end{cases} . \tag{2.11}$$

In this case, we will have 3 equations and 3 unknowns. The unknown variables are (E_s, R_s and X_s). Using the three equations, we can eliminate E_s from the equations as shown in (2.12)

$$\begin{matrix} (R_s \times I_1 + Vx_1)^2 + (X_s \times I_1 + Vy_1)^2 = (R_s \times I_2 + Vx_2)^2 + (X_s \times I_2 + Vy_2)^2 \\ (R_s \times I_1 + Vx_1)^2 + (X_s \times I_1 + Vy_1)^2 = (R_s \times I_3 + Vx_3)^2 + (X_s \times I_3 + Vy_3)^2 \end{matrix} , \tag{2.12}$$

and then we have

$$\begin{matrix} R_s^{\ 2}(I_1^{\ 2} - I_2^{\ 2}) + 2R_s(I_1 \times Vx_1 - I_2 \times Vx_2) + (Vx_1^{\ 2} - Vx_2^{\ 2}) = \\ -X_s^{\ 2}(I_1^{\ 2} - I_2^{\ 2}) + 2X_s(I_2 \times Vy_2 - I_1 \times Vy_1) + (Vy_2^{\ 2} - Vy_1^{\ 2}) \\ \\ R_s^{\ 2}(I_1^{\ 2} - I_3^{\ 2}) + 2R_s(I_1 \times Vx_1 - I_3 \times Vx_3) + (Vx_1^{\ 2} - Vx_3^{\ 2}) = \\ -X_s^{\ 2}(I_1^{\ 2} - I_3^{\ 2}) + 2X_s(I_3 \times Vy_3 - I_1 \times Vy_1) + (Vy_3^{\ 2} - Vy_1^{\ 2}) \end{matrix} . \tag{2.13}$$

To make the equations simpler we can write them as follows:

$$A \times R_s^{\ 2} + B \times R_s + C = -A \times X_s^{\ 2} + D \times X_s + E , \tag{2.14}$$

$$F \times R_s^{\ 2} + G \times R_s + H = -F \times X_s^{\ 2} + K \times X_s + L , \tag{2.15}$$

where:

$A = I_1^2 - I_2^2$, $B = 2\times(I_1\times Vx_1 - I_2\times Vx_2)$, $C = Vx_1^2 - Vx_2^2$, $D = 2\times(I_2\times Vy_2 - I_1\times Vy_1)$, $E = Vy_2^2 - Vy_1^2$, $F = I_1^2 - I_3^2$, $G = 2\times(I_1\times Vx_1 - I_3\times Vx_3)$, $H = Vx_1^2 - Vx_3^2$, $K = 2\times(I_3\times Vy_3 - I_1\times Vy_1)$, $L = Vy_3^2 - Vy_1^2$. (2.16)

If we multiply (2.15) by $(-\frac{A}{F})$ we will have:

$$-\frac{A}{F}\times\left(F\times R_s^{\,2} + G\times R_s + H\right) = -\frac{A}{F}\times\left(-F\times X_s^{\,2} + K\times X_s + L\right), \tag{2.17}$$

$$-A\times R_s^{\,2} - \frac{GA}{F}\times R_s - \frac{HA}{F} = A\times X_s^{\,2} - \frac{KA}{F}\times X_s - \frac{LA}{F}. \tag{2.18}$$

By adding (2.14) to (2.18) the second order terms will be eliminated and we can calculate X_s as a function of R_s, so that

$$\left(B - \frac{GA}{F}\right)\times R_s + \left(C - \frac{HA}{F}\right) = \left(D - \frac{KA}{F}\right)\times X_s + \left(E - \frac{LA}{F}\right), \tag{2.19}$$

and

$$X_s = M\times R_s + N, \tag{2.20}$$

where:

$$M = \frac{BF - AG}{DF - AK}, N = \frac{AL + FC - AH - EF}{DF - AK}. \tag{2.21}$$

Returning to (2.14) and substitute X_s by using (2.20) we have

$$A\times R_s^{\,2} + B\times R_s + C = -A\times(M\times R_s + N)^2 + D\times(M\times R_s + N) + E\ . \tag{2.22}$$

Finally, we obtain

$$A\times\left(1 + M^2\right)\times R_s^{\,2} + \left(B + 2AMN - DM\right)\times R_s + \left(C + AN^2 - DN - E\right) = 0. \tag{2.23}$$

For R_s, (2.23) provides a simple second-order equation, which can easily be solved. It has been derived based on the assumption that the system side parameters remain unchanged for three different system conditions. If for any reason the system side parameters vary for the three points, (2.23) is meaningless and will not have any solutions. The only condition for (2.23) to have a real solution is $\Delta \geq 0$ ($\Delta = b^2 - 4ac$ in $ax^2 + bx + c = 0$); therefore, the sign of Δ can be used as an index for determining the disturbance side. If Δ is greater than or equal to zero, the necessary condition, which is unchanged system side parameters, should be correct, and we will have one or two solutions. A negative Δ can happen due to the variation of the system side parameters, measurement noise, and load switching transients that sometimes exist in power system measurements.

After calculating R_s we can calculate both X_s and E_s from (2.6), and then the feasibility of the solutions can be checked by using the following rules:

- R_s, X_s and E_s should always be positive.
- *X/R* ratio should have feasible values.

Therefore, the proposed three-point algorithm can be used for selecting the data that can be used for the multi-point algorithm. If (2.23) has a solution for every three consecutive points selected from a set of measured data, we can conclude the system side parameters did not vary for that set of measurements. In this case, instead of three points, we can use more measurement points for estimating the system impedance parameters. This process improves the accuracy of the impedance measurement algorithm. The solution for any selected three-point from the set of multipoint data can be used as an initial guess for the multi-point algorithm.

2.3.2 Load Fluctuation Index

The proposed algorithm uses the fluctuations of the loads connected to the system to calculate the system parameters. Therefore, one of the conditions for the input data of the algorithm is variation of the active and reactive power of the load at the substation bus. Since mathematically, the variation of one of the variables, *P* or *Q*, would be enough for the equations to be solved, the fluctuations can be defined as the summation of the absolute variation of P and Q, as stated in (2.24):

$$Fluctuation\ Index = \left(\left| \frac{P_1 - P_2}{P_1} \right| + \left| \frac{Q_1 - Q_2}{Q_1} \right| \right) \times 100 . \tag{2.24}$$

The input data to the algorithm have more than two sets of measurements; therefore, the fluctuation index is the minimum of the summation for the period of measurements, the n points, used for impedance estimation. In order to investigate the relation between the accuracy of the calculated parameters and the defined index, in noise conditions, some sensitivity studies were done. For this purpose, several simulation case studies with different signal-to-noise ratios at different load variations were prepared. The simulation results are plotted in Figure 2.3. For the simulation in this case, the multi-point algorithm using six measurement points was used. The system parameters are explained in Section 2.2.2.

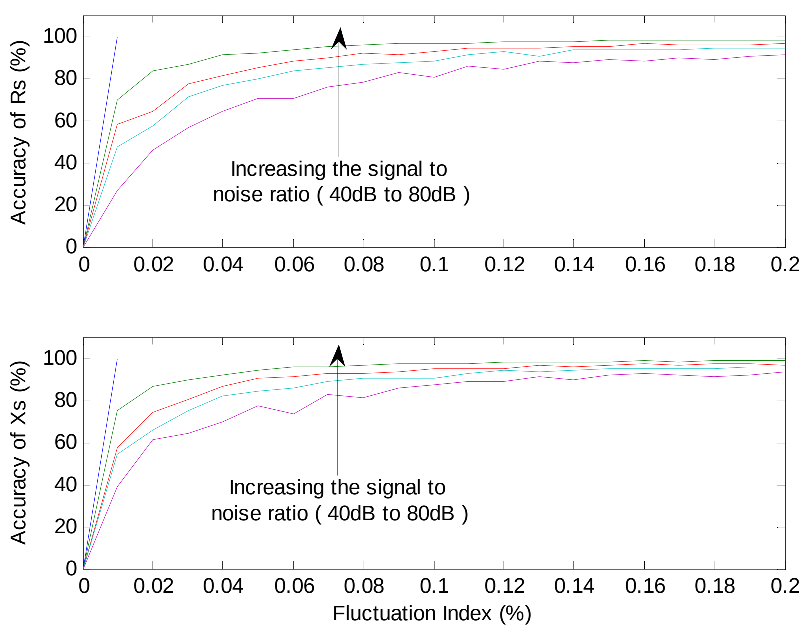

Figure 2.3. Accuracy of the method versus load fluctuations in noise condition

The results in Figure 2.3 show that in noise conditions, the accuracy of the algorithm is increased by increasing the load fluctuations. In the case of real field data, since mathematically the algorithm should work even with a small variation in the load's voltage and current, the required index should not be very large, but its magnitude should be large enough to filter the measurements that have no variations or contain only noise and transients. For this study, the index was chosen to be 0.05%.

2.4 The Proposed Algorithm for Three-Phase Systems

Power systems are usually designed as three-phase systems. If we assume that the system is balanced, the three phase voltages and currents can be transformed to positive, negative and zero sequence voltages and currents. Since the sequences are treated as single-phase circuits, the proposed algorithms in Section 2.2 can be used to calculate the system's positive, negative, and zero sequence equivalent circuit. The proposed algorithm for three-phase systems is explained in the following steps:

- Three to five seconds of waveforms of the three-phase voltages and currents of the feeder are captured with a 15.36 kHz sampling rate.
- Each cycle of the 60Hz three-phase voltage and current waveforms is transformed to the frequency domain by using Fourier transformation.
- The positive sequence voltages and currents for each cycle of the system frequency are calculated by using a sequence transformation matrix.
- The multi-point algorithm, considering the practical issues, is applied to calculate the system's positive sequence equivalent circuit parameters.

The algorithms were verified with the field test data taken from a 25kV feeder in a load-serving substation in Alberta, Canada. The length of the captured data for this test was 5 seconds. The parameters calculated by using the three-point method, for the positive sequence circuit, are plotted in Figure 2.4. The Thevenin voltage is the RMS value of the positive sequence circuit.

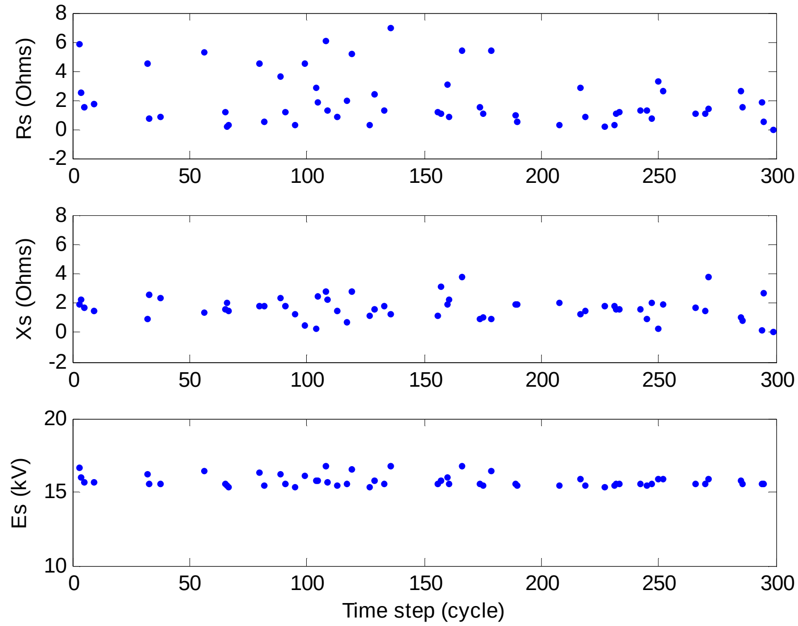

Figure 2.4. Positive sequence parameters using the three-point algorithm

Although the calculated parameters are not constant and vary around the mean value, Figure 2.4 shows that by improving the three-point algorithm, we can calculate the power system's impedance parameters. The variations are due to the measurement noise and transients in the voltages and currents, which may affect the accuracy of the calculated results.

In Figure 2.2, the simulation results show that increasing the number of points used for calculations reduces the sensitivity of the algorithm to the measurement noise. For a real power system, this result is obtained up to the point that one of the parameters of the system changes for the period of measurements. The more points used for calculations, the higher the probability of changing the system Thevenin equivalent circuit parameters for the period of measurements. Changing the system side parameters during the measurements will make the equations unsolvable. Therefore, a trade-off between the number of points and the accuracy of the results will occur.

Several real field data taken from different systems were investigated, and the results show that the multi-point algorithm using six points (6 cycles of waveforms) provides accurate and acceptable results. As an example the parameters of the feeder's positive sequence circuit shown in Figure 2.4 were calculated again by using the multi-point algorithm. For this purpose, six measurements (6 cycles of waveforms) were used to calculate each point, and the results are plotted in Figure 2.5. Again, the Thevenin voltage is the RMS value of the positive sequence circuit.

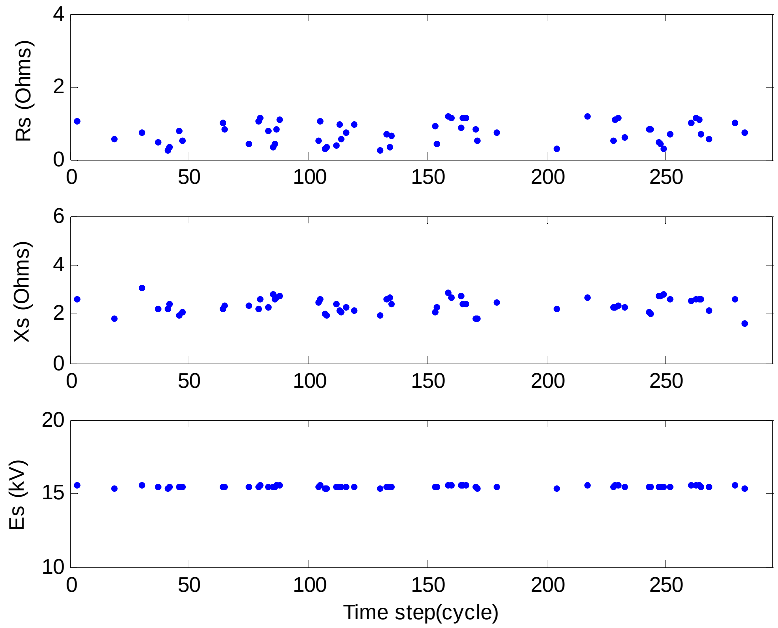

Figure 2.5. Positive sequence parameters using the multi-point algorithm

Figure 2.5 reveals that the results are now more consistent and closer to the actual values (Table 2.2). The modifications made to the algorithm improve the accuracy of the calculated system impedance parameters and make the algorithm practical for calculating real power system impedance parameters.

2.5 Simulation and Experimental Verifications

Some case studies were done and the simulation and experimental results are presented to show the validity of the proposed algorithm.

2.5.1 Simulation Results

For simulation verification, the system side parameters were changed at *t=30s* and *t=60s*, and the load side was changed randomly with a maximum variation of 5%. The measurements are taken as one cycle per every second and the proposed algorithm was applied to estimate the system impedance parameters, and the estimated system parameters and their actual values are plotted in Figure 2.6. The load parameters are explained in Section 2.2.2.

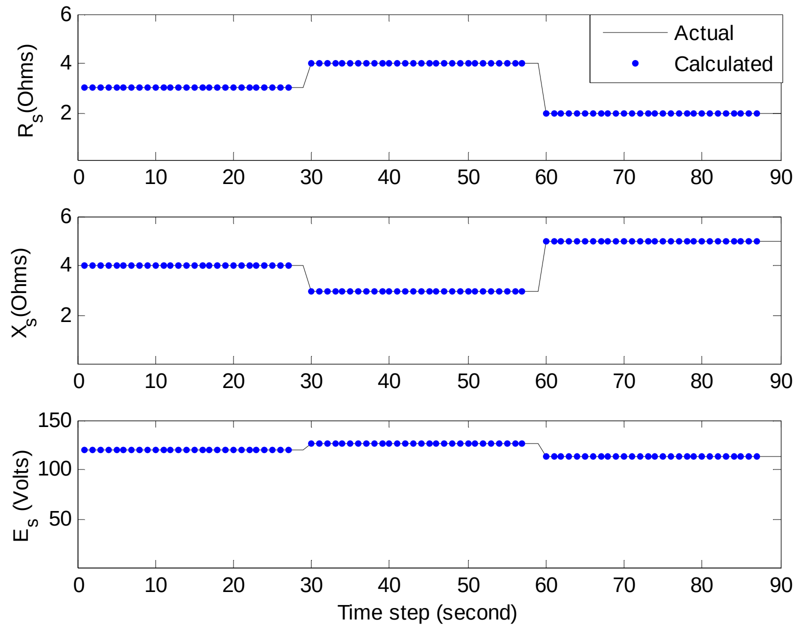

Figure 2.6. Actual and calculated system parameters

Table 2.1 shows the actual and calculated system impedance parameters for the three different stages.

Table 2.1. Simulation results

Stage	**The Calculated values**	**The Actual values**	**Error (%)**
# 1	3.00+j4.00	3.00+j4.00	0.00
# 2	4.00+j3.00	4.00+j3.00	0.00
# 3	2.00+j5.00	2.00+j5.00	0.00

Figure 2.6 and Table 2.1 show that the proposed algorithm provides the exact values of the system impedance and the equivalent voltage source. In some cases, the system parameters (*t=30s and t=60s*) have no solution because of the variation of the system side parameters for the period of measurements. In such cases, (2.23) does not have any solution, and the related Δ value is negative, and since we have used the three-point algorithm, the equations do not have solutions for three consecutive measurements.

2.5.2 Experimental Results

The proposed algorithm was also verified through lab experiments. For this purpose, the system was modeled as a resistance in series with a reactance, and the voltage source was the supply voltage source in the lab facilities at the University of Alberta. The magnitude of the resistance and reactance of the modeled system was much higher than that of the system connected to it. The magnitude of system impedance of the supply voltage can be roughly estimated by connecting a simple resistive load to the supply and measuring the voltage drop of the supply voltage ($Z = \Delta V / I$). Therefore the supply source was considered as an infinite bus. Since mathematically the algorithm works with both waveforms and RMS values, for experimental verification, instead of the voltage and current waveforms, their RMS values and the load's power factor were used for calculations. Every 30 seconds, a data window of voltage and current containing 12 cycles was captured, and the RMS values needed for the calculations were the average values of these 12 cycles, according to the IEC Standard [64]. The characteristics and measurement accuracy of the voltage and current probes used for the measurements are presented in Appendix B.

For this experiment, the load, which was an inductive and passive load, was changed randomly for the period of measurements. The system side parameters, (the resistance and inductance) were changed once after 15 minutes. The calculated and actual values of the system parameters are plotted in Figure 2.7.

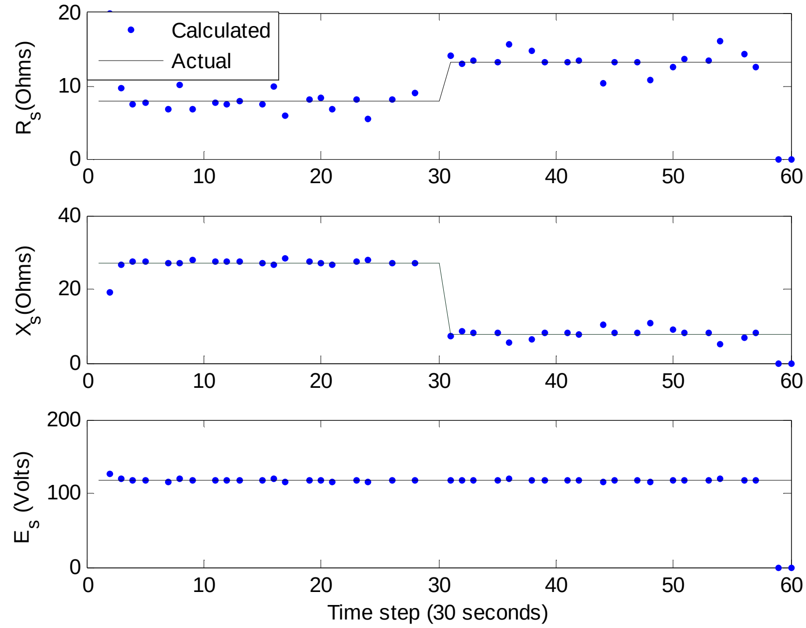

Figure 2.7. Actual and calculated experimental system parameters

The time step in Figure 2.7 is 30 seconds. The results show that the proposed algorithm works properly for experimental data and can also follow and detect the variation of system parameters automatically.

2.6 Implementation and Field Test Verification

In this section, the instrument set-up and field test verifications are explained. Field measurements were conducted on August and September 2007 at load-serving substations in Alberta, Canada, and the field measurements for residential transformers and houses were taken in November and December 2008. The data processing was performed in the power lab at the University of Alberta to determine the system's impedance parameters. The results from two different substations are presented in this chapter, and the calculated parameters for other substations, residential transformers, and houses are presented in Appendix C.

2.6.1 Instrument Set-up

The national instrument NI-6020E 12-bit data-acquisition system with a 15.36 kHz sampling rate controlled by a laptop computer was used for the recording. By using this data-acquisition system, we obtained 256 samples per cycle for each channel of waveform. The captured waveforms were three-phase voltages and the currents at the point of the metering in the load-serving substations. All the measuring points were at 25 kV; therefore, CTs and PTs were used to step down the current and voltages, respectively, to measurable values. The measurements were taken as five seconds per minute, so that in every minute, a five-second data window of three-phase voltage and current waveforms was captured.

2.6.2 Substation One

Site One is a 25 kV load-serving substation and is located in Alberta, Canada. The single-line diagram of the substation and feeders and the measurement points are shown in Figure 2.8.

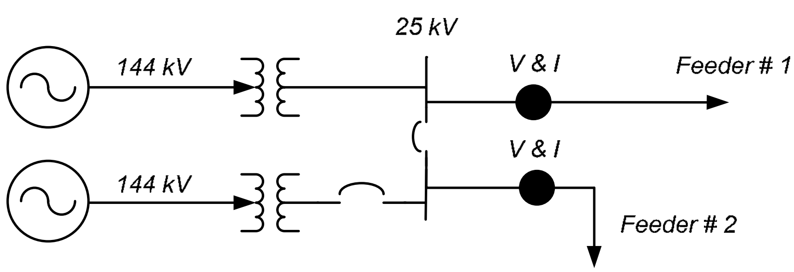

Figure 2.8. Single line diagram of Substation One

The measurements were taken from both feeders at Site One. For this purpose, the data were collected as a five-second data window every minute during a one-hundred minute period. The three-phase waveforms for each feeder were transformed to the frequency domain for every cycle of the 60Hz system frequency, and then, by using the sequence transformation, the positive sequence circuit voltages and currents were calculated. The variation of the RMS values of the positive sequence voltage and the current for Feeder One is shown in Figure 2.9.

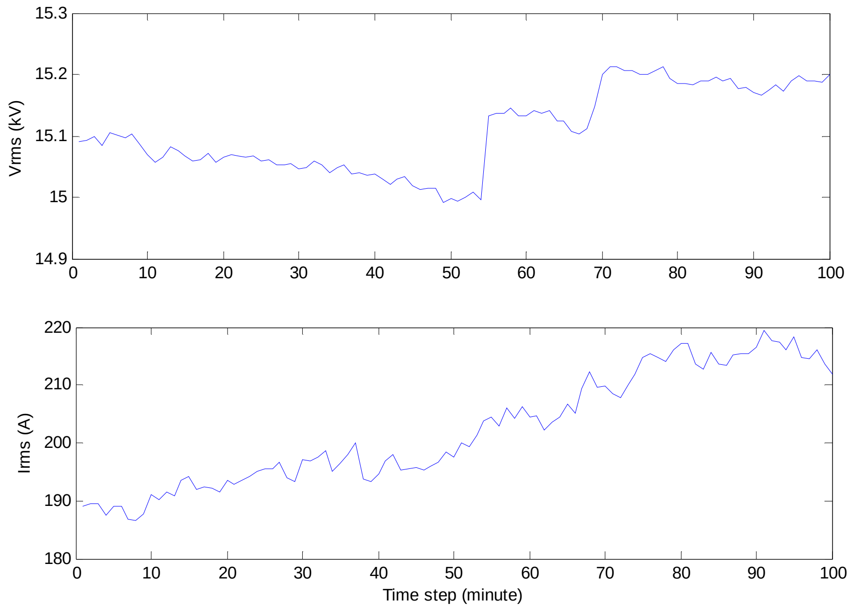

Figure 2.9. Variation of voltage and current at Feeder One in Substation One

The step change in the voltage waveform is the result of the tap changing of the transformer. The positive sequence parameters of the system were calculated for each data window containing six cycles of the waveforms, and the average for every minute was plotted in Figure 2.10, which reveals that if we collect the waveforms continuously, the calculated parameters can be shown continuously on the meters, resulting in a new generation of meters.

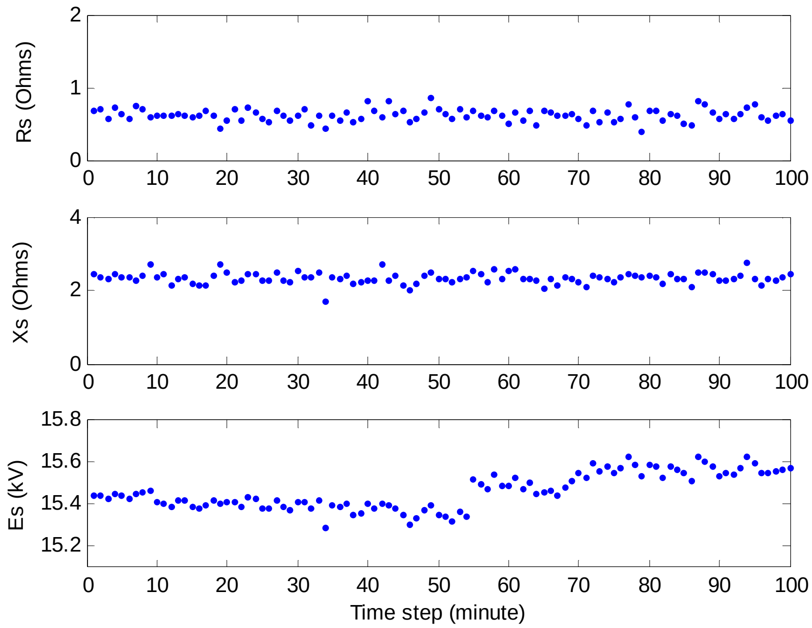

Figure 2.10. Positive sequence parameters of Feeder One, Substation One

The same procedure was applied for Feeder Two, and the mean value of the calculated impedance parameters for the measurement period (100 minutes) for each feeder were compared with the impedance data calculated by using different methods. The other methods involved using the real short-circuit data recorded by PML meters at the substation, and the output of the PSS/E circuit program. The PSS/E provides the simulated total fault current at the substation, which can be used for calculating the system impedance parameters. The F. index is the mean value of the load fluctuation indices defined by (2.24) for the period of measurements. Since the measurement data which result in a calculated impedance parameter are more than 100 points, we assumed a normal distribution function for the distribution of each calculated parameter. By using a 95% confidence level for each calculated parameter, the confidence interval for the impedance parameters was calculated. The results are presented in Table 2.2.

Table 2.2. Substation One, impedance data

Feeder	The Calculated Resistance	The Calculated Inductance	F. index (%)	Real Fault Data	PSS/E Data
# 1	0.628 ± 0.166	j2.271 ± 0.297	0.190	0.623+j2.582	0.751+j2.537
# 2	0.689 ± 0.292	j2.876 ± 0.929	0.148		

Table 2.2 shows that the results calculated by using the proposed algorithm are comparable with those calculated by using other methods. However, the main advantage of the proposed algorithm is the capability for online monitoring and no need for disturbance, comparing to the other methods. The impedances of the transformers connected to Feeders One and Two are 0.040+j1.435 ohms and 0.062+j1.809 ohms, respectively. The averages of the total harmonic distortion (THD) of the voltage and current for Feeder One are 1.386% and 2.485%, respectively. The THD for the voltage and current was calculated as shown in (2.25) and (2.26):

$$THD_V = \frac{\sqrt{\sum_{h=2}^{\infty} V_h^2}}{V_1} \tag{2.25}$$

$$THD_I = \frac{\sqrt{\sum_{h=2}^{\infty} I_h^2}}{I_1} \quad , \tag{2.26}$$

where h represents the harmonic order. Since we are using the fundamental 60Hz values of the waveforms for our calculations, the signal deviations, i.e., the harmonics, have no impact on the performance of the algorithm.

2.6.3 Substation Two

The second substation is also a 25 kV load-serving substation and is located in Alberta, Canada. The single-line diagram of the substation and feeders and the measurement points are shown in Figure 2.11.

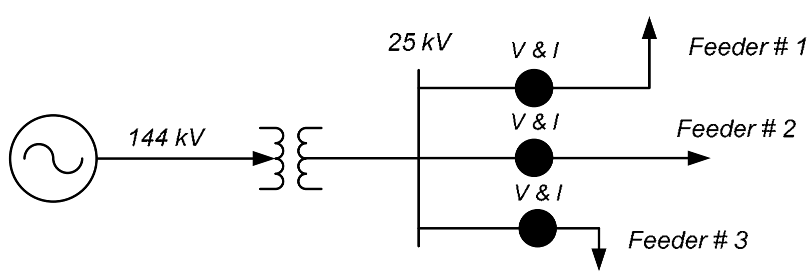

Figure 2.11. Single line diagram of Substation Two

The measurements were taken from all three feeders at this substation. The three-phase voltages and currents were captured again at a rate of five seconds in every minute for one hundred minutes. The waveforms for each feeder were transformed to the frequency domain for every cycle of the 60Hz system frequency, and the positive sequence circuit voltages and currents were calculated. The variations of the RMS values of the positive sequence voltage and current for Feeder One are shown in Figure 2.12.

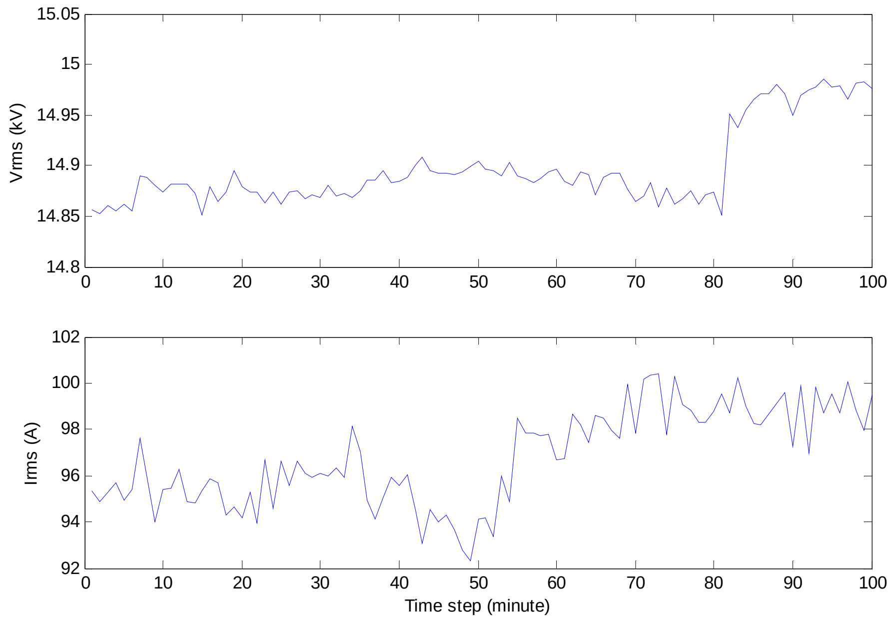

Figure 2.12. Variation of voltage and current at Feeder One in Substation Two

The system's positive sequence parameters were calculated for each data window, and the average for every minute is plotted in Figure 2.13, which shows that, for some cases, the proposed algorithm does not provide any results.

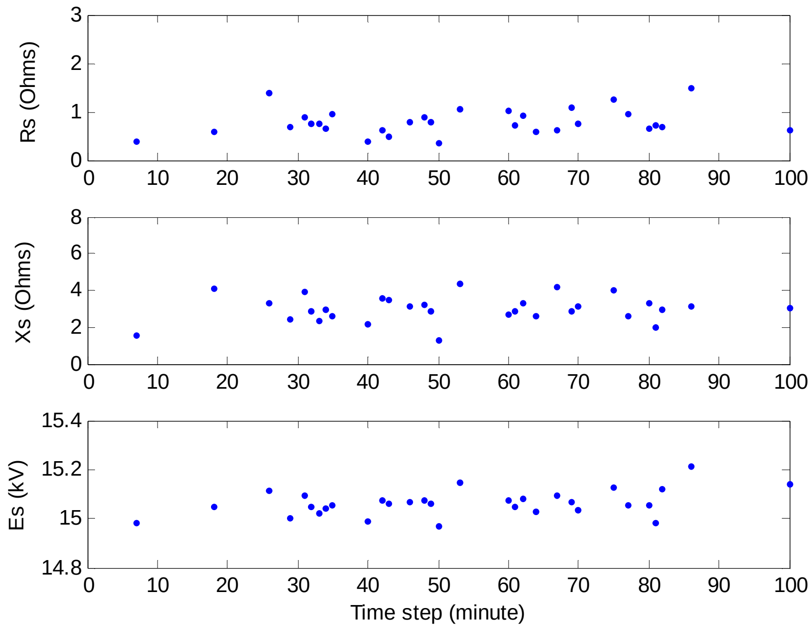

Figure 2.13. Positive sequence parameters of Feeder One, Substation Two

The reason could be the variation of the system side parameters or a small variation of the load's active and reactive power during the five-second measurements. Since the input data, voltage, and current waveforms will be continuously available, this variation will not be a problem when implementing the algorithm. The proposed algorithm using six cycles of the waveform was applied to all the feeders in Substation Two, and, in Table 2.3, the mean value of the calculated impedances for one hundred minutes are compared with that from the other calculation.

Table 2.3. Substation Two, impedance data

Feeder	The Calculated Resistance	The Calculated Inductance	F. index (%)	Real Fault Data	PSS/E Data
# 1	0.538 ± 0.430	$j2.422 \pm 1.435$	0.0781	0.928+j2.913	0.737+j2.602
# 2	0.641 ± 0.459	$j2.559 \pm 1.554$	0.0767		
# 3	0.773 ± 0.336	$j2.768 \pm 1.216$	0.1135		

Table 2.3 also shows the confidence interval for the calculated impedance parameters. The calculated impedances obtained from different feeders by using different methods are slightly different, possible because of the different fluctuation indices and the measurement error. Table 2.2 and Table 2.3 reveal that the greater the fluctuation index,

the more accurate the results, and the smaller the confidence interval, because of the algorithm's better performance in higher load fluctuations, as was shown in Section 2.3.2. In Substation Two, the impedance of the transformer feeding all the feeders is 0.066+j1.777 ohms. The average THD of the voltage and current for Feeder One is also calculated by using (2.25) and (2.26). They are 2.827% and 6.192%, respectively. These amounts have no impact on the calculation of the system impedance parameters.

The algorithm was verified with several field measurements taken from different substations in different locations in Alberta, Canada. The results show that the proposed algorithm can be implemented in power monitors and be used for the online measurement of power system impedance parameters.

2.7 Conclusion

In this chapter, a new algorithm was proposed for the online tracking of power system impedance parameters. The main contributions of this research to the field are the new proposed algorithm; the consideration of the practical issues; and the verifications through computer simulations, lab experiments, and several field tests. The following conclusions are drawn:

- A three-second to five-second data window with sufficient variations is enough for the estimation of impedance parameters,
- The 256 sample per cycle rate of the data-acquisition system is sufficient for the data collection process,
- The algorithm does not depend on the load model and works with the natural variations of any kind of loads,
- Synchronized measurements are not required for calculations, and the method is not sensitive to changes of system frequency and harmonics,
- The required information can be obtained from the meters that are already installed at the substation buses.

The proposed algorithm was verified by using simulations, experiments, and real field data. The verification results show that the proposed method can be implemented for the online monitoring of power system impedance parameters.

Chapter 3

Sensitivity Studies and Additional Applications

This chapter presents some sensitivity studies which were done in order to finalize the impedance measurement algorithm as well as some extra applications of the proposed technique. The sensitivity studies are performed in order to investigate the disturbance side at substation bus, to determine the number of points used for calculations, and also to investigate the fluctuation index at the substation bus. As two extra applications of the method, the impedance measurement algorithm has been applied for the online monitoring of power system harmonic and zero sequence impedance parameters. The method was verified through several real field measurements and the results are presented in this chapter.

3.1 Introduction

The impedance measurement technique presented in Chapter Two, uses the steady state measurements taken at the substation bus for calculation of system impedance parameters. The advantage of the method is the capability to operate under normal conditions without imposing any disturbance on the system and requiring synchronized measurements. However, there are some practical issues that should be considered for implementation of the algorithm. For example, whether the system side parameters remain constant for the measurement period and the load variations is enough for calculations should be investigated. The number of points required for calculations and its effect on the accuracy of the results is also an issue to be determined. Whether the specified fluctuation index defined in Chapter Two is sufficient for impedance measurement in every substation should also be investigated.

In order to answer the above questions and firm up the impedance measurement technique for real field applications, several studies were performed. These studies were done for the data collected from twenty seven feeders in eight different substations. The results presented in this chapter were used to finalize the proposed algorithm.

This chapter also presents the application of the impedance measurement algorithm for online measurement and monitoring of power system harmonic and zero sequence impedance parameters.

The frequency response of a system at specific buses depends mainly on its impedances at different frequencies [10]-[12]. In recent years, the increase in the power demanded by nonlinear loads has not been followed by the appropriate development of the power system; therefore, the network is more likely to be subjected to the injected harmonic disturbances than it was previously. In such cases, harmonic impedances of the network will have an important role in harmonic disturbance propagation due to the system's extension and meshed structure [12].

The knowledge of power system harmonic impedances is necessary for harmonic analysis, harmonic mitigation measures, determination of harmonic limit compliance, prediction of system resonance, and harmonic propagation studies [10]-[30]. In order to utilize the capabilities of widely used power electronic devices and to reduce their negative effects, especially to minimize voltage waveform distortions, detailed models of the interaction between them and the power system they are connected to are necessary. The Thevenin equivalent circuits at fundamental and harmonic frequencies usually provide enough information regarding the effects of the changes in the power electronic device operating conditions on the supply voltage waveform [8]. Moreover, real-time monitoring of the system's harmonic impedances can provide significant improvements to the design and operation of active filters [5], [16]-[18].

The zero sequence impedance of the system seen at the substation bus is important information for power system studies. It is used for calculating the different ground fault levels at substations. It depends upon the path available for the flow of the zero sequence current and also the balancing ampere turns available within the transformer. Generally, a zero sequence current requires a delta winding, or a star connection with the star point grounded. Any impedance in the connection between the star point and earth increases the overall zero sequence impedance and subsequently controls the magnitude of the current that will flow under earth fault conditions.

The various methods that have been proposed to calculate the system's harmonic impedances can be classified into two groups: transient-based and steady state-based methods [11]. The transient-based methods include imposing a disturbance on the power system and then extracting the frequency-dependent network impedances from the transient voltages and currents [3], [14], [65]-[66]. Typically, the switching device is a known local impedance such as a capacitor bank. The main disadvantage of these methods is the need for an external disturbance source and also for a high-speed data-acquisition system to capture high-frequency transients. The steady-state-based methods use the pre- and post-disturbance steady state waveforms to calculate harmonic impedances [1], [65], [67]-[68]. For these methods, the typical disturbances are made by harmonic current injectors produced either by an external source or by switching a network component such as a capacitor or transformer [69]. The main disadvantages of these methods are the need for a disturbance source and their accuracy's dependence on whether any other loads are switched in, and also whether the background distortion remains constant during the measurement interval. Other than the mentioned issues, none of the methods can be used for the online monitoring of the network harmonic impedances. For measurements, both methods need synchronized measurement data and also the injection of disturbances into the power system.

3.2 Sensitivity Studies

In order to finalize the impedance measurement algorithm, in this section several sensitivity studies were performed and the results are presented. The studies are related to the determination of disturbance side, number of points used for calculations and the fluctuation index in different substations.

3.2.1 Disturbance Side

The impedance measurement technique uses the naturally occurring load side disturbances to calculate the system side impedance parameters. As it was explained in Chapter Two, the three point method can be used to determine the disturbance side at the substation bus. In this section the disturbance side detection method is used to investigate the source of disturbance for different feeders in eight substations. If the source of disturbance is the load side then the voltage and current fluctuations can be used to monitor the system impedance parameters. In the following sections the percentage of load side disturbances which can be used for impedance monitoring are presented. The length of data window used for the calculations in this section was from 3 hours to 24 hours for different feeders.

3.2.1.1 Fundamental or Positive Sequence Component

Figure 3.1 shows the average percentage of load side disturbances for fundamental component in different feeders.

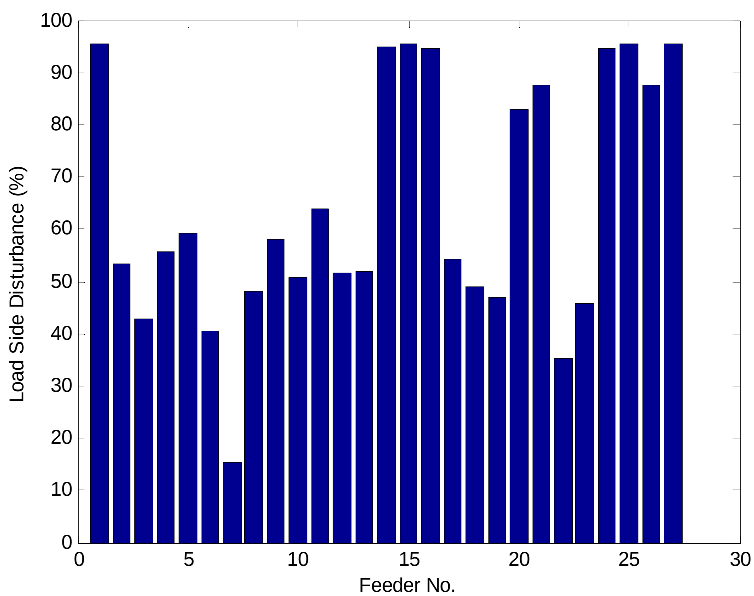

Figure 3.1. The percentage of load side disturbance for different feeders

This figure reveals that for most of the cases the disturbances come from the load side. For some feeders such as the first and last one, almost all the disturbances seen at the substation bus come from the load side and the system side remains constant during the measurement period. Our studies show that there may be some disturbances coming from the system side as well. The data related to this period of time cannot be used for calculation of system side impedance parameters. The disturbance in the system side parameters is usually caused by the variation of system background voltage.

3.2.1.2 Harmonic Components

The average percentage of load side disturbances is also calculated for all the harmonics. The results related to fifth and seventh harmonics are presented in the following figures.

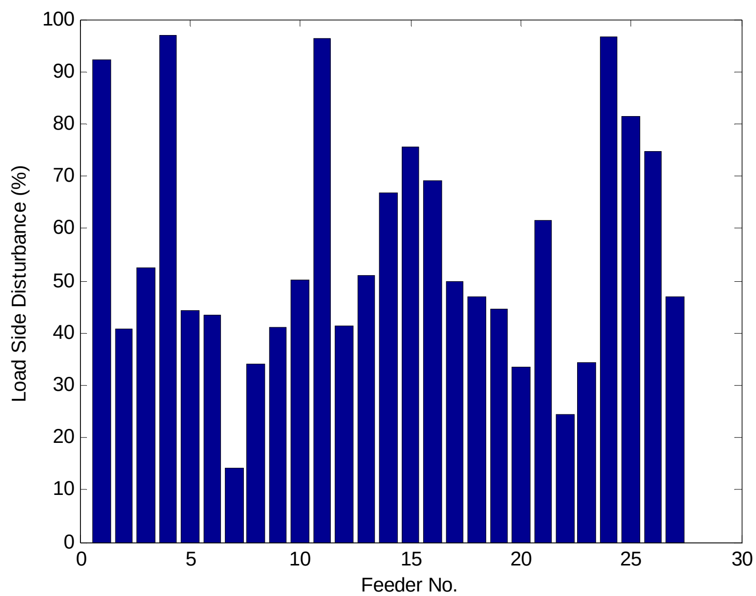

Figure 3.2. The percentage of load side disturbance for fifth harmonic

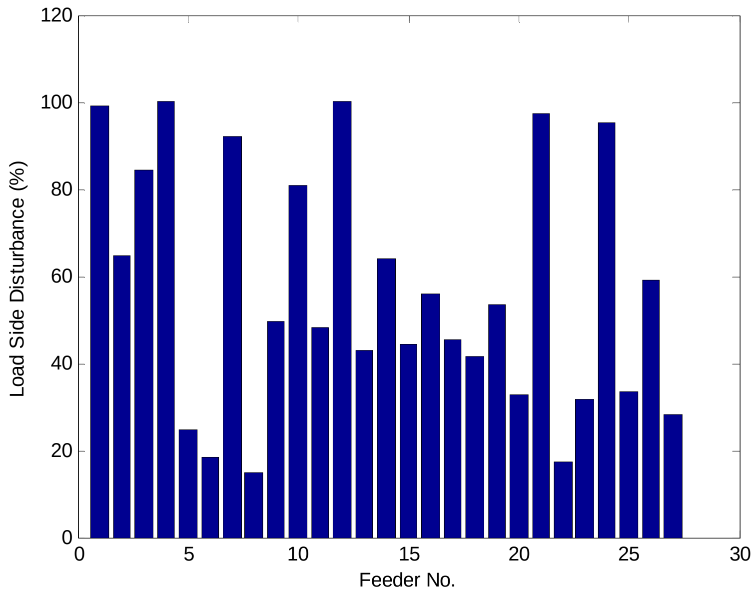

Figure 3.3. The percentage of load side disturbance for seventh harmonic

Figures 3.2 and 3.3 reveal that the percentage of load side disturbance over the measurement period is different for different feeders and different harmonics. However for almost all the feeders we always have disturbances coming from the load side which can be used for monitoring of harmonic impedances.

3.2.1.3 Zero Sequence Components

The average percentage of load side disturbances is also calculated for zero sequence components and the results are plotted in Figure 3.4.

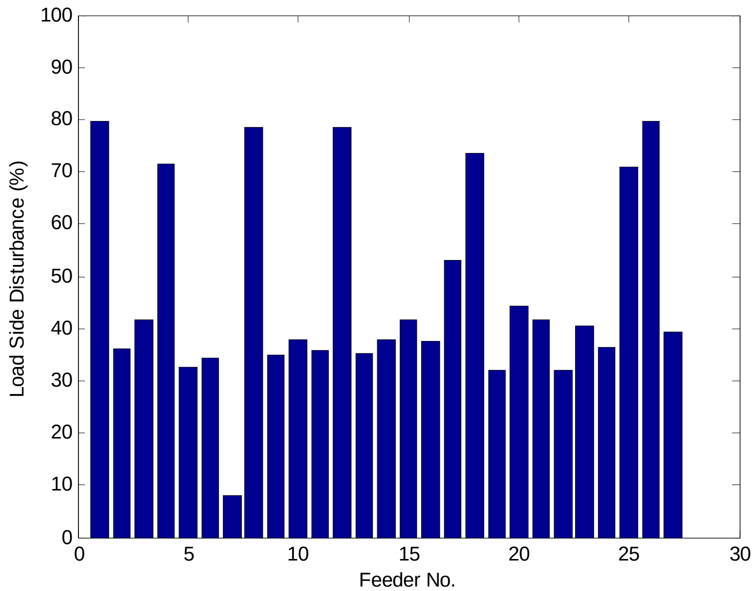

Figure 3.4. The percentage of load side disturbance for zero sequence

It is seen that the average percentage of load side disturbances for zero sequence component is different and always nonzero for all the feeders.

3.2.1.4 Disturbance Side Distribution over 24H

The distribution of average load side disturbances of the feeders over a 24 hour period is plotted in the following figures for fundamental, harmonics and zero sequence components.

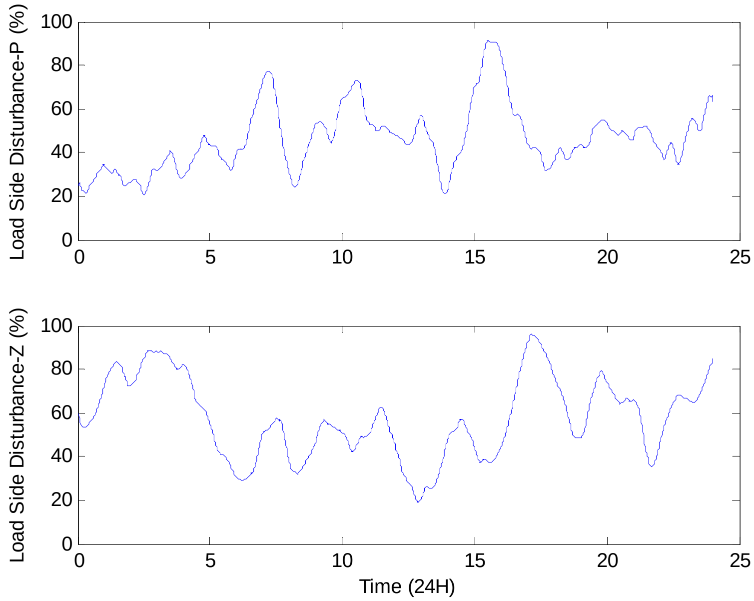

Figure 3.5. Distribution of load side disturbances

Figure 3.5 shows that the percentage of load side disturbances for fundamental and zero sequence components vary during the day without any specific pattern.

The distribution for all the harmonic components was also calculated. As an example the distribution of the percentage of load side disturbances for fifth and seventh harmonics are plotted in Figure 3.6.

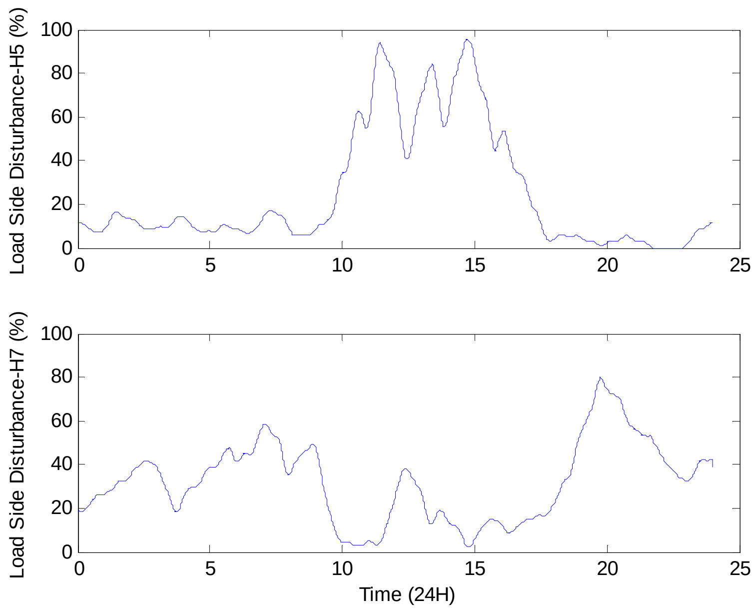

Figure 3.6. Distribution of load side disturbances

It is seen that the percentage of load side disturbances for different harmonics are not the same. Also this value changes during the day but again the important issue is that it is usually large and enough for online monitoring of power system harmonic impedances.

The studies in this section show that the load side disturbances at the substation bus are usually enough for impedance estimations. This is important information and enables us to use the proposed technique for real field applications where we need the system impedance data.

3.2.2 Number of Points Used for Calculations

Chapter Two explained that the three-point method is not applicable for real field measurements. However, the proposed multi-point algorithm is suitable for real applications and is less sensitive to noise and transients.

The simulation results in Figure 2.2, Chapter Two, show that increasing the number of points used for calculations reduces the sensitivity of the algorithm to the measurement noise. This result is obtained while all the system side parameters remain constant. The question is how many points are required and are sufficient for calculations. This section investigates the calculation error for impedance measured from Substations One and Two. As will be shown the multi-point impedance measurement method by using six cycles (n=6) of the voltage and current waveforms is the best choice and provides accurate and acceptable results.

Figure 3.7 shows the calculation error for the resistance and inductance measured at the two feeders in Substation One.

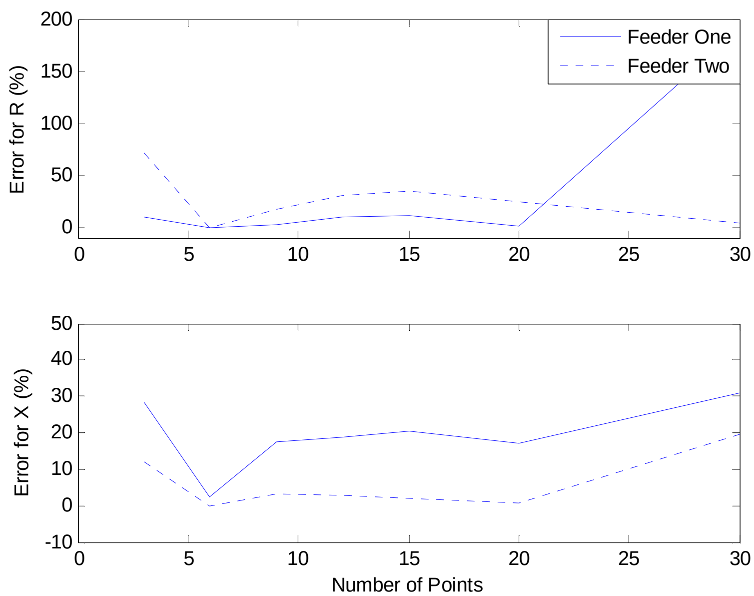

Figure 3.7. Calculation error vs. number of points, Substation One

In Figure 3.7 the calculated parameters are compared with the PSS/E data. As can be seen increasing the number of points does not necessarily increase the measurement's accuracy. The reason is the variation of system side parameters for longer data windows. The same procedure was applied for the three feeders in Substation Two and the results are presented in Figure 3.8.

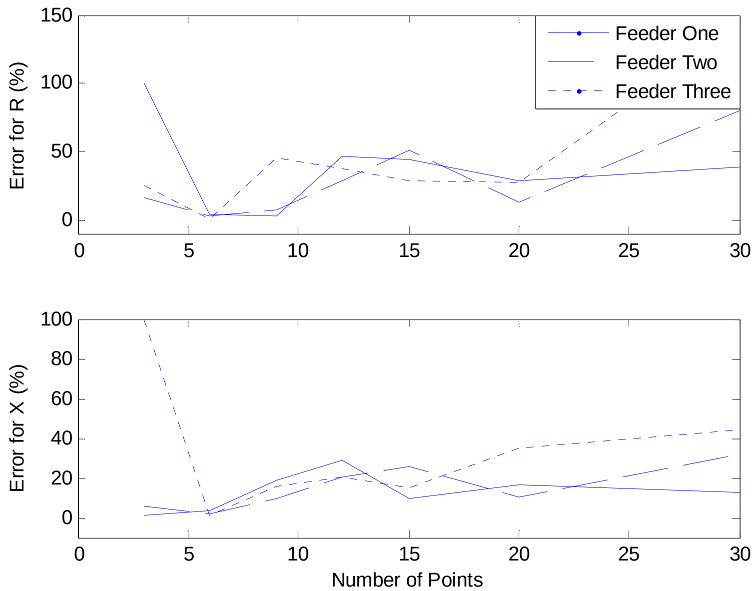

Figure 3.8. Calculation error vs. number of points, Substation Two

Our studies in this section reveals that the multi-point impedance measurement algorithm by using six measurement points from six consequent cycles of voltage and current waveforms provides the most accurate and acceptable results.

3.2.3 Fluctuation Index

The proposed algorithm uses the fluctuations of the loads connected to the system to calculate the system parameters. Therefore, one of the conditions for the input data of the algorithm is variation of the active and reactive power of the load at the substation bus. In order to investigate the relation between the accuracy of the calculated parameters and the defined index, in noise conditions, some sensitivity studies were done in Chapter Two.

The results in Figure 2.3, Chapter Two, show that in noise conditions, the accuracy of the algorithm is increased by increasing the load fluctuations. In the case of real field data, since the accuracy of instruments used for calculations is very high, the signal to noise ratio is also high; therefore, the required index should not be very large, but its magnitude should be large enough to filter the measurements that have no variations or contain only noise and transients. For this study, the index was chosen to be 0.05% and based on the simulation results, since the SNR is high, the accuracy of calculated impedance parameters will be sufficient. As an example the fluctuation index versus the accuracy of calculated system impedance data is plotted for Substation One and Two in the following figures. The PSS/E data was used to calculate the accuracy of calculated parameters in the figures.

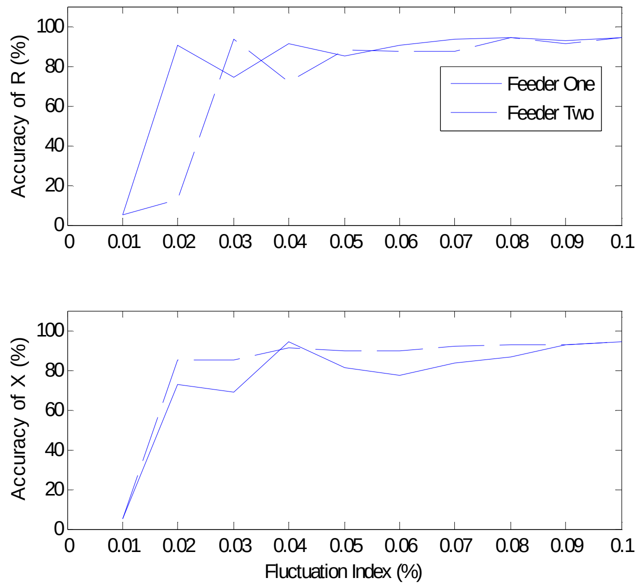

Figure 3.9. Accuracy of R and X vs. fluctuation index in Substation One

Figure 3.9 reveals that the accuracy of calculated parameters increases by increasing the minimum fluctuation index up to a certain point. For this substation the minimum 0.05 provides relatively accurate results. The index versus the accuracy of resistance and reactance in Substation Two is plotted in Figure 3.10.

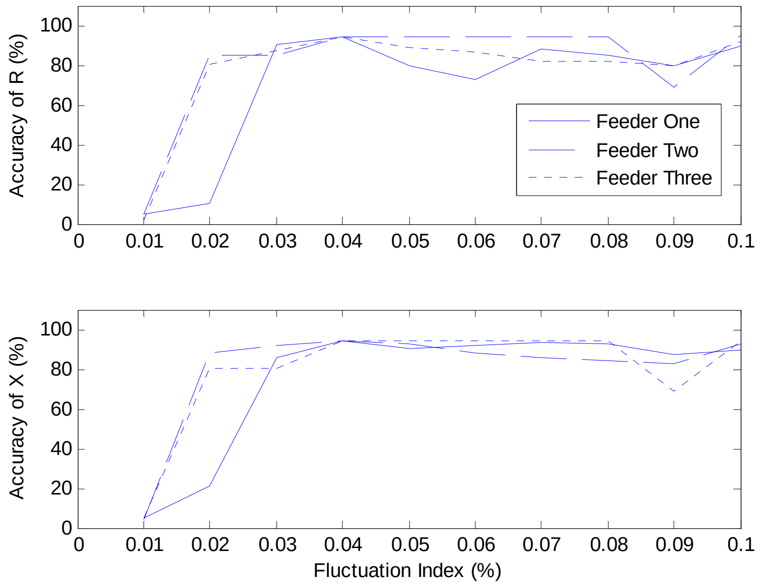

Figure 3.10. Accuracy of R and X vs. fluctuation index in Substation Two

Figure 3.10 shows that for this substation as well the minimum 0.05% for index provides accurate and acceptable results. This study has been done for all the substations and based on the results, the 0.05% fluctuation index is sufficient for selection of appropriate data for impedance monitoring.

In the next following sections the fluctuation index is calculated and plotted for twenty seven feeders in eight different substations. This index was calculated for positive sequence, harmonics and zero sequence voltages and currents of the system and the results are plotted in the next sections.

3.2.3.1 Fundamental or Positive Sequence Component

The average fluctuation indices for fundamental voltage and current of all the feeders over a period of 3 hours to 24 hours for each feeder are plotted in Figure 3.11.

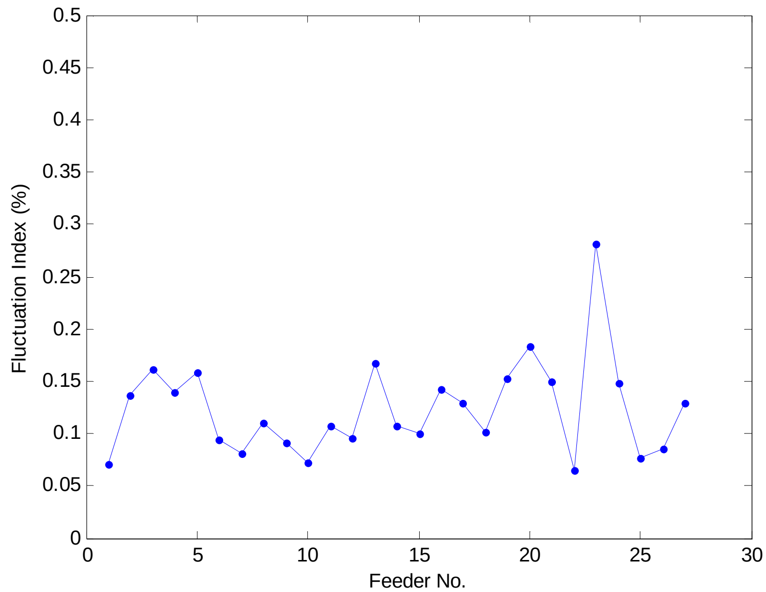

Figure 3.11. Fluctuation index for positive sequence circuit

Figure 3.11 reveals that the fluctuation index for different substations is larger than 0.05%. This means that the system impedance measurement technique is applicable for calculation of impedance data seen from all these substations.

3.2.3.2 Harmonic Components

The fluctuation index was calculated for each harmonic as well and is shown in Figure 3.12.

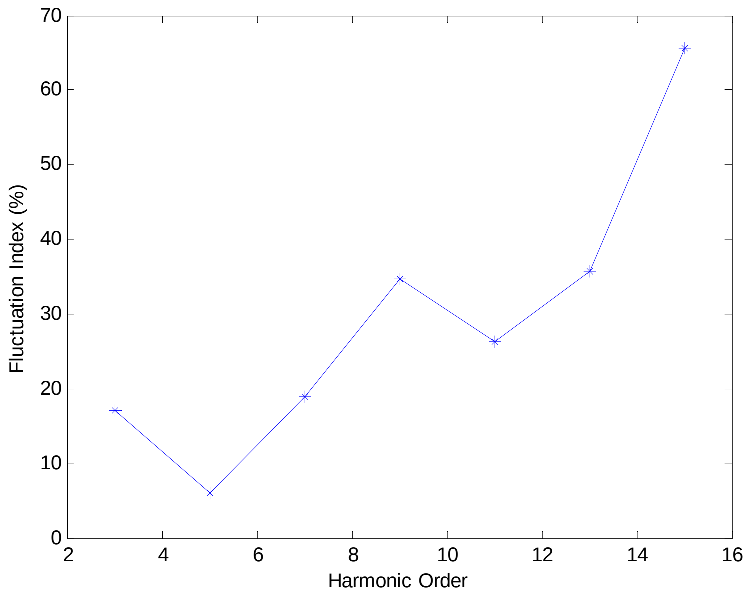

Figure 3.12. Fluctuation index for harmonics

It is seen that the fluctuation index for harmonics is large enough for calculation of harmonic impedances as well.

3.2.3.3 Zero Sequence Components

This index was also calculated for zero sequence voltages and currents and the results are presented in Figure 3.13.

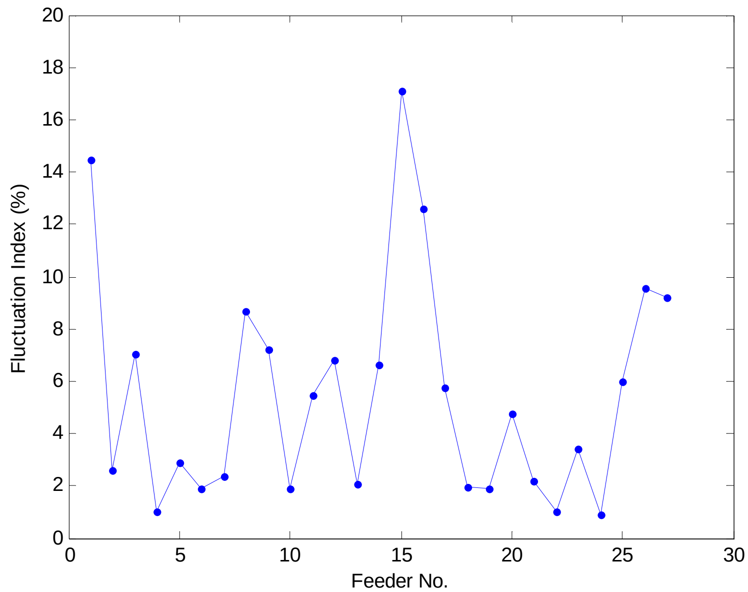

Figure 3.13. Fluctuation index for zero sequence circuit

Figure 3.13 reveals that the load fluctuations are enough for calculation of power system zero sequence impedance parameters.

3.2.3.4 Fluctuation Index Distribution over 24H

The distribution of average fluctuation indices of the feeders over a 24 hour period is plotted in the following figures for fundamental, zero sequence and harmonics.

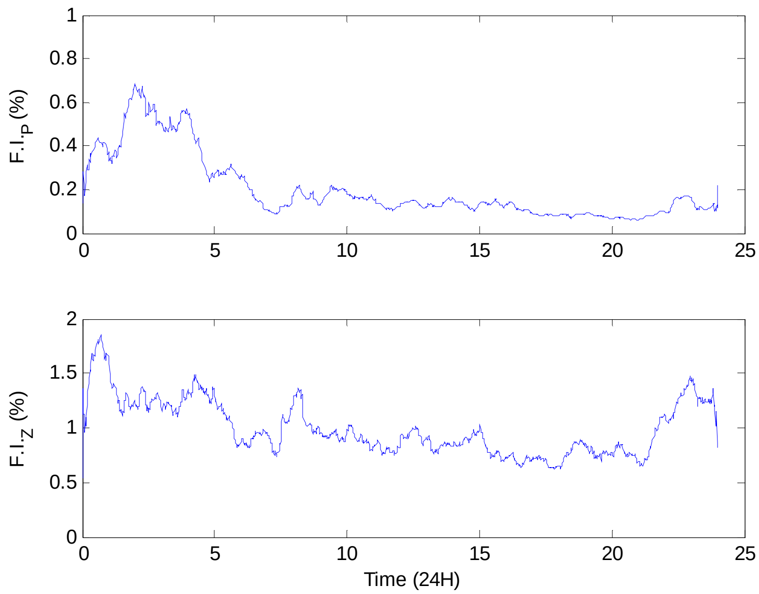

Figure 3.14. Distribution of fluctuation index during 24 hours

Figure 3.14 shows that the fluctuation indices for fundamental and zero sequence components vary during the day. However it is important that during 24 hour its value is more than the minimum required index which is set as 0.05%.

The distribution of this index for all the harmonic components was also calculated. As an example the distribution of fluctuation index for fifth and seventh harmonics are plotted in Figure 3.15.

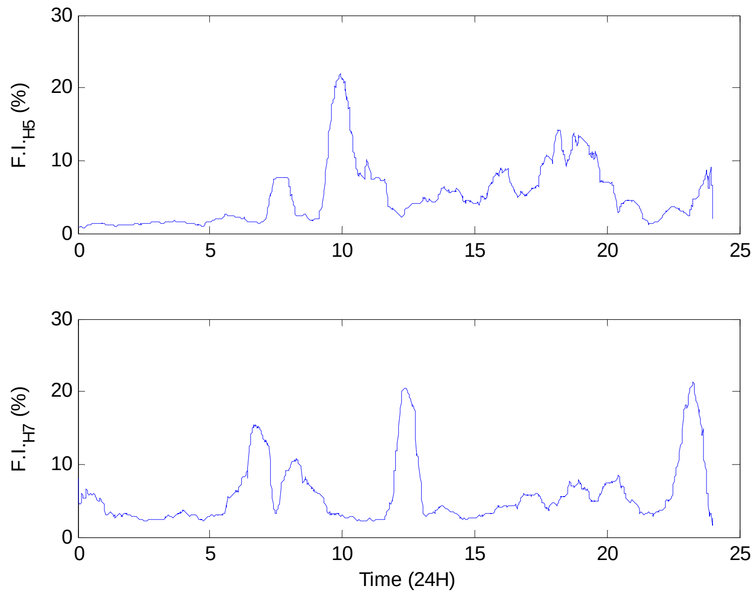

Figure 3.15. Distribution of fluctuation index during 24 hours

It is seen that the fluctuation indices for different harmonics are not the same. Also this value changes during the day but again the important issue is that it is usually large and enough for online monitoring of power system harmonic impedances.

The sensitivity studies in this section shows that the load fluctuation index for power system fundamental, harmonic and zero sequence voltages and currents is sufficient for calculation and online monitoring of system side impedance parameters for each circuit.

3.3 Additional Applications

In this section, based on the research presented in Chapter Two and [70], an algorithm is proposed for the online monitoring of network harmonic impedance parameters and the system's background voltage distortion as well as power system zero sequence impedance parameters. The proposed method requires neither an external disturbance source nor synchronized measurement data. For calculations, it uses the naturally occurring load disturbances connected to the system. Implementation issues are addressed in this section, and the proposed method is verified through real field measurements from different substations. Field measurements were conducted in August and September 2007 at load-serving substations in Alberta, Canada, and the field measurements on residential transformers and houses were taken in November and December 2008. The data-processing was performed in the power lab at the University of Alberta to determine the systems' harmonic impedance parameters and the results related to two different substations are presented in this section. The calculated parameters for the residential transformers and houses are presented in Appendix D.

3.3.1 Harmonic Impedance Measurement

This section presents the harmonic impedance measurement method and the field test verification results.

3.3.1.1 The Proposed Algorithm

The equivalent circuit for the harmonics is the same as that for the positive sequence circuit. Therefore, with some modifications, we can use the algorithm explained in Chapter Two for harmonic impedance measurement. The algorithm and its implementation issues are explained in Chapter Two; therefore, in this chapter, only the application of the method for calculating power system harmonic impedances is presented. The system model used for the harmonic frequencies is the Thevenin equivalent circuit shown in Figure 3.16.

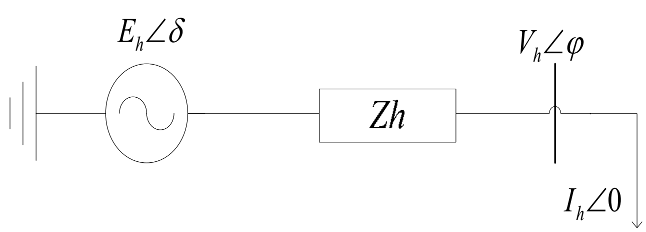

Figure 3.16. Power system model used for harmonics seen at the substation bus

For some harmonics, the Thevenin equivalent voltage will be zero when the system side does not have any harmonic sources and is not generating any harmonic currents. Zero equivalent voltage will not affect the calculation procedure because in this case, the estimated value for the voltage source will be zero. Considering the multi-point algorithm and the implementation issues explained in Chapter Two, in this section we propose an algorithm for calculating power system harmonic impedance parameters. The following steps should be taken:

- Capture the three-phase voltages and currents of the system in a continuous waveform format by using a 256 sample per cycle data-acquisition system (the sampling rate depends on the maximum order of the required harmonic impedance).
- Convert the voltages and currents of each cycle of the 60-Hz waveforms, for each phase, to the frequency domain by using Fourier transformation.
- Assuming that the system impedance matrix is balanced, convert the system's three-phase voltages and currents phasors to positive, negative, and zero sequences for each harmonic including the fundamental frequency.
- Apply the multi-point algorithm to the system's harmonic voltages and currents to calculate the impedance parameters of each circuit.

Since the system impedance matrix is balanced at the substation point, we can assume the system harmonic impedance matrix is also balanced. In this scenario, because of the different phase angle properties of the harmonic voltages and currents, they will be dominant in different sequences. For example, if the first harmonic with the fundamental frequency has positive sequence properties, then the system voltages can be assumed to be in the following format:

$$\begin{aligned}\tilde{V}_a &= |V| Cos(\omega t) \\ \tilde{V}_b &= |V| Cos(\omega t - 120^0), \\ \tilde{V}_c &= |V| Cos(\omega t + 120^0)\end{aligned} \tag{3.1}$$

and the second harmonic can be shown as follows:

$$\begin{aligned}\tilde{V}_a &= |V| Cos\left[2\times(\omega t)\right] = |V| Cos(2\omega t) \\ \tilde{V}_b &= |V| Cos\left[2\times(\omega t - 120^0)\right] = |V| Cos\left[2\omega t - 240^0\right] = |V| Cos(2\omega t + 120^0) \\ \tilde{V}_c &= |V| Cos\left[2\times(\omega t + 120^0)\right] = |V| Cos\left[2\omega t + 240^0\right] = |V| Cos(2\omega t - 120^0).\end{aligned} \tag{3.2}$$

As (3.2) reveals the second-order harmonic will have negative sequence properties. For the third harmonic, we will have

$$\begin{aligned}
\tilde{V}_a &= |V|\,Cos\left[3\times(\omega t)\right] = |V|\,Cos(3\omega t) \\
\tilde{V}_b &= |V|\,Cos\left[3\times(\omega t - 120^0)\right] = |V|\,Cos\left[3\omega t - 360^0\right] = |V|\,Cos(3\omega t) \\
\tilde{V}_c &= |V|\,Cos\left[3\times(\omega t + 120^0)\right] = |V|\,Cos\left[3\omega t + 360^0\right] = |V|\,Cos(3\omega t).
\end{aligned} \tag{3.3}$$

Equations (3.3) show that the third harmonic has zero sequence properties. The other harmonics' properties can be found similarly and are listed in Table 3.1.

Table 3.1. Harmonic order and sequences

Positive Seq.	**Negative Seq.**	**Zero Seq.**
1	2	3
4	5	6
7	8	9
10	11	12
13	14	15

In order to calculate the harmonic impedances for each harmonic, first we have to check the sequence in which the harmonic voltage and currents will show up. This requirement for calculating the harmonic impedances of a three-phase system has been considered for all the calculations in this section. The algorithm was applied to real field data, and the results are presented in the next sections.

3.3.1.2 Substation One

The first substation is a 25 kV load-serving substation located in Alberta, Canada. The single-line diagram of the substation and feeders and the measurement points are shown in Figure 3.17.

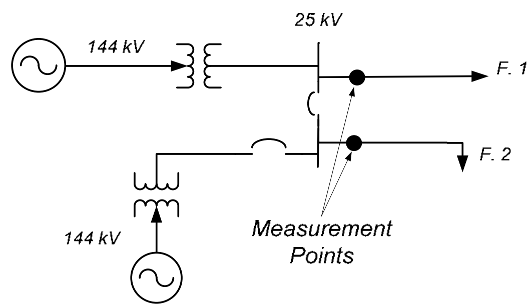

Figure 3.17. Single line diagram of Substation One

The measurements were taken from both feeders at Site One. The data were collected in a five-second data window in every minute for one hour. The three-phase waveforms for each feeder were transformed to the frequency domain for every cycle of the 60Hz system frequency. The impedances of the transformers connected to Feeders One and Two were 0.040+j1.435 ohms and 0.062+j1.809 ohms, respectively. The RMS of the voltage and current at Feeder One at this substation is plotted in Figure 3.18. Each plotted value is the average of the voltage or current during five seconds of measurements.

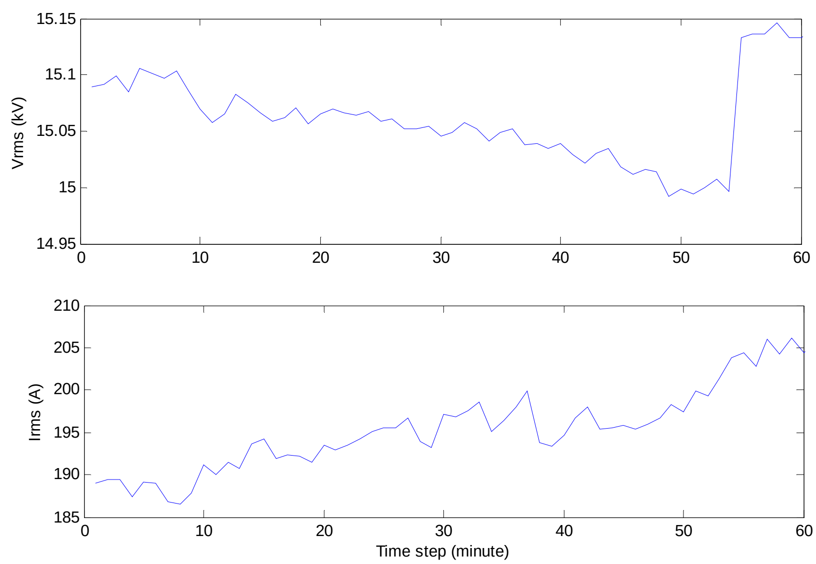

Figure 3.18. Voltage and current at Feeder One, Substation One

Figure 3.18 reveals that the voltage and current have some variations, which were used for estimating the system side harmonic impedance parameters. After applying the sequence transformation, for the current system, the magnitude of the harmonic voltages of the two feeders are plotted in Figure 3.19.

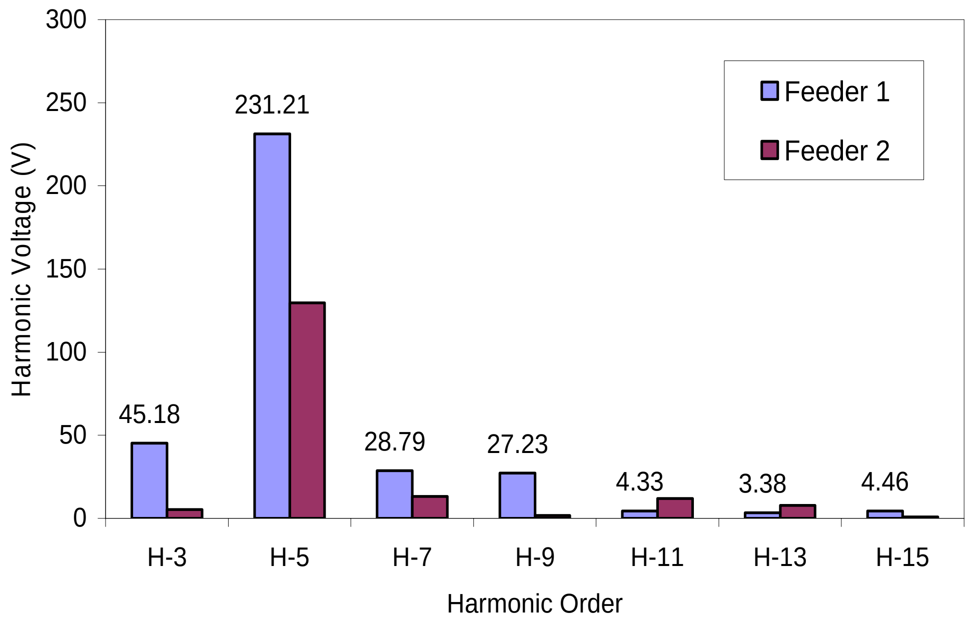

Figure 3.19. Harmonic voltages at two feeders in Substation One

As Figure 3.17 shows, the two feeders were supplied with two different transformers. Since the loads and the feeders' transformer impedance characteristics differed, the feeders' harmonic voltages also differed. Figure 3.19 reveals that the fifth harmonic is the largest harmonic component of the voltage at Feeder One at Substation One. The harmonic components of the currents for the two feeders are plotted in Figure 3.20.

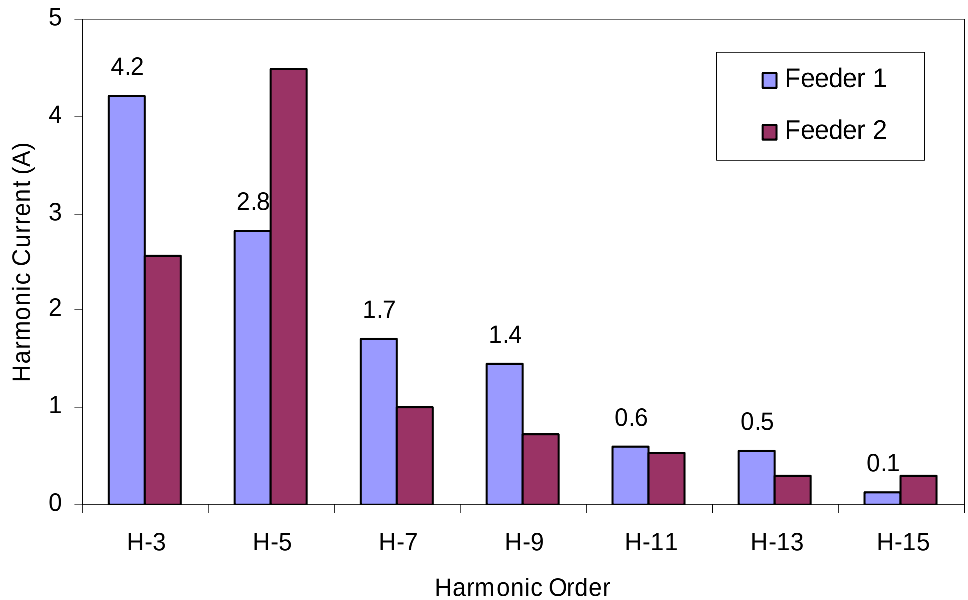

Figure 3.20. Harmonic currents at two feeders in Substation One

Figure 3.20 shows that the third and fifth harmonic currents are the largest components in the current spectrum in Substation One. After calculating the corresponding voltage and current for each harmonic, we can use the proposed algorithm to calculate the harmonic impedances of the system. The proposed algorithm uses the naturally occurring fluctuations of the loads connected to the system, at different harmonics, to calculate the system parameters. Therefore, we can define the fluctuation index, as defined in Chapter Two for the fundamental frequency. The fluctuation index will represent the level of the load fluctuations, and the higher this index, the more accurate the calculated parameters. The fluctuation index for the harmonics is defined as the summation of the absolute variation of P_h and Q_h, as stated in (3.4):

$$Fluctuation\ Index = \left(\left| \frac{P_{h1} - P_{h2}}{P_{h1}} \right| + \left| \frac{Q_{h1} - Q_{h2}}{Q_{h1}} \right| \right) \times 100, \tag{3.4}$$

where P_h and Q_h are the active and reactive powers of the harmonics and are defined in the same way as for the fundamental frequency. Since the data used for the algorithm had more than two sets of measurements, the fluctuation index is the minimum of the summation for the period of the measurements used for the impedance estimation. The fluctuation index, which is the mean value of the load fluctuation indices for the period of measurement (one hour), is plotted in Figure 3.21 for all the harmonics for the two feeders.

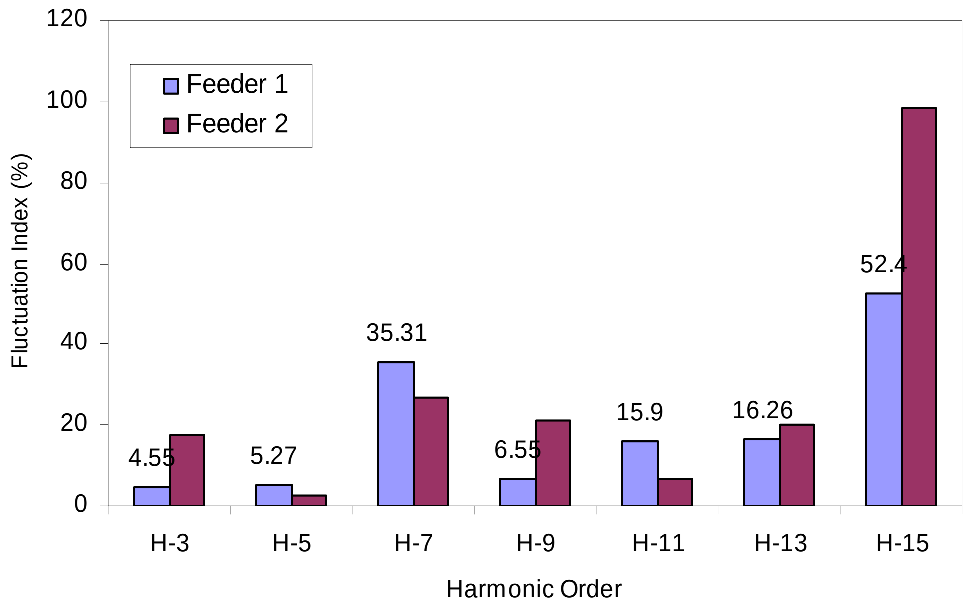

Figure 3.21. Fluctuation index for the feeders in Substation One

Figure 3.21 reveals that the fluctuation index increases as the harmonic order increases. The reason is the large variation of the higher-order harmonic voltages and currents, in percentages, compared to that of the lower harmonics. For harmonic impedance estimation, the minimum required fluctuation index was assumed to be one percent.

The harmonic impedances of the system were calculated for this substation by using the proposed algorithm. As an example, the variation of Feeder One's seventh harmonic voltages and currents, which appeared in positive sequence after the sequence transformation was applied, is plotted in Figure 3.22 for the period of one hour.

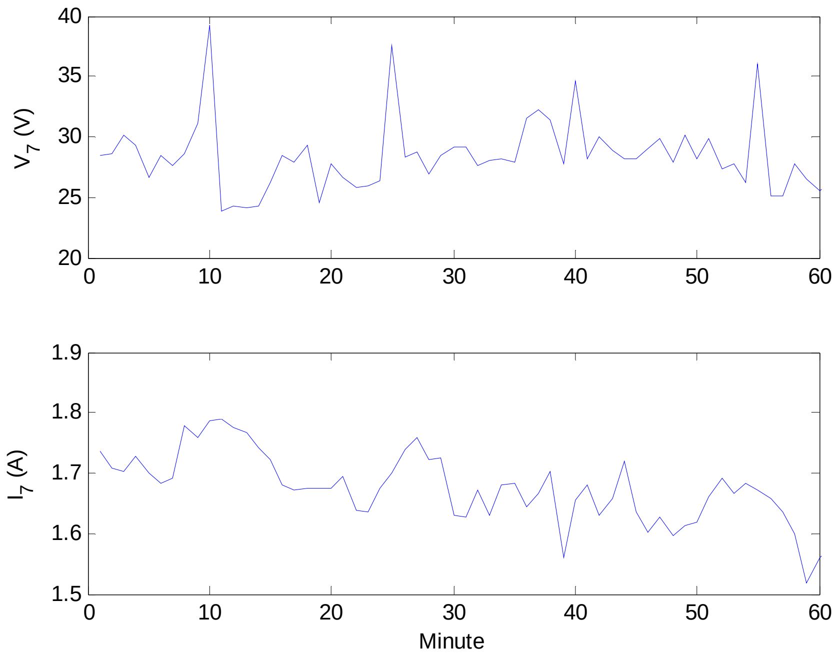

Figure 3.22. Variation of seventh harmonic voltage and current at Feeder One

The seventh harmonic impedance parameters were calculated by using the proposed method, and the results for the period of one hour are shown in Figure 3.23.

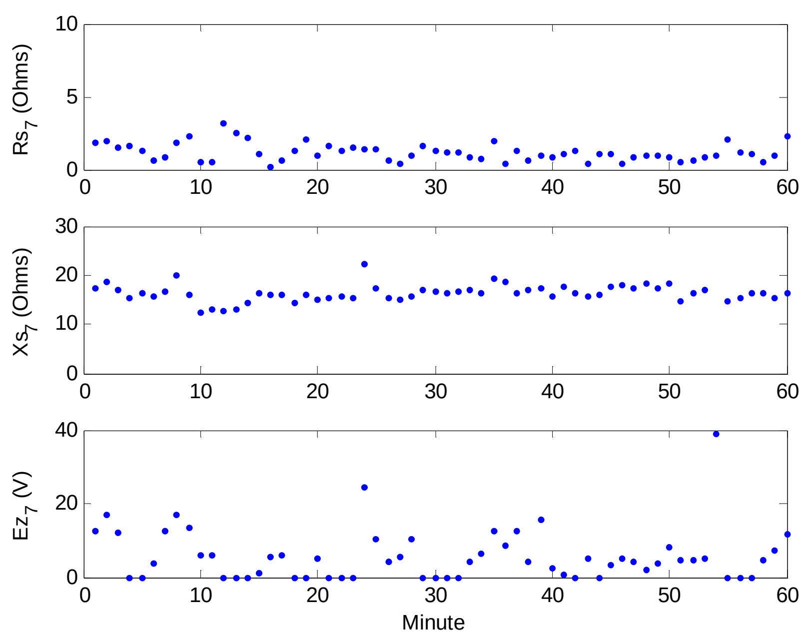

Figure 3.23. Seventh harmonic circuit parameters of Feeder One

Figure 3.23 reveals that in some cases, the calculated background voltage distortion for the seventh harmonic is zero, so that in these cases, no background voltage distortion occurs from the system side. In these periods, the loads connected to the feeder are responsible for all the voltage distortions occurring at the substation bus and associated with the seventh harmonic. The other loads connected to the transformer in the substation could be the reason for the non-zero background voltage of the seventh harmonic voltage.

The algorithm was applied to all the harmonic voltages and currents of the substation, and the average of the results for the period of one hour is presented in Figure 3.24.

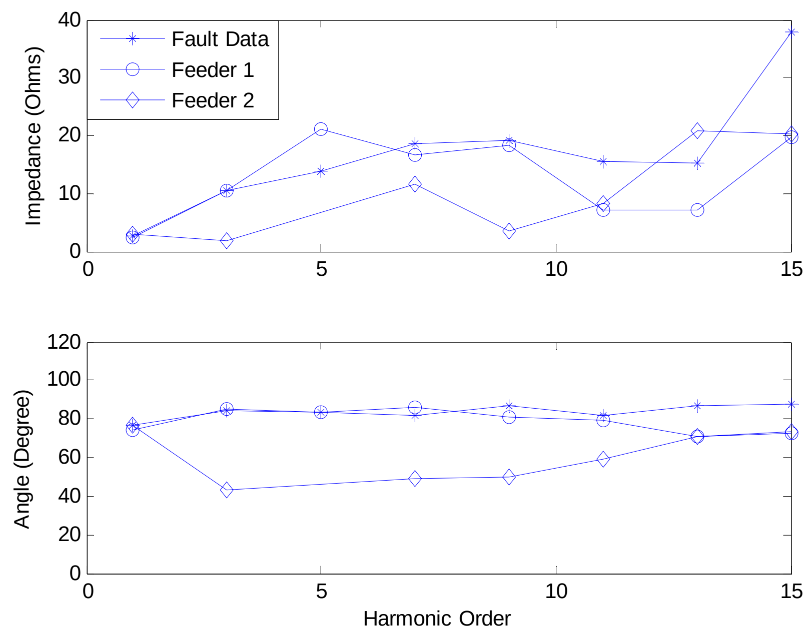

Figure 3.24. Harmonic impedances of two feeders in Substation One

Figure 3.24 also shows the harmonic impedances calculated by using the real fault data recorded by the PML meter at the substation. This figure reveals that the calculated harmonic impedances from the proposed method are comparable to those calculated from the recorded fault data. The second algorithm uses the pre- and post-disturbance voltage and currents to estimate the system harmonic impedances. The recorded fault voltage and current waveforms used for the harmonic impedance calculations at Substation One are plotted in Figure 3.25.

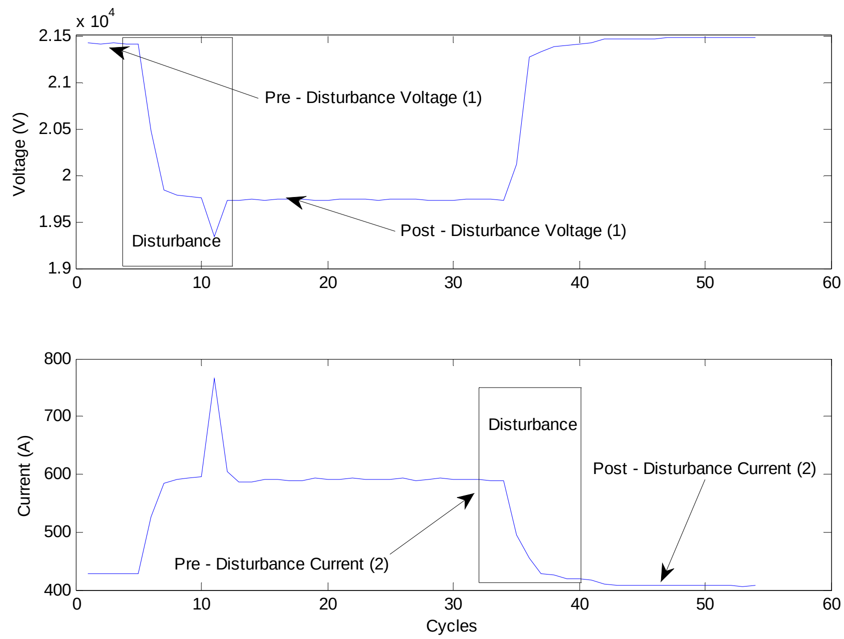

Figure 3.25. A sample recorded fault at feeder one in Substation One

The two disturbances in the recorded data window can both be used for harmonic impedance estimation. By using the pre- and post-disturbance values of the voltage and current for each harmonic and inserting them in (3.5), the power system harmonic impedances can be calculated:

$$Z_{Hs} = -\frac{V_{H\_pre} - V_{H\_post}}{I_{H\_pre} - I_{H\_post}}, \tag{3.5}$$

where Z_{Hs} is the system harmonic impedance, and V_H and I_H are the system's harmonic voltages and currents, respectively. The practical considerations and details of the algorithm can be found in [11].

The harmonic resistance of the system is plotted in Figure 3.26. The calculated harmonic impedances for the one-hour period were more than one hundred points. Therefore, we assumed a normal distribution function for each calculated parameter. The confidence interval of the harmonic resistance and inductances, using a 95% confidence level, is shown in the figures [71].

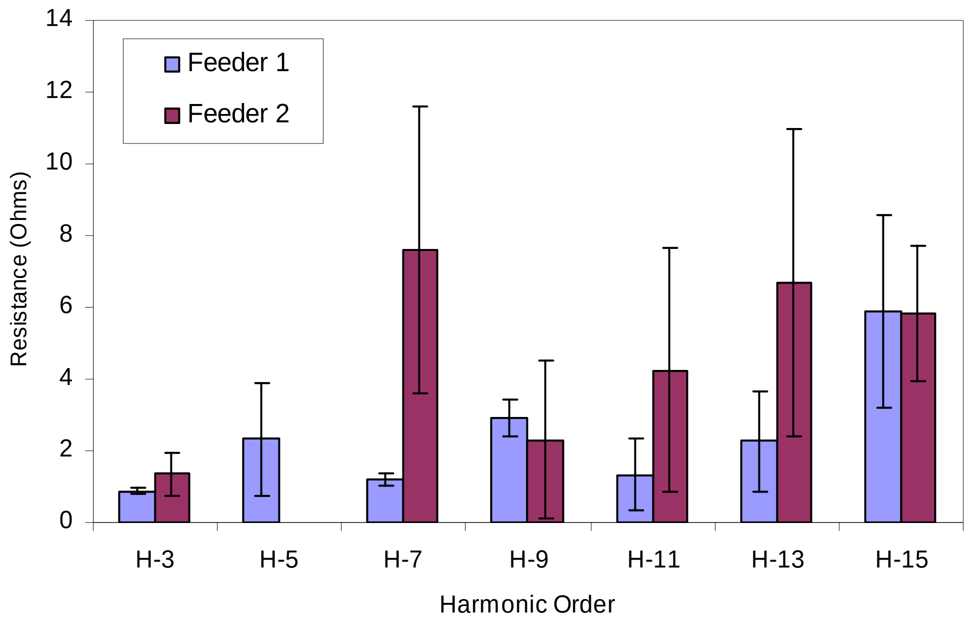

Figure 3.26. Harmonic resistances of two feeders in Substation One

The harmonic reactance of the system is plotted in Figure 3.27. The confidence interval of the calculated reactances is also shown in this figure.

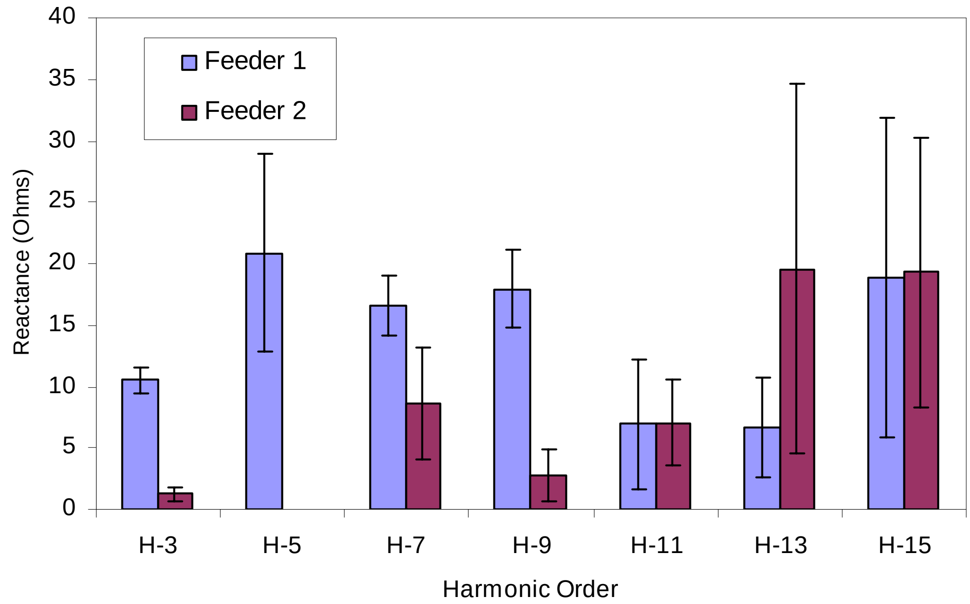

Figure 3.27. Harmonic reactances of two feeders in Substation One

Figures 3.26 and 3.27 reveal that for some harmonics, the confidence interval for the calculated system impedance is very large. In such cases, although the fluctuation index is high, the magnitude of the voltage and current is very low compared to the fundamental voltage and current, as shown in Figures 3.19 and 3.20. Therefore, the signal-to-noise ratio for these cases decreases, and this result will reduce the accuracy and, consequently, increase the confidence interval for the estimated parameters. For online monitoring, this effect will not be a problem because we have access to data at any time, and we can use data from different operating times that have smaller confidence intervals for the estimated parameters.

3.3.1.3 Substation Two

The second substation is also a 25 kV load-serving substation located in Alberta, Canada. The single-line diagram of the substation and feeders and the measurement points are shown in Figure 3.28.

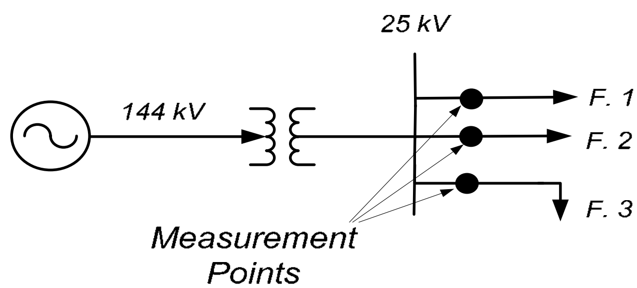

Figure 3.28. Single line diagram of Substation Two

The measurements were taken from all the feeders at Site Two. The data were collected as a five-second data window in every minute for one hour. The three-phase waveforms for each feeder were transformed to the frequency domain for every cycle of the 60Hz system frequency. The impedance of the transformers connected to the feeders was 0.066+j1.777 ohms. The RMS of the voltage and current at Feeder One in this substation is plotted in Figure 3.29. Each plotted value is the average of the voltage or current during five seconds of measurements.

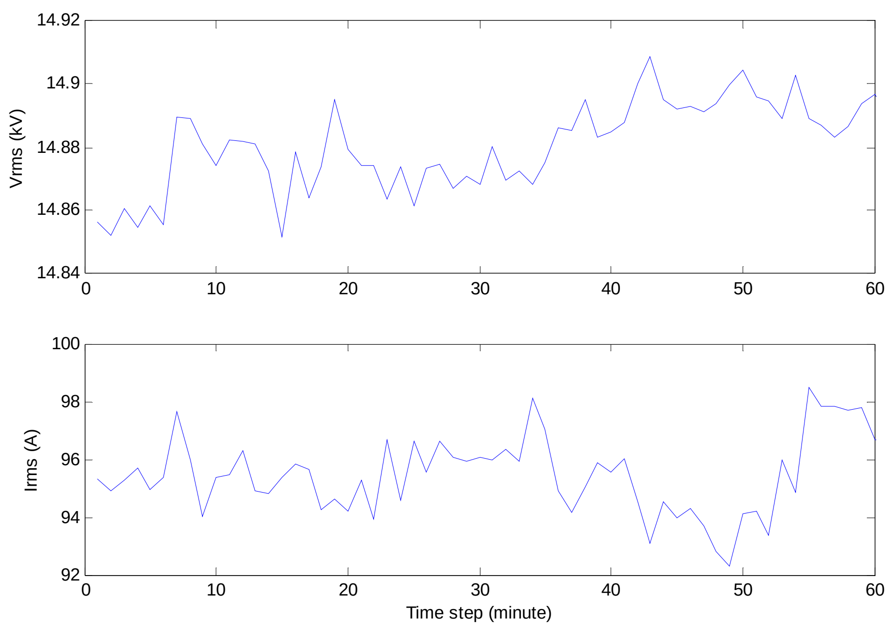

Figure 3.29. Variation of voltage and current at Feeder One in Substation Two

Figure 3.29 reveals that the voltage and current at this feeder at Substation Two also have large variations and are not constant for the measurement period. After applying the sequence transformation, for the current system, the magnitude of the harmonic voltages and currents of the three feeders was plotted in Figure 3.30.

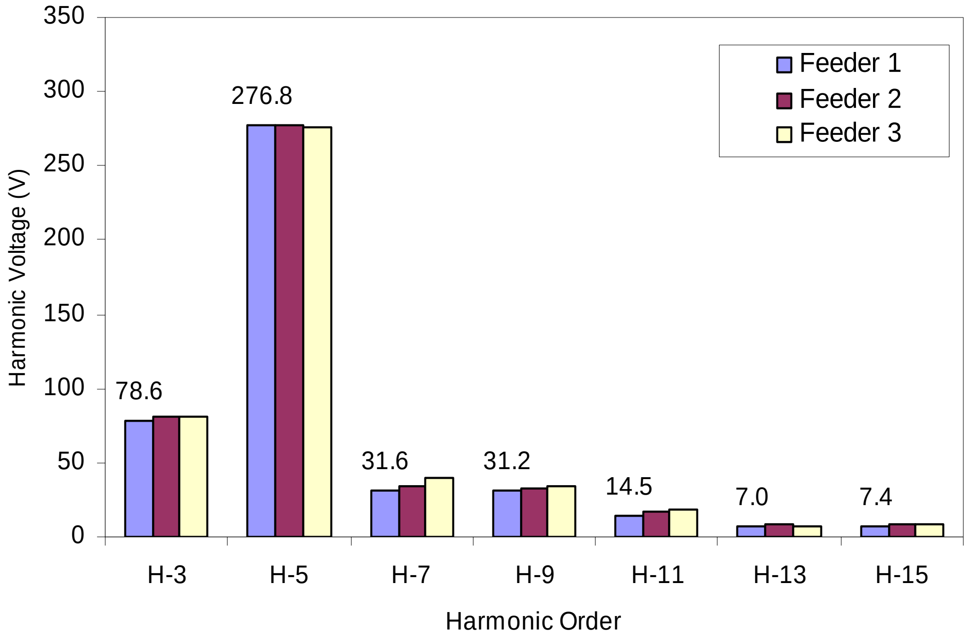

Figure 3.30. Harmonic voltages at three feeders in Substation Two

As Figure 3.28 reveals, all three feeders were supplied with the same transformer. Therefore, their fundamental and harmonic voltages should be the same as shown in Figure 3.30. The harmonic components of the currents for the three feeders are plotted in Figure 3.31.

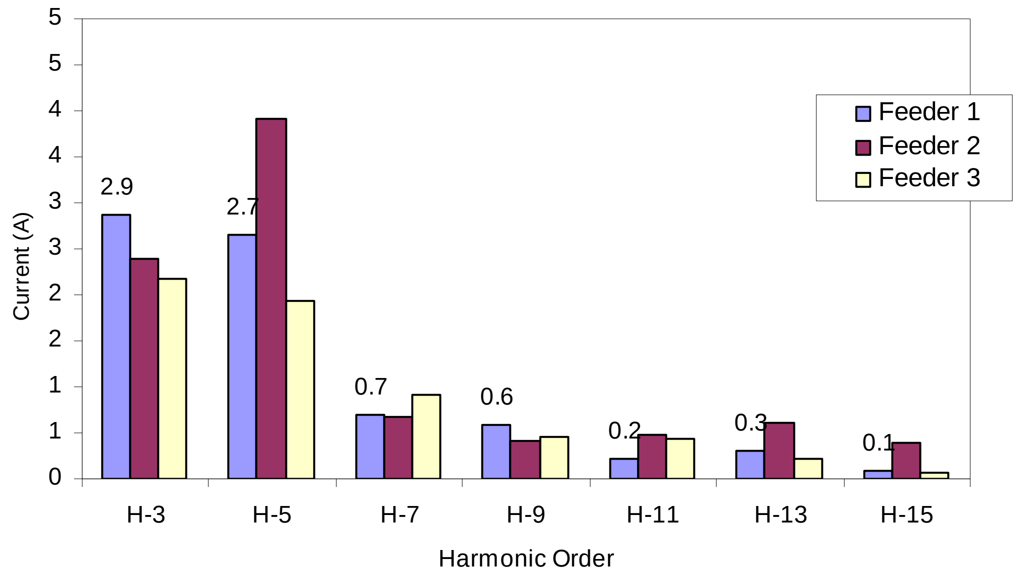

Figure 3.31. Harmonic currents at three feeders in Substation Two

Figure 3.31 shows that for this substation as well, the third and fifth harmonic currents are the largest component in the current spectrum. The fluctuation index for the feeders at Substation Two was also calculated by using (3.4), and the results are plotted in Figure 3.32.

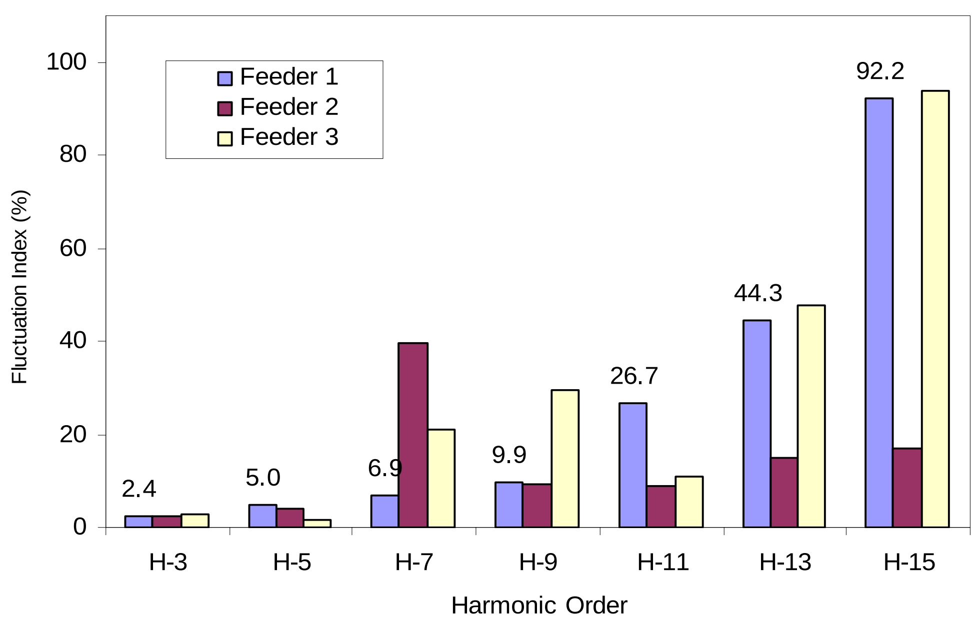

Figure 3.32. Fluctuation index for the feeders in Substation Two

Figure 3.32 reveals that the index differs for different feeders and harmonics. The system's calculated harmonic impedances for all three feeders are plotted in Figure 3.33 and compared with the calculated results from the real fault data.

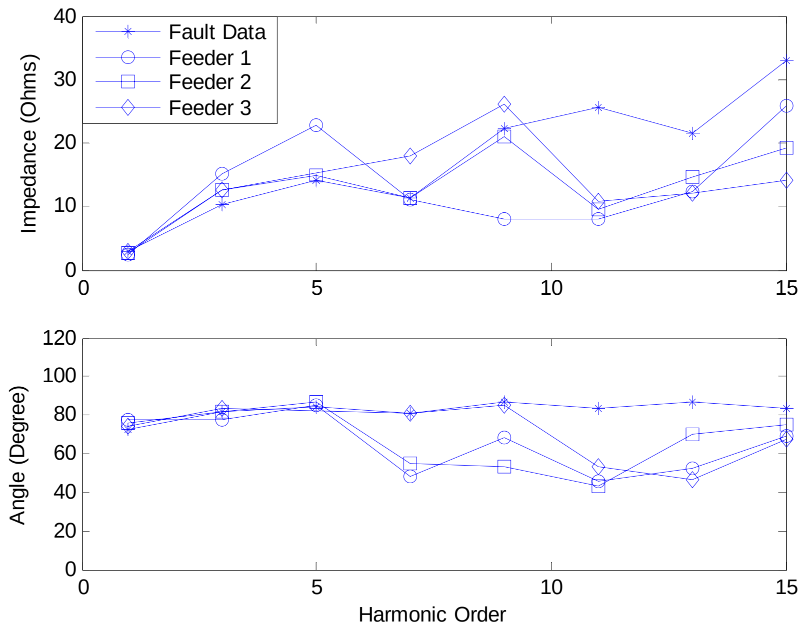

Figure 3.33. Harmonic impedances of three feeders in Substation Two

As Figure 3.33 reveals, the harmonic impedances calculated for this substation are also comparable to those calculated by using the real fault data. The system's harmonic resistance for this substation is also plotted in Figure 3.34. Here again, the calculated harmonic impedances for the one-hour period were more than one hundred points and we assumed a normal distribution function for each calculated parameter. The confidence interval of the harmonic resistance and inductances, using a 95% confidence level, are shown in the figures.

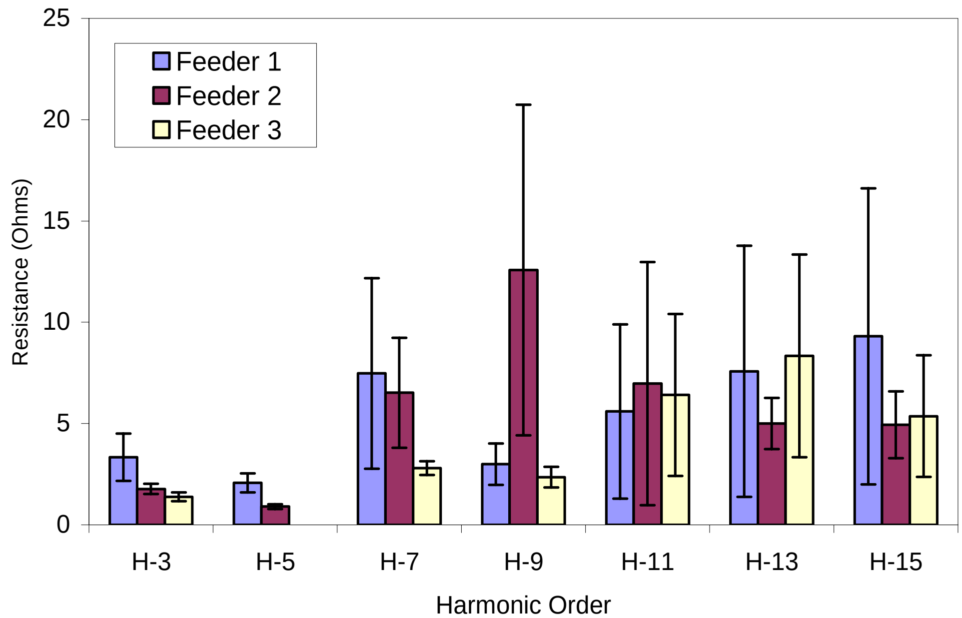

Figure 3.34. Harmonic impedances of two feeders in Substation One

The harmonic reactance of the system is plotted in Figure 3.35. The confidence interval of the calculated reactances is also shown in this figure.

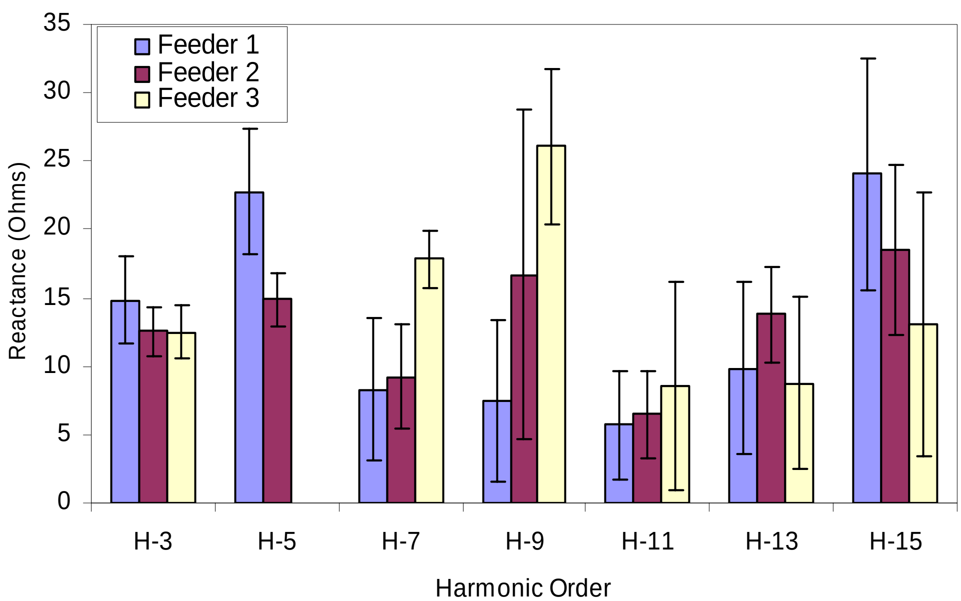

Figure 3.35. Harmonic impedances of two feeders in Substation One

If the waveforms are available continuously, the calculated parameters will be available continuously, and by using the two indices, the fluctuation, and the confidence interval, we can track the system harmonic impedances. If the loads connected to the feeder generate more distortions and inject more harmonics into the system, calculating the system harmonic impedances by using the proposed method will be easier and more accurate.

3.3.2 Zero Sequence Impedance Measurement

This section presents the zero sequence impedance measurement method and the field test verification results.

3.3.2.1 The Proposed Algorithm

The equivalent for the zero sequence circuit is the same as that for the positive sequence circuit. The only difference is that the equivalent voltage of the Thevenin circuit for the zero sequence might be zero. This voltage will not affect the calculation procedure because in this case, the estimated value for the voltage source will be zero.

The algorithm and its implementation issues are explained in Chapter Two; therefore, in this chapter the final algorithm for zero sequence impedance estimation is presented. Considering the basic algorithm and implementation issues explained in Chapter Two, in this section we propose the final algorithm for calculating power system zero sequence impedance parameters. The following steps should be taken:

- Capture the system's three-phase voltages and currents in a continuous waveform format by using a 256 sample per cycle data-acquisition system (the sampling rate could be less since the frequency of the zero sequence voltages and currents is 60 Hz),
- Convert the voltages and currents of each cycle of the 60-Hz waveforms, for each phase, to the frequency domain by using Fourier transformation,
- Assuming that the system impedance matrix is balanced, convert the system's three-phase voltage and current phasors to positive, negative and zero sequences for each cycle of the fundamental frequency,
- While considering the implementation issues, apply the multi-point algorithm to the system's zero sequence voltages and currents to calculate the zero sequence impedance

parameters.

The algorithm was applied to real field data, and the results are presented in the next sections.

3.3.2.2 Substation One

The first substation is a 25 kV load-serving substation located in Alberta, Canada. The single-line diagram of the substation and feeders and the measurement points are shown in Figure 3.36.

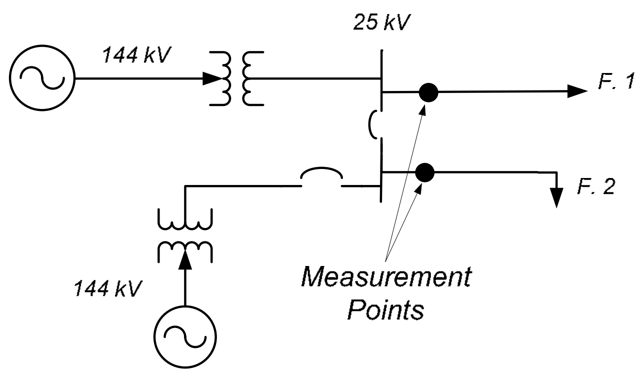

Figure 3.36. Single-line diagram of Substation One

The variation of the zero sequence voltage and current for Feeder One at Substation One is shown in Figure 3.37.

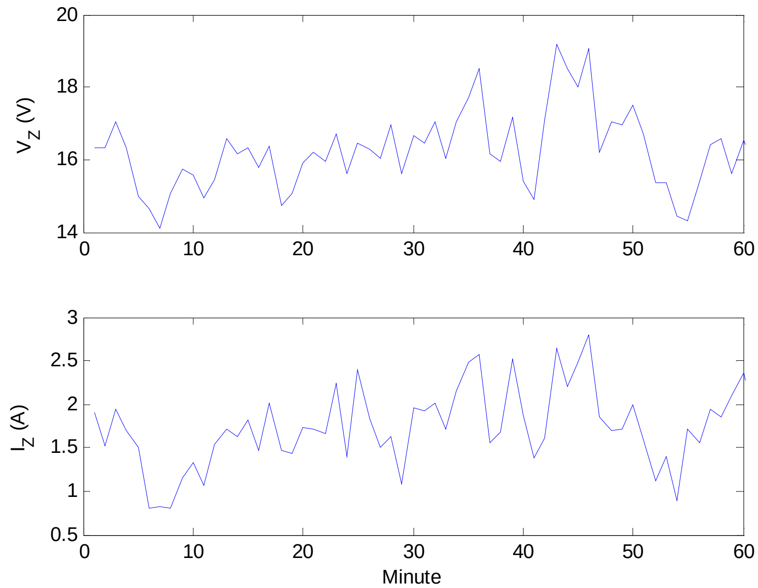

Figure 3.37. Zero sequence voltage and current at Feeder One, Substation One

After calculating the corresponding voltage and current for the zero sequence circuit, we can use the proposed algorithm to calculate the zero sequence impedances of the system. The proposed algorithm uses the naturally occurring fluctuations of the loads connected to the system to calculate its zero sequence impedance parameters. Therefore, we can define the fluctuation index as it was defined in Chapter Two for the fundamental frequency. The fluctuation index will represent the level of load fluctuations appearing in the zero sequence components of the voltages and currents, and the higher this index, the more accurate the calculated parameters. The fluctuation index for the zero sequence parameters is defined as the summation of the absolute variation of P_z and Q_z, as stated in (3.6).

$$\mathit{Fluctuation\ Index} = \left(\left| \frac{P_{z1} - P_{z2}}{P_{z1}} \right| + \left| \frac{Q_{z1} - Q_{z2}}{Q_{z1}} \right| \right) \times 100\,, \tag{3.6}$$

where P_z and Q_z are the active and reactive powers for the zero sequence components and are defined in the same way as they were defined for the fundamental frequency:

$$\begin{aligned} P_z &= V_{xz} \times I_z \\ Q_z &= V_{yz} \times I_z \end{aligned}, \tag{3.7}$$

where V_{xz} and V_{yz} are the x and y components of the voltage, respectively, when the angle of I_z is zero. Since the data used for the algorithm had more than two sets of measurements, the fluctuation index is the minimum of the summation for the period of the measurements used for impedance estimation. The average fluctuation index, which is the mean value of the load fluctuation indices for the one-hour period of measurement, for Feeders One and Two, is %4.38 and %7.13, respectively. The proposed algorithm was used to calculate the system's zero sequence impedance parameters. The calculated zero sequence impedance parameters for Feeder One are plotted in Figure 3.38. In this figure, each plotted value is the raw average of the calculated parameters for the period of five-second data window.

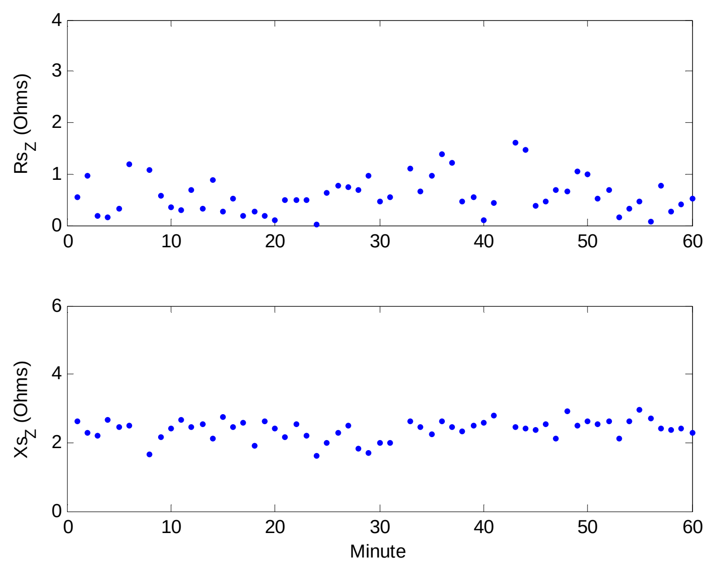

Figure 3.38. Zero sequence circuit parameters of Feeder One, Substation One

The zero sequence impedance parameters seen from Feeder Two were also calculated. The mean value of the calculated impedance parameters for the one-hour measurement period for Feeders One and Two are 0.341+j2.181 and 0.386+j2.152, respectively. Since the transformer type and loading conditions for the two feeders were similar, the system's zero sequence impedance can be considered as the average of the calculated parameters for the two feeders. The calculated parameters are compared in Table 3.2 with the zero sequence impedance data calculated by using different methods. The other methods involved using the real fault data recorded by the PML meters at the substation, and the data from the PSS/E circuit program.

Since the measurement data which resulted in a calculated zero sequence impedance parameter were more than 100 points, we assumed a normal distribution function for the distribution of each calculated parameter. Using a 95% confidence level for each calculated parameter, the confidence interval for the zero sequence impedance parameters are calculated. The results are presented in Table 3.2.

Table 3.2. Zero sequence impedance data for Substation One

Feeder	The Calculated Resistance	The Calculated Inductance	F. index (%)	Real Fault Data	PSS/E Data
# 1	0.341 ± 0.312	$j2.181 \pm 0.467$	4.38	0.211+j2.043	0.10+j1.441
# 2	0.386 ± 0.209	$j2.152 \pm 0.513$	7.13		

Table 3.2 shows that the results calculated by using the proposed algorithm are comparable with the results calculated by using the other methods. The slight difference could be the result of measurement error or transients in the system. Since the data are available continuously, the average of the calculated set of values with smaller confidence intervals could be selected as the final values.

3.3.2.3 Substation Two

The second substation is also a 25 kV load-serving substation located in Alberta, Canada. The single-line diagram of the substation and feeders and the measurement points are shown in Figure 3.39.

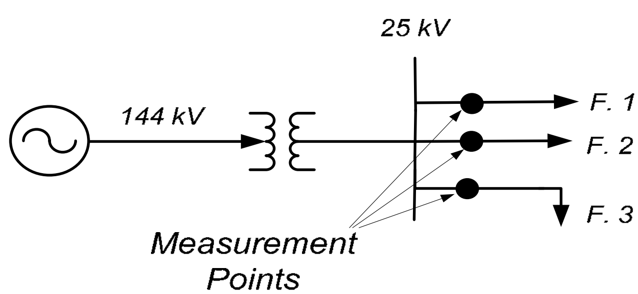

Figure 3.39. Single-line diagram of Substation Two

The zero sequence impedance parameters were calculated for Substation Two as well. The variation of the zero sequence voltages and currents for Feeder One at Substation Two is shown in Figure 3.40. This feeder's zero sequence voltage and current are larger compared to those for Feeder One at Substation One. This difference could be the result of having a different transformer or grounding conditions or different kind of loads in the two substations.

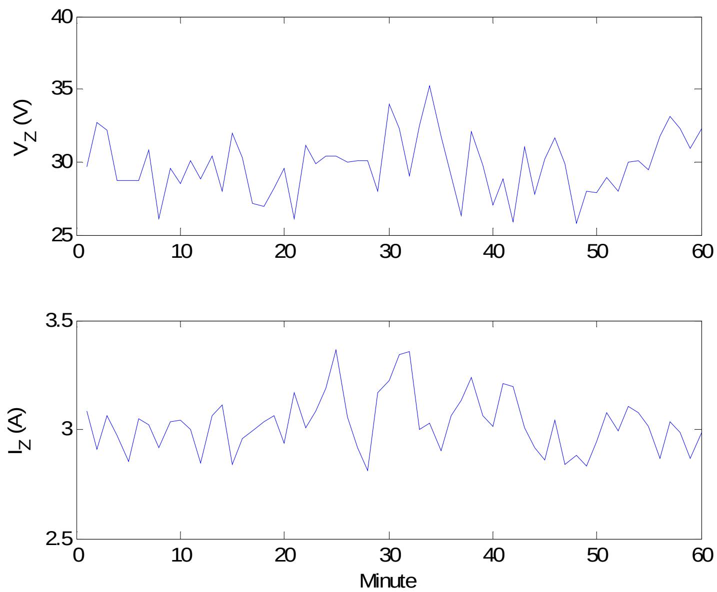

Figure 3.40. Zero sequence voltage and current at Feeder One, Substation Two

The voltage and current data at substation two were recorded for all three feeders. The average fluctuation index for the zero sequence voltages and currents in the three feeders during this period is %9.14, %12.32 and %14.1. The proposed algorithm was applied for estimating the zero sequence impedance parameters of the three feeders. The calculated zero sequence impedance parameters for Feeder One are plotted in Figure 3.41. In this figure, each plotted value is the raw average of the calculated parameters for the period of the five-second data window.

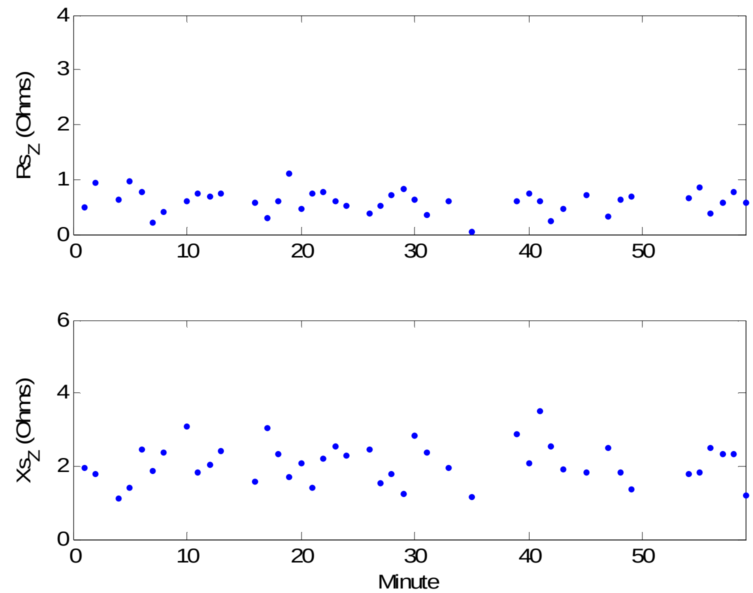

Figure 3.41. Zero sequence circuit parameters of Feeder One, Substation Two

The feeder's average zero sequence impedance for the period of one hour is 0.491+j2.625, 0.640+j3.271 and 0.514+j2.898. For this substation, because there is only one transformer and the feeders have almost the same kind of loads, the equivalent zero sequence impedance could be considered as the average of the three feeders.

The average zero sequence impedance for Substation Two is compared in Table 3.3 with the zero sequence impedance data calculated by using different methods. For this substation also, since the measurement data which result in a calculated zero sequence impedance parameter were more than one hundred points, we assumed a normal distribution function for the distribution of each calculated parameter. Using a 95% confidence level for each calculated parameter, the confidence interval for the zero sequence impedance parameters are calculated. The results are presented in Table 3.3.

Table 3.3. Zero sequence impedance data for Substation Two

Feeder	The Calculated Resistance	The Calculated Inductance	F. index (%)	Real Fault Data	PSS/E Data
# 1	0.491 ± 0.330	$j2.625 \pm 0.835$	9.14	0.290+j2.8967	0.3436+j3.002
# 2	0.640 ± 0.287	$j3.271 \pm 0.712$	12.32		
# 3	0.514 ± 0.261	$j2.898 \pm 0.613$	14.10		

Given the results shown in Tables 3.2 and 3.3, the proposed method could be applied to the zero sequence voltages and currents to calculate the zero sequence impedances of the power system. This impedance, combined with the positive sequence impedance calculated in Chapter Two, can be used for the online measurement of different kinds of substation fault levels.

3.4 Conclusion

In this chapter, some sensitivity studies are presented which were done to finalize the impedance measurement algorithm. The studies were done for twenty seven feeders in eight different substations and are related to some practical issues such as the disturbance side determination, the number of points used for the multi-point algorithm, and the fluctuation index criteria. Through these studies, the proposed algorithm was improved and finalized. Furthermore, by extending the impedance measurement technique, an algorithm was proposed for the online tracking of power system harmonic and zero sequence impedance parameters. The main contributions of this research to the field are the new proposed algorithm that can be used for online measurements, the consideration of practical issues, and the verifications through several field tests. Our studies show that a three-second to five-second data window with sufficient variations is enough for the estimation of harmonic and zero sequence impedance parameters. The 256 sample per cycle rate of the data-acquisition system is sufficient for the data collection process, depending on the maximum frequency of the required harmonic impedance. The algorithm does not depend on the load model and works with the natural variations of any kind of loads and synchronized measurements are not required for calculations.

The required information can be obtained from the meters that are already installed at the substation buses. The proposed algorithm was verified by using several field measurements. The verification results show that the proposed method is capable for the online monitoring of power system harmonic and zero sequence impedance parameters.

Chapter 4

Online Measurement of the Load Model Parameters

Load model parameters have become critical information for the accurate analysis of power systems. In particular, voltage stability limits derived from simulations may be highly influenced by the load models used in both static and dynamic analysis. This chapter proposes a newly developed algorithm for the online measurement and monitoring of power system load model parameters. For this purpose, the existing load modeling algorithms in the literature are reviewed, the load parameter measurement problem is formulated, and solution algorithms are proposed. An algorithm is proposed to detect the tap movement by using the step change in the voltage waveform. Some sensitivity studies were done to investigate the characteristics of the tap movements. The proposed tap change detection and load modeling algorithms were applied to several field measurements from different substations.

4.1 Introduction

The loads in power systems play an important role in power system planning, control and stability analysis [31], [72]-[80]. Having reliable models of the loads is essential for the purpose of power system simulation studies, designing automatic control systems and optimizing their configuration [34]. This chapter describes the development of a useful practical technique to measure and track the load model parameters at load-serving substations. According to electric circuit theories, a disturbance coming from the upstream side can be used to estimate the parameters in the downstream side, namely the load parameters. Since the algorithm should be capable of online monitoring, a disturbance which has a high frequency of occurrence and also is large enough is required for the estimation procedure. The natural disturbances in the system are usually very small in terms of magnitude, and their source, either from the system or the load side, is not easily determined; therefore, they are not appropriate for the online measurement of load parameters. One of the disturbances in power systems which is large enough and has a high chance of occurrence is the operation of the Under Load Tap Changer (ULTC) of the substation transformers, which was chosen in this research to estimate the load parameters.

To accomplish this project, the characteristics of the tap movements occurring at the secondary of the transformers in the substations were investigated. For this purpose, an algorithm was developed to detect the tap change and record the corresponding three-phase voltages and currents by using the Labview program. The data-acquisition systems were installed in four different substations across Edmonton and captured all the tap movements occurring, at 14 different transformers supplying different types of load feeders, for a period of one week. Based on our experiences, tap movement has a high chance of occurring and can happen in any loading condition and at any time during the day, seven days a week. This fact is very important and enabled us to use the tap changes to monitor the load at any required time during the week.

Our study shows that tap movement creates a system side voltage step change with sufficient magnitude for load parameters estimations. This step change in voltage creates similar disturbances in the corresponding active power and reactive power consumed by the loads and the load response to this step change in the voltage can be used for determining load behavior and estimating the load model parameters. The main focus of this chapter is to calculate the static and transient load model parameters by using the exponential load model. A set of estimation algorithms was developed accordingly. This chapter further presents the implementation of the proposed method and its field experiences.

4.2 Review of the Existing Load Modeling Algorithms

Obtaining detailed and accurate models of power system loads can be a more complicated task than modeling other power system components, such as synchronous machines. The problem can be summarized as follows [31], [81]:

- Loads are time-variant and stochastic, and their composition changes with the time of day and week, the seasons, the weather, and over time.
- There are many diverse load components.
- New load compositions are added to the system.
- Precise information about the composition and mix of loads is not usually available.
- Load models must be verified with actual measurements of the dynamic response.
- The ownership and location of load devices in customer facilities are not directly accessible to the electric utility.
- The characteristics of many load components, particularly for large voltage or frequency variations, are uncertain.

Accurate load modeling has been a challenging problem for power system engineers for decades. Over the past 30 years, two types of methods have been proposed, which are presented in the following sections.

4.2.1 Component-Based Approaches

The component-based approaches use information about the load composition, such as the NAICS codes and associated computer models, to compute the parameters [82]-[85]. Power system load aggregation can be performed analytically by lumping together similar loads based on the load type [31], [35], and using predetermined values for each parameter of the load. This approach is theoretically sound but has a number of implementation problems. For example, how do we classify the loads into different types that have similar voltage-dependent characteristics? What are the valid models for different load types and at different times and seasons? The component-based approach has also the disadvantage of requiring an extensive survey to collect load composition information; however, after deregulation, transmission-system planners may not be able to access such information. As well, making an accurate mathematical model is difficult for the following reasons [86]:

- Errors always exist in the nominal values given by the manufacturer.
- Simplifications and assumptions will certainly introduce errors.
- The load's characteristics that are ignored for some applications may be important for other applications.

Therefore, the component-based approaches are not suitable for the online monitoring of load model parameters.

4.2.2 Measurement-Based Approaches

The difficulties of the component-based approaches have led to the development of the second type of method in recent years – direct measurement of the load parameters [87]-[97]. To be successful, however, this method has to rely on voltage disturbances. Since many intentional voltage disturbances cannot be created due to power quality concerns and costs, the direct measurement method can be performed only under special arrangements. This constraint has made the method expensive to use and has limited its application to spot-checking the characteristics of certain load. Some attempts have been made to use naturally occurring voltage disturbances to measure the load characteristics. For example, [76], [86], [88] showed how to estimate load parameters by using captured voltage disturbances. However, these papers never addressed the problem of how often such disturbances occur and how representative they are. In fact, the disturbances collected and reported by these papers are few in number and irregular in occurrence. As a result, the estimated load parameters cannot represent the load behavior at different times and seasons. This lack of representativeness has severely limited the use of such methods.

One type of voltage disturbance that occurs frequently, is the disturbance caused by the operation of the Under Load Tap Changer (ULTC) transformers. Reference [87] performed extensive load tests on the BC Hydro system and found that the load responses due to the ULTC disturbances were sufficient to capture the voltage-dependent load characteristics. However, the ULTC disturbances were created intentionally in that work so its results also suffer from a lack of representativeness.

Based on the above experiences, this chapter proposes a method that can measure voltage-dependent load parameters at any given day and on demand. This method uses the natural tap movements as the source of voltage disturbances. Although the concept is simple, whether the natural tap movements can indeed yield disturbances with sufficient magnitude and frequency that can be used to determine the load parameters adequately and continuously must be verified. Through extensive field measurements on 14 transformers serving various loads, the above issue was settled. The results show that the disturbances caused by natural tap movement are quite suitable for load parameter estimation.

4.3 Algorithms for Load Parameter Estimations

This section explains the load response characteristics and the basic form of the proposed algorithms for load parameter estimation. Several experiments were done to investigate the effect of magnitude of voltage disturbance on the calculated load model parameters and some sensitivity studies are performed in order to finalize the algorithm. In this study, the step changes in the voltage caused by the operation of ULTCs were used for load parameter estimations. During our field experiences, the time required for tap movement was usually a few cycles, with the probability of a disturbance occurring on both the system and load side simultaneously being very low. Through extensive field measurements and experiments it is shown that the voltage step change created by operation of ULTCs is sufficient for online monitoring of load model parameters.

4.3.1 Load Response Characteristics

In a power transmission system, load refers to the collective power demand of the various electricity users served by a feeder or by a substation. The voltage-dependent load characteristics, also called (voltage-dependent) load models, denote the real and reactive power demands of the loads as affected by their supply voltage. This chapter's main focus is to investigate the voltage dependency characteristics of the loads in transient and steady-state conditions. Once we have the load model parameters for one specific model (the exponential model), we can estimate the parameters for different static load models such as the ZIP model [82].

When a step voltage change such as a tap movement is applied to the load, it generally has a response very close to that shown in Figure. 4.1.

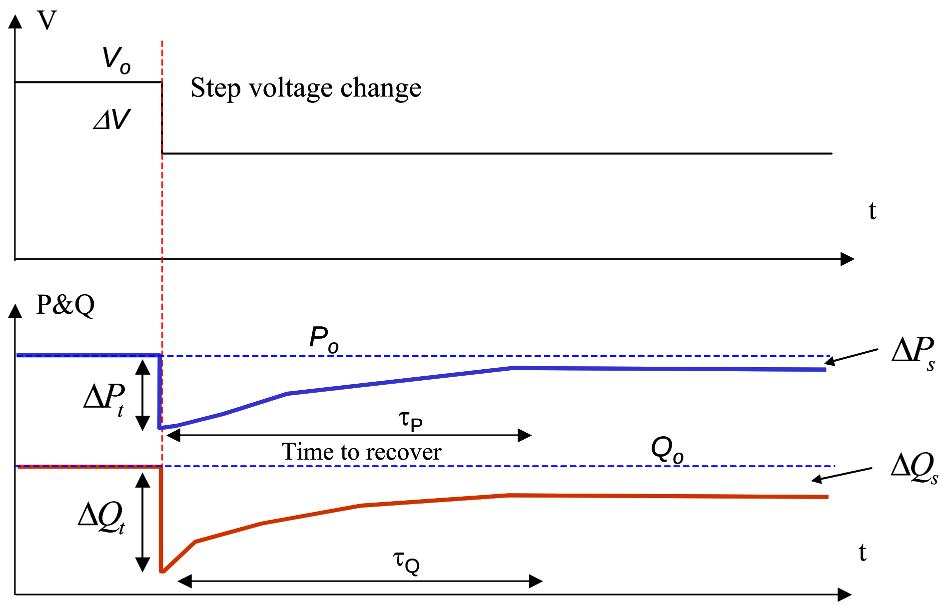

Figure 4.1. The general load response characteristics

The responses can be characterized using the following six variables:

- Transient load responses ΔP_t and ΔQ_t: They represent how the load's power demand will change immediately when a voltage change is applied.
- Steady-state load responses ΔP_s and ΔQ_s: They represent how the load's power demand will change eventually after it's response to step voltage change has reached the steady-state.
- Time to recover τ_p and τ_q: They represent how long it will take for the load to reach a new steady-state.

Extensive research work has shown that these variables are related to the voltage and the pre-disturbance power demand according to the following equations:

$$P_s = P_0 \left(\frac{V}{V_0} \right)^a ,$$
$$P_t = P_0 \left(\frac{V}{V_0} \right)^\alpha , \tag{4.1}$$
$$P(t) = (P_0 - \Delta P_s) + (\Delta P_s - \Delta P_t) e^{-\frac{t}{\tau_P}} .$$

The above equations (similar for Q) assume that the load demand recovers from its transient values to its steady-state values in an exponential function, which is an acceptable approximation of the actual situation. Once the above six load parameters are determined, a dynamic load model can be established. A variety of equations have been proposed for the dynamic load model. No matter what equations are used, these six load parameters contain the most important information of the loads and this thesis proposes algorithms to measure and monitor them in a continuous format.

4.3.2 Estimation of Load Model Parameters

The static model's parameters are the exponents "*a*" and "*b*". With these exponents equal to 0, 1, or 2, the model represents the constant power, constant current or constant impedance characteristics, respectively. For composite loads, their values depend on the aggregate characteristics of the load components. The exponent "*a*" (or "*b*") is nearly equal to the slope $\Delta P/\Delta V$ or ($\Delta Q/\Delta V$) at $V = V_0$, and if $V \neq V_0$, the exponents can be calculated from (4.2) by assuming P_0 and V_0 as the initial values or the pre-disturbance active power and voltage, and assuming P and V as the post-disturbance values.

$$a = \log(\frac{P}{P_0}) \Big/ \log(\frac{V}{V_0}) . \tag{4.2}$$

The same procedure can be used to calculate "*b*", α and β. For composite system loads, the exponent "*a*" usually ranges between 0.5 and 1.8, and the exponent "*b*" is typically between 1.5 and 6. A significant characteristic of the exponent "*b*" is that it varies as a nonlinear function of the voltage. This variation is caused by magnetic saturation in the distribution transformers and motors. At higher voltages, Q tends to be significantly higher [79].

As shown in Section 4.3, the average tap movement for different transformers is around one percent. This one-percent step change in the voltage creates a step change in the corresponding active and reactive power. For instance, the active and reactive power step changes, caused by the operation of the ULTC, for two different step-up and –down tap movements are plotted in Figure 4.2.

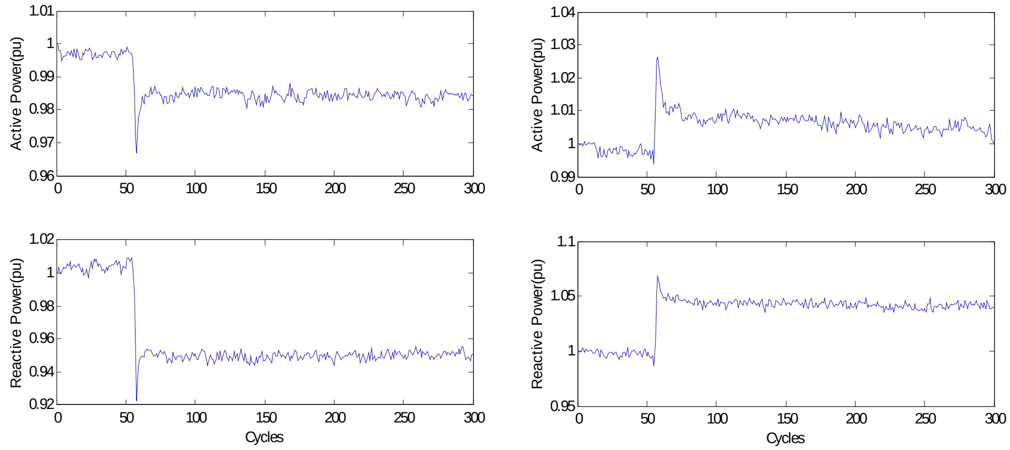

Figure 4.2. Two sample tap movement active and reactive power transients

Figure 4.2 shows that the transient in the active and reactive power for these cases, and also for almost all the tap movements of the transformers, dies out in at most one second.

In order to calculate the load model parameters, we need the steady state and transient active and reactive power and the corresponding voltage. The first step in calculating the load model parameters is to detect the starting point, or the exact occurrence time of the step change. Since an entire tap change occurs in around 5 cycles, a moving window can be used for detecting it.

If the calculated DV is greater than 0.5, then "t" can be considered as the starting point of the tap movement (Tap_{sp}). DV is calculated from the following equation:

$$DV = \left| \frac{V(t) - V(t+5)}{V(t)} \right| \times 100\,. \tag{4.3}$$

The vector V is constructed out of the 60-Hz component of the voltage of phase "A" for each cycle of the waveform.

After detecting the tap movement instant, the procedure explained below is applied to calculate the load model parameters:

1. Calculation of the pre-tap values as the average of the five cycles before starting the tap movement:

$$V_0 = \sum_{t=Tap_{sp}-5}^{Tap_{sp}-1} \frac{V(t)}{5},$$
$$P_0 = \sum_{t=Tap_{sp}-5}^{Tap_{sp}-1} \frac{P(t)}{5}, \tag{4.4}$$
$$Q_0 = \sum_{t=Tap_{sp}-5}^{Tap_{sp}-1} \frac{Q(t)}{5}.$$

The vectors *V, P* and *Q* are the positive sequence voltage and active and reactive power associated with the 60-Hz component of the waveforms. The reason to average the five-cycle window is because we assume the load side parameters do not have a significant change during the five cycle period which is a valid assumption. This fact was verified by different tap movements' data and the results are shown in section 4.3.4.

2. Calculation of steady-state post-tap values as the average of five cycles and 60 cycles after starting the tap movement since the transient will die out in at most one second (60 cycles):

$$V_s = \sum_{t=Tap_{sp}+60}^{Tap_{sp}+64} \frac{V(t)}{5},$$
$$P_s = \sum_{t=Tap_{sp}+60}^{Tap_{sp}+64} \frac{P(t)}{5}, \tag{4.5}$$
$$Q_s = \sum_{t=Tap_{sp}+60}^{Tap_{sp}+64} \frac{Q(t)}{5}.$$

Having the pre- and post-tap values for voltage, real and reactive power, the load parameters, *"a"* and *"b"* can be calculated from (4.1).

3. Calculation of transient post-tap values, P_t and Q_t as they are the peak of real and

reactive power immediately after the tap movement. They can be easily determined by using (4.6).

$$\begin{aligned} P_t &= peak\{P(t), t = Tap_{sp} : Tap_{sp} + 10\} \\ Q_t &= peak\{Q(t), t = Tap_{sp} : Tap_{sp} + 10\} \end{aligned} \tag{4.6}$$

Having P_t and Q_t we can calculate α and β by using (4.1).

4. Calculate the parameters τ_p and τ_q. They can be estimated by monitoring the actual waveforms or using (4.1). They will be the required times for the real and reactive power to get to their steady state values after the tap movement. Since the moment of tap movement and the steady-state and transient values are already known, τ_p and τ_q can be easily estimated. In the cases that two tap movements occur simultaneously, the algorithms are still applicable since the waveforms will be similar with either a larger step change or a two-consecutive step changes.

4.3.3 Voltage Disturbance Effects on Load Model Parameters

Although mathematically the load model parameters can be estimated from any voltage step change, it is important to verify whether the parameters are sensitive to the magnitude of the step change. Through extensive field tests on BC Hydro's system, reference [87] showed that the 1% voltage drop caused by a single tap movement gives the same load parameters as a 15% voltage drop.

In this section for further investigation of the issue, several experiments with different loads were set up to see how the magnitude of step change will affect the load parameters. For these experiments the loads included a 2 hp three-phase induction machine with various loading conditions in parallel with a bank of variable resistors, and a variable frequency drive supplied by three-phase 208 phase-to-phase voltages. The following steps were taken for calculation of load model parameters:

- Detect the step changes in the three-phase voltage ,

- Record the pre and post disturbance three-phase voltage and current waveforms using a window of 5 cycles of the 60Hz system frequency,
- Calculate the positive sequence voltage, active and reactive power for each cycle of the captured window,
- Calculate the load model parameters

The results shown in this section are related to two different cases which have the following loads:

1. A fully loaded induction machine working in parallel with a bank of resistors.
2. A variable frequency drive powering a loaded induction machine in parallel with a bank of resistors.

The experiments were done under the following conditions:

- The voltage disturbance occurred in the steps of 1.5%, 2.5%, 5%, 7.5%, and 10%.
- The disturbance occurs at t = 1 Second
- The pre-disturbance value was the average of 5 cycles before the disturbance (55-59)
- The post-disturbance value was the average of 5 cycles 30 cycles after the disturbance (90-94)
- For each voltage step value, 10 experiments were done
- The time difference between each experiment was 10 seconds
- All the experiments were in three-phase system

The two cases were investigated and the parameters of the models were calculated for them.

4.3.3.1 Fully loaded induction machine in parallel with resistor bank

In this experiment a three-phase, 2 hp induction machine and a resistor bank are considered as the three phase loads connected to the system. As an example, the variations of active and reactive power after a 5% step change in voltage are plotted in Figure 4.3.

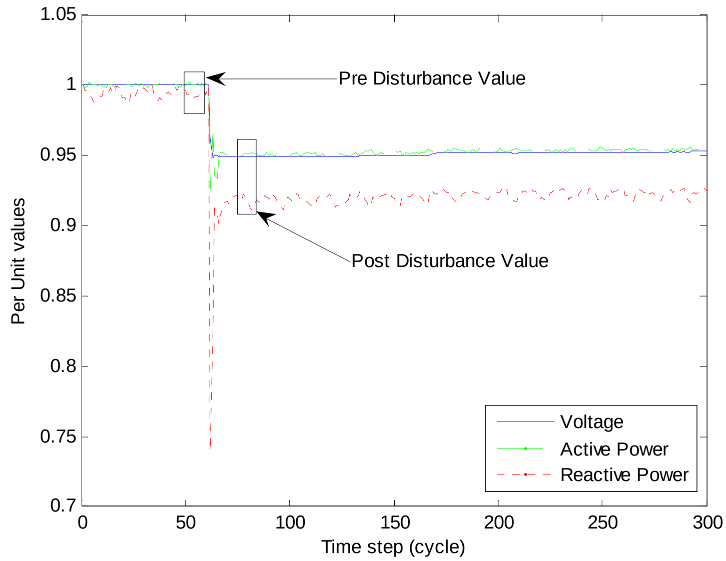

Figure 4.3. The variation of voltage, active and reactive power

Figure 4.3 shows the averaging window which has been used for getting the pre and post disturbance values. The experiments have been done with step changes of 1.5%, 2.5%, 7.5% and 10%. The calculated load model parameters versus the magnitude of step change in the voltage are plotted in the following figures.

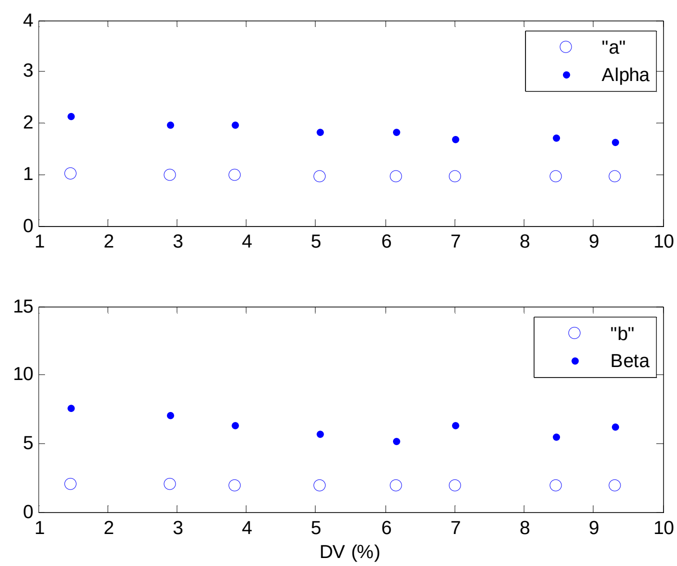

Figure 4.4. The variation of voltage, active and reactive power

The required time to recover for this load is also plotted in Figure 4.5.

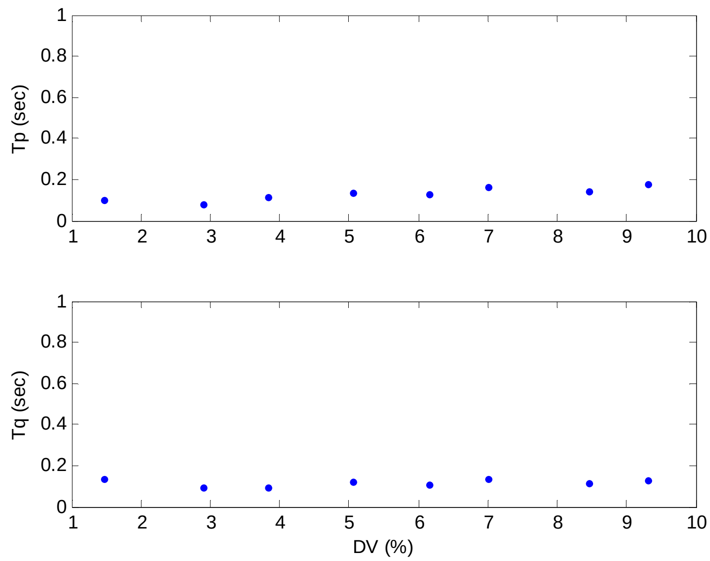

Figure 4.5. The calculated load model parameters

The experiments done in this section show that the six load parameters for the induction machine operating in parallel with a resistor bank, do not depend on the magnitude of step voltage change significantly and they are mainly dependent on the characteristics of the load itself.

4.3.3.2 Variable frequency drive in parallel with resistor bank

For this experiment a three-phase variable frequency drive, driving the 2 hp induction machine and a resistor bank were considered as the three phase loads connected to the system. As an example, the variations of active and reactive power after a 5% step change in voltage are plotted in Figure 4.6.

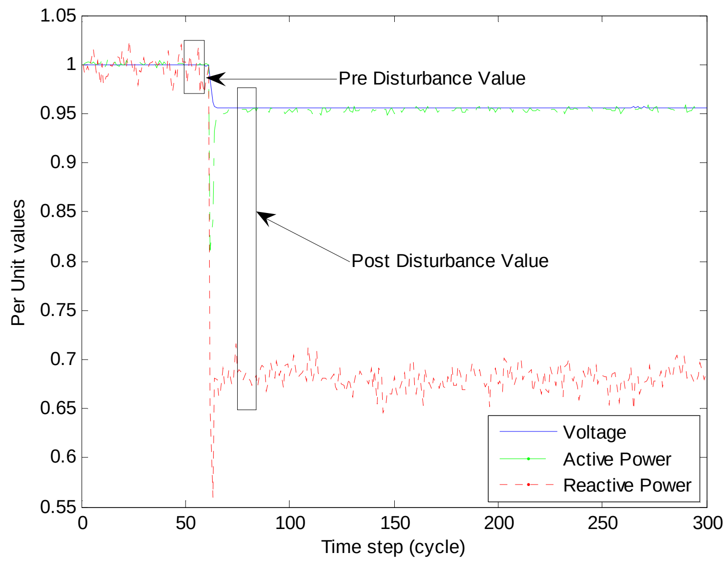

Figure 4.6. The variation of voltage, active and reactive power

Figure 4.6 shows the averaging window which has been used for getting the pre and post disturbance values. The calculated load model parameters versus the magnitude of step change in the voltage are plotted in the following figures.

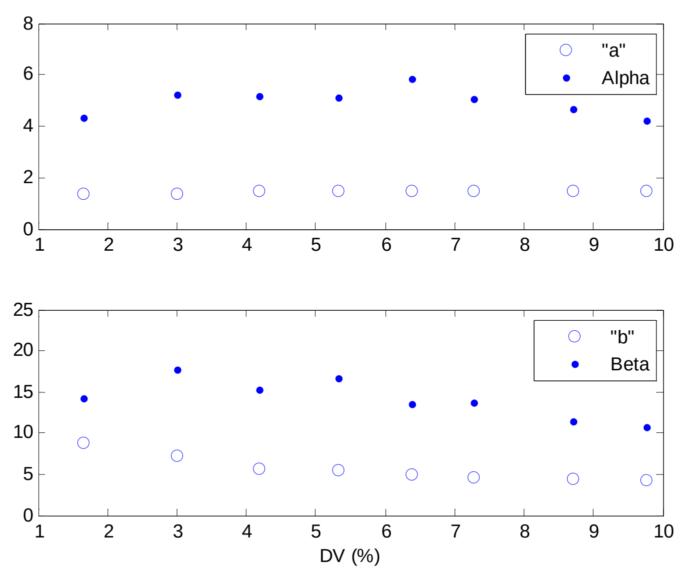

Figure 4.7. The variation of voltage, active and reactive power

The required time to recover for this load is also plotted in Figure 4.8.

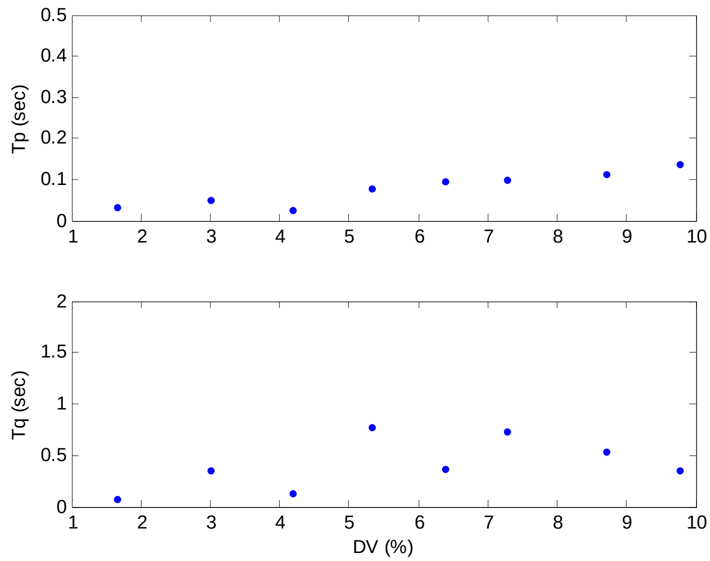

Figure 4.8. The calculated load model parameters

The calculated results show that the load model parameters can be determined by using a disturbance in the voltage and the corresponding active and reactive power. In this project the tap changer will be used to determine the parameters of the loads connected to different feeders in the substation.

Further to the cases mentioned above, the lab experiments have were done for the induction machine, resistor bank and variable frequency drive in different loading conditions. The experiments done in this section show that the six load parameters do not depend on the magnitude of step voltage change significantly and they are mainly dependent on the characteristics of the load itself. This is very important finding and shows that although the step changes in voltage created by the operation of ULTC are not very large, they still can be used for calculation of the load model parameters. This issue has also been confirmed and reported in [36] and [87].

4.3.4 Sensitivity Studies

In this part some sensitivity studies are presented. These studies were performed in order to finalize the load modeling algorithm and apply it to the real field measurements data. The parameters to be determined are the length of window used for averaging the pre-tap voltage, real and reactive power, the length of window used for averaging the post-tap voltage, real and reactive power, and the time span between pre- and post-tap values.

4.3.4.1 Averaging the Pre-tap Values

In order to reduce the effect of noise and transients in the calculated parameters, the pre-tap values are built up from averaging a data window. Several sensitivity studies were done to find the best data window length for averaging. For this purpose the load parameters of different kind of loads were plotted versus the length of data window used for averaging. Our studies show that a five-cycle data window for averaging provides accurate and acceptable results. As an example the calculated “a” and “b” are plotted versus the length of data window for a sample tap movement in Figure 4.9.

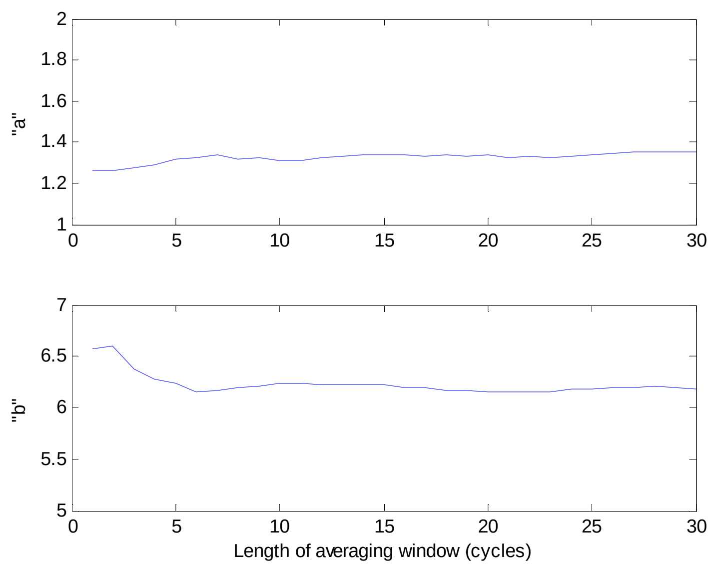

Figure 4.9. Load parameters versus length of pre-tap averaging window

Figure 4.9 shows that increasing the length of window more than five cycles will not affect the parameters and this confirms the appropriate selection of five-cycle data window for averaging the pre-tap values.

4.3.4.2 Averaging the Post-tap Values

The same procedure was applied to determine the length of window used for averaging the post-tap values. Our studies on several tap movements captured from different transformers show that the five-cycle data window provides accurate and acceptable results. As an example for a single tap movement, the results are shown in Figure 4.10.

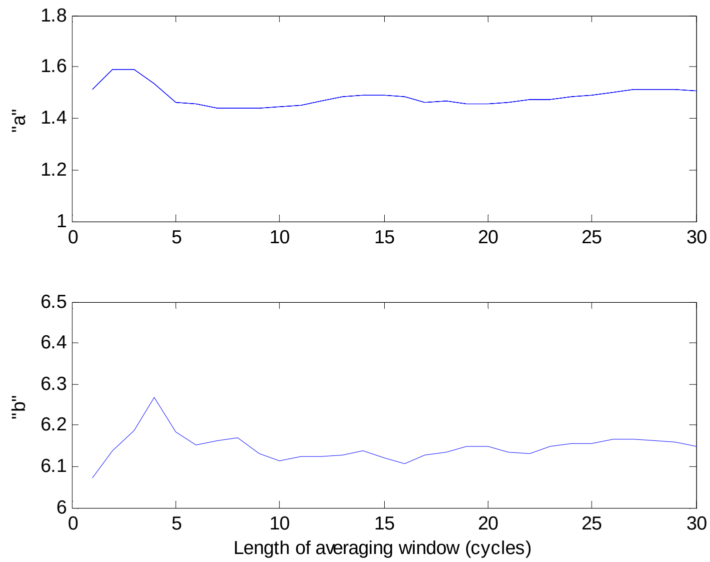

Figure 4.10. Load parameters versus length of post-tap averaging window

It is seen that by increasing the length of averaging window more than five cycles, the results will not change significantly and this value was selected for averaging the post-tap values.

4.3.4.3 Time Span between Pre- and Post-Tap Values

The tap movement usually occurs in a few cycles. However, its effect on real and reactive power will continue for a while. In order to calculate the post-tap values for estimation of load parameters, we need to select the time span between the pre- and post-tap values. For this purpose several sensitivity studies were performed and several cases were investigated. The filed test results show that for almost all the transformers, the transients in real and reactive power will die out after one second. As an example the results related to a specific tap movement are plotted in Figure 4.11.

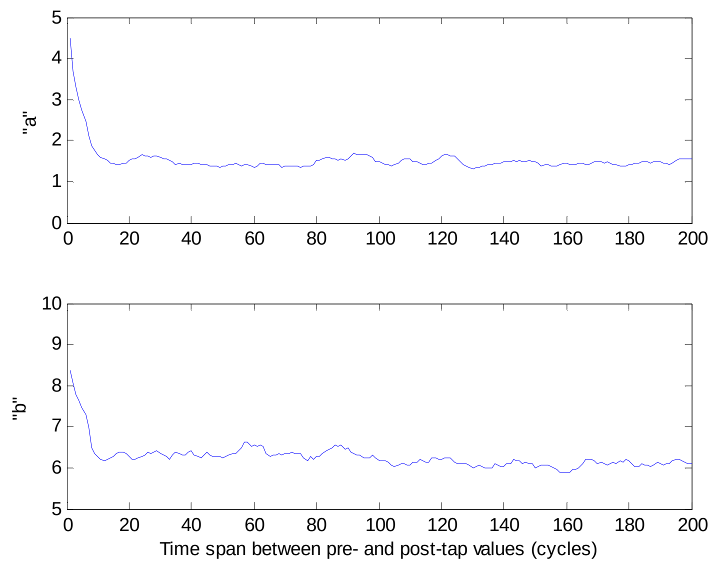

Figure 4.11. Load parameters versus time span

Figure 4.11 reveals that selection of one second for the time span between the pre- and post-tap values is an appropriate choice and provides accurate results.

The sensitivity studies performed in this section helped us to determine the required parameters for the proposed load modeling algorithm. These parameters were used to calculate the load model parameters for all the transformers in this and the next chapter.

4.4 Characteristics of the ULTC Movement

In a power transmission system, the load is the collective power demand of the various electricity users served by a feeder or by a substation. The proposed measurement scheme for calculating the load model parameters is shown in Figure 4.12. This system uses the disturbance responses recorded at substation meters to estimate the load characteristics of the downstream system.

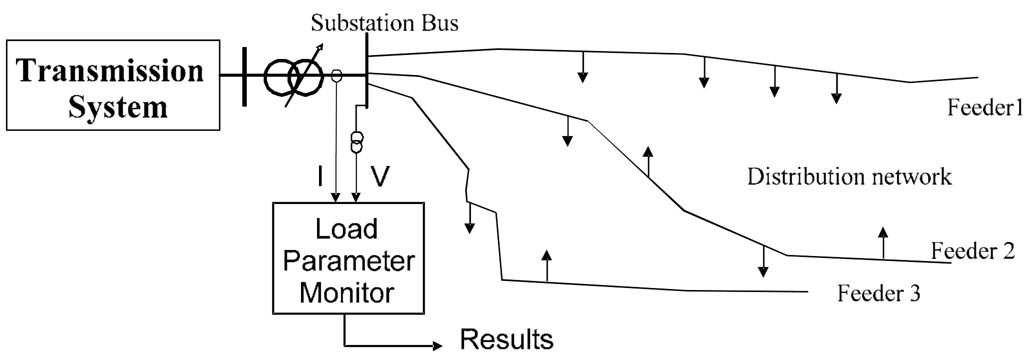

Figure 4.12. The proposed measurement system

The data needed for this system are the substation bus voltages and feeder or the transformer line currents. The data are recorded in the waveform format with a sample rate of at least 16 samples per cycle. The data are collected in a continuous stream, and the system's outputs are the load model parameters as functions of time. According to electric circuit theories, when a disturbance occurs at the system side, the voltage and current waveforms can be used for estimating the load side parameters. The disturbance can be any kind of distortion in the voltage or current waveforms, such as continuous variations of the load voltage and current, or step changes caused by transformers' taps. Since the probability that variations or disturbances will occur on both the system and load side simultaneously is, practically, very low, it is reasonable to assume that the parameters on the non-disturbance side are constant for the disturbance period. Once the disturbance side is determined, the measurement data can be used to calculate the system or load side parameters.

This project is based on the use of the tap movement effect on voltages and currents for calculating load model parameters. In this section, the characteristics of the ULTC movements are explained. For this purpose, the measurement devices were installed in four different substations to capture the tap movements occurring in 14 transformers during a one-week period. The data are captured from the city of Edmonton transformers identified in Table 4.1. These substations are 15 kV substations supplying commercial and residential loads. The loads are classified as mostly commercial, which has roughly 70% commercial loads; mostly residential, which has roughly 70% residential loads; and the substations that have roughly equal amounts of commercial and residential loads. The list of transformers and their load types are presented in Table 4.1.

Table 4.1. List of transformers and substations under study

Substation	Transformer No.	Transformer Name	Transformer load types
One (14.4 kV)	1	M1.1	Commercial and residential
	2	M2.1	Commercial and residential
	3	M3.1	Commercial and residential
Two (14.4 kV)	4	P1.1	Commercial and residential
	5	P1.2	Mostly Residential
	6	P2.7	Mostly Residential
	7	P2.8	Mostly Residential
Three (14.4 kV)	8	J3.1	Mostly Commercial
	9	J3.3	Mostly Commercial
	10	J3.8	Mostly Commercial
	11	J4.2	Mostly Commercial
	12	J4.7	Mostly Commercial
Four (14.4 kV)	13	C1.2	Mostly Residential
	14	C2.8	Commercial and residential

As Figure 4.12 reveals, each transformer supplies several feeders, and the measurements are taken at the secondary side of the transformers. Therefore, the collection of feeders connected to each transformer is considered as a load.

Some characteristics of the tap changes such as the voltage step change, frequency of occurrence, time of occurrence, and the time required for tap movement are explained in the following sections.

4.4.1 Voltage Disturbance Characteristics

According to the manufacturers of the ULTC, the total range of the regulation and size of the individual steps for tap movements are most often specified as 10% voltage in 33 steps of 0.625% voltage per step [98]. Exact information about the transformers in the substations is not always available to detect the operation of the ULTC and to adjust the recordings. Thus, to remain in a safe margin, the step change can be assumed to be 0.5% of the initial voltage. In a 15kV line-to-line voltage, or an 8.4 kV line-to-ground voltage, the tap movement step will be around 42 volts. This value was used only to detect the operation of the ULTC; however, for load parameter estimations, the actual step change was calculated from the real recorded waveforms.

Figure 4.13 shows the minimum, maximum and the average values of the voltage disturbance, caused by the operation of the ULTC, during the period of measurement. The average magnitude of the step changes in the voltage is evidently close to one percent and is almost the same for all the transformers in the different substations.

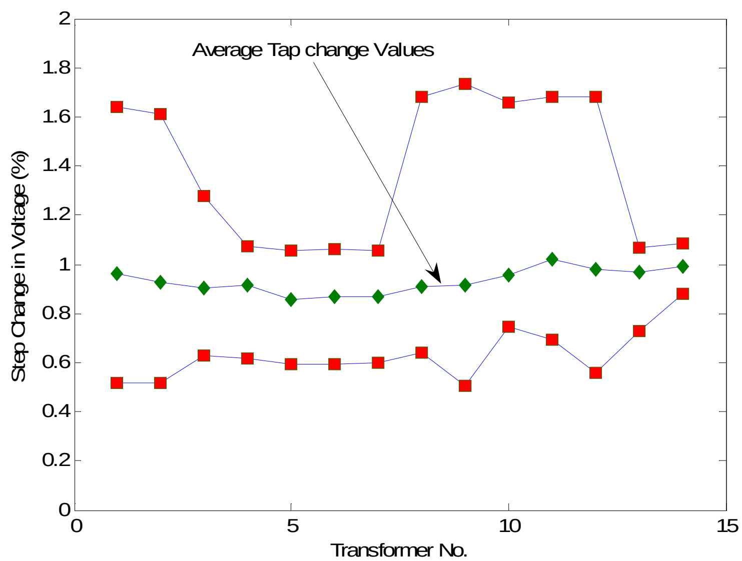

Figure 4.13. The minimum, average and maximum voltage step change

Figure 4.13 shows that most of the transformers have similar maximum and minimum values. Since the voltage change characteristics for Transformers One, Two and Eight to Twelve are similar, we grouped them together and grouped the rest of transformers as another group. Transformers One and Five, which each reside in a different group were selected for further illustrations. The magnitude of the step change in the voltage caused by the tap change for Transformers One and Five are presented in Figure 4.14.

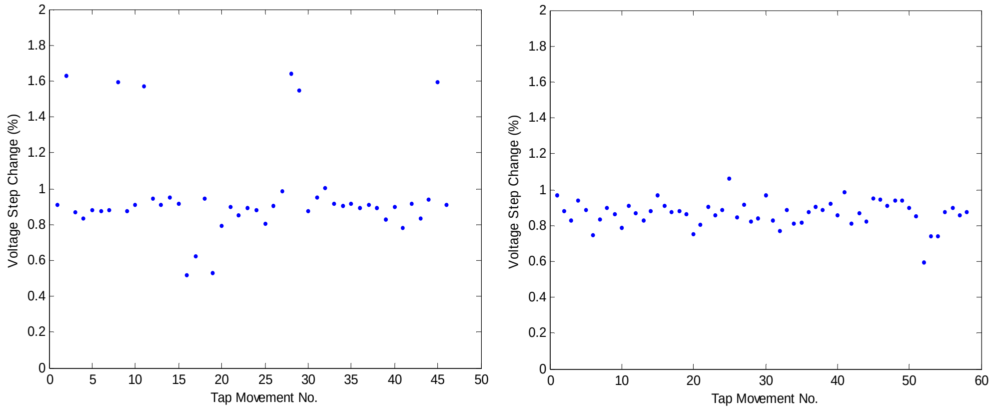

Figure 4.14. The step change in voltage for Transformers One and Five

During the one-week measurement period, 46 and 59 tap movements occurred for Transformers One and Five, respectively. Figure 4.14 reveals that for Transformer One, some tap movements have values greater than the others. Since the magnitude of the step change in the voltage is almost twice that of the rest, we can assume that in such cases the tap moved for two steps. As an example, two tap movements, with different steps, are shown in Figure 4.15.

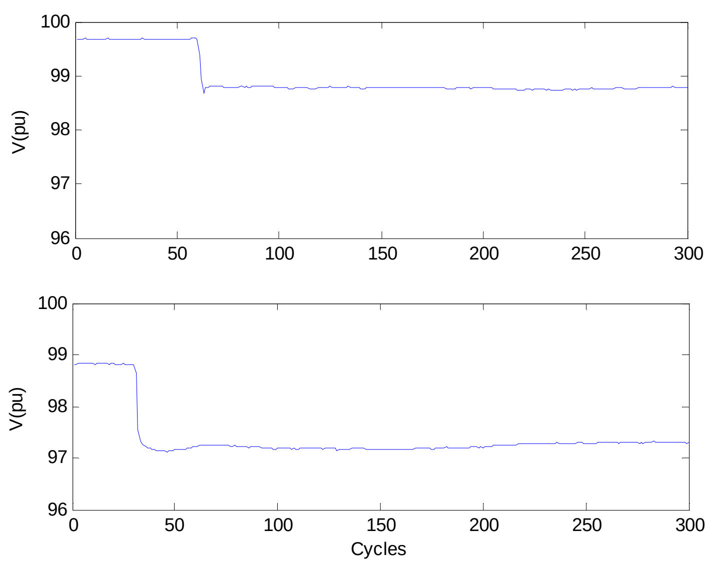

Figure 4.15. The step change in voltage for two sample tap movements

Figure 4.15 shows that the voltage change properties in terms of the transient time look the same. The only difference is the magnitude of the step change, which is two times larger for one of the movements.

The distributions of the magnitude of the step change in the voltage caused by the tap change for Transformers One and Five are presented in Figure 4.16.

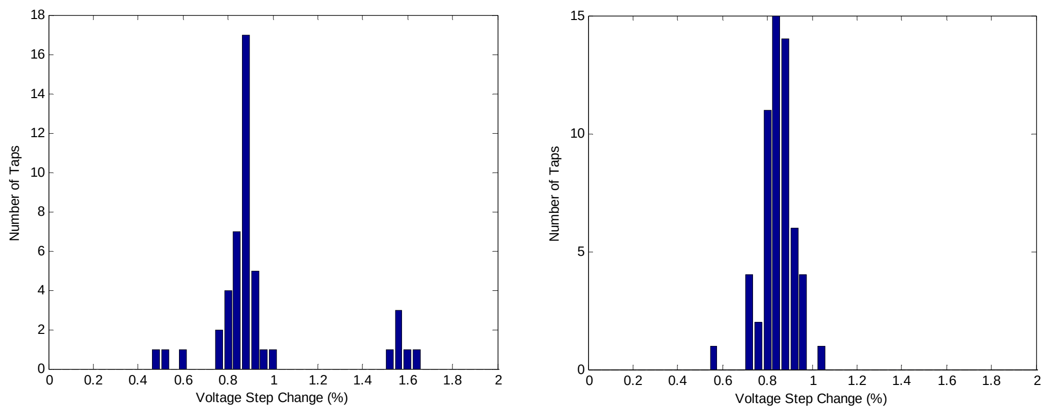

Figure 4.16. Distribution of voltage disturbances, Transformers One and Five

Figure 4.16 shows that the distribution function is similar to the normal distribution function with the mean value close to %0.9.

4.4.2 The Frequency of Tap Movement

Figure 4.17 shows the average number of tap movements per day for different transformers that could be used for load model calculations. For this purpose, the averages for the weekdays and weekends are plotted separately.

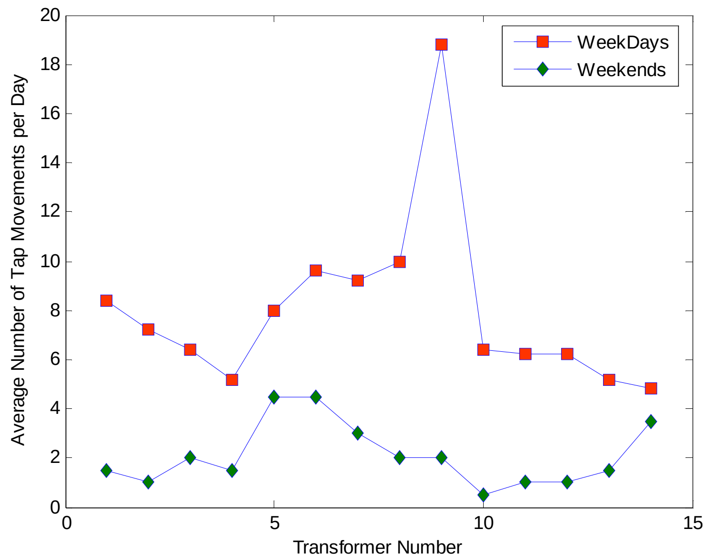

Figure 4.17. The average number of tap movement

As Figure 4.17 reveals, enough tap movements per day usually occur for the online tracking of load parameters. Also, the number of tap movements for weekdays usually exceeds the number for weekends. The reason is likely related to the degree of the variation of the loads on weekends. The lesser variation of loads on weekends results in less need for voltage regulation and operation of the ULTC.

4.4.3 Times of Tap Movement

Tap movement can happen at any time during the day. In order to show when the tap movement occurred during our experiments, the distribution of the tap movement occurrence time is plotted in Figure 4.18 for Transformers, One and Five, for a period of one week.

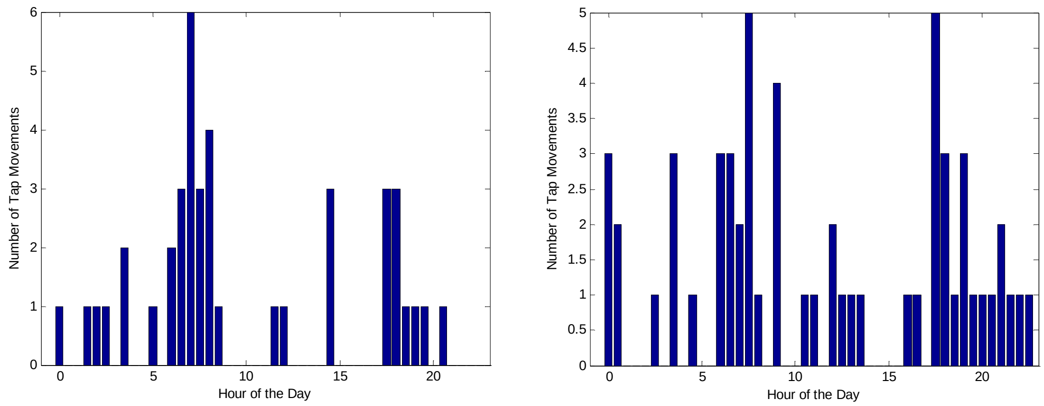

Figure 4.18. Distribution of ULTC operation time, Transformers One and Five

As Figure 4.18 reveals, tap movement can occur at almost any time of the day. This property could be very helpful in presenting the load model parameters in an online format. For the hours of the day in which we do not have any tap movements, the load model parameters can be estimated through interpolation methods.

4.4.4 Required Moment for Tap Movement

Tap movement usually takes place relatively quickly, or within five cycles of the fundamental frequency. As an example, the step changes in the voltage caused by a tap movement for two different step-up and –down movements are shown in Figure 4.19.

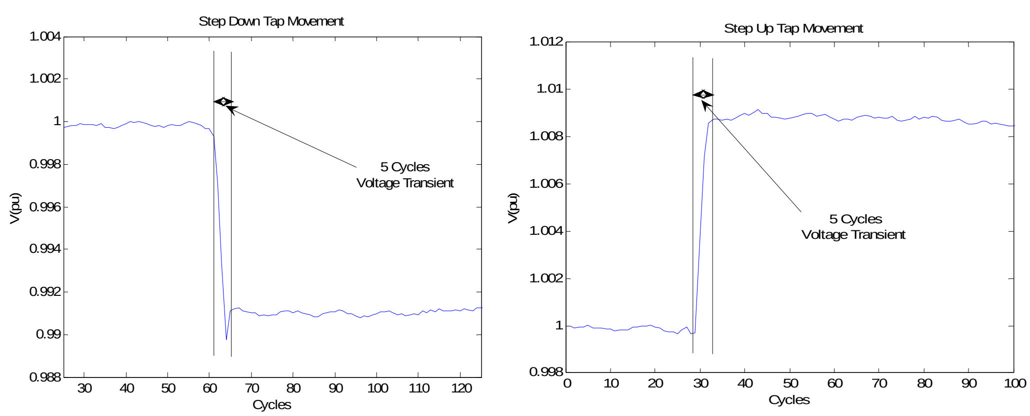

Figure 4.19. Two sample tap movement voltage transients

Figure 4.19 shows that the voltage has almost no transient. This result was checked by examining all the tap movements from the different substations. In some cases, two tap changes occurred simultaneously, so that the step change in voltage, consequently, almost occurred twice. In these cases, as shown in Figure 4.15, the tap movement characteristics in terms of the time required for the tap movement and the transients associated with the step change in the voltage are almost the same as the single tap movement characteristics. This property of tap movement is very useful since we can assume that the load side is constant during this process; therefore, load modeling becomes possible and meaningful. This property also helped us to develop our recording procedure, which is explained in the next sections.

4.5 Data Recording and the Final Algorithm

The characteristics of tap movements are explained in Section 4.4. Knowing the characteristics of tap movement and its effect on the system's voltage, we can develop an algorithm to detect and record the tap changes. In this section, the data-recording procedure and how the tap movement can be used for modeling the loads in the system are presented. This section concludes by presenting the flowchart of the final algorithm proposed for calculating load model parameters.

4.5.1 Data Collection Procedure

The national instrument NI-6020E 12-bit data-acquisition system with a 15.36 kHz sampling rate for each channel, controlled by a laptop computer, was used to record the three-phase voltages and currents at the point of metering in the substations for a period of four weeks. All the measuring points were at 15 kV systems; therefore, CTs and PTs were used to step down the recorded current and voltages, respectively, to measurable values. Two different recording procedures were used simultaneously to record the data, as is explained in the following sections.

4.5.1.1 Auto Snapshot Recording

In order to obtain the load profile data, we had to monitor and capture the three-phase voltages and currents during the measurements. For this purpose, the labview program was used to capture 12 cycles of the waveforms in every 12 seconds. Therefore, we obtained five snapshots per minute and 300 snapshots of the three-phase voltages and currents per hour.

4.5.1.2 Tap Movement Recording

The other data which had to be captured simultaneously were the tap movement instant waveforms. In order to record this type of data, the labview program was used, and the tap movement was captured based on the variation of the voltages. Since the tap movement causes a step change in the voltage, either a decrease or an increase, and this step change occurs within a few cycles, checking the voltage of phase "A" every second and comparing it to the voltage at the previous second helped us to detect the tap movement. If the step change in the voltage was larger than 0.5%, then tap movement had occurred, and the three-phase voltages and currents were recorded for a period of five or twelve seconds, which included four to ten seconds of data after tap movement instant. A twelve-second period was used to check whether the load had a dynamic response, which would last for this period of time. Our field tests on the four substations and 14 transformers showed that the dynamic responses of the load caused by the tap movement were very small and died out in, at most, one second. Therefore, the twelve-second period was sufficient for capturing the tap movement and estimating the transient and static load model parameters.

For the five-second recordings, the snapshot was recorded as a five-second snapshot or 300 cycles. In order to determine whether the snapshot should be considered as a tap change and to detect the instant of the tap movement's beginning, the following procedure was applied:

1. Three different voltages and the active and reactive power at three different time instants were recorded:

$$V_1 = \sum_{t=1}^{10} \frac{V(t)}{10},\ V_2 = \sum_{t=71}^{110} \frac{V(t)}{10},\quad V_3 = \sum_{t=111}^{120} \frac{V(t)}{10}, \tag{4.7}$$

The vector V is constructed of the 60-Hz component of the voltage of phase "A" for each cycle of the waveform.

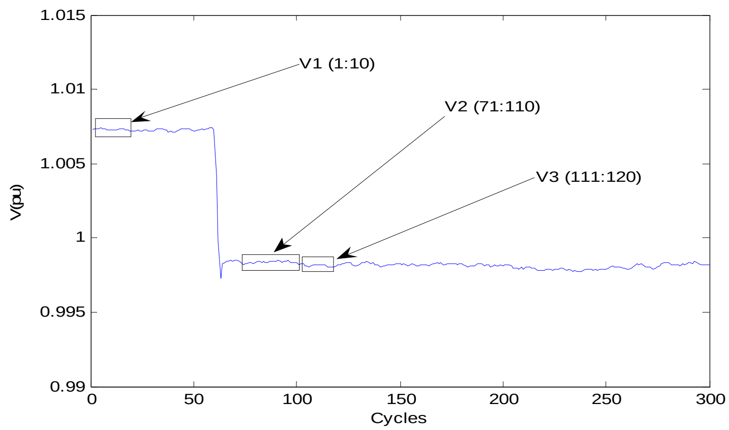

Figure 4.20. The step change in voltage caused by tap movement

2. The variation of the voltage for (V_1,V_2) and (V_2,V_3) is calculated as follows:

$$DV_1 = \left|\frac{V_2 - V_1}{V_1}\right| \times 100,$$

$$DV_2 = \left|\frac{V_3 - V_2}{V_2}\right| \times 100. \qquad (4.8)$$

3. According to the transformers' manufacturers, the minimum tap change is a step change around 0.625%; therefore, an index of 0.5% is appropriate for determining tap change occurrence. The following conditions should be satisfied for a snapshot to be considered as a tap change:

- $DV_1 > 0.5.$
- $DV_2 < 0.3.$ (4.9)

The reason for the second condition is to avoid the cases where the voltage fluctuates. In such cases, the data recorder will assume the ULTC has operated, but, in fact, the tap has not moved, and the changes in the system loading conditions have caused the voltage to change, and the first condition becomes true.

4.5.2 Flowchart of the Final Algorithm

The proposed algorithm can be implemented in the following steps:

Step 1. Detect the step changes in the three-phase voltage through the following procedure,

Step 1.1. Record the transformer's three-phase voltage and current for two consecutive seconds in a sliding window format,

Step 1.2. Calculate the 60-Hz component of the voltage of phase "A" for the first six cycles of each second,

Step 1.3. Calculate the step change in voltage; if the step change is greater than 0.5%, a tap movement has been occurred,

Step 2. If a tap movement occurred, go to step 3; otherwise, go to step 1.

Step 3. Record the pre- and post- disturbance three-phase voltage and current waveforms as follows:

Step 3.1. Record the transformer's three-phase voltage and current for the period of 20 cycles before to 10 seconds after the tap movement.

Step 4. Calculate the load model parameters by using the algorithm explained in Section 4.4,

Step 5. Save the calculated parameters and keep them until the reporting period is over,

Step 6. If the data-reporting period is over, calculate the load model parameters as the average of the parameters that have been calculated so far.

Step 7. Go to step 1.

4.6 Field Measurement Results

Field measurements were conducted in June and July 2009 at different substations in the city of Edmonton, Alberta. The data processing was performed in the power lab at the University of Alberta to determine the load model parameters of the transformers.

4.6.1 The Substations and Transformers under Study

Four substations were studied for this project. Measurements were done for two to five transformers at each substation. The substations' names and the measured transformers, nominal voltage, average load per day, and the load types are presented in Table 4.2.

Table 4.2. List of measured transformers and the average loads

Substation	Transformer Name	Transformer load types	Average Transformer Load per day (S = P + jQ)
One (14.4 kV)	M1.1	Commercial and residential	22.5 MW + j8.1 MVar
	M2.1	Commercial and residential	20.5 MW + j7.5 MVar
	M3.1	Commercial and residential	21.8 MW + j4.1 MVar
Two (14.4 kV)	P1.1	Commercial and residential	18.3 MW + j5.1 MVar
	P1.2	Mostly Residential	27.5 MW + j7.8 MVar
	P2.7	Mostly Residential	26.2 MW + j7.1 MVar
	P2.8	Mostly Residential	22.8 MW + j6.2 MVar
Three (14.4 kV)	J3.1	Mostly Commercial	38.6 MW + j14.4 MVar
	J3.3	Mostly Commercial	32.1 MW + j11.9 MVar
	J3.8	Mostly Commercial	18.8 MW + j9.5 MVar
	J4.2	Mostly Commercial	24.1 MW + j10.6 MVar
	J4.7	Mostly Commercial	25.2 MW + j10.1 MVar
Four (14.4 kV)	C1.2	Mostly Residential	21.8 MW + j5.1 MVar
	C2.8	Commercial and residential	16.8 MW + j5.3 MVar

The average transformer load per day is presented as only a rough value in order to allow the different transformers' loads to be compared.

4.6.2 Grouping Similar Loads

All the measured transformer loads in the substations were grouped into four groups based on the load profiles, the load levels of the transformers, and the information received from technicians at the substations. Table 4.3 shows the four constructed groups.

Table 4.3. List of different load groups

Group	Members	Description
I	M1.1, M2.1, M3.1	Commercial and residential (larger loads)
II	P1.1, C2.8	Commercial and residential (smaller loads)
III	C1.2, P1.2, P2.7, P2.8	Mostly residential
IV	J3.1, J3.3, J3.8, J4.2, J4.7	Mostly commercial

In order to show the load profiles of the transformers, the power profiles of the members of each group are plotted in the following Figures 4.21-4.24.

A. Group I - Commercial and Residential

This group of loads has both commercial and residential load types. As Figure 4.21 reveals, the peaks of the loads occur in the evening, and the loads during working hours are also high.

(a)

M1.1

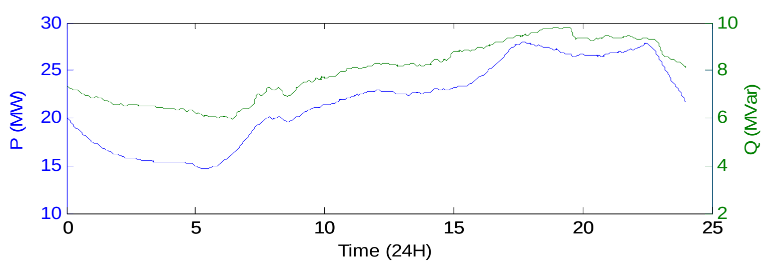

(b)

M1.2

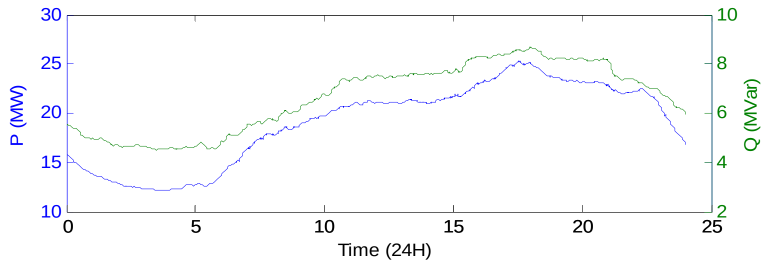

(c)

M1.3

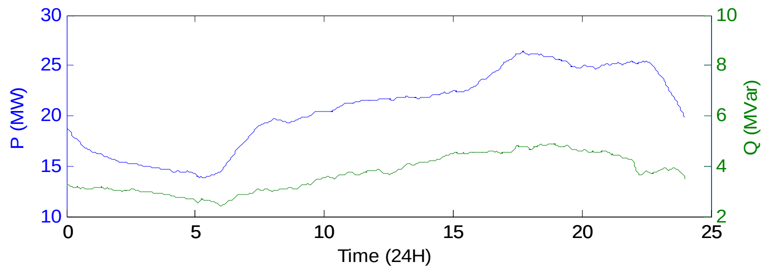

Figure 4.21. Load profile of Group I

B. Group II - Commercial and Residential

This group of loads also has both commercial and residential load types. The peaks of the loads here occur in the evening and during working hours. The differences between this group loads and Group I are that Group II has less load variation and much less load peaks.

(a)

P1.1

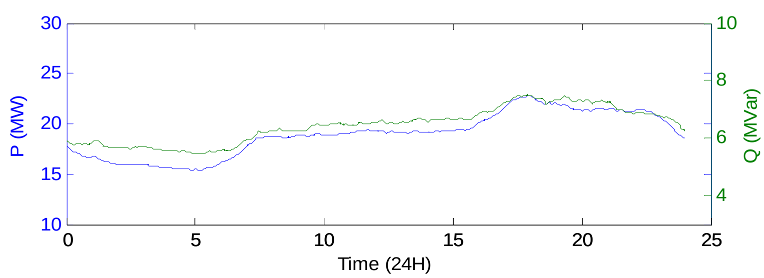

(b)

C2.8

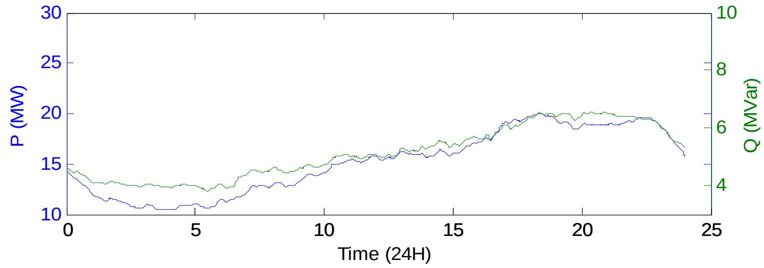

Figure 4.22. Load profile of Group II

C. Group III - Mostly Residential

This group of loads has more residential than commercials loads. The peaks of the loads occur in the evening, and the loads during working hours are also high. As Figure 4.23 shows, the difference between Group III and the previous groups is its higher peaks in the evenings and its larger average power factor. The higher peaks could be caused by larger residential loads in the evenings.

(a)

C1.2

(b)

P1.2

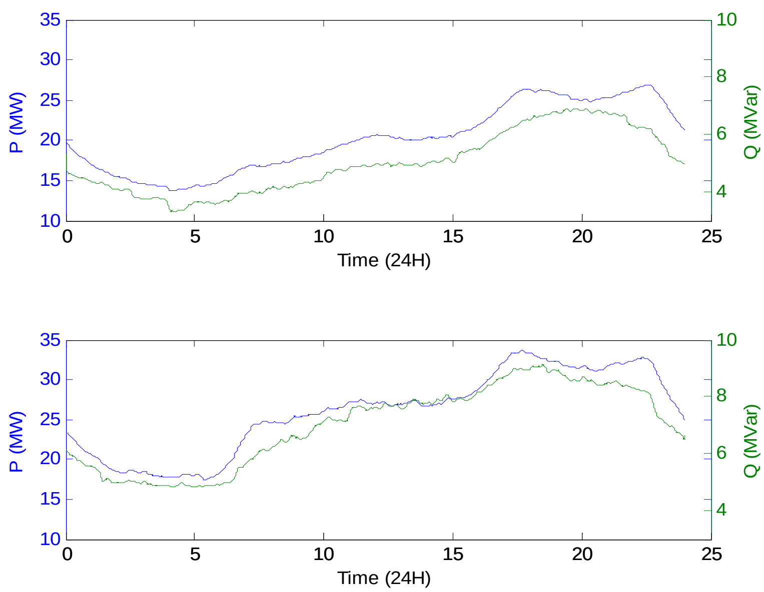

(c)

P2.7

(d)

P2.8

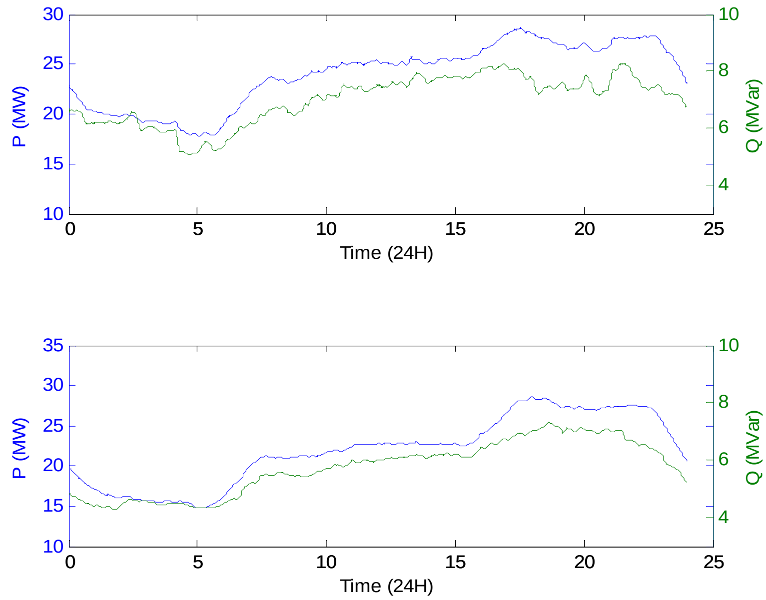

Figure 4.23. Load profile of Group III

D. Group IV - Mostly Commercial

This group of loads is constructed mainly from commercial loads. Figure 4.24 reveals, that the peak of the loads occurs during working hours. The difference between Group IV and the previous groups is Group IV's higher peaks during the day, larger loads, lower power factor, and small peaks in the evening.

(a)

J3.1

(b)

J3.3

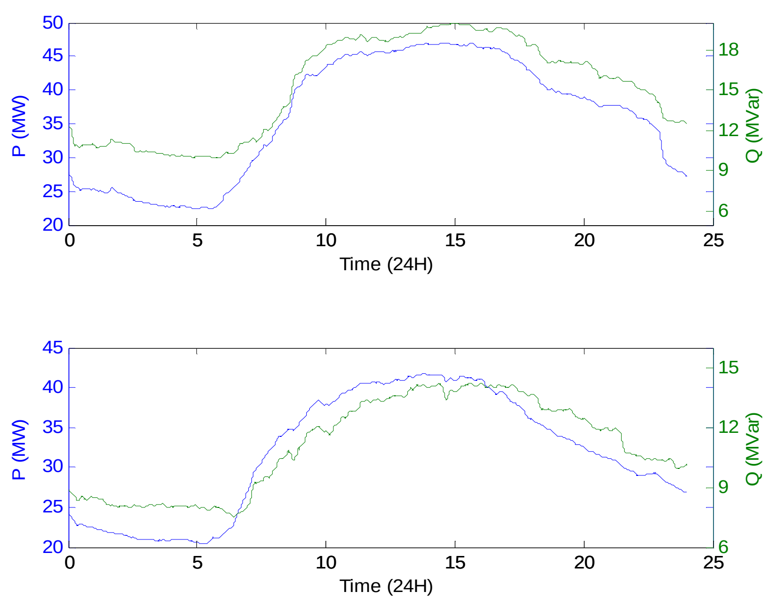

(c) J3.8

(d) J4.2

(e) J4.7

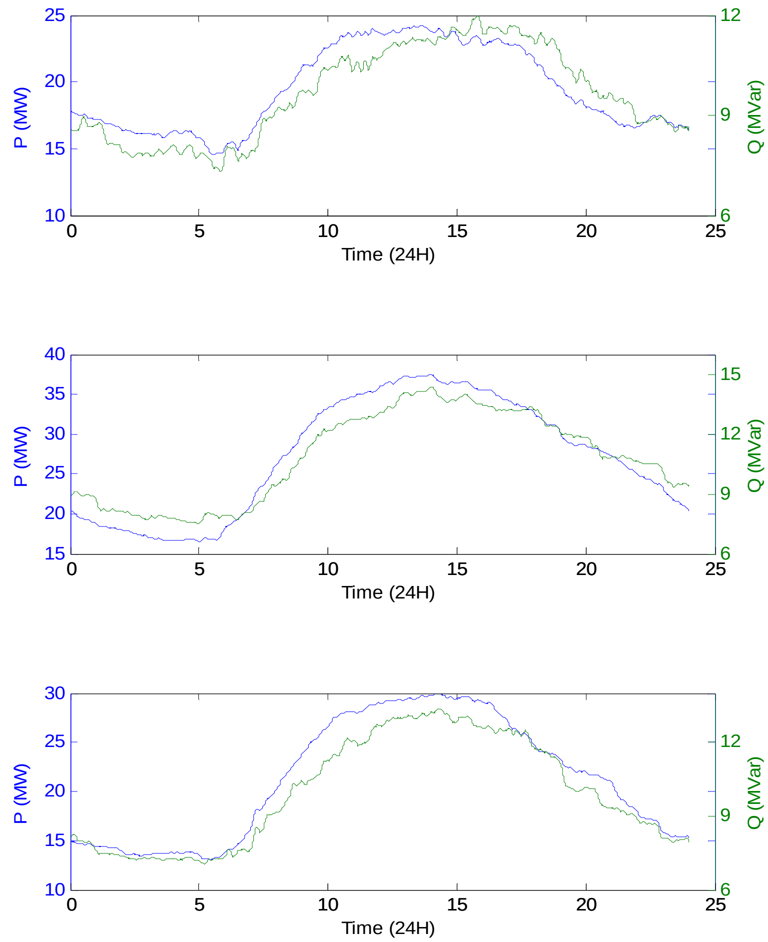

Figure 4.24. Load profile of Group IV

Although some of the Four groups are similar and could be merged together, for better differentiation and observation of the load parameter variations, the groups have been kept separate.

4.7 Conclusions

This chapter presented a practical and effective method for the online monitoring of voltage-dependent load model parameters. The method was verified through several experiments and extensive field test results. The data collected from the tests were analyzed to show the various characteristics and sensitivities of the tap movements. The main advantages of using natural tap movements for load parameter estimation are summarized as follows:

- Tap movements occur on a daily basis, so load parameters can be collected consistently, frequently, and predictably.
- Tap movements cause a step voltage change. If no other disturbances occur at the same instant, as is commonly the case, the load parameters can be estimated by using simple and reliable algorithms.
- Pre-established disturbance signatures uniquely suitable to detect tap movements can be used to detect and capture these disturbances.
- Since many such disturbances occur, if one misses some of them because of various uncertainties, the accuracy of the calculations will not be decreased. In fact, selecting only high-quality disturbances improves the reliability and quality of the results.
- System operators can create these disturbances intentionally with a desired disturbance severity (i.e., by varying the amount of DV produced by the tap changer). As a result, the proposed technique can estimate load parameters 'on demand'.
- Finally, the results do not need to be "verified", for the load parameters are actually measured from the step-change disturbances rather than with sophisticated algorithms using complex disturbance waveforms.

Since the load parameters can be obtained many times a day, their online tracking becomes possible, and real-time power system applications such as dynamic security assessment can use the measured load parameters as input.

Chapter 5

Characteristics of Load Data Parameters

This chapter presents the characteristics of the load data parameters. For this purpose, the basic load model parameters calculated for four different substations' transformers are presented. Then the typical load parameters for different load types are calculated and shown. The load parameters are investigated while considering the load profiles. The effect of a step change in the voltage on the load model parameters and the variation of the load parameters through the variation of the pre-tap values is studied. The pre-tap values are the pre-tap voltage, the pre-tap active power, and the pre-tap reactive power. Finally, some abnormal tap movement results that should not be considered for load modeling are presented.

5.1 Introduction

Different loads respond differently to the variation of their supply voltage. Their response depends on their characteristics. One way to investigate the load responses to variations in the voltage is to investigate the characteristics of the load data parameters. In this chapter, several sensitivity studies are presented to explain the characteristics of load parameters and to modify the final load modeling algorithm. As an example, the effect of the magnitude of a step change in the voltage on the load parameters is investigated. The results show that the magnitude of the step changes or tap movement does not significantly affect the calculated parameters, so that any step change in the voltage caused by tap movement, regardless of its magnitude, can be used to estimate the load parameters. As well, the pre-tap values of the voltage and the active and reactive power and their effects on the estimated load parameters were studied, and the observations showed that the pre-tap values did not affect the load parameters. This important fact shows that the estimated load parameters depended on only the load types and not their size, just as they do in reality.

Moreover, our research shows that not all tap changes can be used for load estimation, because of the variation of the loads connected to the transformer while the ULTC is operating. For this reason, the tap movement detection algorithm was modified to capture only the tap changes that could be used for online measurement and, consequently, to improve the accuracy of the algorithm.

Through a sensitivity analysis of several field measurements, the final algorithm for the online measurement of load model parameters was developed. The measured transformers are from four different substations serving different types of loads. These transformers are classified into four groups of commercial and residential transformers. Of the transformers under study, the residential transformers had the lowest, and the commercial transformers had the highest values for the load model parameters.

The sensitivity studies show that the tap movements occurring in the secondary side of power transformers in load-serving substations created a system side disturbance that can be used for estimating load model parameters. A tap change can happen at any time and in any loading conditions, and the disturbance magnitude of the step change in the voltage is large enough for calculating the load model parameters. Therefore, the methodology developed in this research fulfills the requirement for the online measurement of load model parameters.

5.2 The Basic Load Model Parameters of the Transformers

The load modeling procedure explained in Chapter Four was used to calculate the load model parameters of all the transformers in the substations. Table 5.1 to 5.6 present the calculated load model parameters for the transformers for weekdays and weekends separately. Since the load variation is considerable during a 24-hour period, the 24 hours were divided into six segments of four hours each. The tables also show the substation, transformer, and bus numbers. The average of the load model parameters during a 24-hour period is shown in the table's last column.

Table 5.1. Load model parameters for different transformers ("a")

Substation	**Transformer & Day**		**"a"**						
			AM			**PM**			
	F.	**D.**	**0 to 4**	**4 to 8**	**8 to 12**	**12 to 4**	**4 to 8**	**8 to 12**	**Average**
One	M1.1	WD	**1.44**	**1.19**	**0.95**	**1.03**	**1.06**	**1.17**	**1.14**
		WE	---	1.18	1.41	1.54	---	---	1.37
	M2.1	WD	**1.32**	**1.36**	**1.33**	**1.39**	**1.23**	**1.27**	**1.32**
		WE	---	---	1.16	---	---	---	1.16
	M3.1	WD	**1.48**	**1.34**	**1.09**	**1.12**	**1.29**	**1.22**	**1.26**
		WE	1.53	1.27	---	---	---	0.93	1.25
Two	P1.1	WD	**0.78**	**1.06**	**0.60**	**0.46**	**0.86**	**0.67**	**0.74**
		WE	0.62	0.45	0.79	---	---	---	0.62
	P1.2	WD	**1.11**	**1.09**	**1.04**	**1.37**	**1.08**	**0.98**	**1.11**
		WE	0.87	0.89	1.11	0.79	---	---	0.91
	P2.7	WD	**0.85**	**1.05**	**0.98**	**1.01**	**1.11**	**0.93**	**0.99**
		WE	1.34	0.74	1.01	0.78	1.06	1.09	1.00
	P2.8	WD	**1.24**	**1.26**	**1.29**	**1.16**	**1.02**	**1.13**	**1.18**
		WE	---	1.05	1.04	---	0.84	---	0.98
Three	J3.1	WD	**0.85**	**0.80**	**0.71**	**0.52**	**0.70**	**0.85**	**0.74**
		WE	---	---	0.64	---	---	---	0.64
	J3.3	WD	**1.01**	**0.91**	**0.69**	**0.88**	**0.93**	**0.94**	**0.89**
		WE	---	1.00	1.04	---	---	---	1.02
	J3.8	WD	---	**0.72**	**0.48**	---	**1.02**	**1.28**	**0.88**
		WE	---	2.21	---	0.45	---	---	1.33
	J4.2	WD	**1.09**	**0.83**	**0.85**	**0.98**	**0.91**	**0.84**	**0.92**
		WE	---	---	0.77	---	---	---	0.77
	J4.7	WD	**0.75**	**1.02**	**0.95**	**0.37**	**0.81**	**0.91**	**0.80**
		WE	---	---	0.63	---	---	---	0.63
Four	C1.2	WD	**1.14**	**1.08**	**1.09**	**1.29**	---	**1.12**	**1.14**
		WE	---	---	1.37	---	---	1.05	1.21
	C2.8	WD	**0.89**	**0.91**	**0.87**	**0.96**	---	**0.98**	**0.92**
		WE	1.12	---	1.03	---	0.81	1.03	1.00

The calculated “b” parameter is shown in Table 5.2.

Table 5.2. Load model parameters for different transformers (“b”)

Substation	Transformer & Day		“b”						
			AM			PM			Average
	T.	D.	0 to 4	4 to 8	8 to 12	12 to 4	4 to 8	8 to 12	
One	M1.1	WD	**6.39**	**5.34**	**5.21**	**4.85**	**4.52**	**5.31**	**5.27**
		WE	---	5.11	5.80	5.37	---	---	5.43
	M2.1	WD	**6.05**	**5.13**	**5.06**	**4.29**	**4.01**	**5.18**	**4.95**
		WE	---	---	5.45	---	---	---	5.45
	M3.1	WD	**8.74**	**8.26**	**7.95**	**7.42**	**6.41**	**8.41**	**7.87**
		WE	7.94	7.92	---	---	---	8.63	8.16
Two	P1.1	WD	**3.69**	**3.60**	**3.10**	**3.12**	**3.48**	**3.44**	**3.40**
		WE	3.91	3.37	3.34	---	---	---	3.54
	P1.2	WD	**6.67**	**5.70**	**5.55**	**5.59**	**4.91**	**5.56**	**5.66**
		WE	6.49	5.89	4.83	4.82	---	---	5.51
	P2.7	WD	**5.19**	**4.96**	**5.45**	**5.02**	**5.68**	**5.23**	**5.25**
		WE	6.25	5.13	4.91	4.14	4.46	4.26	4.86
	P2.8	WD	**6.29**	**5.93**	**5.90**	**5.22**	**5.11**	**5.74**	**5.70**
		WE	---	6.35	5.55	---	4.30	---	5.40
Three	J3.1	WD	**5.32**	**4.83**	**3.86**	**3.48**	**4.01**	**4.60**	**4.35**
		WE	---	---	4.06	---	---	---	4.06
	J3.3	WD	**6.11**	**5.39**	**4.70**	**4.21**	**5.01**	**5.97**	**5.23**
		WE	---	5.46	6.70	---	---	---	6.08
	J3.8	WD	---	**5.72**	**5.63**	---	**5.23**	**5.48**	**5.52**
		WE	---	8.84	---	4.71	---	---	6.78
	J4.2	WD	**6.13**	**5.45**	**4.92**	**4.26**	**4.54**	**5.07**	**5.06**
		WE	---	---	4.21	---	---	---	4.21
	J4.7	WD	**5.23**	**4.95**	**4.52**	**4.04**	**4.08**	**5.22**	**4.67**
		WE	---	---	4.19	---	---	---	4.19
Four	C1.2	WD	**5.99**	**6.34**	**5.40**	**4.33**	---	**5.64**	**5.54**
		WE	---	---	5.30	---	---	5.10	5.20
	C2.8	WD	**4.94**	**5.06**	**4.28**	**3.97**	---	**4.47**	**4.55**
		WE	4.37	---	4.31	---	4.07	4.39	4.29

The calculated α parameter is shown in Table 5.3.

Table 5.3. Load model parameters for different transformers (α)

Substation	**Transformer & Day**		**α**						
			AM			**PM**			**Average**
	F.	**D.**	**0 to 4**	**4 to 8**	**8 to 12**	**12 to 4**	**4 to 8**	**8 to 12**	
One	M1.1	WD	**3.69**	**3.13**	**4.20**	**4.18**	**2.63**	**3.26**	**3.52**
		WE	---	3.25	4.32	4.51	---	---	4.03
	M2.1	WD	**2.96**	**3.00**	**3.78**	**4.72**	**2.31**	**3.00**	**3.30**
		WE	---	---	3.92	---	---	---	3.92
	M3.1	WD	**4.07**	**4.28**	**3.86**	**4.50**	**3.41**	**3.81**	**3.99**
		WE	4.12	4.38	---	---	---	3.9	4.13
Two	P1.1	WD	**1.51**	**2.02**	**1.46**	**1.08**	**1.64**	**1.60**	**1.55**
		WE	1.53	2.5	1.35	---	---	---	1.79
	P1.2	WD	**2.40**	**3.32**	**2.41**	**2.37**	**2.15**	**2.02**	**2.44**
		WE	2.43	3.56	2.91	2.84	---	---	2.94
	P2.7	WD	**2.16**	**2.21**	**2.15**	**2.12**	**2.09**	**1.78**	**2.08**
		WE	2.09	2.36	2.24	2.05	2.13	1.93	2.13
	P2.8	WD	**2.93**	**3.72**	**2.79**	**2.79**	**2.47**	**2.41**	**2.85**
		WE	---	3.16	3.01	---	2.84	---	3.00
Three	J3.1	WD	**2.06**	**2.19**	**2.16**	**1.29**	**1.73**	**1.83**	**1.88**
		WE	---	---	2.38	---	---	---	2.38
	J3.3	WD	**1.70**	**1.87**	**1.62**	**1.58**	**1.72**	**1.70**	**1.70**
		WE	---	1.93	2.01	---	---	---	1.97
	J3.8	WD	---	**2.07**	**3.12**	---	**1.46**	**1.88**	**2.13**
		WE	---	2.21	---	1.66			1.94
	J4.2	WD	**2.03**	**2.36**	**1.81**	**1.61**	**1.73**	**1.74**	**1.88**
		WE	---	---	1.79	---	---	---	1.79
	J4.7	WD	**1.85**	**2.77**	**1.49**	**1.55**	**1.48**	**1.57**	**1.78**
		WE	---	---	1.54	---	---	---	1.54
Four	C1.2	WD	**3.28**	**4.75**	**3.27**	**2.59**	---	**2.67**	**3.31**
		WE	---	---	3.65	---	---	2.98	3.32
	C2.8	WD	**2.63**	**4.17**	**3.12**	**2.36**	---	**2.44**	**2.78**
		WE	2.75	---	3.15	---	2.08	2.35	2.58

The calculated β parameter is shown in Table 5.4.

Table 5.4. Load model parameters for different transformers (β)

Substation	**Transformer & Day**		β						
			AM			**PM**			
	F.	**D.**	**0 to 4**	**4 to 8**	**8 to 12**	**12 to 4**	**4 to 8**	**8 to 12**	**Average**
One	M1.1	WD	**9.61**	**7.68**	**7.98**	**8.60**	**7.30**	**8.78**	**8.23**
		WE	---	7.85	8.02	8.65	---	---	8.17
	M2.1	WD	**8.54**	**7.66**	**8.11**	**8.05**	**6.96**	**8.63**	**7.86**
		WE	---	---	7.93	---	---	---	7.93
	M3.1	WD	**11.63**	**11.78**	**11.73**	**13.40**	**11.54**	**13.60**	**12.02**
		WE	11.32	11.35	---	---	---	11.65	11.34
Two	P1.1	WD	**7.00**	**7.88**	**6.75**	**6.19**	**7.24**	**6.91**	**7.01**
		WE	6.95	6.59	6.59	---	---	---	6.71
	P1.2	WD	**9.16**	**9.91**	**7.87**	**7.86**	**7.64**	**7.78**	**8.49**
		WE	9.32	10.24	7.26	8.05	---	---	8.72
	P2.7	WD	**8.16**	**8.92**	**8.43**	**8.18**	**8.07**	**7.84**	**8.35**
		WE	8.73	9.18	8.42	7.93	8.12	8.06	8.48
	P2.8	WD	**9.23**	**9.81**	**8.78**	**7.99**	**8.19**	**8.74**	**8.80**
		WE	---	10.02	9.31	---	8.35	---	9.23
Three	J3.1	WD	**7.64**	**7.04**	**6.87**	**5.34**	**6.27**	**7.43**	**6.63**
		WE	---	---	6.97	---	---	---	6.97
	J3.3	WD	**10.13**	**8.76**	**7.78**	**6.80**	**8.09**	**9.51**	**8.31**
		WE	---	8.96	8.14	---	---	---	8.55
	J3.8	WD	---	**7.20**	**8.10**	---	**6.14**	**7.66**	**7.15**
		WE	---	7.24	---	6.1	---	---	6.67
	J4.2	WD	**8.26**	**7.65**	**6.30**	**5.58**	**6.31**	**7.42**	**6.82**
		WE	---	---	6.21	---	---	---	6.21
	J4.7	WD	**7.47**	**8.08**	**6.00**	**5.62**	**6.23**	**6.89**	**6.68**
		WE	---	---	5.96	---	---	---	5.96
Four	C1.2	WD	**11.04**	**11.79**	**9.07**	**8.23**	---	**9.42**	**10.03**
		WE	---	---	9.38	---	---	9.33	9.38
	C2.8	WD	**7.68**	**8.02**	**7.56**	**6.11**	**6.72**	**6.89**	**7.22**
		WE	7.86	---	8.01	---	6.84	7.16	7.57

The calculated T_p parameter is shown in Table 5.5.

Table 5.5. Load model parameters for different transformers (T_p)

Substation	Transformer & Day		T_p						
			AM			PM			
	F.	D.	0 to 4	4 to 8	8 to 12	12 to 4	4 to 8	8 to 12	Average
One	M1.1	WD	**0.15**	**0.17**	**0.13**	**0.16**	**0.15**	**0.13**	**0.15**
		WE	---	0.17	0.12	0.15	---	---	0.15
	M2.1	WD	**0.11**	**0.17**	**0.12**	**0.13**	**0.13**	**0.12**	**0.13**
		WE	---	---	0.12	---	---	---	0.12
	M3.1	WD	**0.19**	**0.16**	**0.17**	**0.13**	**0.16**	**0.16**	**0.16**
		WE	0.19	0.15	---	---	---	3.9	1.41
Two	P1.1	WD	**0.09**	**0.11**	**0.10**	**0.11**	**0.10**	**0.08**	**0.10**
		WE	0.1	0.1	0.11	---	---	---	0.10
	P1.2	WD	**0.13**	**0.14**	**0.13**	**0.13**	**0.09**	**0.13**	**0.13**
		WE	0.13	0.12	0.14	0.13	---	---	0.13
	P2.7	WD	**0.13**	**0.13**	**0.12**	**0.11**	**0.11**	**0.11**	**0.12**
		WE	0.13	0.12	0.13	0.11	0.12	0.11	0.12
	P2.8	WD	**0.12**	**0.17**	**0.15**	**0.15**	**0.13**	**0.13**	**0.14**
		WE	---	0.16	0.14	---	0.13	---	0.14
Three	J3.1	WD	**0.09**	**0.11**	**0.13**	**0.08**	**0.11**	**0.10**	**0.10**
		WE	---	---	0.13	---	---	---	0.13
	J3.3	WD	**0.08**	**0.11**	**0.09**	**0.09**	**0.09**	**0.10**	**0.09**
		WE	---	0.12	0.09	---	---	---	0.11
	J3.8	WD	---	**0.08**	**0.10**	**0.18**	**0.10**	**0.09**	**0.11**
		WE	---	0.09	---	0.17	---	---	0.13
	J4.2	WD	**0.10**	**0.13**	**0.10**	**0.12**	**0.10**	**0.09**	**0.11**
		WE	---	---	0.11	---	---	---	0.11
	J4.7	WD	**0.09**	**0.11**	**0.09**	**0.07**	**0.09**	**0.10**	**0.09**
		WE	---	---	0.08	---	---	---	0.08
Four	C1.2	WD	**0.16**	**0.20**	**0.14**	**0.17**	---	**0.15**	**0.16**
		WE	---	---	0.13	---	---	0.15	0.14
	C2.8	WD	**0.14**	**0.18**	**0.15**	**0.16**	**0.13**	**0.14**	**0.15**
		WE	0.14	---	0.14	---	0.13	0.15	0.14

The calculated T_q parameter is shown in Table 5.6.

Table 5.6. Load model parameters for different transformers (T_q)

Substation	**Transformer & Day**		T_q						
			AM			**PM**			
	F.	**D.**	**0 to 4**	**4 to 8**	**8 to 12**	**12 to 4**	**4 to 8**	**8 to 12**	**Average**
One	M1.1	WD	**0.13**	**0.18**	**0.19**	**0.25**	**0.17**	**0.16**	**0.19**
		WE	---	0.18	0.18	0.24	---	---	0.20
	M2.1	WD	**0.14**	**0.20**	**0.14**	**0.15**	**0.20**	**0.15**	**0.17**
		WE	---	---	0.15	---	---	---	0.15
	M3.1	WD	**0.17**	**0.21**	**0.16**	**0.18**	**0.22**	**0.20**	**0.19**
		WE	0.18	0.23	---	---	---	11.65	0.21
Two	P1.1	WD	**0.24**	**0.26**	**0.25**	**0.29**	**0.29**	**0.25**	**0.27**
		WE	0.23	0.24	0.25	---	---	---	0.24
	P1.2	WD	**0.18**	**0.17**	**0.18**	**0.12**	**0.17**	**0.14**	**0.16**
		WE	0.18	0.18	0.19	0.13	---	---	0.17
	P2.7	WD	**0.19**	**0.22**	**0.23**	**0.21**	**0.18**	**0.20**	**0.21**
		WE	0.18	0.22	0.22	0.21	0.19	0.19	0.20
	P2.8	WD	**0.21**	**0.17**	**0.19**	**0.17**	**0.18**	**0.17**	**0.18**
		WE	---	0.15	0.18	---	0.19	---	0.17
Three	J3.1	WD	**0.13**	**0.14**	**0.20**	**0.19**	**0.16**	**0.17**	**0.16**
		WE	---	---	0.21	---	---	---	0.21
	J3.3	WD	**0.17**	**0.21**	**0.18**	**0.19**	**0.17**	**0.17**	**0.18**
		WE	---	0.2	0.19	---	---	---	0.20
	J3.8	WD	---	**0.14**	**0.14**	**0.15**	**0.11**	**0.14**	**0.14**
		WE	---	0.15	---	0.16	---	---	0.16
	J4.2	WD	**0.12**	**0.15**	**0.14**	**0.16**	**0.15**	**0.15**	**0.14**
		WE	---	---	0.13	---	---	---	0.13
	J4.7	WD	**0.11**	**0.21**	**0.18**	**0.13**	**0.16**	**0.17**	**0.16**
		WE	---	---	0.18	---	---	---	0.18
Four	C1.2	WD	**0.13**	**0.19**	**0.17**	**0.21**	---	**0.18**	**0.17**
		WE	---	---	0.18	---	---	0.19	0.18
	C2.8	WD	**0.18**	**0.19**	**0.17**	**0.17**	**0.13**	**0.16**	**0.17**
		WE	0.18	---	0.17	---	0.12	0.17	0.16

The presented load model parameter for each segment is the average of the parameter during the four-hour segment. In some cases where no tap movement occurred, the value is shown as ‘---‘. In practice, the parameter for this segment could be estimated by interpolating from the other segments. Therefore, we can obtain the load model parameters for any time during the day.

5.3 Typical Load Parameters for Different Load Types

As was explained in Chapter Four, the measured transformers are grouped into four different types. In order to compare the load parameters in the different groups, in this section the average of the load parameters in each group is presented in Table 5.7.

Table 5.7. The calculated load parameters for different groups

Transformer Type \ Hour of Day		0 to 4	4 to 8	8 to 12	12 to 16	16 to 20	20 to 23
Commercial and Residential	"a"	1.193	1.119	1.027	1.008	1.046	1.070
	Alpha	2.974	3.322	3.287	3.369	2.391	2.821
	T_p	0.137	0.159	0.132	0.139	0.135	0.125
	"b"	5.891	5.415	5.259	4.822	4.459	5.341
	Beta	8.891	8.604	8.424	8.469	7.953	8.961
	T_q	0.171	0.208	0.181	0.209	0.204	0.183
Mostly Residential	"a"	1.055	1.068	1.092	1.054	1.047	1.035
	Alpha	2.691	3.500	2.653	2.467	2.232	2.221
	T_p	0.134	0.160	0.132	0.142	0.111	0.127
	"b"	6.112	5.734	5.378	4.920	5.195	5.442
	Beta	9.401	10.105	8.539	8.065	7.965	8.447
	T_q	0.178	0.189	0.194	0.174	0.174	0.172
Mostly Commercial	"a"	0.944	1.002	0.771	0.681	0.894	0.911
	Alpha	1.910	2.251	2.040	1.538	1.624	1.744
	T_p	0.091	0.108	0.099	0.107	0.096	0.096
	"b"	5.710	5.367	4.736	4.228	4.588	5.243
	Beta	8.375	7.746	7.010	5.890	6.610	7.780
	T_q	0.133	0.170	0.166	0.165	0.150	0.161

The tabulated load parameters are related to three groups, commercial and residential, mainly residential, and mainly commercial. As Table 5.7 shows, the calculated parameters for the residential loads are almost larger than those for the commercial loads. This finding is more clear in Figures 5.1, 5.2 and 5.3.

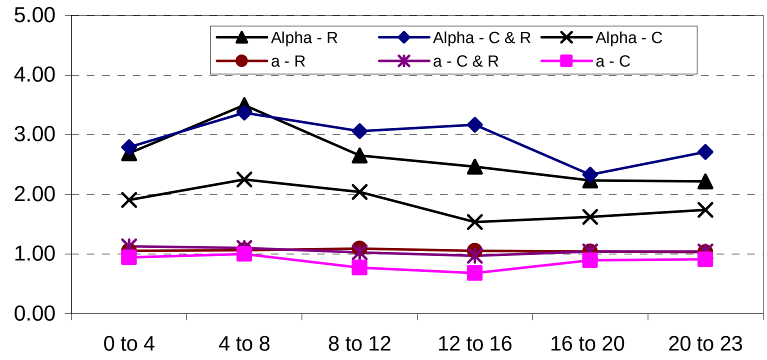

Figure 5.1. Typical calculated “a” and α for different groups of loads

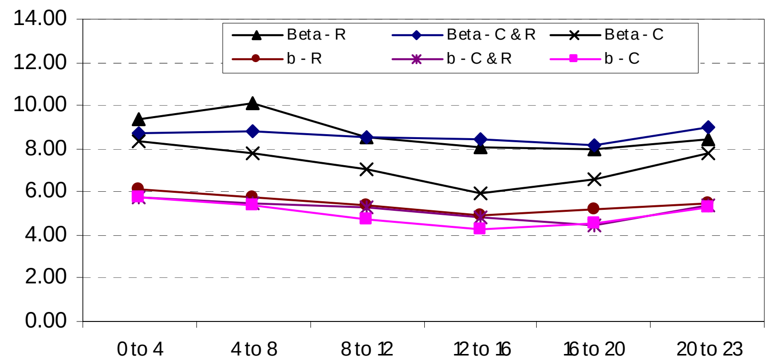

Figure 5.2. Typical calculated “b” and β for different groups of loads

Figures 5.1 and 5.2 show that the transient load parameters α and β, for all the three groups of loads, are larger than *“a”* and *“b”*. It is also seen that the commercial loads have the lowest values for the four load parameters, α, β, *“a”* and *“b”*. The calculated *“a”* and *“b”* are the highest for the residential loads during the day.

Figure 5.3 shows the calculated τ_p and τ_q for different groups of loads.

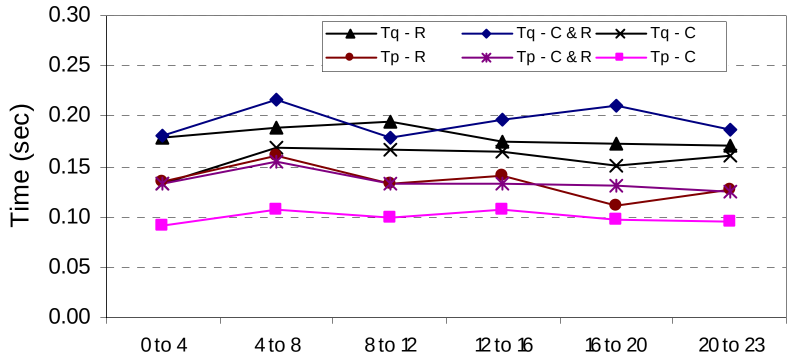

Figure 5.3. Typical calculated τ_p and τ_q for different groups of loads

It reveals that the recovery time for reactive power is longer than the one for real power. It also reveals that the commercial loads have the shortest recovery time while the longest recovery time varies for residential and "commercial and residential" load types.

The variation of load parameters in percentage of the mean values during the day, for different load types, is presented in Table 5.8.

Table 5.8. Average variation of load parameters during the day (%)

Group	a	b	α	β	τ_p	τ_q
Commercial and residential	4.1	10.1	4.9	7.2	2.8	6.6
Mostly residential	1.6	11.2	8.2	5.6	7.6	4.1
Mostly commercial	10.9	11.7	5.3	9.3	10.1	6.7

Table 5.8 reveals that the load parameters *"a"*, *"b"*, τ_p and τ_q have more variations for commercial loads, while from the other two parameters, variation of α and β is maximum for residential and commercial loads, respectively.

The studies in this section show that the load parameters are varying during the day and their daily variations are not similar for different types of loads, which makes the online monitoring of the load parameters more reasonable.

5.4 Load Parameters versus Load Profiles

This section presents the load profiles and the calculated load model parameters for the substations. Figures 5.4-5.7 show the time of the tap change and the load variation simultaneously. In order to see the time of tap movement, only the parameters “a” and “b” are shown in the figures. The calculated parameters are for a period of one week. Since more than one parameter was calculated for each hour, the average for each hour is shown in the figures. As they reveal, the tap movements occurred at different load levels, even at the peak of the load. The calculated results for only two transformers from each substation are presented here, and the rest are presented in Appendix E.

A. Substation One

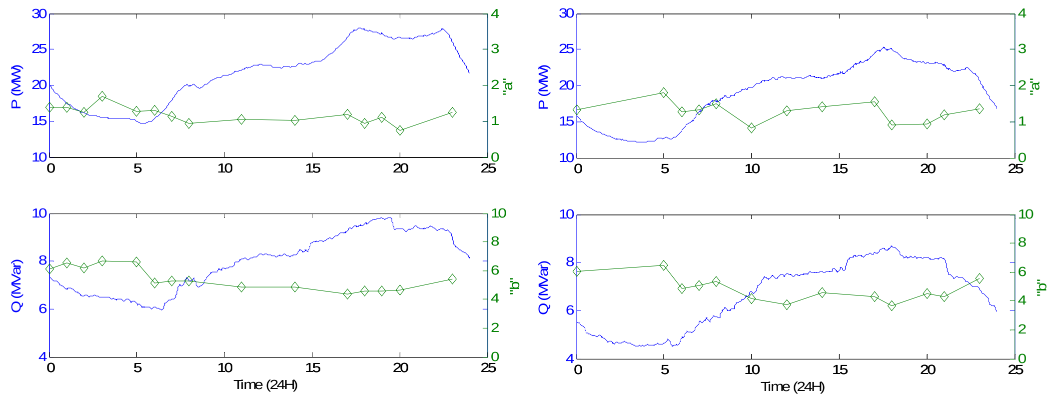

Figure 5.4. Transformers M1.1 & M2.1–Commercial and Residential

B. Substation Two

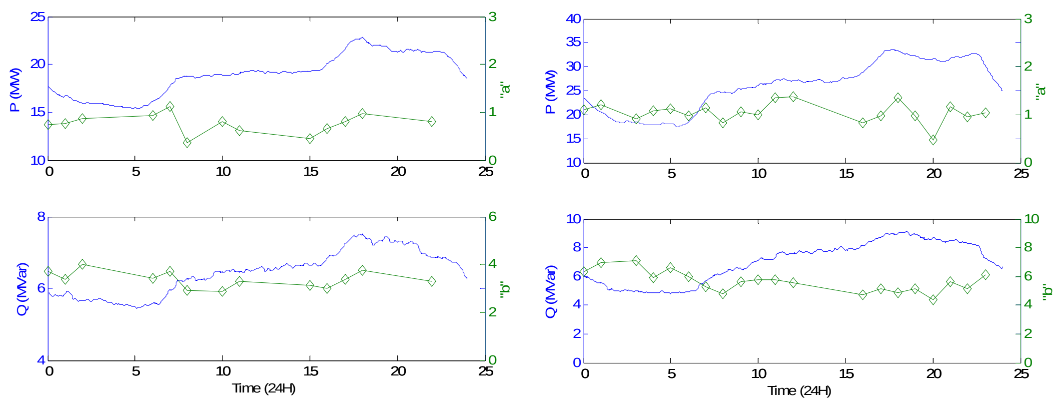

Figure 5.5. Transformers P1.1–Commercial & Residential & P1.2–Residential

C. Substation Three

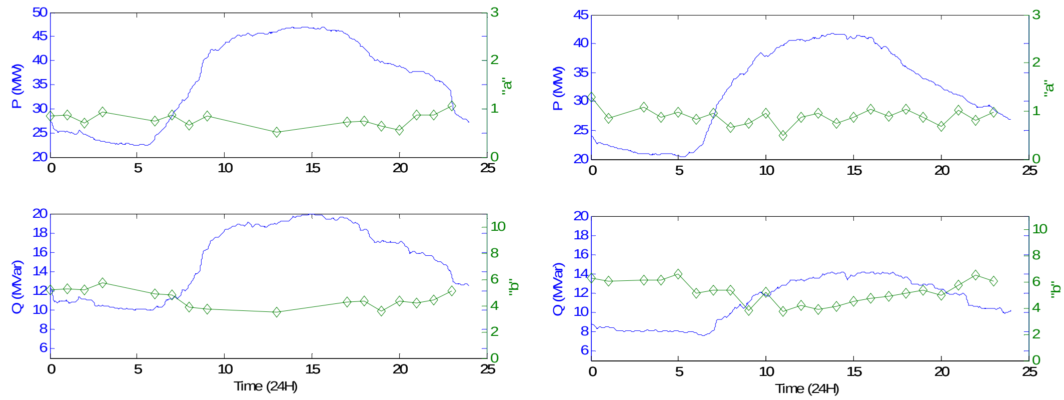

Figure 5.6. Transformer J3.1 & J3.3–Mostly Commercial

D. Substation Four

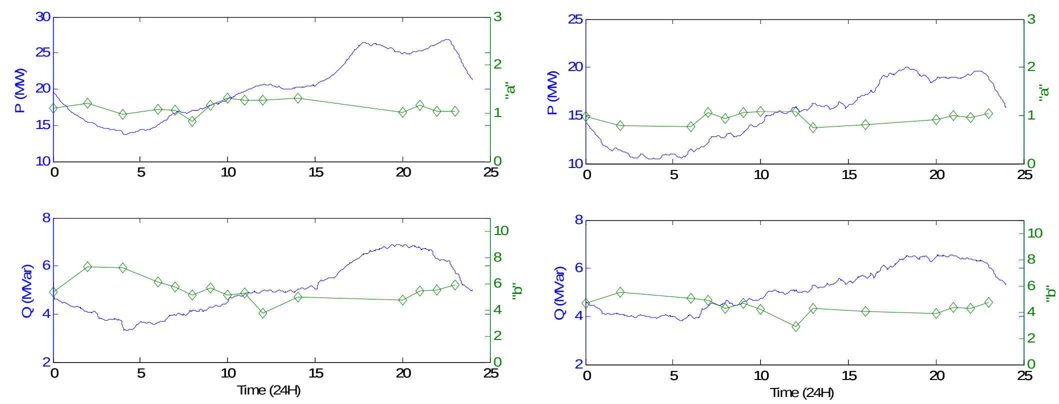

Figure 5.7. Transformers C1.2-Residential & C2.8-Commercial & Residential

The load profiles and calculated load parameters for all the transformers were studied, and Figures 5.4-5.7 show that the load profiles of each group are similar and that the calculated load parameters are almost the same for the transformers in the same group. Tap movement can occur at any time. Thus one can obtain accurate load models for every hour of the day. The load model parameters vary during each 24-hour period, based on the type of loads connected to the system.

5.4.1 Load Classifications According to Groups

The load profiles and calculated load model parameters for the different groups defined in Chapter Four are plotted together in Figures 5.8-5.11.

A. Group I – Commercial and Residential

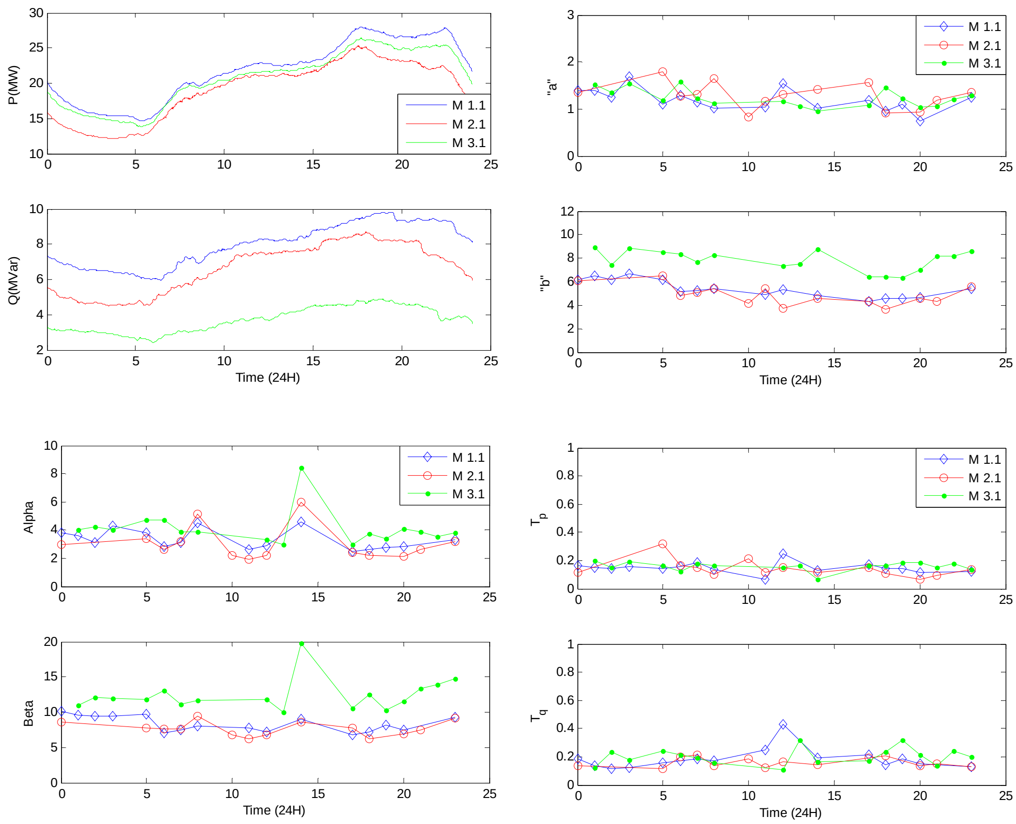

Figure 5.8. Power profile, Load model parameters during 24H

B. Group II – Commercial and Residential

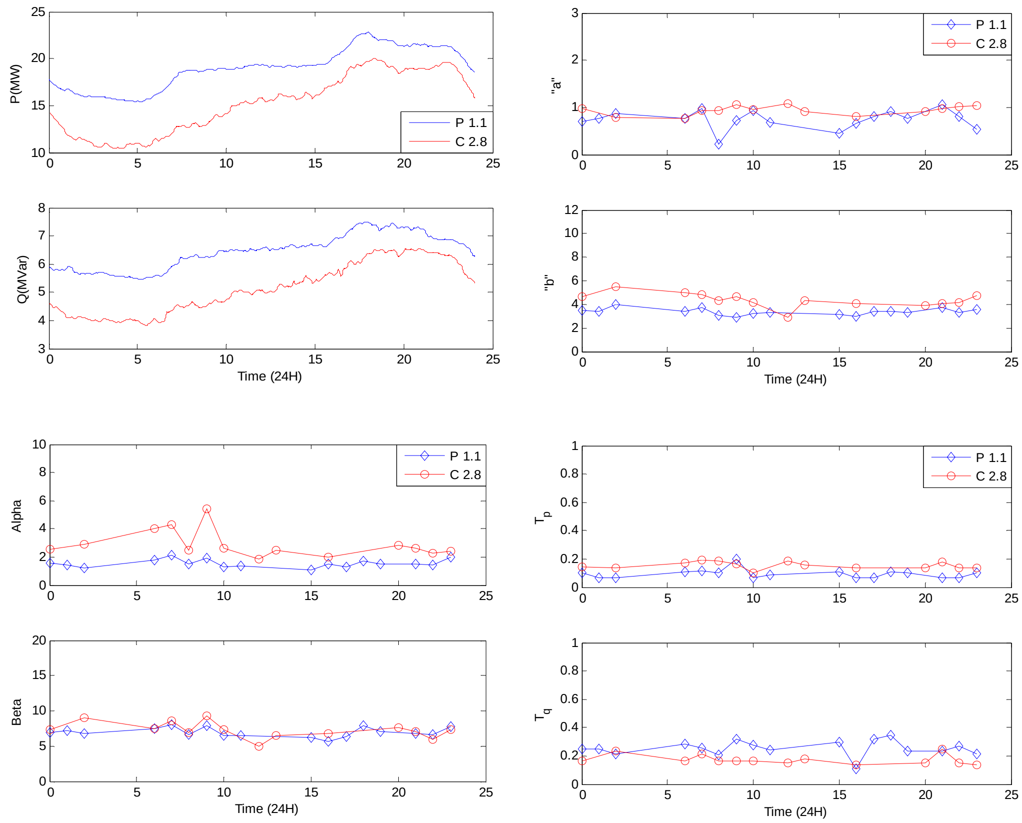

Figure 5.9. Power profile, Load model parameters during 24H

C. Group III – Mostly Residential

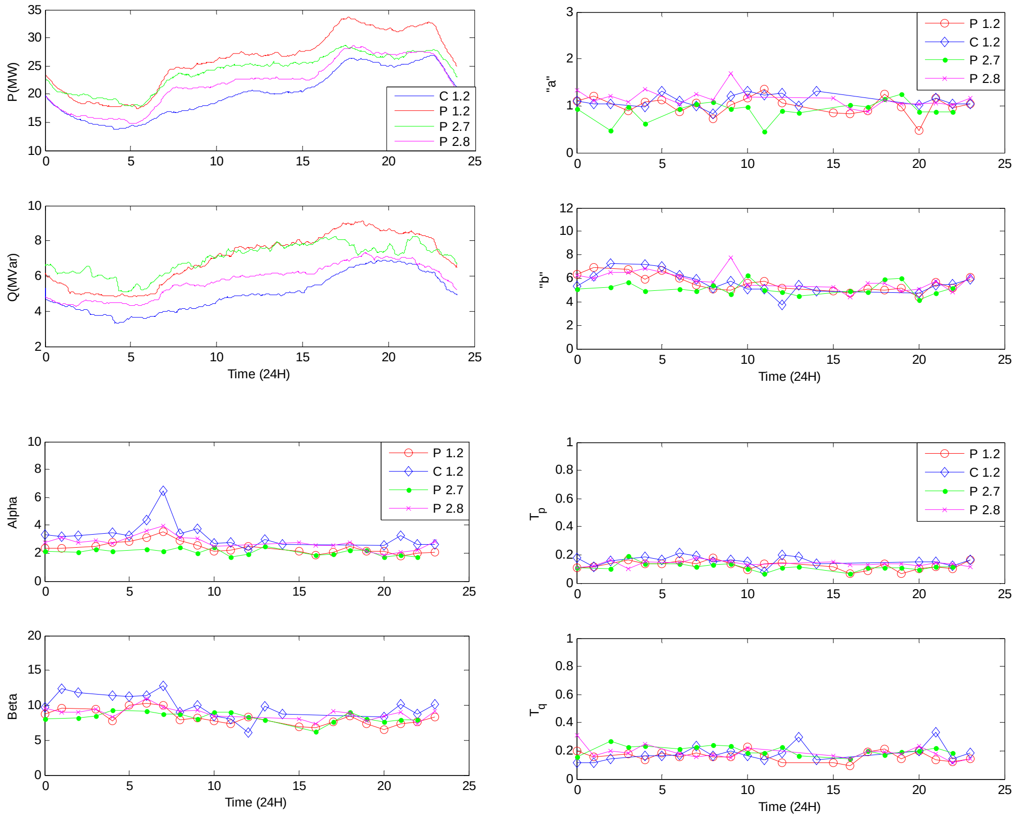

Figure 5.10. Power profile, Load model parameters during 24H

D. Group IV – Mostly Commercial

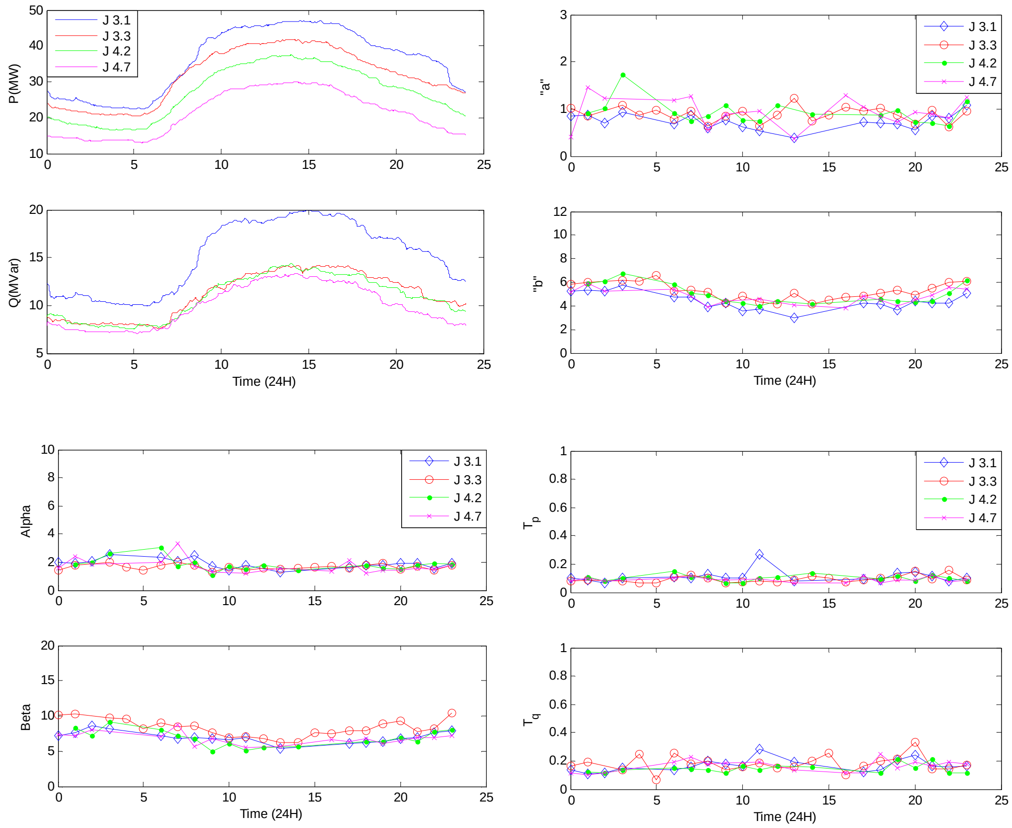

Figure 5.11. Power profile, Load model parameters during 24H

Figures 5.8-5.11 show that the load profiles of each group are similar and that the calculated load parameters are almost the same for transformers in the same group. Since the load types and load profiles of the transformers are similar, we expected to have similar model parameters for the loads in each group, and the plotted graphs confirm this expectation.

The following are the conclusions for this study:

- A tap movement can happen at any time during the day.
- The load parameters vary during each 24-hour period.
- The parameters vary based on the type of load.
- Similar loads have similar transformer load profiles.
- Similar loads have similar load parameters.

5.5 Load Parameters as Affected by Voltage Step Change

The load model parameters versus the step change in the voltage caused by tap movement are plotted in Figures 5.12-5.15 for the weekdays. For each plot, the taps occurring during a one-week period are shown. These entire tap movements were used to calculate the load model parameters. The calculated results for only two transformers from each substation are presented here, and the rest are presented in Appendix E.

A. Substation One

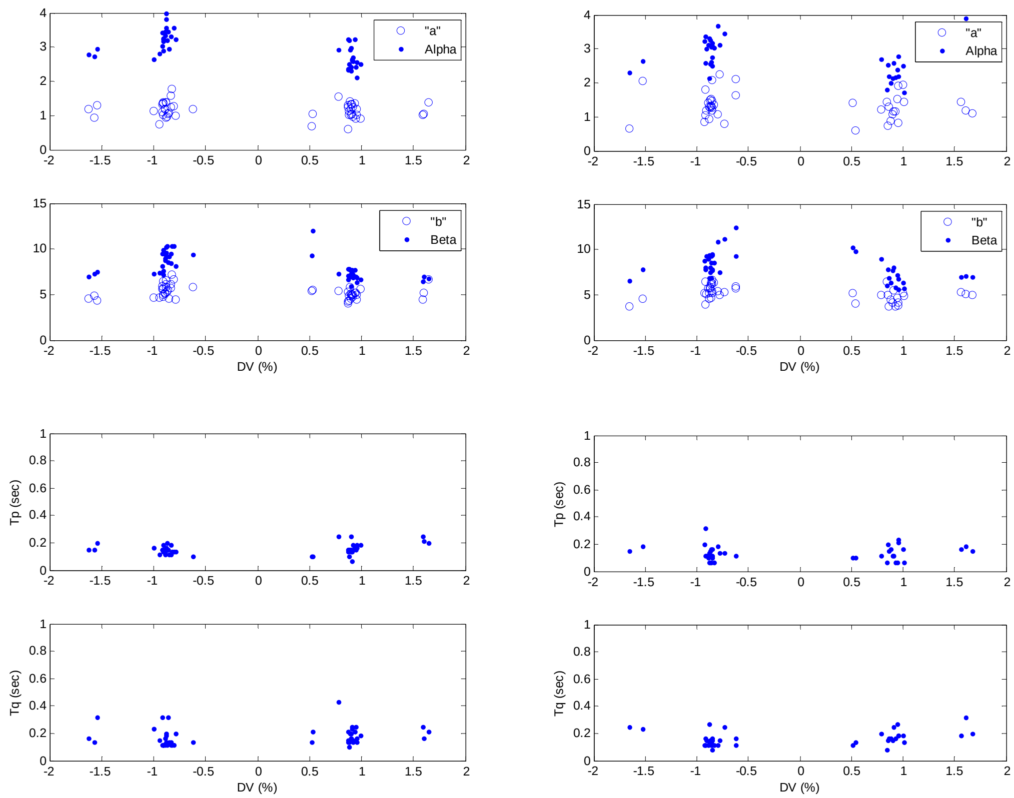

Figure 5.12. Transformers M1.1 & M2.1–Commercial and Residential

B. Substation Two

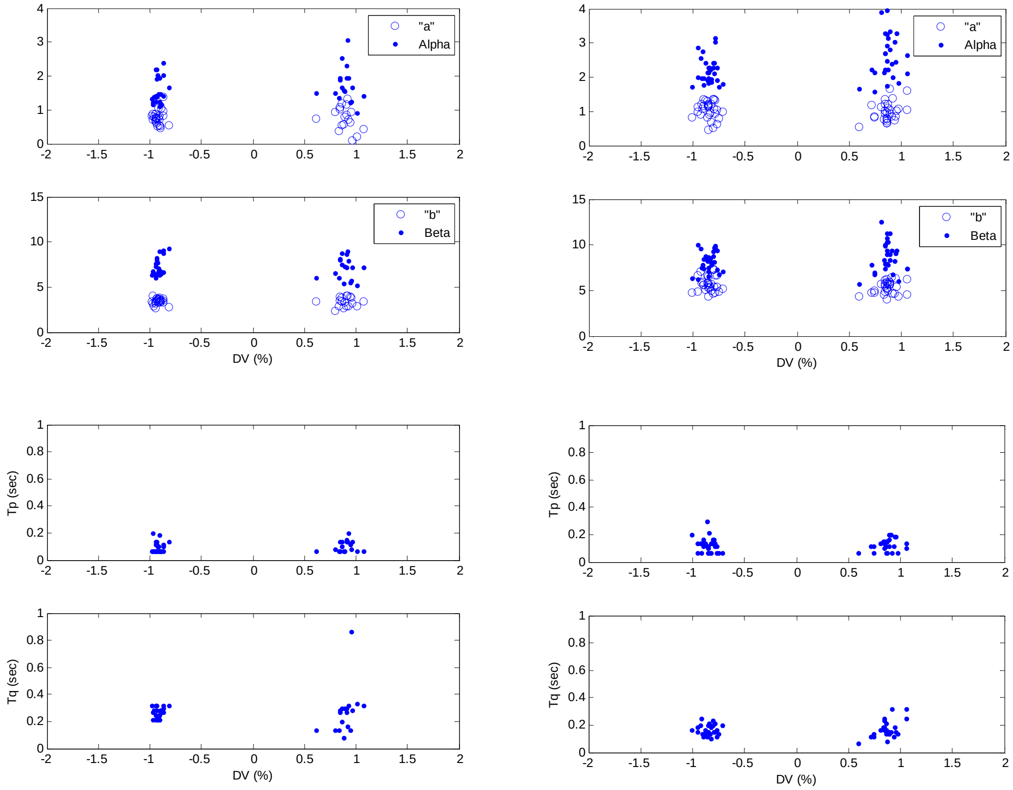

Figure 5.13. Transformers P1.1-Commercial, Residential & P1.2-Residential

C. Substation Three

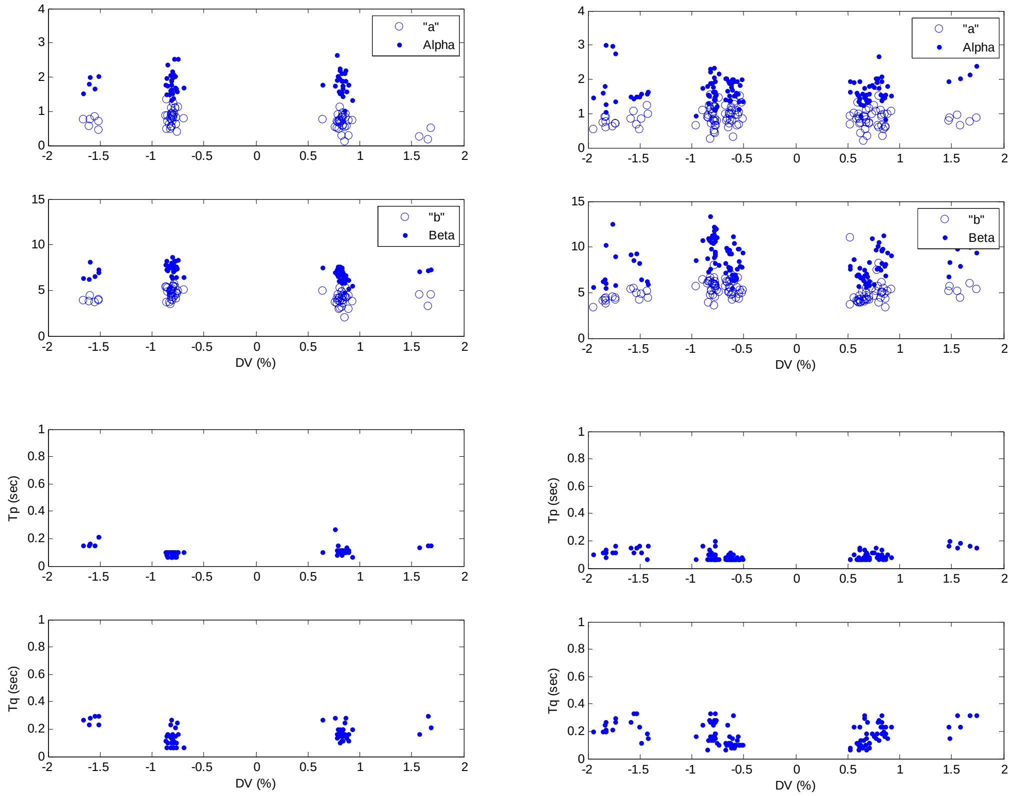

Figure 5.14. Transformer J3.1 & J3.3–Mostly Commercial

D. Substation Four

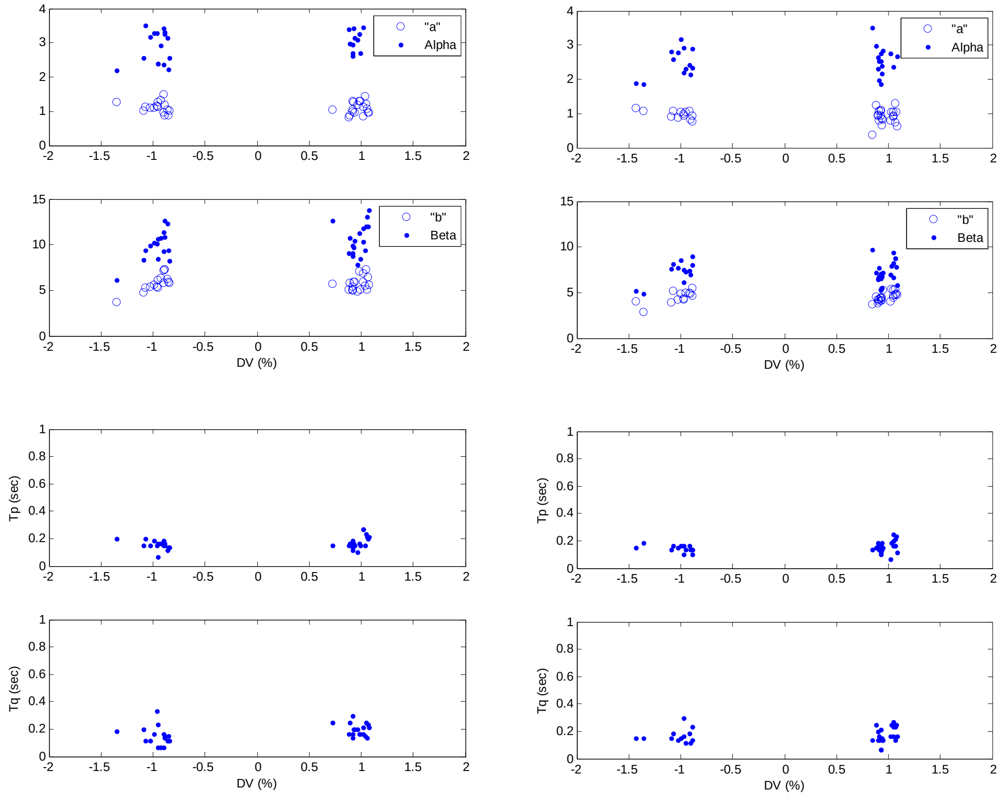

Figure 5.15. Transformers C1.2-Residential & C2.8-Commercial, Residential

Figures 5.12-5.15 show that almost all the step changes are around one percent of the initial voltage and that the step-up and –down tap changes did not affect the calculated load model parameters for all the measured transformers. This very important information doubles the number of tap movements that can be used for load modeling and therefore increases the accuracy of the calculated results.

The following are the conclusions from this study:

- Almost all the tap changes cause a step change in voltage of around one percent.
- The step-up or step-down tap movements are the same in terms of the parameters' calculations.
- Both the step-up and step-down tap movements provide the same load data parameters.
- The tap movements can happen at any time in each 24-hour period.
- The step change in the voltage does not depend on the time of tap movement.

5.6 Load Parameters as Affected by Pre-tap Values of the Loads

In this section, the effects of the pre-tap voltage and the active and reactive power on the load model parameters are investigated. All the calculated parameters shown in Figures 5.16-5.19 are for the weekdays. The calculated parameters for only one transformer from each substation are presented here, and the rest are presented Appendix E.

A. Substation One

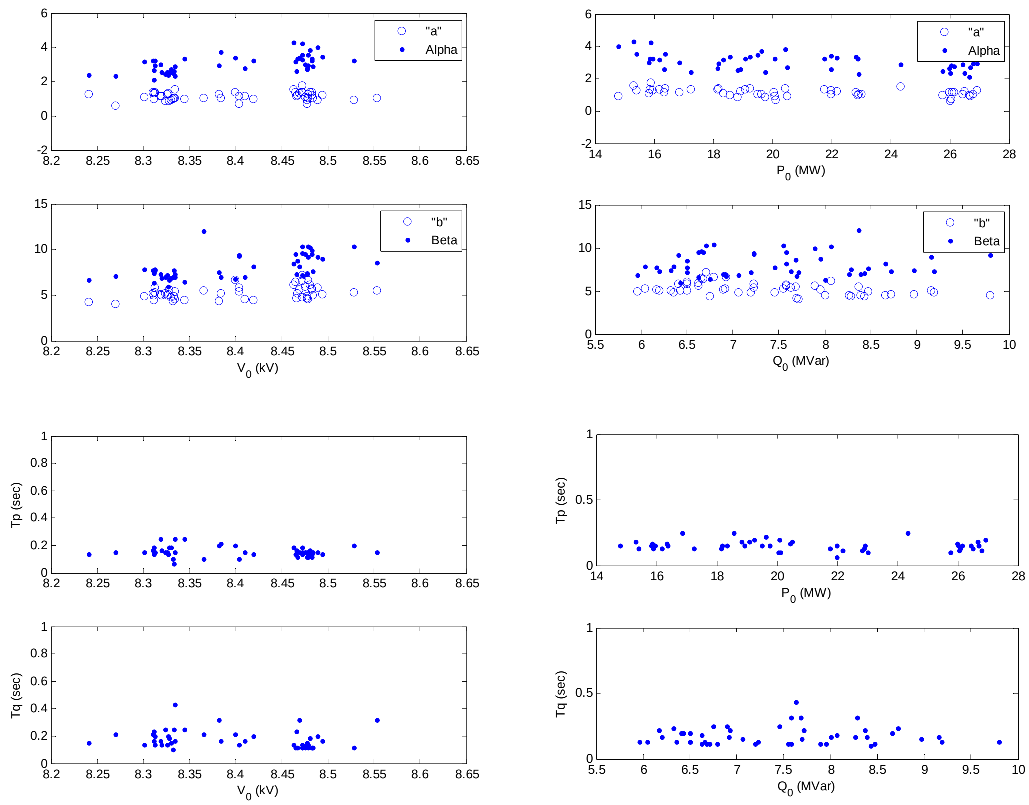

Figure 5.16. Transformer M1.1–Commercial and Residential

B. Substation Two

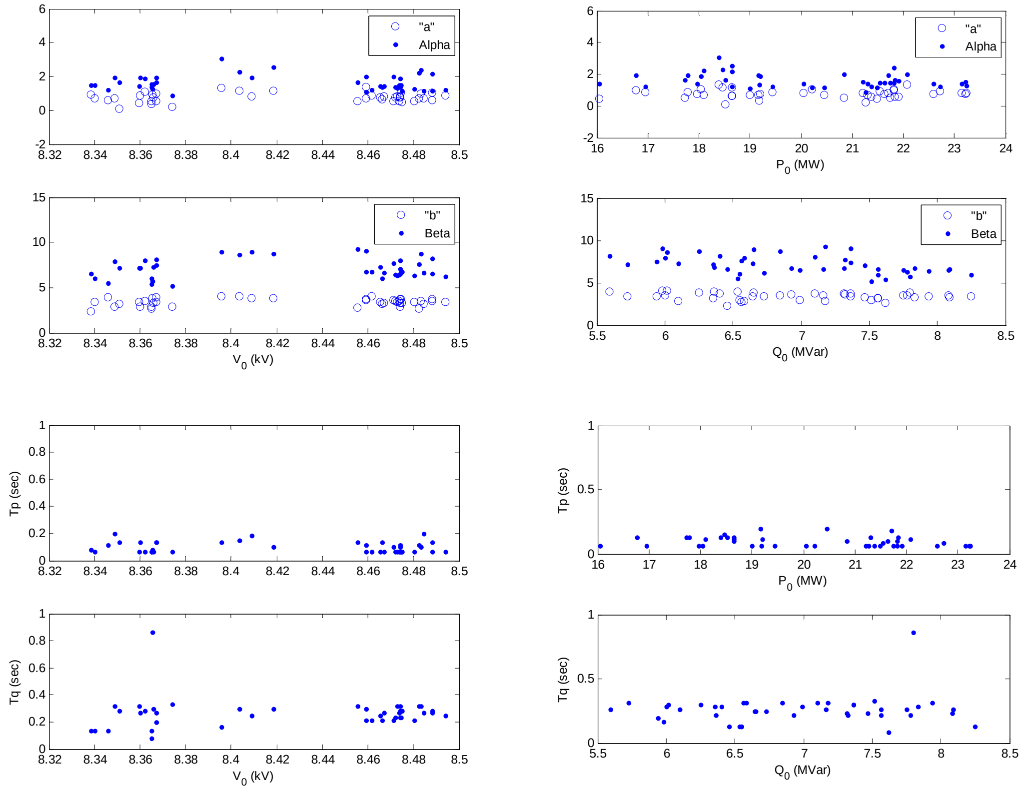

Figure 5.17. Transformer P1.1–Commercial and Residential

C. Substation Three

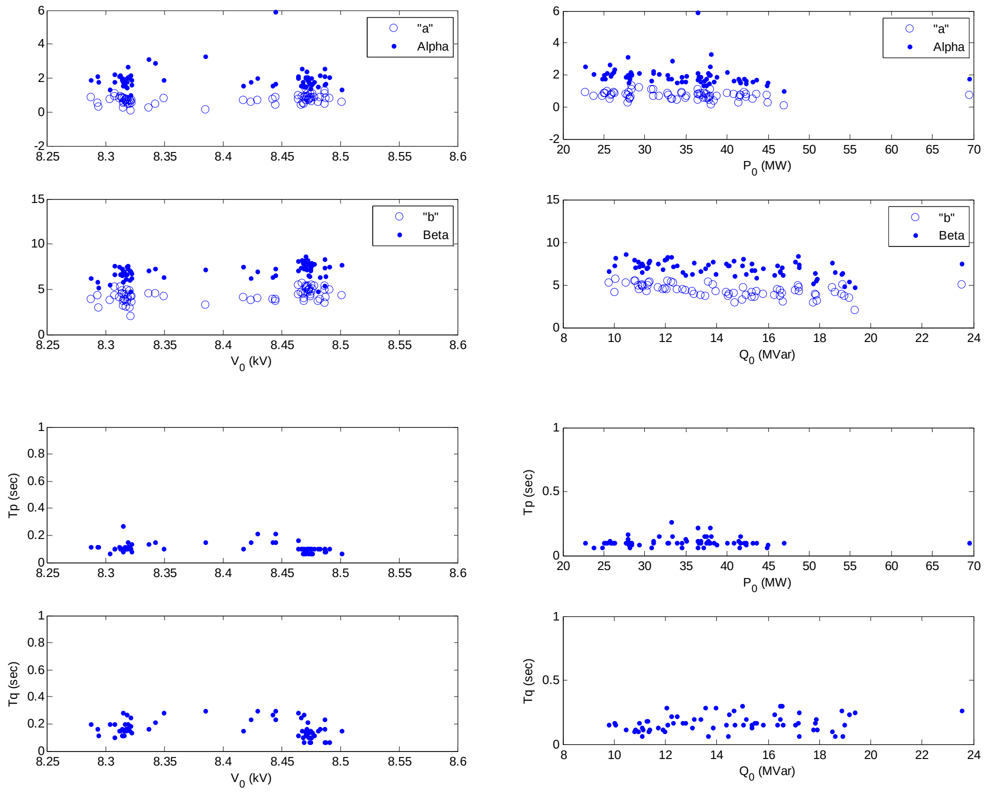

Figure 5.18. Transformer J3.1–Mostly Commercial

D. Substation Four

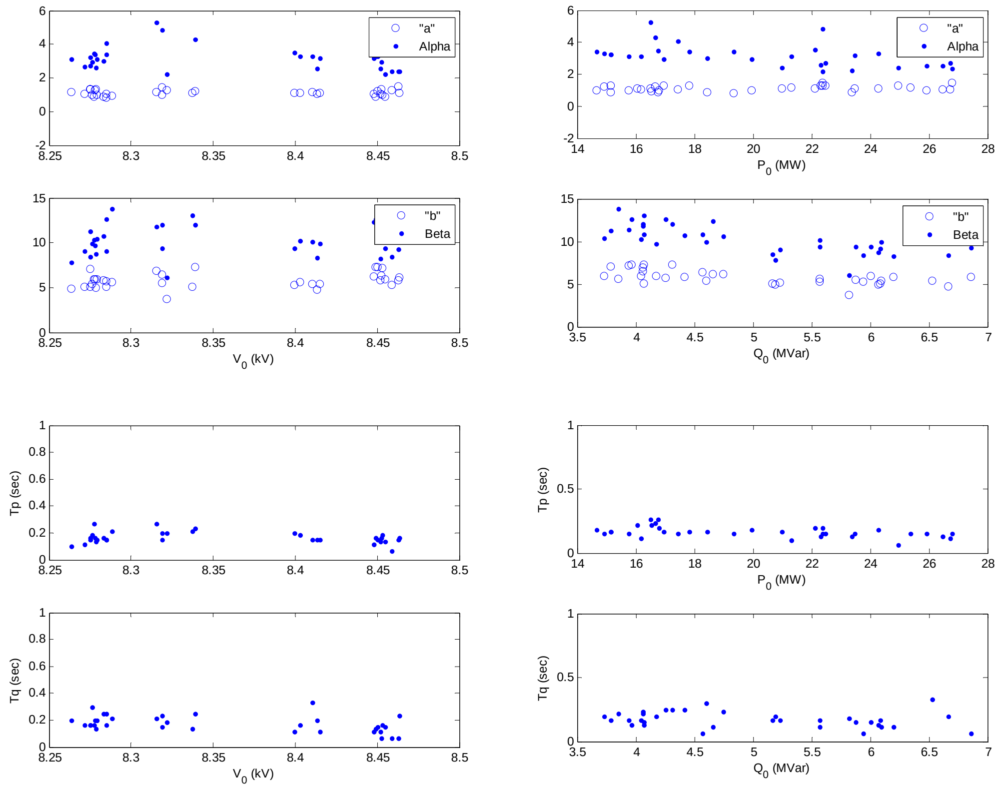

Figure 5.19. Transformer C1.2–Mostly Residential

The results show that the calculated parameters are not functions of pre-tap values and do not depend on them. Since the plots for a period of one week, the small deviation in the calculated parameters could be the result of variations in the load kinds for different days and different times of the day.

Our conclusions are presented as follows:

- The tap movements can occur at any initial voltage.
- The tap movements can occur at any initial active or reactive power.
- The load model parameters do not depend on the pre-tap voltage.
- The load model parameters do not depend on the pre-tap active or pre-tap reactive power.

5.7 Abnormal Cases

The load modeling algorithm is based on the fact that the system side changes while the load side is constant. In this condition, if the load and system change at the same time, the load side parameters cannot be identified. Therefore, for the load modeling procedure, the cases in which the load varies during the tap movement cannot be used for calculating the load model parameters and should be omitted from the calculations. This section investigates the abnormal cases where the tap movement data cannot be used for estimating the load model parameters. For this purpose, all the tap data captured from all the transformers were investigated. The results show that if the load was not constant during a tap movement, then the step change in the voltage and the corresponding changes in the active and reactive power were not useful for load parameters estimation.

As an example from three of the substations, one transformer was selected, and the voltage and active and reactive power for one case where the values of “a” and “b” were suspicious were plotted.

5.7.1 Substation One, Transformer M1.2

Figure 5.19 shows the variation of the load for a 24-hour period. As figure 5.20 shows, the calculated parameters have large variation even within a one-hour period.

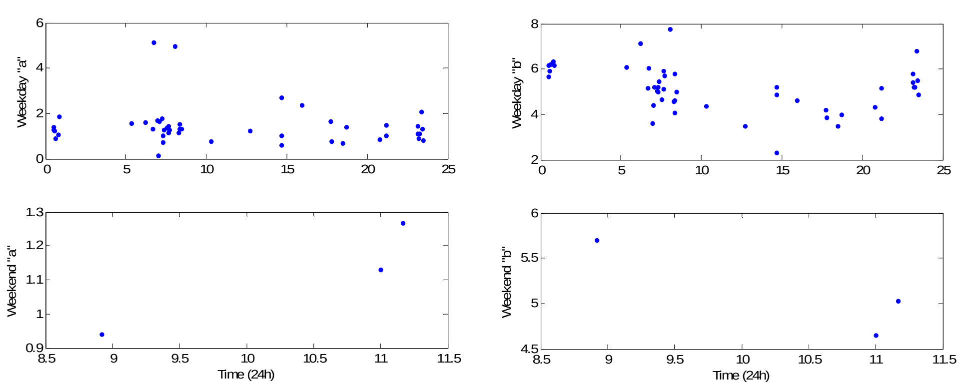

Figure 5.20. Transformer M1.2–Commercial and Residential

As an example, one of the most severe cases is presented in detail in Table 5.9.

Table 5.9. An example of an abnormal case for Transformer M1.2

Calculated Parameter	**Value**
DV	0.84%
DP	4.24%
DQ	6.71%
Load Power Factor	0.943
Time of Day	8:03 am
Calculated "a"	4.96
Calculated "b"	7.76

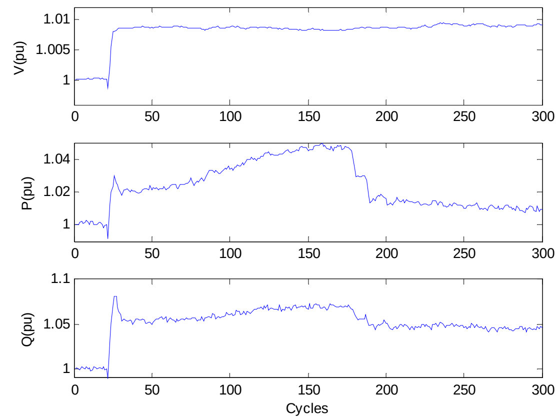

The calculated "a" and "b" for this case are very different from the others. The snapshot reveals the reason, which is the variation of the load during and right after the tap movement. This case should be omitted from calculations.

5.7.2 Substation Two, Transformer P2.7

In this substation, we have the same problem, which is investigated below. The variations of the load model parameters are plotted in Figure 5.21.

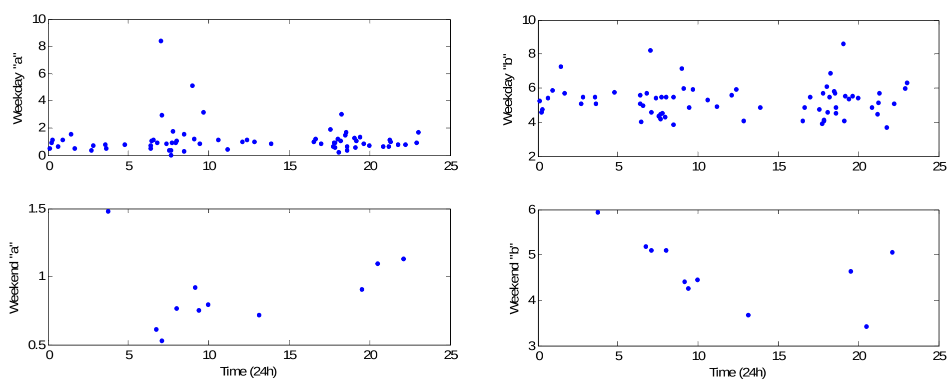

Figure 5.21. Transformer P2.7–Mostly Residential

In Figure 5.21, some of the calculated parameters seem strange. One of these cases was further investigated, and the results are presented in Table 5.10.

Table 5.10. An example of an abnormal case for Transformer P2.7

Calculated Parameter	**Value**
DV	0.96%
DP	0.38%
DQ	4.30%
Load Power Factor	0.963
Time of Day	7:31 am
Calculated “a”	0.39
Calculated “b”	4.38

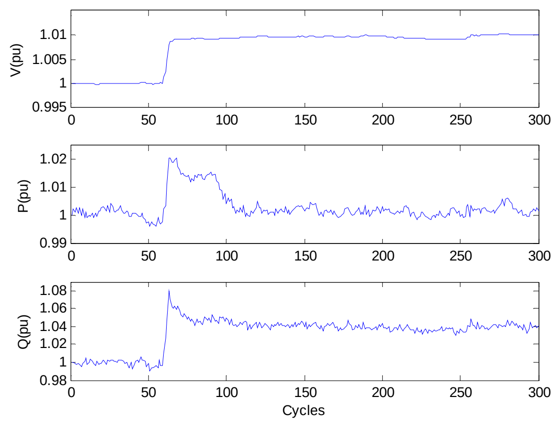

Here again, the variation of the load right after the tap movement leads to an inaccurate calculation of the load model parameters.

5.7.3 Substation Three, Transformer J4.7

The next substation is Substation Three, and the transformer is J4.7. The variation of the load model parameters for a 24-hour period is plotted in Figure 5.22.

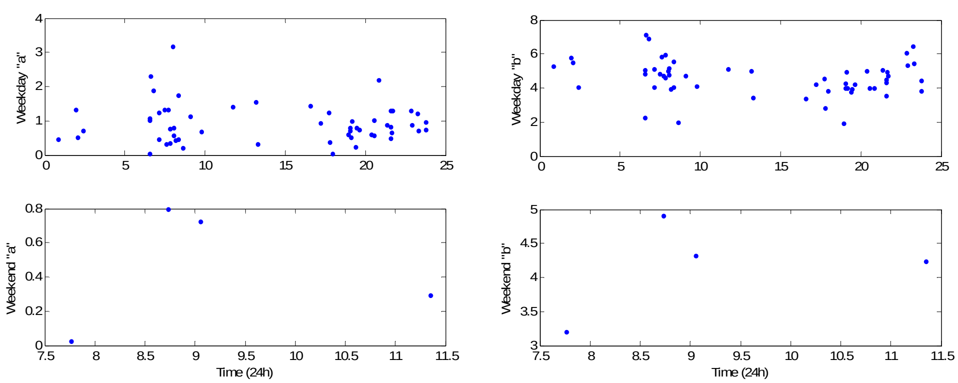

Figure 5.22. Transformer J4.7–Mostly Commercial

As an example, one of the most severe cases is presented in detail in Table 5.11.

Table 5.11. An example of an abnormal case for Transformer J4.7

Calculated Parameter	**Value**
DV	-0.85%
DP	-0.04%
DQ	1.93%
Load Power Factor	0.881
Time of Day	6:34 am
Calculated "a"	0.051
Calculated "b"	2.26

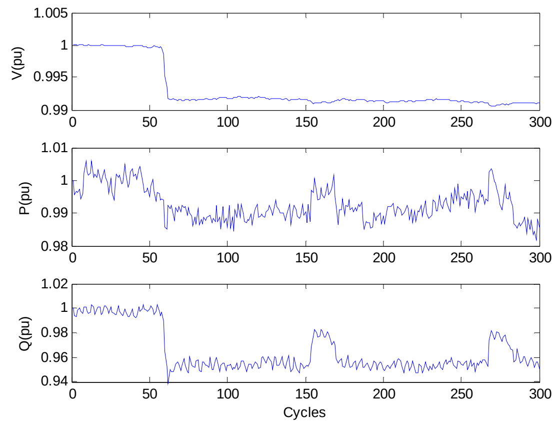

The load modeling algorithm is based on the fact that the system side changes while the load side is constant. In this condition, if the load and system change at the same time, the load and system parameters cannot be identified. Therefore, for the load modeling procedure, the cases in which the load varies during a tap movement cannot be used for calculating the load model parameters and should be omitted from the calculations.

A simple algorithm for detecting these kinds of tap movements is to detect the variation in the load after the tap movement for the period of 300 cycles. Since we already know the tap movement instant from the variation of the voltage, the step change in the power can be detected. For a snapshot to be valid, the step change in the power at the tap movement instant should be much larger (300%) than the load variation during 300 cycles. By using this criterion, the load modeling procedure will be improved, and the calculated parameters will be more accurate. This method has been already used for the calculated load parameters in the previous sections.

5.8 Conclusions

In this chapter, the characteristics of load data parameters are presented. Several sensitivity studies were done, and the load data parameters of several transformers in four different substations were investigated. The following conclusions are drawn:

- Tap movement can happen at any time during the day.
- The load parameters vary during a 24-hour period, and their variation is based on the type of load.
- Similar loads have similar transformer load profiles and load parameters.
- The step-up or step-down tap movements are the same in terms of the parameters' calculations, and both provide the same load data parameters.
- The step change in the voltage does not depend on the time of the tap movement.
- A tap movement can occur at any initial voltage and active and reactive power.
- The load model parameters do not depend on the pre-tap voltage and pre-tap active and pre-tap reactive power.
- For the same hour of the day, the load parameters are almost the same; however, the pre-tap voltage and the active and reactive power could be dissimilar.

The proposed algorithm was verified by using several measurements taken from different substations, with different loading conditions. The field test verification results show that the proposed algorithm can fulfill the load modeling requirements.

Chapter 6

Conclusions and Future Work

This chapter summarizes the main findings of the thesis and provides suggestions for extending and improving its research.

6.1 Thesis Conclusions and Contributions

In this thesis, a set of algorithms was proposed for the online measurement and monitoring of some power system parameters. These parameters are power system impedance, harmonic impedance, zero sequence impedance, as well as power system load model parameters. The main conclusions and contributions of the thesis can be summarized as follows:

- A new algorithm was proposed for the online tracking of power system impedance parameters. The main contributions of the research to the field are the new proposed algorithm; the consideration of practical issues; and the verifications through computer simulations, lab experiments, and several field tests. The research results show that a three-second to five-second data window with sufficient variations is enough for estimating impedance parameters. The algorithm proposed for this purpose does not depend on the load model and works with the natural variations of any kind of loads. Synchronized measurements are not also required for our calculations, and the method is not sensitive to changes in system frequency and harmonics.

  The proposed algorithm was verified by using simulations, experiments, and real field data. The verification results show that the proposed method can be implemented for the online monitoring of power system impedance parameters, for which no other appropriate and reliable method has yet been proposed. The required information can be obtained from the meters that are already installed at the substation buses.

- A second algorithm was proposed for the online tracking of power system harmonic and zero sequence impedance parameters. The main contributions of this part of the thesis to the research area are the new proposed algorithm, which can be used for online measurements; the consideration of practical issues; and the verifications through several field tests. The studies done in this part illustrate that a three-second to five-second data window with sufficient variations is enough for estimating harmonic and zero sequence impedance parameters. The 256-sample-per-cycle rate of the data-acquisition system is sufficient for the data-collection process, depending on the maximum frequency of the required harmonic impedance. The algorithm does not depend on the load model and works with the natural variations of any kind of loads, and synchronized measurements are not required for our calculations. The proposed algorithm was verified by using real field data. The verification results show that the proposed method fulfills the requirement for the online monitoring of power system harmonic and zero sequence impedance parameters.

- A practical and effective method for the online monitoring of voltage-dependent load model parameters was proposed. The method was verified through several experiments and extensive field test results. The data collected from the tests were analyzed to show the various characteristics of tap movements, and their sensitivities. Using natural tap movements for load parameter estimation has several advantages. The tap movements occur on a daily basis, so the load parameters can be collected consistently, frequently, and predictably. They cause a step voltage change. If no other disturbances occur at the same instant, as is commonly the case, load parameters can be estimated by using simple and reliable algorithms. Also, pre-established disturbance signatures uniquely suitable for detecting them can be used to detect and capture these disturbances. Since many such disturbances occur, if one misses some of them because of various uncertainties, the accuracy of the calculations will not be decreased. In fact, selecting only high-quality disturbances improves the reliability and quality of the results.

System operators can create these disturbances intentionally with a desired disturbance severity (i.e., by varying the amount of *DV* produced by the tap changer). As a result, the proposed technique can estimate load parameters 'on-demand'. Finally, the results do not need to be "verified" for the load parameters are actually measured from step-change disturbances and not with sophisticated algorithms using complex disturbance waveforms. Since the load parameters can be obtained many times a day, their online tracking becomes possible, and real-time power system applications such as dynamic security assessment can use the measured load parameters as input.

- Lastly, the characteristics of load data parameters were investigated. Several sensitivity studies were done, and the load data parameters of several feeders in four different substations were investigated. The research done in this area shows that tap movement can happen at any time during the day and that the load parameters vary during a 24-hour period, and their variation is based on the type of load.

  Similar loads have similar feeder load profiles and load parameters, and the step-up or step-down tap movements are the same in terms of the parameters' calculations, and both provide the same load data parameters. As well, the step change in the voltage does not depend on the time of the tap movement. It can occur at any initial voltage and active and reactive power, and the load model parameters do not depend on the pre-tap voltage and pre-tap active and pre-tap reactive power.

  The proposed algorithm for load modeling was verified by experiments and by using several measurements taken from different substations, with different loading conditions. The field test verification results show that the proposed algorithm can fulfill the online load modeling requirements.

6.2 Suggestion for Future Work

The research work performed and presented in this thesis can be extended in the following directions:

- The power system impedance measurement method can be improved and extended to estimate the system impedance and equivalent voltage source of multi-phase systems. When the system impedance matrix is not symmetric, the symmetrical components method cannot be used, and instead of one value for the system impedance, the whole system impedance matrix should be estimated. Practical considerations such as the choice of the disturbance side detection method and the definition of the fluctuation index, should be dealt with accordingly.

- The harmonic impedance measurement method can be used to calculate the system side harmonic impedances and estimate the harmonic contribution of harmonic generating loads at the point of common coupling. The algorithm can also be improved to be applied for the systems where the harmonic impedance matrix is not symmetric, to calculate the harmonic impedance matrix of the system.

- The impedance estimation method is capable of determining the Thevenin equivalent circuit parameters of the loads as well. The next step then would be to determine the fundamental and harmonic impedances of the loads connected to the system. In this case, the load model parameters where the load could be modeled as a Thevenin circuit could be estimated by using the proposed method. In harmonic studies, the proposed method could be used to determine the harmonic impedances of the loads. This process would lead to the determination of the system's and load's harmonic contributions at the interfacing point.

- The load modeling algorithm could be improved to detect other kind of disturbances such as capacitor switching in the system and to use the disturbance for load parameter estimations. The effect of tap change on the voltages and currents in residential transformers and in houses could also be detected and used to estimate the load parameters seen from residential transformers and houses. The algorithms also could be extended to measure and monitor the frequency-dependent load model parameters.

Chapter 7

References

[1] A. De Oliveira, J.C. De Oliveira, J.W. Resende and M.S. Miskulin, "Practical approaches for AC system harmonic impedance measurements", *IEEE Trans. Power Delivery*, vol. 6, issue 4, pp. 1721-1726, Oct. 1991.

[2] L. S. Czarnecki and Z. Staroszczyk, "On line measurement of equivalent parameters for harmonic frequencies of a power distribution system and load," IEEE Transactions on Instrumentation and Measurement, vol. 45, no. 2, pp. 467–472, 1996.

[3] M. Nagpal, W. Xu, and J. Sawada, "Harmonic impedance measurement using three phase transients," IEEE Transactions on Power Delivery, vol. 13, no. 1, pp. 272–277, 1998.

[4] W. C. Beattie and S. R. Matthews, "Measurement of harmonic impedance from analysis of transients generated by capacitors," 3rd International Conference Advances in Power System Control, Operation and Management, (Hong Kong), pp. 97–102, IEE, 1995.

[5] Z. Staroszczyk, "Time dependant power systems impedance-interpretation and measuring problems," in IEEE instrumentation and measurement technology conference (IMTC99): Measurements for the new millenium, vol. 2, (Italy), pp. 795–800, 1999.

[6] M. Tsukamoto, S. Ogawa, Y. Natsuda, Y. Minowa, and S. Nishimura, "Advanced technology to identify harmonics characteristics and results of measuring.," in Ninth International Conference on Harmonics and Quality of Power (A. Domijan, ed.), vol. 1, (Orlando, FL, USA), pp. 341–346, IEEE, 2000.

[7] J. P. Rhode, A. W. Kelley, and M. E. Baran, "Line impedance measurement: A nondisruptive wideband technique," in IAS Annual Meeting, vol. 3, (Orlando,Florida, USA), pp. 2233–2240, IEEE, 1995.

[8] G. Fusco, A. Losi, and M. Russo, “Constrained Least Squares Methods for Parameter Tracking of Power System Steady-State Equivalent Circuits”, *IEEE Trans. Power Delivery*, vol. 15, issue 3, pp. 1073-1080, 2000.

[9] K. Vu, M. M. Begovic, D. Novosel, and M. M. Saha, “Use of local measurements to estimate voltage-stability margin”, *IEEE Trans. Power Systems*, vol. 14, issue 3, pp. 1029-1035, Aug. 1999.

[10] W. Wang, E.E. Nino and W. Xu, "Harmonic impedance measurement using a thyristor-controlled short circuit," *Generation, Transmission & Distribution, IET*, vol.1, no.5, pp.707-713, September 2007.

[11] W. Xu, E.E. Ahmed, X. Zhang and X. Liu, "Measurement of network harmonic impedances: practical implementation issues and their solutions," *Power Delivery, IEEE Transactions on*, vol.17, no.1, pp.210-216, Jan 2002.

[12] J. Martinon, P. Fauquembergue, J. Lachaume and M. Meunier, "A new statistical approach of harmonic propagation in transmission systems," *Power Delivery, IEEE Transactions on*, vol.11, no.2, pp.1032-1040, Apr 1996.

[13] M. Sumner, B. Palethorpe and D.W.P. Thomas, "Impedance measurement for improved power quality-Part 1: the measurement technique," *Power Delivery, IEEE Transactions on*, vol.19, no.3, pp. 1442-1448, July 2004.

[14] A. A. Girgis, McManis and R. Brent, "Frequency Domain Techniques for Modeling Distribution or Transmission Networks Using Capacitor Switching Induced Transients," *Power Engineering Review, IEEE*, vol.9, no.7, pp.74-75, July 1989.

[15] M. Sumner, B. Palethorpe, D.W.P. Thomas, P. Zanchetta and M.C. Di Piazza, "A technique for power supply harmonic impedance estimation using a controlled voltage disturbance," *Power Electronics, IEEE Transactions on* , vol.17, no.2, pp.207-215, Mar 2002.

[16] B. Palethorpe, M. Sumner, and D. W. P. Thomas, “System impedance measurement for use with active filter control,” in *Proc. IEE PEVD’00 Conf.*, London, U.K., Sept. 2000, pp. 24–28.

[17] M. C. di Piazza, P. Zanchetta, M. Sumner, and D. W. P. Thomas, “Estimation of load impedance in a power system,” in *Proc. IEEE PES ICHQP’00*, Orlando, FL, Oct. 2000, pp. 520–525.

[18] Z. Staroszczyk, "A method for real-time, wide-band identification of the source impedance in power systems," *IEEE Trans. Instrum. Meas.*, vol. 54, no. 1, pp. 377–385, Feb. 2005.

[19] C. Xie, S.B. Tennakoon, R. Langella, D. Gallo, A. Testa, A. Wixon, "Harmonic impedance measurement of 25 kV single phase AC supply systems," *Harmonics and Quality of Power, 2000. Proceedings. Ninth International Conference on,* vol.1, no., pp.214-219 vol.1, 2000.

[20] J. Hui, H. Yang, S. Lin, M. Ye, "Assessing Utility Harmonic Impedance Based on the Covariance Characteristic of Random Vectors," *Power Delivery, IEEE Transactions on*, vol.25, no.3, pp.1778-1786, July 2010.

[21] M.J. Bridgeman, R.E. Morrison, S.B. Tenakoon, "Measurement of harmonic impedance on an LV system utilising power capacitor switching and consequent predictions of capacitor induced harmonic distortion," *Harmonics And Quality of Power, 1998. Proceedings. 8th International Conference on*, vol.2, no., pp.1141-1145 vol.2, 14-18 Oct 1998.

[22] Yao Xiao, J.C. Maun, H.B. Mahmoud, T. Detroz, Stephane Do, "Harmonic impedance measurement using voltage and current increments from disturbing loads," *Harmonics and Quality of Power, 2000. Proceedings. Ninth International Conference on*, vol.1, no., pp.220-225 vol.1, 2000.

[23] R.S. Thallam, S. Mogri, R.S. Burton, "Harmonic impedance and harmonic interaction of an AC system with multiple DC infeeds," *Power Delivery, IEEE Transactions on*, vol.3, no.4, pp.2064-2071, Oct 1988.

[24] X.Y Xiao, H.G. Yang, "Assessing harmonic impedance by synchronously layered distortion waves based on wavelet," *Electric Utility Deregulation, Restructuring and Power Technologies, 2004. (DRPT 2004). Proceedings of the 2004 IEEE International Conference on*, vol.2, no., pp. 653- 657 Vol.2, 5-8 April 2004.

[25] W.R.A Ryckaert, J.A.L. Ghijselen, J.A.A. Melkebeek, J.J.M. Desmet, J. Driesen, "The influence on harmonic propagation of the resistive shunt harmonic impedance location along a distribution feeder and the influence of distributed capacitors," *Harmonics and Quality of Power, 2004. 11th International Conference on*, vol., no., pp. 129- 135, 12-15 Sept. 2004.

[26] A.O. Ba, A.O. Barry, "Active filter analysis by the harmonic impedance compensation method (part 1)," *Electrical and Computer Engineering, 2003. IEEE*

CCECE 2003. Canadian Conference on, vol.1, no., pp. 663- 667 vol.1, 4-7 May 2003.

[27] G. Moreau, H.H. Le, G. Croteau, G. Beaulieu, E. Portales, "Measurement system for harmonic impedance of the network and validation steps," *Quality and Security of Electric Power Delivery Systems, 2003. CIGRE/PES 2003. CIGRE/IEEE PES International Symposium*, vol., no., pp. 69- 73, 8-10 Oct. 2003.

[28] R. Langella, A. Testa, "A New Method for Statistical Assessment of the System Harmonic Impedance and of the Background Voltage Distortion," *Probabilistic Methods Applied to Power Systems, 2006. PMAPS 2006. International Conference on*, vol., no., pp.1-7, 11-15 June 2006.

[29] Zhenyu Fan, E. Johan, "Harmonic Impedance Analysis in the Presence of Static Var Compensator (SVC)," *Power Systems Conference and Exposition, 2006. PSCE '06. 2006 IEEE PES*, vol., no., pp.1485-1492, Oct. 29 2006-Nov. 1 2006.

[30] G. R. Slemon, E. A. Ismailov, "An Analysis of the Harmonic Impedance of a Saturated Induction Machine," *Power Apparatus and Systems, IEEE Transactions on* , vol.PAS-99, no.4, pp.1663-1669, July 1980.

[31] IEEE Task Force on Load Representation for Dynamic Performances, “Load representation for dynamic performance analysis,” *IEEE Trans. Power Systems*, vol. 8, no. 2, pp. 472–482, May 1993.

[32] L. Pereira, D. Kosterev, P. Mackin, D. Davies, J. Undrill, W. Zhu, “An Interim Dynamic Induction Motor Model for Stability Studies in the WSCC,” *IEEE Trans. Power Systems*, vol.17, no. 4, pp. 1108-1115, November 2002.

[33] IEEE Task Force Report, “Standard Load Models for Power Flow and Dynamic Performance Simulation,” *IEEE Trans. Power Systems*, Vol. 10, No. 3, pp. 1302-1313, August 1995.

[34] V. Knyazkin, C. A. Canizares, L.H. Soder, “On the parameter estimation and modeling of aggregate power system loads Power Systems,” *IEEE Trans. Power Systems,* vol. 19, Issue 2, pp. 1023- 1031 May 2004.

[35] “Bibliography on load models for power flow and dynamic performance simulation,” *IEEE Trans. Power Systems*, vol. 10, pp. 523–538, Feb. 1995.

[36] L.M. Korunovic, D.P. Stojanovic, J.V. Milanovic, "Identification of static load characteristics based on measurements in medium-voltage distribution network," *Generation, Transmission & Distribution, IET*, vol.2, no.2, pp.227-234, March 2008.

[37] M. Sadeghi, G.A. Sarvi, "Determination of ZIP parameters with least squares optimization method," *Electrical Power & Energy Conference (EPEC), 2009 IEEE*, vol., no., pp.1-6, 22-23 Oct. 2009.

[38] K. Morison, H. Hamadani, Lei Wang, "Load Modeling for Voltage Stability Studies," *Power Systems Conference and Exposition, 2006. PSCE '06. 2006 IEEE PES*, vol., no., pp.564-568, Oct. 29 2006-Nov. 1, 2006.

[39] Rung-Fang Chang , Rong-Ceng Leou , Chan-Nan Lu, "Distribution transformer load modeling using load research data," *Power Delivery, IEEE Transactions on* , vol.17, no.2, pp.655-661, Apr 2002

[40] P. Ju, E. Handschin, "Identifiability of load models [power systems]," *Generation, Transmission and Distribution, IEE Proceedings-* , vol.144, no.1, pp.45-49, Jan 1997.

[41] P. Ju, F. Wu, Z.Y. Shao, X.P. Zhang, H.J. Fu, P.F. Zhang, N.Q. He, J.D. Han, "Composite load models based on field measurements and their applications in dynamic analysis," *Generation, Transmission & Distribution, IET*, vol.1, no.5, pp.724-730, September 2007.

[42] W. Xu, Y. Mansour, "Voltage stability analysis using generic dynamic load models," *Power Systems, IEEE Transactions on* , vol.9, no.1, pp.479-493, Feb 1994.

[43] Jin Ma , Dong Han , Ren-Mu He , Zhao-Yang Dong , D.J. Hill, "Reducing Identified Parameters of Measurement-Based Composite Load Model," *Power Systems, IEEE Transactions on* , vol.23, no.1, pp.76-83, Feb. 2008.

[44] Y. Baghzouz, C. Quist, "Determination of static load models from LTC and capacitor switching tests," *Power Engineering Society Summer Meeting, 2000. IEEE*, vol.1, no., pp.389-394 vol. 1, 2000.

[45] A. K. Ghosh, D.L. Lubkeman, R.H. Jones, "Load modeling for distribution circuit state estimation," *Power Delivery, IEEE Transactions on*, vol.12, no.2, pp.999-1005, Apr 1997.

[46] J.A. Martinez, J. Martin-Arnedo, "Advanced load models for voltage sag studies in distribution networks," *Power Engineering Society General Meeting, 2004. IEEE*, vol., no., pp. 614- 619, vol.1, 6-10 June 2004.

[47] J.A. Martinez, J. Martin-Arnedo, J.V. Milanovic, "Load modeling for voltage sag studies," *Power Engineering Society General Meeting, 2003, IEEE* , vol.4, no., pp. 2513 Vol. 4, 13-17 July 2003.

[48] K. Rudion, H. Guo, H. Abildgaard, Z.A. Styczynski, "Non-linear load modeling — Requirements and preparation for measurement," *Power & Energy Society General Meeting, 2009. PES '09. IEEE*, vol., no., pp.1-7, 26-30 July 2009.

[49] Jin Ma, Zhao-yang Dong, Ren-mu He, D.J. Hill, "Measurement-based Load Modeling using Genetic Algorithms," *Evolutionary Computation, 2007. CEC 2007. IEEE Congress on*, vol., no., pp.2909-2916, 25-28 Sept. 2007.

[50] J.H. Shi, He Renmu, "Measurement-based load modeling-model structure," *Power Tech Conference Proceedings, 2003 IEEE Bologna* , vol.2, no., pp. 5 pp. Vol.2, 23-26 June 2003.

[51] A. Maitra, A. Gaikwad, P. Pourbeik, D. Brooks, "Load model parameter derivation using an automated algorithm and measured data," *Power and Energy Society General Meeting - Conversion and Delivery of Electrical Energy in the 21st Century, 2008 IEEE* , vol., no., pp.1-7, 20-24 July 2008.

[52] D. Asber, S. Lefebvre, M. Saad, C. Desbiens, "Modeling of Distribution Loads for Short and Medium-Term Load Forecasting," *Power Engineering Society General Meeting, 2007. IEEE*, vol., no., pp.1-5, 24-28 June 2007.

[53] L.M. Vargas, J. Jatskevich, J.R. Marti, "Load modeling of an induction motor operated with a variable frequency drive," *Electric Power Conference, 2008. EPEC 2008. IEEE Canada*, vol., no., pp.1-7, 6-7 Oct. 2008.

[54] Haibin Wang, N.N. Schulz, "A load modeling algorithm for distribution system state estimation," *Transmission and Distribution Conference and Exposition, 2001 IEEE/PES*, vol.1, no., pp.102-105 vol.1, 2001.

[55] D. Kosterev, A. Meklin, J. Undrill, B. Lesieutre, W. Price, D. Chassin, R. Bravo, S. Yang, "Load modeling in power system studies: WECC progress update," *Power and Energy Society General Meeting - Conversion and Delivery of Electrical Energy in the 21st Century, 2008 IEEE* , vol., no., pp.1-8, 20-24 July 2008.

[56] J.H. Park, Y.M. Park, K.Y. Lee, "Composite modeling for adaptive short-term load forecasting," *Power Systems, IEEE Transactions on* , vol.6, no.2, pp.450-457, May 1991.

[57] L. Asiminoaei, R.Teodorescu, F. Blaabjerg, and U. Borup, “A new method of on-line grid impedance estimation for PV inverter”, *Nineteenth Annual IEEE Applied Power Electronics Conference and Exposition, APEC '04,* vol. 3, pp. 1527–1533, 2004.

[58] M. Sumner, D. W. P. Thomas and P. Zanchetta, “Power System Impedance Estimation for Improved Active Filter Control, using Continuous Wavelet Transforms”, *PES TD 2005/2006*, pp. 653– 658, May 21-24, 2006.

[59] A.V. Timbus, R. Teodorescu, F. Blaabjerg and U. Borup, **“**Online grid impedance measurement suitable for multiple PV inverters running in parallel”, *Twenty-First Annual IEEE Applied Power Electronics Conference and Exposition, APEC '06,* pp. 19-23 March 2006.

[60] M. Bahadornejad and G. Ledwich, “System Thevenin Impedance Estimation Using Signal Processing on Load Bus Data,” *Proceedings of 6th International Conference on Advances in Power System Control, Operation and Management*, APSCOM, pp. 274–279, Nov. 2003.

[61] T. Tayjasanant, Chun Li and W. Xu, “A resistance sign-based method for voltage sag source detection”, *IEEE Trans. Power Delivery*, vol. 20, no. 4, Oct. 2005.

[62] K. Vu, and D. Novosel, “Voltage instability predictor (VIP)--method and system for performing adaptive control to improve voltage stability in power systems”, U.S. Patent 6 219 591, May 15, 1998.

[63] J. L. Santos, F.P.M, Barbosa, “Voltage stability evaluation using the relation between impedances”, Proceedings of the 12th IEEE Mediterranean Electrotechnical Conference, vol. 3, pp. 927 – 930, 2004.

[64] *Electromagnetic compatibility (EMC), Part 4: Testing and measurement techniques, Section 30: Power Quality Measurement Methods*, IEC standard 61000-4-30, 2003.

[65] A. Robert and T. Deflandre, “Guide for assessing the network harmonic impedances,” CIGRE 36.05, Working Group CC02 Rep., Mar. 1993.

[66] A. S. Morched and P. Kundur, “Identification and modeling of load characteristics at high frequencies,” IEEE Trans. Power Syst., vol. PWRS-2, Feb. 1987.

[67] E. Duggan and R. E. Morrison, “A noninvasive technique for the measurement of power system harmonic impedance,” in Proc. Int. Conf. Electricity Distribution (CIRED), 1991, Paper 2.02.

[68] J. Bergeal and L. Moller, “Analysis of the spectrum impedance of a network, use of digital methods,” in Proc. Int. Conf. Electricity Distribution (CIRED), 1983, Paper c.05.

[69] T. Tayjasanant, "A graphic user interface-based program for voltage sag- and flicker-source detection," Power Engineering Conference, IPEC 2007, International, vol., no., pp.1213-1218, 3-6 Dec. 2007.

[70] S. A. Arefifar and W. Xu, "Online Tracking of Power System Impedance Parameters and Field Experiences," *Power Delivery, IEEE Transactions on*, vol.24, no.4, pp.1781-1788, Oct. 2009.

[71] A.P.S. Meliopoulos, F. Zhang and S. Zelingher, "Power system harmonic state estimation," *Power Delivery, IEEE Transactions on*, vol.9, no.3, pp.1701-1709, Jul 1994.

[72] J. V. Milanovic and I. A. Hiskens, "Effects of load dynamics on power system damping," *IEEE Trans. Power Syst.*, vol. 10, no. 2, pp. 1022–1028, May 1995.

[73] IEEE Task Force on Load Representation for Dynamic Performance, "Standard load models for power flow and dynamic performance simulation," *IEEE Trans. Power Syst.*, vol. 10, no. 3, pp. 1302–1313, Aug. 1995.

[74] C. Concordia and S. Ihara, "Load representation in power systems stability studies," *IEEE Trans. Power App. Syst.*, vol. PAS-101, no. 4, pp. 969–977, Apr. 1982.

[75] J. M. Undrill and T. F. Laskowski, "Model selection and data assembly for power system simulation," *IEEE Trans. Power App. Syst.*, vol. PAS-101, no. 9, pp. 3333–3341, Sep. 1982.

[76] H. Renmu, Ma Jin, D.J. Hill, "Composite load modeling via measurement approach," Power Systems, IEEE Transactions on , vol.21, no.2, pp. 663- 672, May 2006.

[77] R. H. Craven and M. R. Michael, "Load representations in the dynamic simulation of the Queensland Power System," *J. Elect. Electron. Eng.*, vol. 3, no. 1, pp. 1–7, 1983.

[78] I. A. Hiskens and J. V. Milanovic, "Load modeling in studies of power system damping," *IEEE Trans. Power Syst.*, vol. 10, no. 4, pp. 1781–1788, Nov. 1995.

[79] P. Kundur, Power System Stability and Control. New York: McGraw-Hill, 1994.

[80] A. Gebreselassie and J. H. Chow, "Investigation of the effects of load models and generator voltage regulators on voltage stability," *Int. J. Elect. Power Energy Syst.*, vol. 16, no. 2, pp. 83–89, 1994.

[81] A. Maitra, A. Gaikwad, P. Zhang, M. Ingram, D.L. Mercado, W.D. Woitt, "Using System Disturbance Measurement Data to Develop Improved Load Models",

Power Systems Conference and Exposition, PSCE '06. 2006 IEEE PES, pp.1978-1985, Oct. 29-Nov. 1 2006.

[82] E. Vaahedi, M.A. Fl-Kady, J.A. Libaque-Esaine, V.F. Carvalho, "Load Models for Large-Scale Stability Studies from End-User Consumption," Power Systems, IEEE Transactions on , vol.2, no.4, pp.864-870, Nov. 1987.

[83] General Electric Company, “Load Modeling for Power Flow and Transient Stability Computer Studies,” EPRI, Rep. EL-5003, vol. 1–4, Jan. 1987.

[84] W. W. Price, K. A. Wirgau, A. Murdoch, J. V. Mitsche, E. Vaahedi, and M. A. El-kady, “Load modeling for load flow and transient stability computer studies,” *IEEE Trans. Power Syst.*, vol. 3, no. 1, pp. 180–187, Feb. 1988.

[85] Dong Han, Jin Ma, Ren-mu He, Zhao-yang Dong, "A Real Application of Measurement-Based Load Modeling in Large-Scale Power Grids and its Validation," Power Systems, IEEE Transactions on , vol.24, no.4, pp.1756-1764, Nov. 2009.

[86] Jinyu Wen, Shaorong Wang, Shijie Cheng, Q.H. Wu, D.W. Shimmin, "Measurement based power system load modeling using a population diversity genetic algorithm," Power System Technology, 1998. Proceedings. POWERCON '98. 1998 International Conference on, vol.1, no., pp.771-775 vol.1, 18-21 Aug 1998.

[87] W. Xu, E. Vaahedi, Y. Mansour, J. Tamby, "Voltage stability load parameter determination from field tests on BC Hydro's system," Power Systems, IEEE Transactions on, vol.12, no.3, pp.1290-1297, Aug 1997.

[88] Byoung-Kon Choi, Hsiao-Dong Chiang, Yinhong Li, Hua Li, Yung-Tien Chen, Der-Hua Huang, M.G. Lauby, "Measurement-based dynamic load models: derivation, comparison, and validation," Power Systems, IEEE Transactions on, vol.21, no.3, pp.1276-1283, Aug. 2006.

[89] Byoung-Kon Choi, Hsiao-Dong Chiang, "Multiple Solutions and Plateau Phenomenon in Measurement-Based Load Model Development: Issues and Suggestions," Power Systems, IEEE Transactions on, vol.24, no.2, pp.824-831, May 2009.

[90] Qian Ai, Danzhen Gu, Chen Chen, "New Load Modeling Approaches Based on Field Tests for Fast Transient Stability Calculations," Power Systems, IEEE Transactions on , vol.21, no.4, pp.1864-1873, Nov. 2006.

[91] J.Y. Wen, L. Jiang, Q.H. Wu, S.J. Cheng, "Power system load modeling by learning based on system measurements," Power Delivery, IEEE Transactions on, vol.18, no.2, pp. 364- 371, April 2003.

[92] Ma Jin, H. Renmu, D.J. Hill, "Load modeling by finding support vectors of load data from field measurements," Power Systems, IEEE Transactions on , vol.21, no.2, pp. 726- 735, May 2006.

[93] H. Renmu, M. Jin, D. J. Hill, "Composite load modeling via measurement approach", *IEEE Trans. Power System*, vol. 21, no.2, pp. 663-672, May 2006.

[94] D. J. Hill, "Nonlinear dynamic load models with recovery for voltage stability studies," *IEEE Trans. Power Systems*, vol. 8, no. 1, pp. 166–176, Feb. 1993.

[95] D. Karlsson and D. J. Hill, "Modeling and identification of nonlinear dynamic loads in power systems," IEEE Trans. Power Syst., vol. 9, no. 1, pp. 157–166, Feb. 1994.

[96] C. J. Lin, Y. T. Chen, C. Y. Chiou, C. H.Huang, "Dynamic Load Models in Power system Using the Measurement Approach," *IEEE Trans. Power System*, vol. 8, no.1, pp. 309-315, Feb. 1993.

[97] J. C. Wang, et al., "Development of a Frequency-dependent Composite Load Model Using the Measure Approach," *IEEE Trans. Power Systems*, vol. 9, no.3, pp. 1546-1556, Aug. 1994.

[98] D.W. Holladay, C.H. Grigg, B.D. Dallman, "Equipment Performance Study on Voltage Regulators," Power Delivery, IEEE Transactions on, vol.23, no.4, pp.2496-2512, Oct. 2008.

Appendix A

The Gauss-Newton Algorithm

The Gauss–Newton algorithm is a method used to solve non-linear least squares problem. It can be seen as a modification of Newton's method for finding a minimum of a function. Unlike Newton's method, the Gauss–Newton algorithm can only be used to minimize a sum of squared function values, but it has the advantage that second derivatives, which can be challenging to compute, are not required. Non-linear least squares problems arise for instance in non-linear regression, where parameters in a model are sought such that the model is in good agreement with available observations. The method is named after the mathematicians Carl Friedrich Gauss and Isaac Newton. In this section the method is described and convergence properties are explained.

A.1 Description

Given m functions $r_1, \ldots, r_m$ of n variables $\beta = (\beta_1, \ldots, \beta_n)$, with $m \geq n$, the Gauss–Newton algorithm finds the minimum of the sum of squares

$$S(\beta) = \sum_{i=1}^{m} r_i^2(\beta). \tag{A.1}$$

Starting with an initial guess $\beta^{(0)}$ for the minimum, the method proceeds by the iterations

$$\beta^{(s+1)} = \beta^{(s)} + \Delta \tag{A.2}$$

where the increment Δ is the solution to the normal equations:

$$(J_r^T J_r)\Delta = -J_r^T r \tag{A.3}$$

Here, r is the vector of functions r_i, and J_r is the $m \times n$ Jacobian matrix of r with respect to β, both evaluated at β^s. The superscript T denotes the matrix transpose. In data fitting, where the goal is to find the parameters β such that a given model function $y = f(x, \beta)$ fits best some data points (x_i, y_i), the functions r_i are the residuals

$$r_i(\beta) = y_i - f(x_i, \beta) \tag{A.4}$$

Then, the increment Δ can be expressed in terms of the Jacobian of the function f, as

$$(J_f^T J_f)\Delta = -J_f^T r. \tag{A.5}$$

The assumption $m \geq n$ in the algorithm statement is necessary, as otherwise the matrix $J_r^T J_r$ is not invertible and the normal equations cannot be solved. The Gauss–Newton algorithm can be derived by linearly approximating the vector of functions r_i. Using Taylor's theorem, at each iteration we can write:

$$r(\beta) \approx r(\beta^s) + J_r(\beta^s)\Delta\,. \tag{A.6}$$

With $\Delta = \beta - \beta^s$. The task of finding Δ minimizing the sum of squares of the right-hand side, i.e.,

$$\min \left\| r(\beta^s) + J_r(\beta^s)\Delta) \right\|_2^2, \tag{A.7}$$

is a linear least squares problem, which can be solved explicitly, yielding the normal equations in the algorithm. The normal equations are m linear simultaneous equations in the unknown increments, Δ. They may be solved in one step, using Cholesky decomposition, or, better, the QR factorization of J_r. For large systems, an iterative method, such as the conjugate gradient method, may be more efficient. If there is a linear dependence between columns of J_r, the iterations will fail as $J_r^T J_r$ becomes singular.

A.2 Convergence Properties

It can be shown that the increment Δ is a descent direction for S, and, if the algorithm converges, then the limit is a stationary point of S. However, convergence is not guaranteed, not even local convergence as in Newton's method. The rate of convergence of the Gauss–Newton algorithm can approach quadratic. The algorithm may converge slowly or not at all if the initial guess is far from the minimum or the matrix $J_r^T J_r$ is ill-conditioned. For example, consider the problem with $m = 2$ equations and $n = 1$ variable, given by

$$\begin{aligned} r_1(\beta) &= \beta + 1 \\ r_2(\beta) &= \lambda\beta^2 + \beta - 1. \end{aligned} \tag{A.8}$$

The optimum is at $\beta = 0$. If $\lambda = 0$ then the problem is in fact linear and the method finds the optimum in one iteration. If $|\lambda| < 1$ then the method converges linearly and the error decreases asymptotically with a factor $|\lambda|$ at every iteration. However, if $|\lambda| > 1$, then the method does not even converge locally.

Appendix B

Instruments Specifications

In this section the characteristics of the Data-Acquisition Device and voltage and current probes that were used for the measurements are presented.

B.1 Data Acquisition Device

The data were collected by using the National Instruments' NI DAQPad-6020E USB data-acquisition system, which has the following characteristics:

Inputs:	8 differential BNC analog inputs (12-bit)
Sampling Rate:	100 KS/s
<u>Maximum Quantization Error</u>	
10/1, Voltage Probe & 100mV/A, Current Probe	$\frac{1}{2}\times\frac{1}{2^{12}}\times 10$ = 0.00122 (A/V)
100/1, Voltage Probe & 10mV/A, Current Probe	$\frac{1}{2}\times\frac{1}{2^{12}}\times 100$ = 0.0122 (A/V)

B.2 Current Probes

The used current probes are the Fluke 80i-110s AC/DC Current Clamp, manufactured by Fluke. This type of probes has the following specification:

Current Range:	0.1 to 100A DC or 0.1 to 70A AC
Basic Accuracy (DC to 1kHz):	100mV/A setting: 50mA to 10A +/- 3% of reading + 50mA 10mV/A setting: 50mA to 40A +/- 4% of reading + 50mA 40A to 80A +/- 12% of reading + 50mA 80 to 100A +/- 15% of reading
Output Signal:	10A range: 100mV/A | 100A range: 10mV/A
Bandwidth:	1Hz to 20kHz

B.3 Voltage Probes

The voltage probes are the Differential Probe for the Power Management, Model 4232, manufactured by Probe Master. This type of probes has the following specification:

Bandwidth:	DC to 25 MHz (-3dB)
Accuracy:	±2%
Attenuation Ratio:	1:10 and 1:100
Input Voltage:	+70V (DC + Peak AC) or 50Vrms for 1/10
Max. Differential:	+700V (DC +Peak AC) or 500Vrms for 1/100
Max. Common Mode	+700V (DC + Peak AC) or 500Vrms
Output Voltage	
Max. Amplitude:	+7V (into 2K OHM load)
Offset (Typical):	<+5mV, -10°C to 40°C
Noise (Typical):	1.5 to 2mV

Appendix C

Thevenin Impedance Measurement at Different Points of System

C.1 Substation Level

C1.1 Substation Three

The single-line diagram of Substation Three and the feeders selected for measurements are shown in Figure C.1. The measurements are taken at the metering points of the feeders. The Feeders One, Two, Three and Four were chosen to calculate the system equivalent circuit parameters.

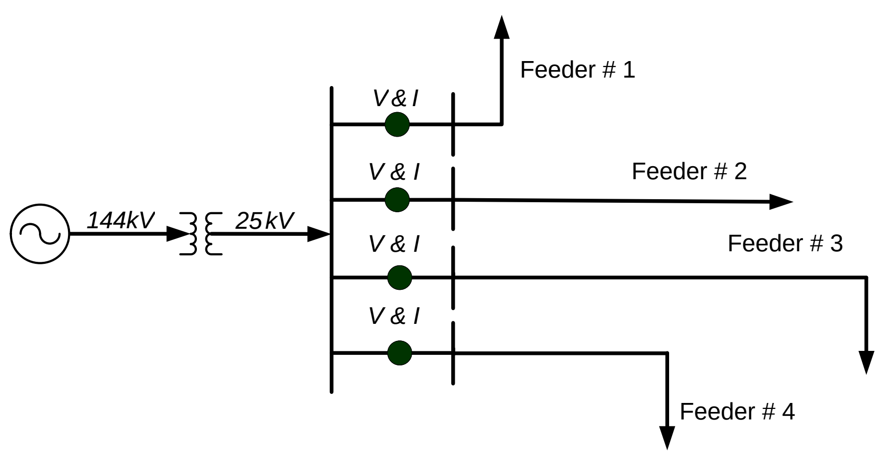

Figure C.1. Single-line diagram of Substation Three

The equivalent circuit parameters of the system seen from the selected feeders are calculated and presented in the following sections.

1. Feeder One

The variations of RMS values of positive sequence voltage and current of this feeder during the measurements are shown in Figure C.2.

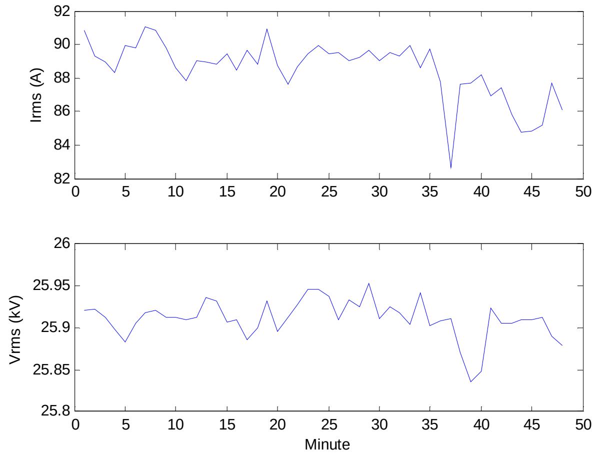

Figure C.2. Voltage and current of Feeder One in Substation Three

The positive sequence parameters of the system are calculated and shown in Figure C.3.

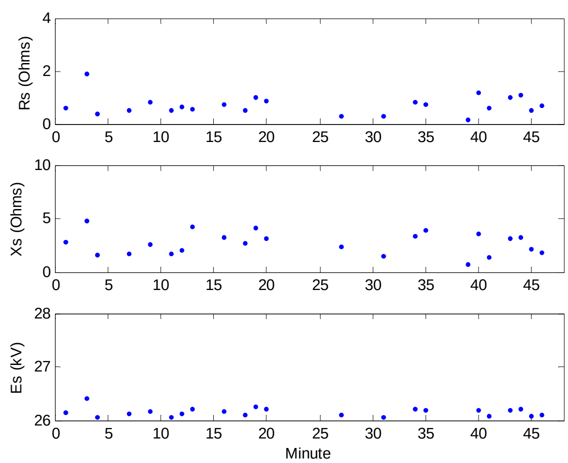

Figure C.3. Circuit parameters of Feeder One in Substation Three

2. Feeder Two

The variations of RMS values of positive sequence voltage and current of this feeder during the measurements are shown in Figure C.4.

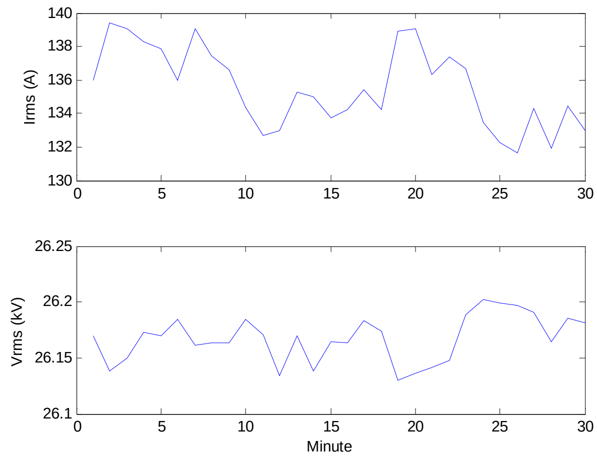

Figure C.4. Voltage and current of Feeder Two in Substation Three

The positive sequence parameters of the system are calculated and shown in Figure C.5.

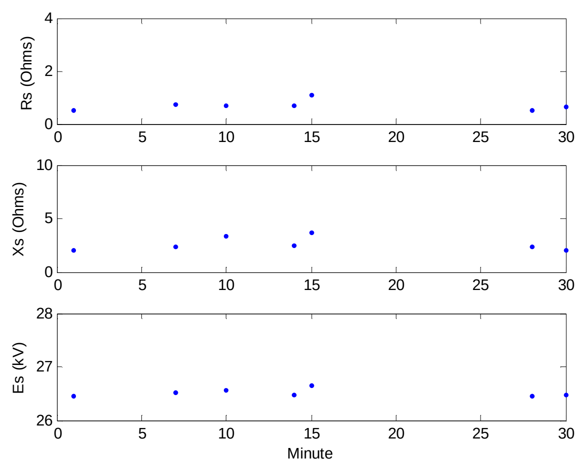

Figure C.5. Circuit parameters of Feeder Two in Substation Three

3. Feeder Three

The variations of RMS values of positive sequence voltage and current of this feeder during the measurements are shown in Figure C.6.

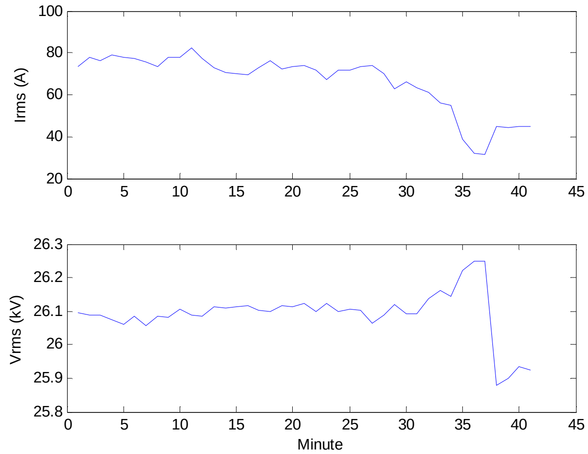

Figure C.6. Voltage and current of Feeder Three in Substation Three

The positive sequence parameters of the system are calculated and shown in Figure C.7.

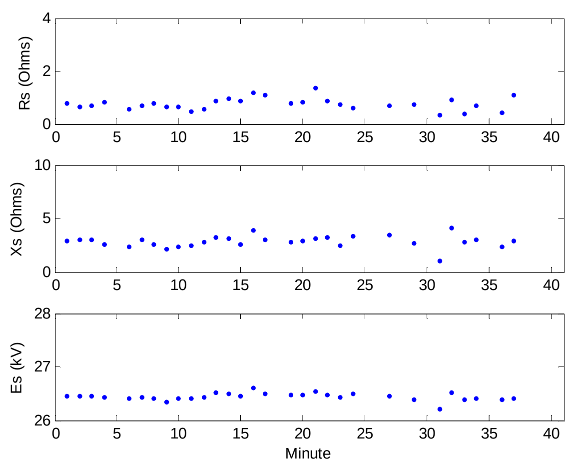

Figure C.7. Circuit parameters of Feeder Three in Substation Three

Figure C.7 reveals that for $t > 38$, the system voltage has a large variation, which could be caused by the transformer tap changer, the algorithm does not provide any results.

4. Feeder Four

The variations of RMS values of positive sequence voltage and current of this feeder during the measurements are shown in Figure C.8.

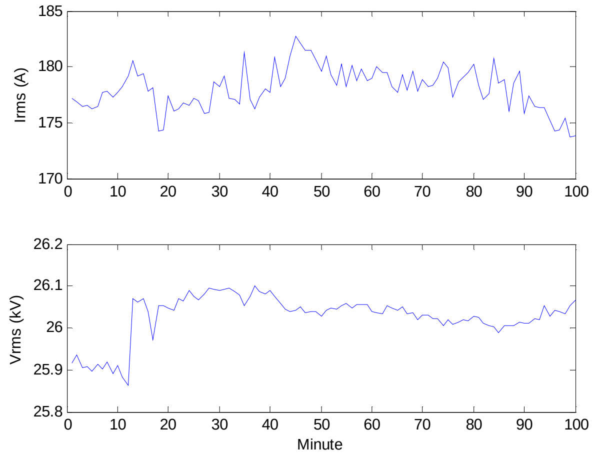

Figure C.8. Voltage and current of Feeder Four in Substation Three

The positive sequence parameters of the system are calculated and shown in Figure C.9.

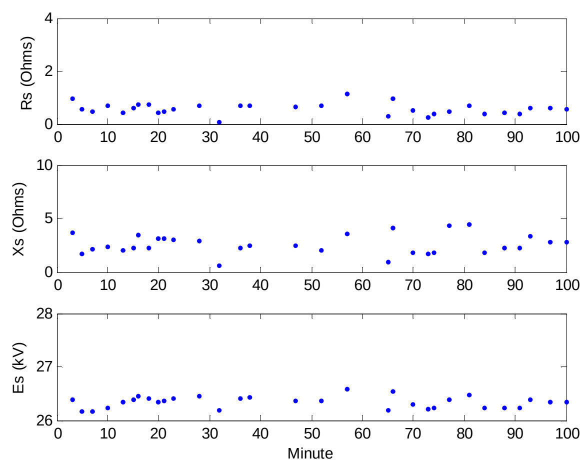

Figure C.9. Circuit parameters of Feeder Four in Substation Three

The results show that, in spite of different voltage and current variations at the feeders, the equivalent circuit parameters of the substation seen from them are almost equal. The slight difference could be the result of accuracy of different CTs and PTs and data-acquisition systems used for measurements.

Summary and Comparison

In this section the average of calculated system impedance for each feeder in Substation Three is tabulated and compared with that of the other methods. Table C.1 shows the calculated impedance for each feeder and the average of the fluctuation index for the period of measurements.

Table C.1. Calculated system impedances for Substation Three

Substation	**Feeder**	**Calculated Impedance**	**F. Index (%)**	**Real Fault Data**	**PSS/E Data**
Three	**# 1**	0.719+j2.679	0.1490	0.296+j2.833	0.589+j1.697
	# 2	0.689+j2.623	0.0805		
	# 3	0.755+j2.843	0.1575		
	# 4	0.571+j2.572	0.1515		

As can be seen the proposed algorithm provides acceptable results and the little difference could be the result of measurement errors.

C1.2 Substation Four

The single-line diagram of Substation Four and the feeders selected for measurements are shown in Figure C.10. The measurements are taken at the metering point of the feeders. The Feeders One, Two and Three were chosen to calculate the system equivalent circuit parameters.

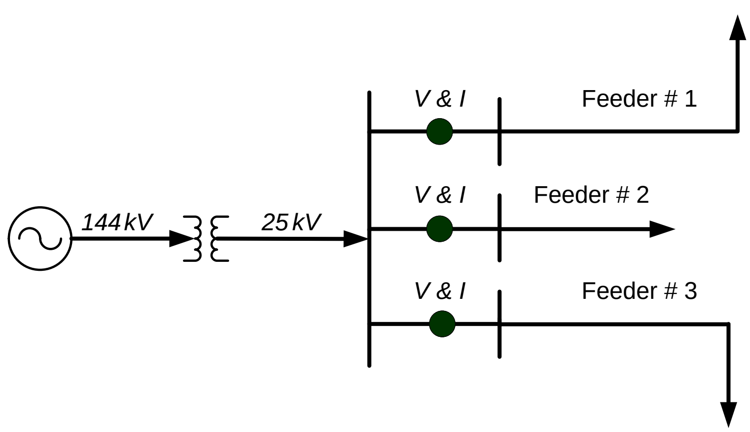

Figure C.10. Single-line diagram of Substation Four

1. Feeder One

The variations of RMS values of positive sequence voltage and current of this feeder during the measurements are shown in Figure C.11.

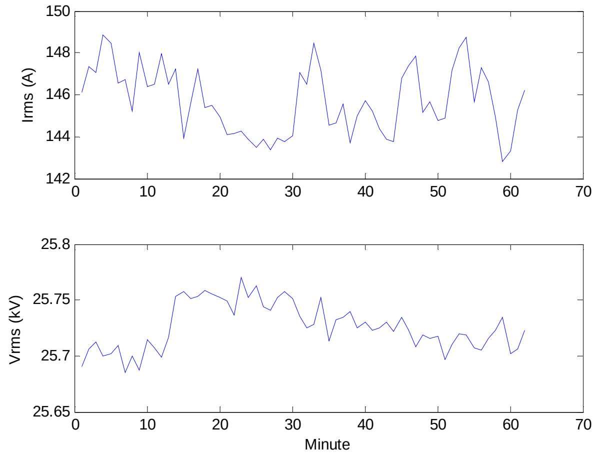

Figure C.11. Voltage and current of Feeder One in Substation Four

The positive sequence parameters of the system are calculated and shown in Figure C.12.

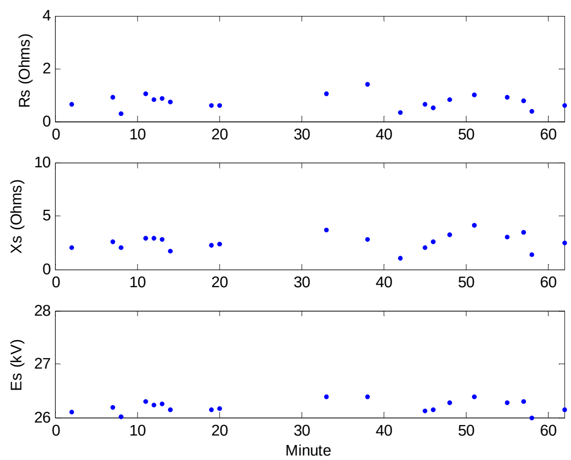

Figure C.12. Circuit parameters of Feeder One in Substation Four

2. Feeder Two

The variations of RMS values of positive sequence voltage and current of this feeder during the measurements are shown in Figure C.13.

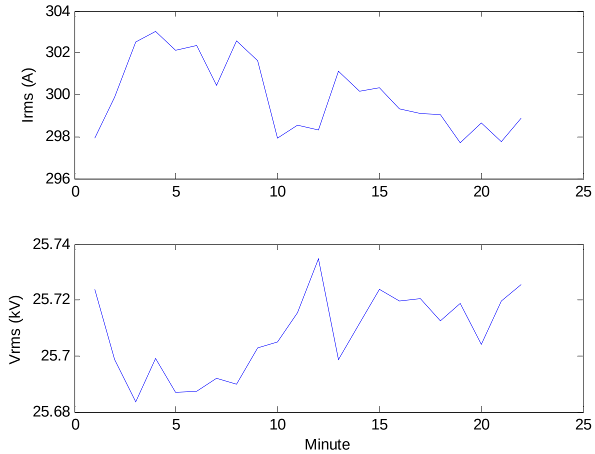

Figure C.13. Voltage and current of Feeder Two in Substation Four

The positive sequence parameters of the system are calculated and shown in Figure C.14.

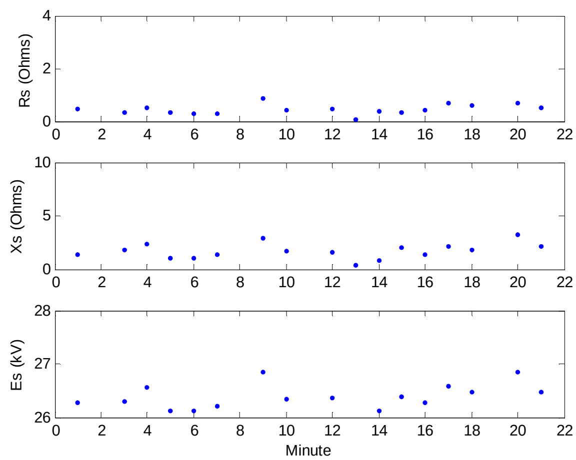

Figure C.14. Circuit parameters of Feeder Two in Substation Four

2. Feeder Three

The variations of RMS values of positive sequence voltage and current of this feeder during the measurements are shown in Figure C.15.

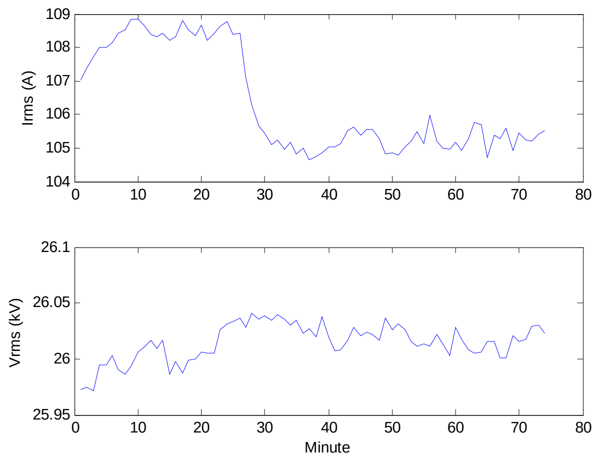

Figure C.15. Voltage and current of Feeder Three in Substation Four

The positive sequence parameters of the system are calculated and shown in Figure C.16.

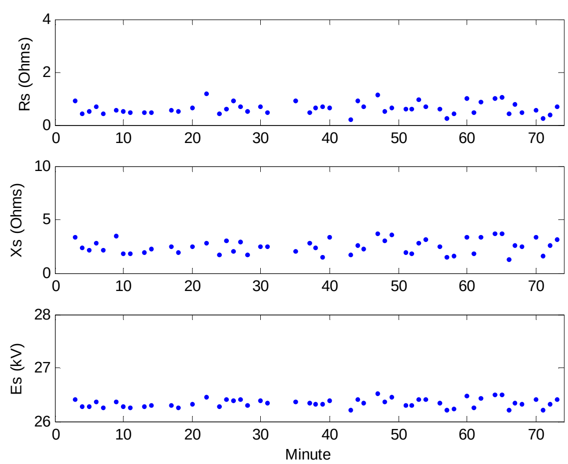

Figure C.16. Circuit parameters of Feeder Three in Substation Four

Summary and Comparison

In this section the average of calculated system impedance for each feeder in Substation Four is tabulated and compared with that of the other methods. Table C.2 shows the calculated impedance for each feeder and average of fluctuation index for the period of measurements.

Table C.2. Calculated system impedances for Substation Four

Substation	**Feeder**	**Calculated Impedance**	**F. Index (%)**	**Real Fault Data**	**PSS/E Data**
Four	**# 1**	0.749+j2.572	0.0729	0.164+j2.403	0.585+j2.115
	# 2	0.450+j1.726	0.0687		
	# 3	0.631+j2.492	0.1305		

Table C.2 shows that the proposed algorithm provides acceptable results and again the little difference could be the result of measurement errors.

C.2 Residential Transformer Level

This section presents the application of the multi-point system impedance measurement method for estimation of system Thevenin impedance seen from residential transformers. Residential transformers are single-phase double-circuit transformers, located all around the city near the customers and supply the residential customers with two different voltage levels, 240V and 120V. The primary voltage of these transformers is usually supplied directly from 15 kV substations using underground cables. For this research the measurements were taken as five seconds every minute with the resolution of 256 samples per second. Variation of the voltage and current at the measurement point are plotted in Figure C.17.

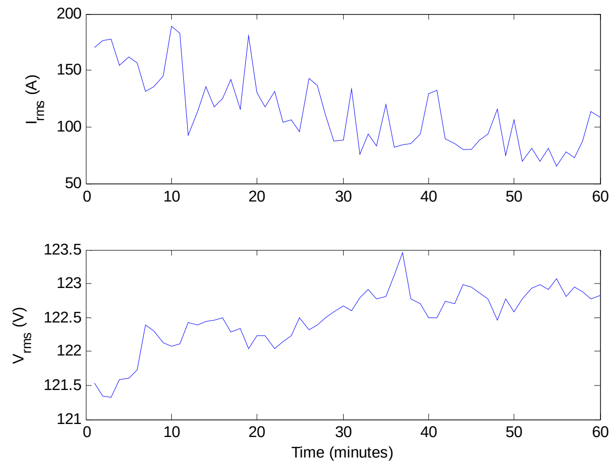

Figure C.17. Voltage and current at the residential transformer

The fluctuation index, defined in Chapter Two, is 1.453% for the period of measurements. The multi-point algorithm was used to calculate the system side parameters and the results are shown in Figure C.18.

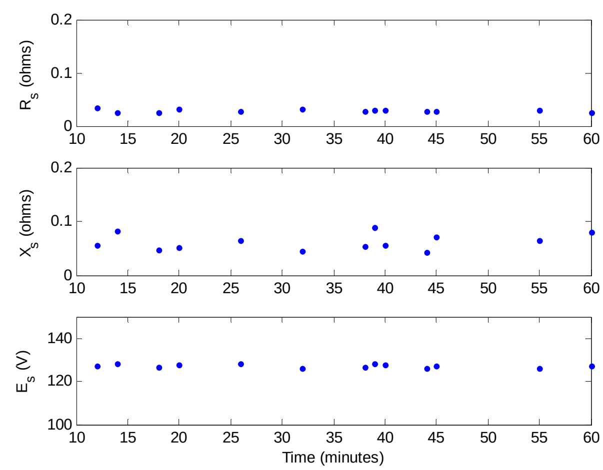

Figure C.18. Impedance parameters seen at the residential transformer

The average calculated impedance for this transformer is 0.0292+j0.0619 ohms. As Figure C.18 reveals, for some periods of time, the parameters are not calculated. The reason is the variation of system side parameters during the measurements. For further illustrations, Table C.3 is provided for a sample 5 second snapshot captured at different system's voltage levels.

Table C.3. Disturbance source detection at different points of the system

Measurement Level \ Disturbance Source	**Load Side only**	**System Side only**	**Both Sides**
House	18.64%	45.76%	35.59%
Residential Transformer	16.61%	64.74%	18.64%
Substation Transformer	62.37%	36.09%	1.53%

Table C.3 shows that at the residential transformers, the system side is mainly the disturbance source while at the substation transformer the disturbance side is the load side. The load disturbance only which will result in calculation of system side impedance parameters is maximum at the substation level and minimum in residential transformer level. This is the reason that makes the impedance estimation more difficult at the residential transformers. However, it is not still impossible; with using more data we can get more accurate and reliable results.

C.3 House Level

This section presents the application of the multi-point system impedance measurement method for estimation of system Thevenin impedance seen from house level. For this research the measurements were taken as five seconds every minute with the resolution of 256 samples per second. Variation of the voltage and current at the measurement point are plotted in Figure C.19.

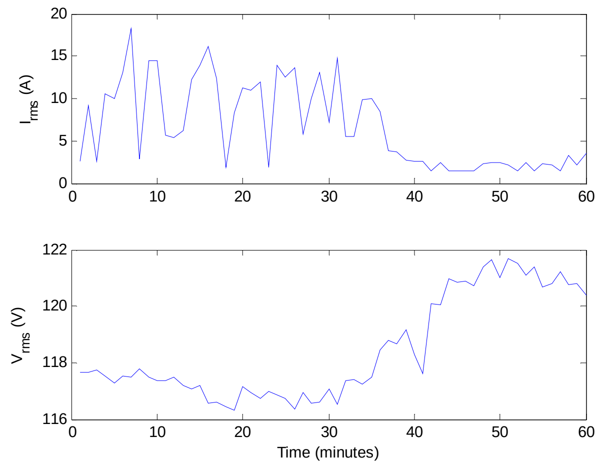

Figure C.19. Voltage and current at the house level

The fluctuation index, defined in Chapter Two, is 3.191% for the period of measurements. The multi-point algorithm was used to calculate the system side parameters and the results are shown in Figure C.20.

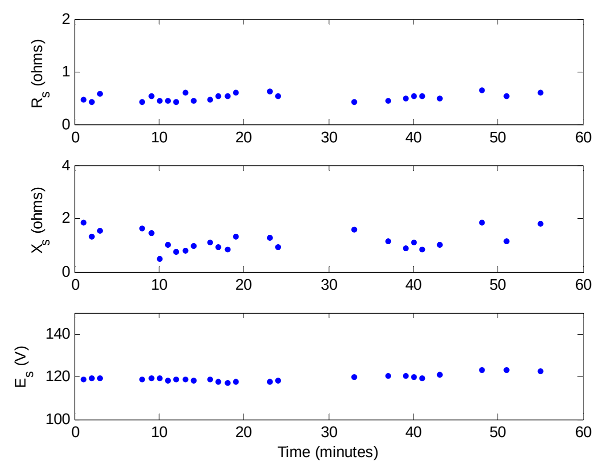

Figure C.20. Impedance parameters seen at the house level

The average calculated impedance for this transformer is 0.52+j1.20 ohms. As Figure C.20 reveals, for some periods of time, the parameters are not calculated. The reason is again, the variation of system side parameters during the measurements as presented in Table C.3.

Appendix D

Harmonic Impedance Measurement at Different Points of System

D.1 Residential Transformer Level

In this section the modified multi-point algorithm was used to calculate the system side harmonic impedances seen at the residential transformers. Residential transformers are single-phase double-circuit transformers, located all around the city near the customers and supply the residential customers with two different voltage levels, 240V and 120V. The primary voltage of these transformers is usually supplied directly from 15 kV substations by using underground cables. The average harmonic voltages for one-hour at the measurement point are plotted in Figure D.1.

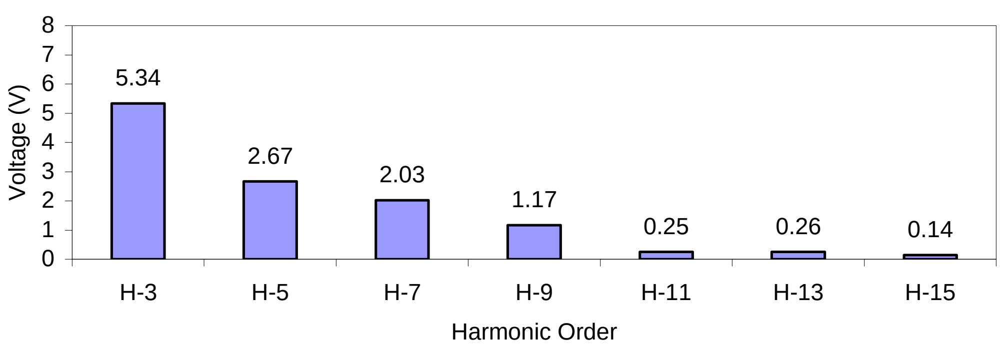

Figure D.1. Harmonic voltages at the residential transformer level

The average harmonic currents for the measurement period are also plotted in Figure D.2.

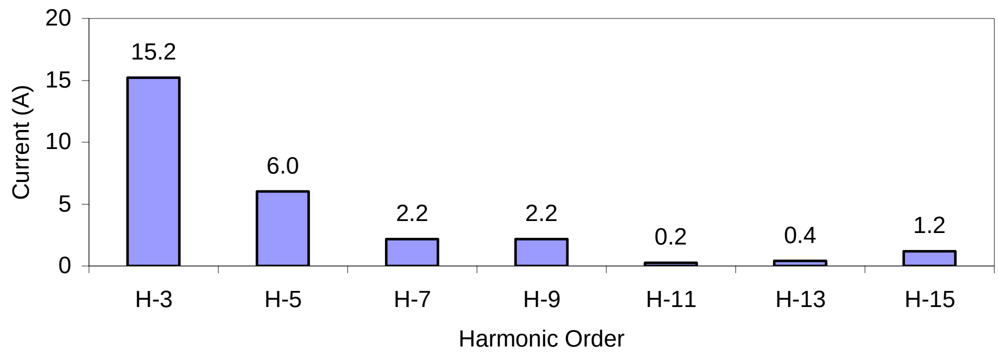

Figure D.2. Harmonic currents at the residential transformer level

Figure D.2 shows that the harmonic voltage and currents are different for different harmonics. For example the harmonics 11, 13 and 15 have very low magnitudes of voltages and currents (less than 1% of fundamental component) which may affect the calculation results. Applying the multi-point algorithm we will have the following values for the harmonic impedances.

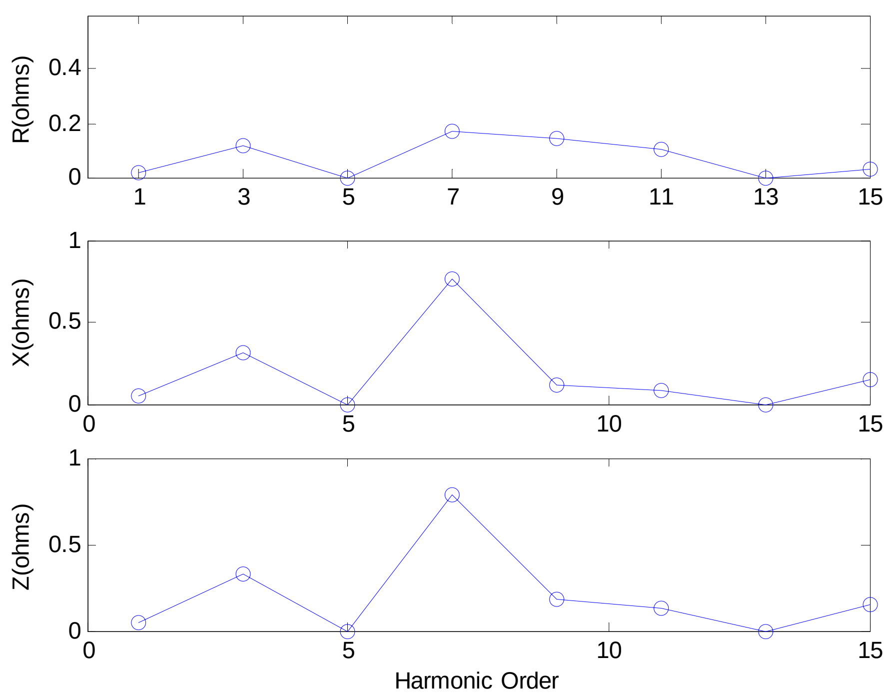

Figure D.3. Calculated harmonic impedances using multi-point algorithm

Some of the calculated results seemed to be incorrect. To look further into the problem we needed the average fluctuation index for the period of measurements. The average fluctuation indices, defined in Chapter Three, for each harmonic was calculated and plotted in Figure D.4.

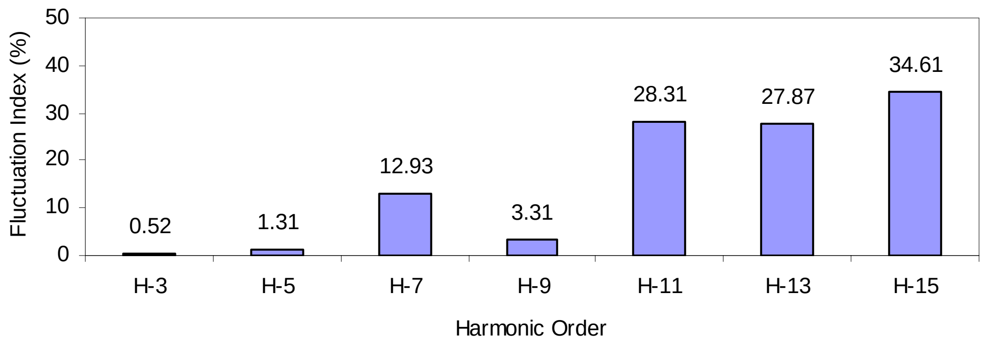

Figure D.4. Fluctuation index at the residential transformer point

It is seen that the fluctuation index for some harmonics are very high and for some is low. The reason to have high fluctuation index is the low magnitude of harmonic voltages and currents especially for the 11th, 13th and 15th harmonic order. In order to have accurate and reliable results, the magnitude of harmonic voltages and currents firstly and then the fluctuation index should be high. Therefore in this case, the 9th, 11th, 13th, and 15th calculated harmonic impedances are not reliable, and we should check other data windows for calculating them. If we consider the reliable impedances and plot the trend of impedances we will have the following graphs for R_h, X_h and $Z_{h..}$

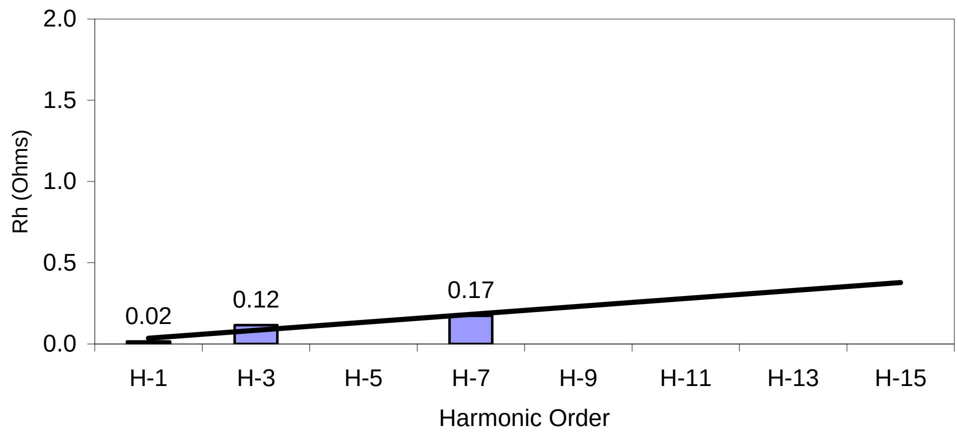

Figure D.5. Calculated resistance at the residential transformer point

The calculated system's harmonic inductance is plotted in Figure D.6.

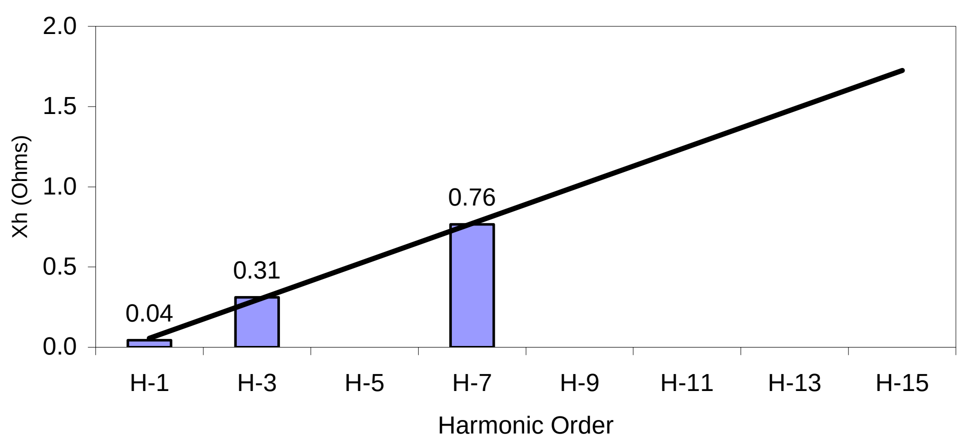

Figure D.6. Calculated reactance at the residential transformer point

The calculated system's harmonic impedance for different harmonics is plotted in Figure D.7.

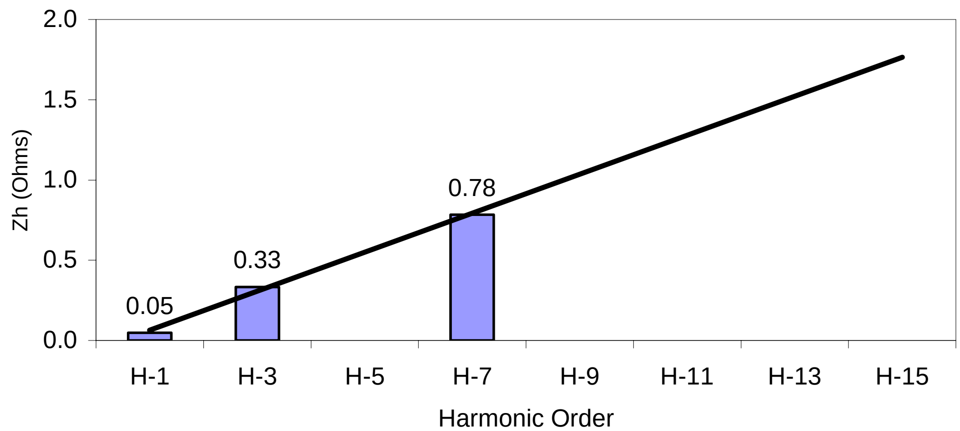

Figure D.7. Calculated impedance at the residential transformer point

As can be seen by using the magnitude of harmonic voltages and currents and the fluctuation index, the reliable calculated parameters from each snapshot can be selected and the rest can be estimated from the other data windows.

D.2 House Level

In this section the modified multi-point algorithm is used to calculate the system side harmonic impedances seen at the house level. The average harmonic voltages for one hour at the measurement point are plotted in Figure D.8.

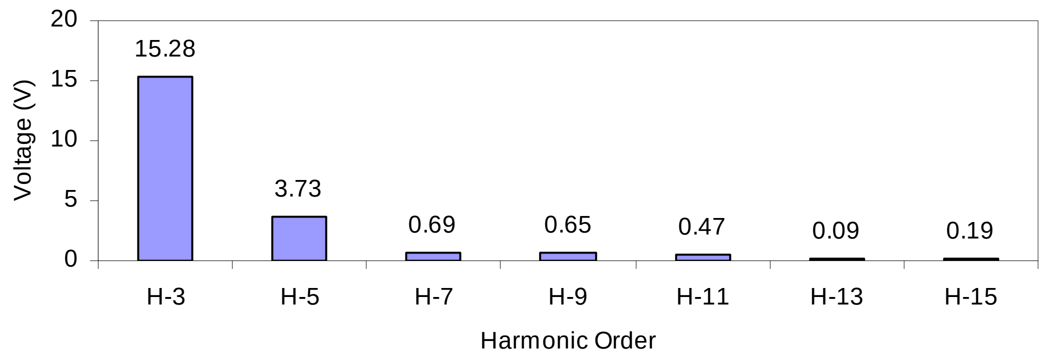

Figure D.8. Harmonic voltages at the house level

The average harmonic currents for the measurement period are also plotted in Figure D.9.

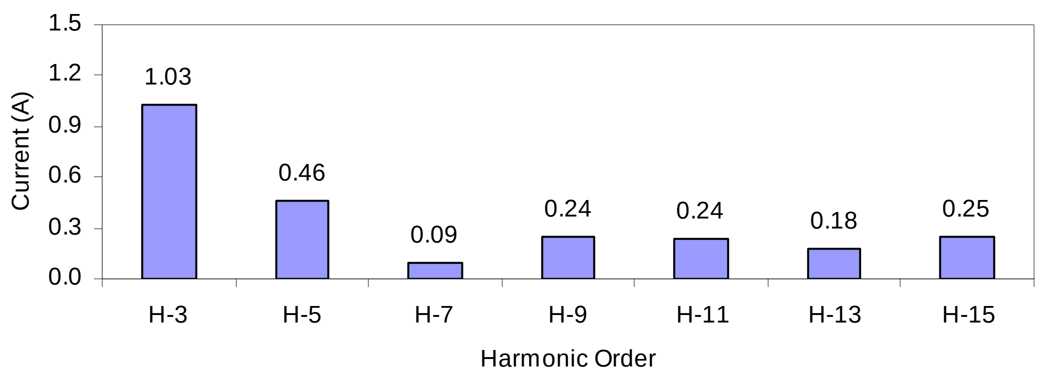

Figure D.9. Harmonic voltages at the house level

It can be seen that the harmonic voltage and currents are different for different harmonics. Harmonics 7 to 15 have very low values for voltages and currents comparing to 3rd and 5th harmonic. This may affect the accuracy of calculated results. Applying the multi-point algorithm we will have the following values for the harmonic impedances.

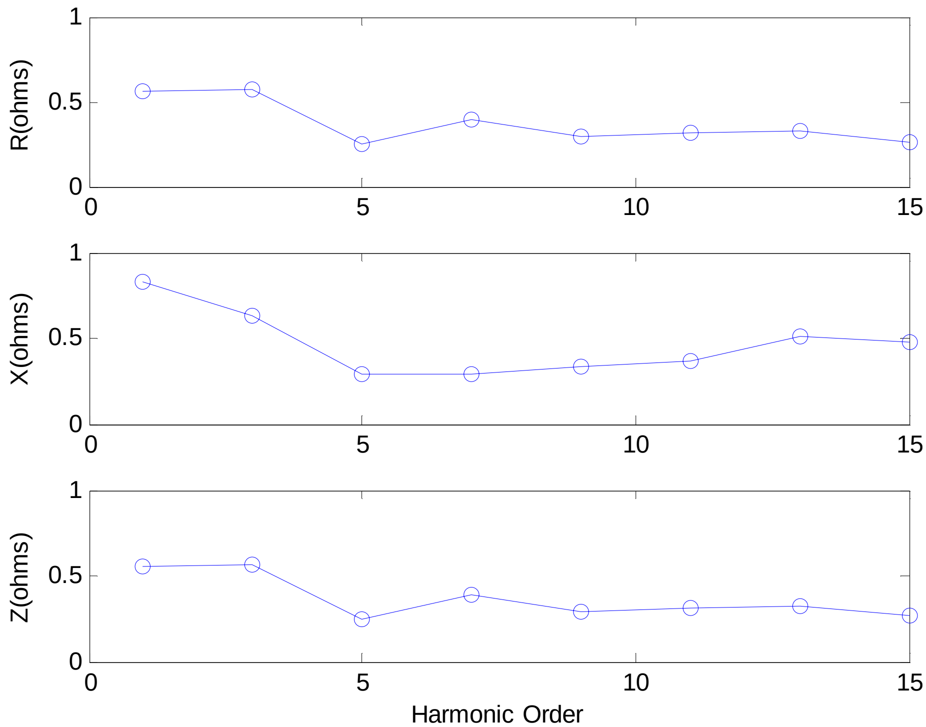

Figure D.10. Calculated harmonic impedances using multi-point algorithm

The average fluctuation indices, defined in Chapter Three, for each harmonic is calculated and plotted in Figure D.11.

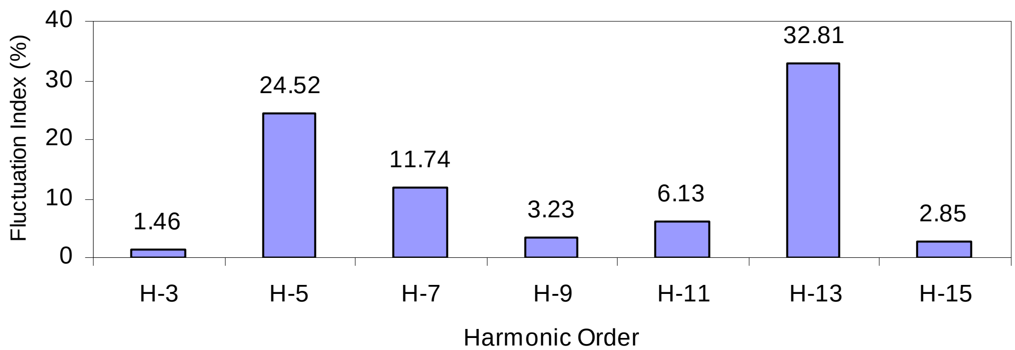

Figure D.11. Fluctuation index at the house point

Figure D.11 reveals that the fluctuation index for some harmonics is very high and for some is low. The reason to have high fluctuation index is again the low magnitude of harmonic voltages and currents especially for the 11th to 15th harmonic. In order to have accurate and reliable results, the magnitude of harmonic voltages and currents firstly and then the fluctuation index should be high. If we consider the reliable impedances and plot the trend of impedances we will have the following graphs for R_h, X_h and Z_h..

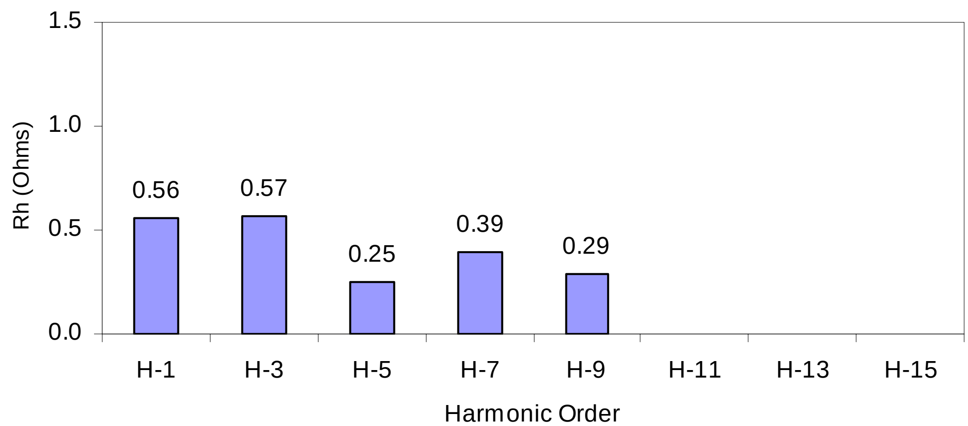

Figure D.12. Calculated resistance at the house point

The calculated system's harmonic inductance is plotted in Figure D.13.

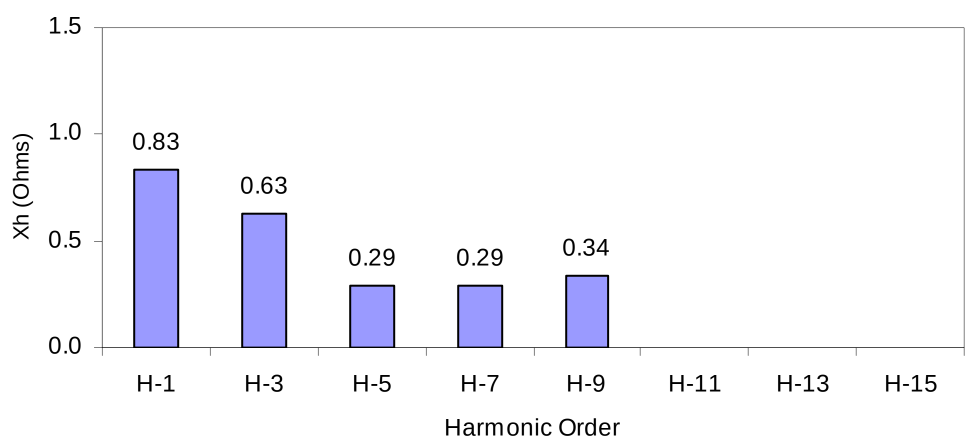

Figure D.13. Calculated inductance at the house point

The calculated system's harmonic impedance for different harmonics is plotted in Figure D.14.

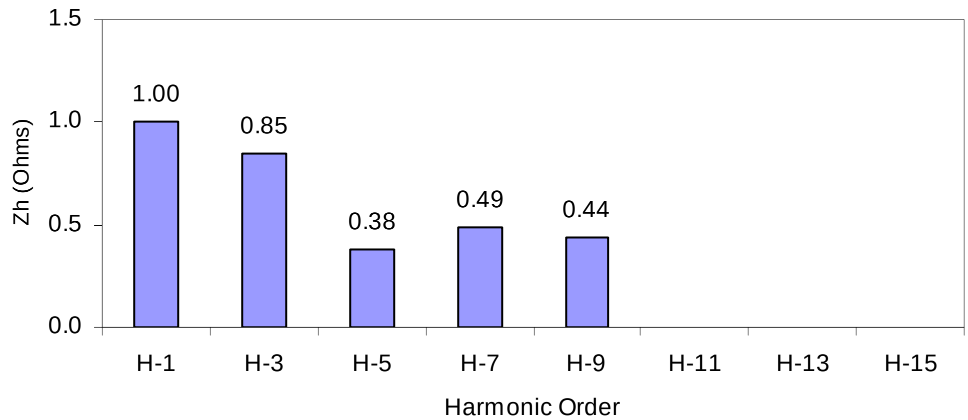

Figure D.14. Calculated impedance at the house point

As can be seen by using the magnitude of harmonic voltages and currents at any measurement point in the power system and the fluctuation index, the reliable calculated parameters from each snapshot can be selected and the rest can be estimated from the other data windows.

Appendix E

Characteristics of Load Parameters for all Substations

E.1 Load Profiles and Average Load Parameters

In the following tables the load profile and the average of calculated load power factor for the weekdays of each group is presented.

1. Group I - Commercial and Residential

This group of loads has both commercial and residential load types.

Table E.1. Load profiles and load parameters of Group I

Load Parameters			Load Profile
M1.1	Power Factor	0.94	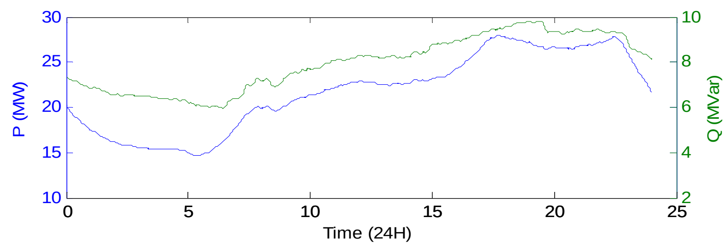
M1.2	Power Factor	0.94	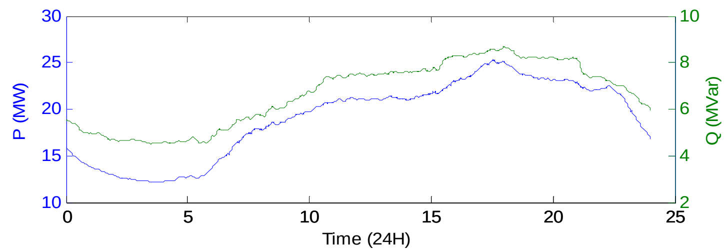
M1.3	Power Factor	0.98	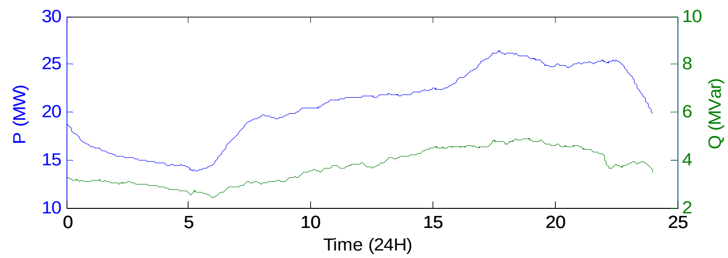

Table E.1 shows that the load active power profile is almost the same for all the transformers, the reactive power profile is almost the same for M1.1 and M1.2 but different from M1.3. Transformer Three has less reactive load and larger power factor than the other two and as presented in the table the corresponding load model parameter, "b", is different from the others.

2. Group II - Commercial and Residential

This group of load has also both commercial and residential load types with lesser load variation and peaks comparing to the loads in Group I.

Table E.2. Load profiles and load parameters of Group II

<table>
<tr><th colspan="3">Load Parameters</th><th>Load Profile</th></tr>
<tr><td>P1.1</td><td>Power Factor</td><td>0.94</td><td>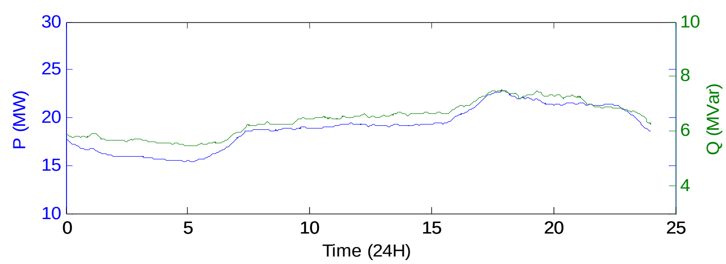
</td></tr>
<tr><td>C2.8</td><td>Power Factor</td><td>0.94</td><td>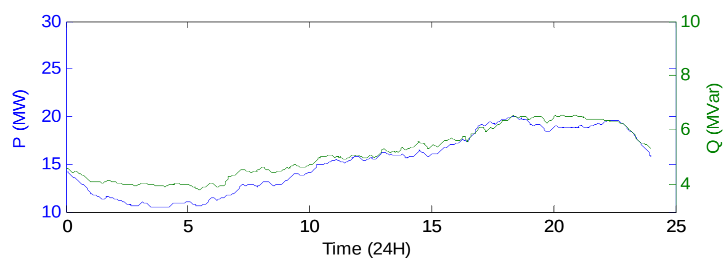
</td></tr>
</table>

The calculated load model parameters for this two groups and the average load power factor before tap movement is presented in the table. It can be seen that the load power factor is almost the same which correspond to the same load type and the load model parameters are close to each other.

3. Group III - Mostly Residential

This group of load has more residential loads than commercials. The average power factor of this kind of loads is also larger than the other two groups.

Table E.3. Load profiles and load parameters of Group III

Load Parameters			Load Profile
C1.2	**Power Factor**	0.96	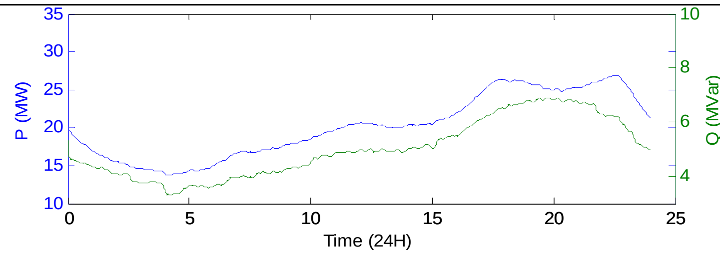
P1.2	**Power Factor**	0.96	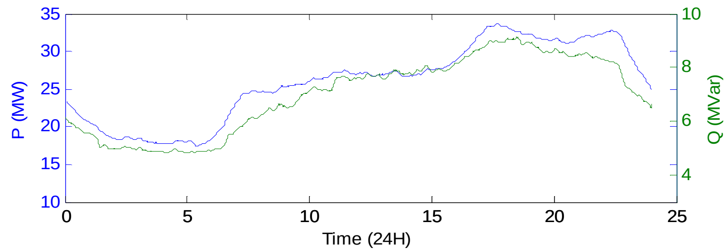
P2.7	**Power Factor**	0.95	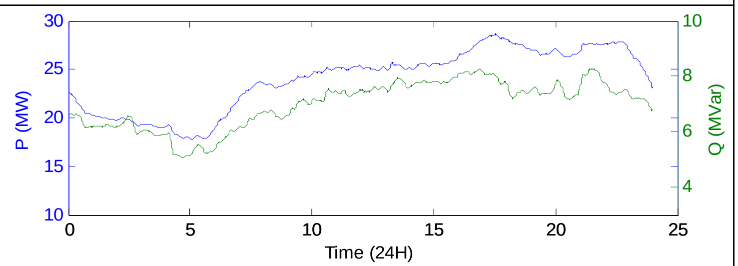
P2.8	**Power Factor**	0.96	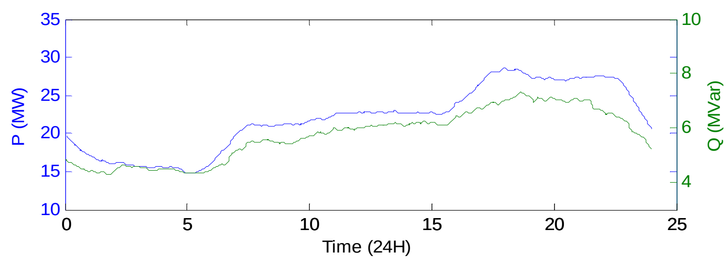

Table E.3 shows that the more similar load profiles, leads to closer calculated load model parameters.

4. Group IV - Mostly Commercial

This group of load is mostly constructed from commercial loads.

Table E.4. Load profiles and load parameters of Group IV

Load Parameters			**Load Profile**
J3.1	**Power Factor**	0.92	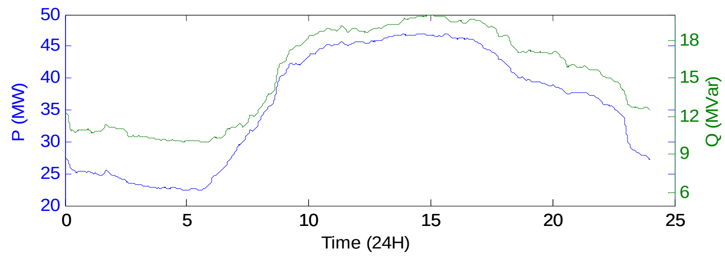
J3.3	**Power Factor**	0.94	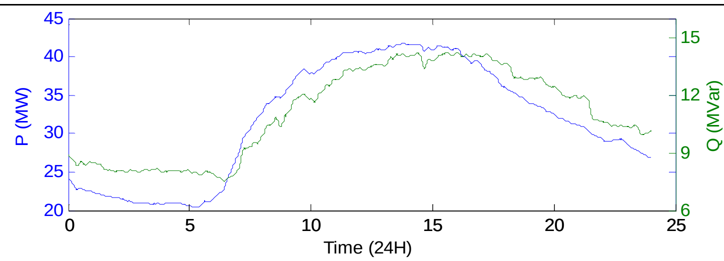
J3.8	**Power Factor**	0.92	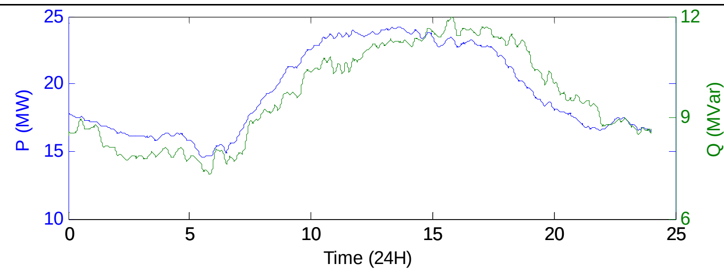
J4.2	**Power Factor**	0.92	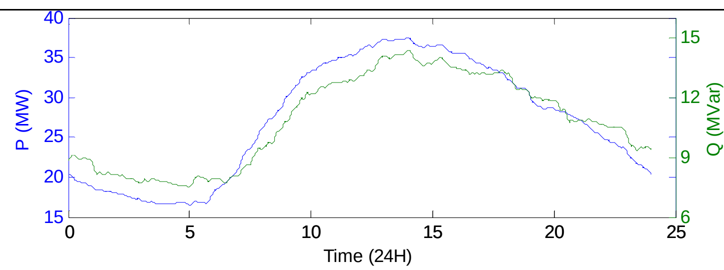
J4.7	**Power Factor**	0.89	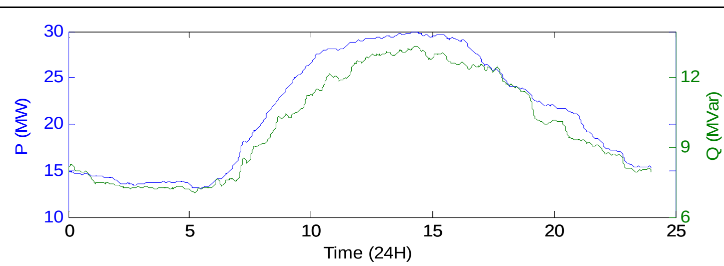

E.2 Load Power Factors of Transformers

Table E.5 presents the average calculated load power factors for the transformers.

Table E.5. The transformers' loads' power factors

Substation	Transformer & Day		Load Power Factor					
	T.	D.	0 to 4	4 to 8	8 to 12	12 to 16	16 to 20	20 to 23
One	M1.1	WD	**0.924**	**0.938**	**0.944**	**0.938**	**0.952**	**0.944**
		WE	0.925	0.938	0.942	0.954	0.953	0.943
	M2.1	WD	**0.934**	**0.941**	**0.947**	**0.941**	**0.948**	**0.944**
		WE	0.935	0.942	0.951	0.947	0.952	0.948
	M3.1	WD	**0.983**	**0.983**	**0.987**	**0.987**	**0.989**	**0.988**
		WE	0.986	0.984	0.989	0.989	0.99	0.992
Two	P1.1	WD	**0.938**	**0.948**	**0.943**	**0.94**	**0.946**	**0.944**
		WE	0.944	0.942	0.945	0.949	0.948	0.945
	P1.2	WD	**0.96**	**0.967**	**0.964**	**0.967**	**0.965**	**0.963**
		WE	0.96	0.963	0.964	0.956	0.966	0.964
	P2.7	WD	**0.954**	**0.957**	**0.959**	**0.957**	**0.961**	**0.957**
		WE	0.952	0.951	0.959	0.955	0.959	0.951
	P2.8	WD	**0.956**	**0.967**	**0.964**	**0.959**	**0.966**	**0.966**
		WE	0.96	0.964	0.964	0.962	0.959	0.967
Three	J3.1	WD	**0.915**	**0.932**	**0.932**	**0.929**	**0.915**	**0.917**
		WE	0.922	0.935	0.935	0.931	0.919	0.92
	J3.3	WD	**0.928**	**0.95**	**0.953**	**0.948**	**0.937**	**0.933**
		WE	0.932	0.928	0.948	0.95	0.938	0.935
	J3.8	WD	**0.931**	**0.94**	**0.956**	**0.947**	**0.91**	**0.895**
		WE	0.935	0.902	0.958	0.948	0.912	0.901
	J4.2	WD	**0.902**	**0.935**	**0.942**	**0.939**	**0.925**	**0.921**
		WE	0.911	0.936	0.935	0.942	0.926	0.923
	J4.7	WD	**0.879**	**0.903**	**0.921**	**0.921**	**0.903**	**0.888**
		WE	0.91	0.908	0.887	0.933	0.908	0.89
Four	C1.2	WD	**0.967**	**0.97**	**0.971**	**0.966**	**0.973**	**0.971**
		WE	0.968	0.973	0.971	0.97	0.971	0.975
	C2.8	WD	**0.941**	**0.943**	**0.947**	**0.95**	**0.959**	**0.95**
		WE	0.951	0.95	0.947	0.953	0.945	0.955

The 24 hour day has been split to six segments. Each segment includes four hours which makes the comparisons easier. It also shows the substation name, transformer and bus number.

E.3 Load Parameters versus Load Profiles

The load profiles and the calculated static load model parameters are shown in this section.

1. Substation One

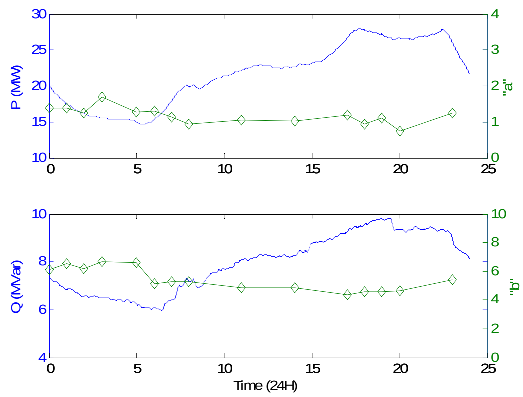

Transformer M2.1 – Commercial and Residential

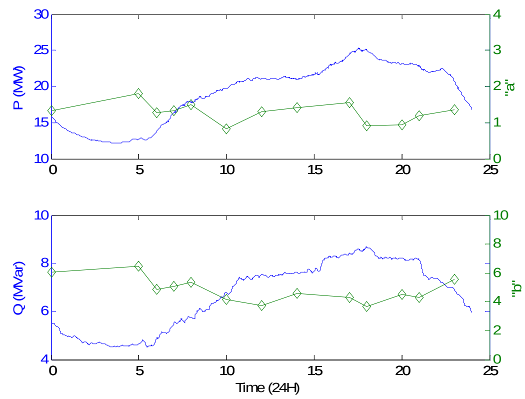

Transformer M2.2 – Commercial and Residential

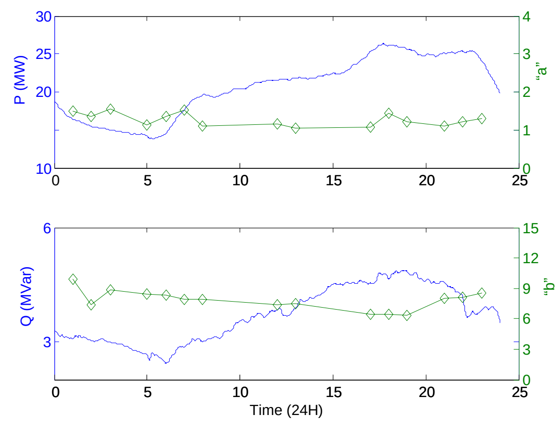

Transformer M3.1 – Commercial and Residential

Figure E.1 Load parameters vs. load profiles - Substation One

2. Substation Two

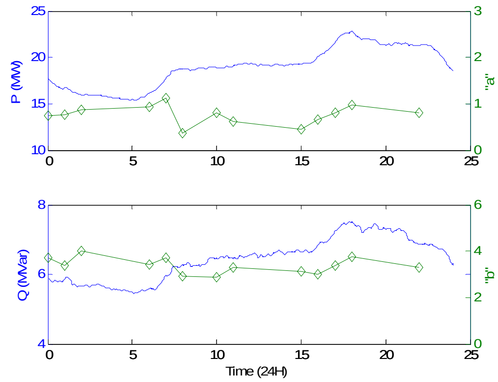

Transformer P1.1 – Commercial and Residential

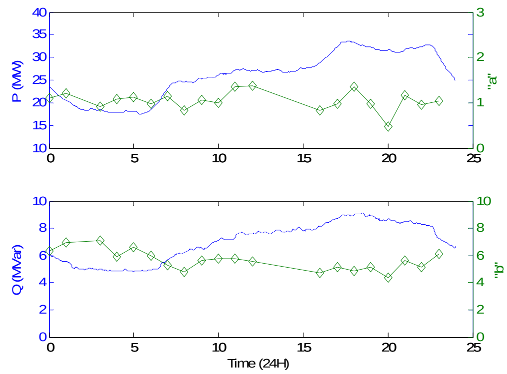

Transformer P1.2 – Mostly Residential

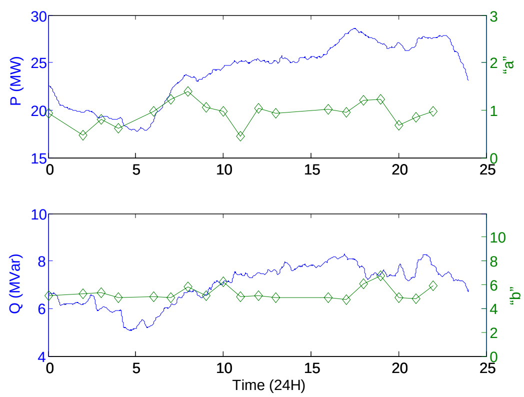

Transformer P2.7 – Mostly Residential

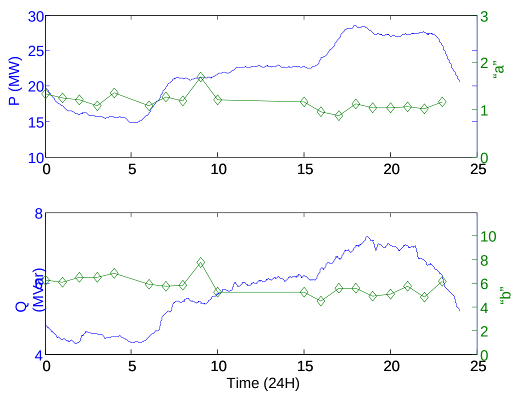

Transformer P2.8 – Mostly Residential

Figure E.2. Load parameters vs. load profiles - Substation Two

3. Substation Three

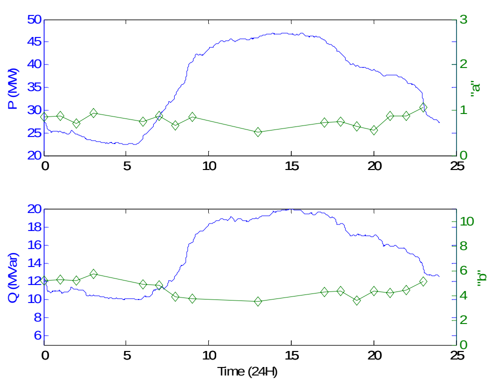

Transformer J3.1 – Mostly Commercial

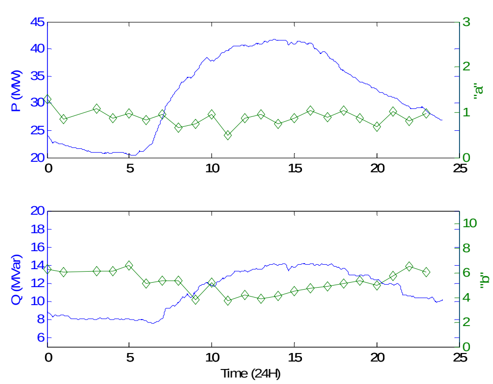

Transformer J3.3 – Mostly Commercial

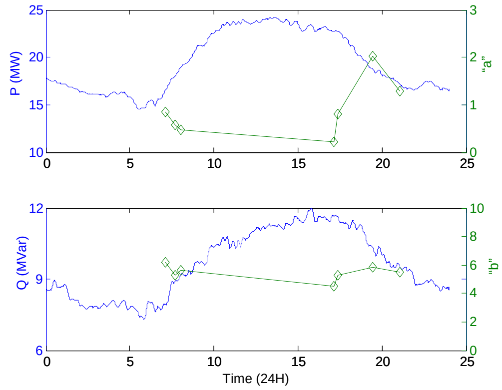

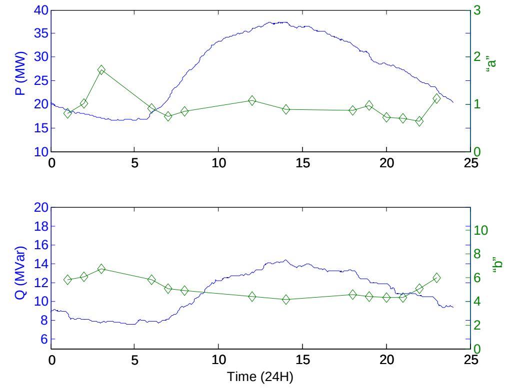

Transformer J3.8 – Mostly Commercial

Transformer J4.2 – Mostly Commercial

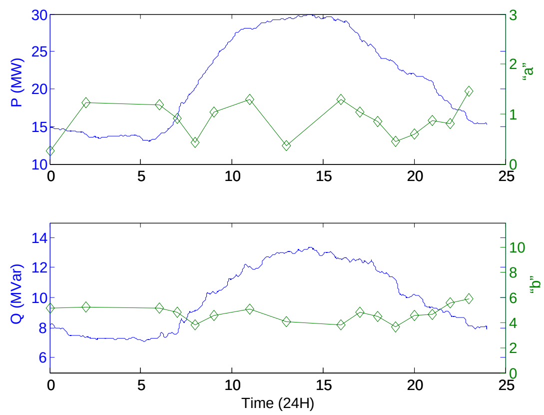

Transformer J4.7 – Mostly Commercial

Figure E.3. Load parameters vs. load profiles - Substation Three

4. Substation Four

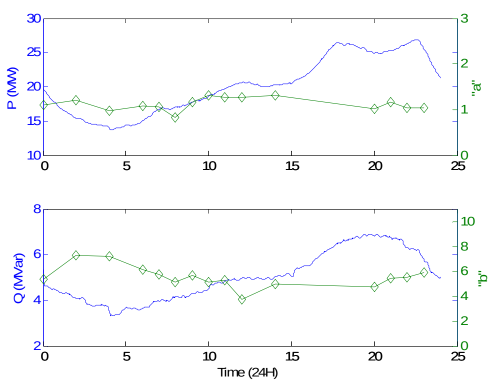

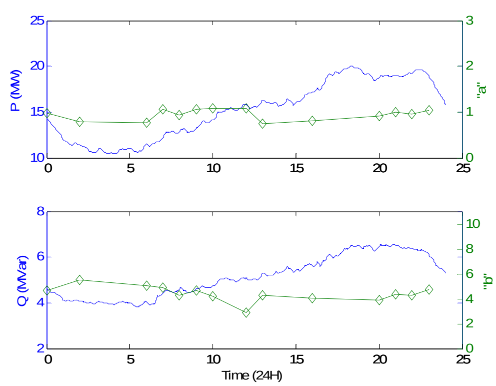

Transformer C1.2 – Mostly Residential

Transformer C2.8 – Commercial and Residential

Figure E.4. Load parameters vs. load profiles - Substation Four

E.4 Load Parameters as Affected by Voltage Step Change

The step change in voltage caused by tap movement is plotted in the following figures for the weekdays.

1. Substation One

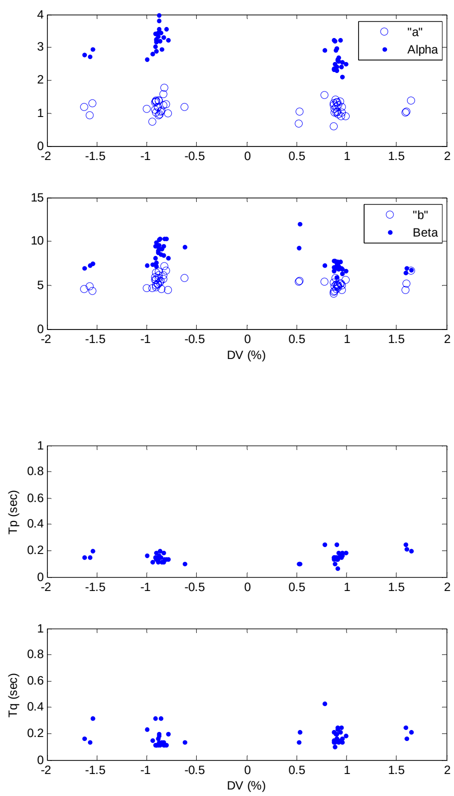

Transformer M1.1 – Commercial and Residential

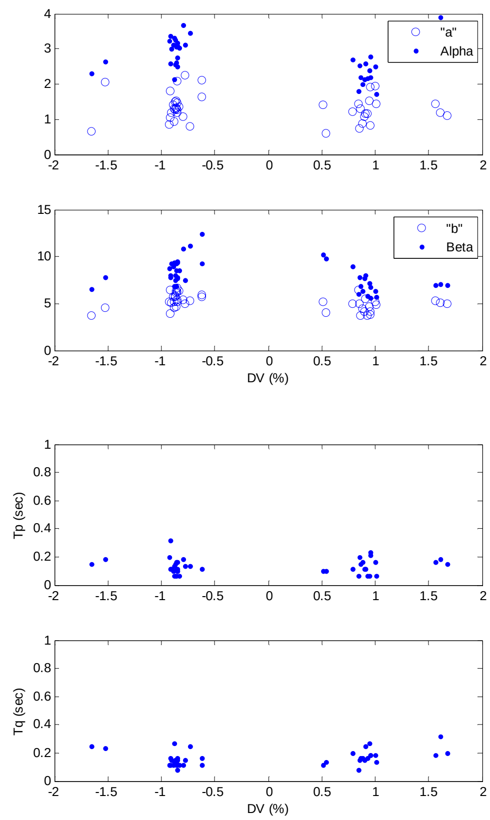

Transformer M2.1 – Commercial and Residential

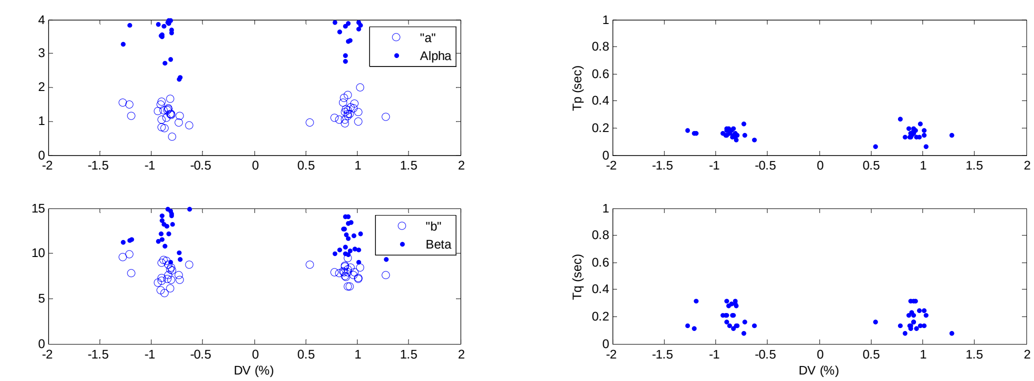

Transformer M3.1 – Commercial and Residential

Figure E.5. Load parameters vs. voltage step change - Substation One

2. Substation Two

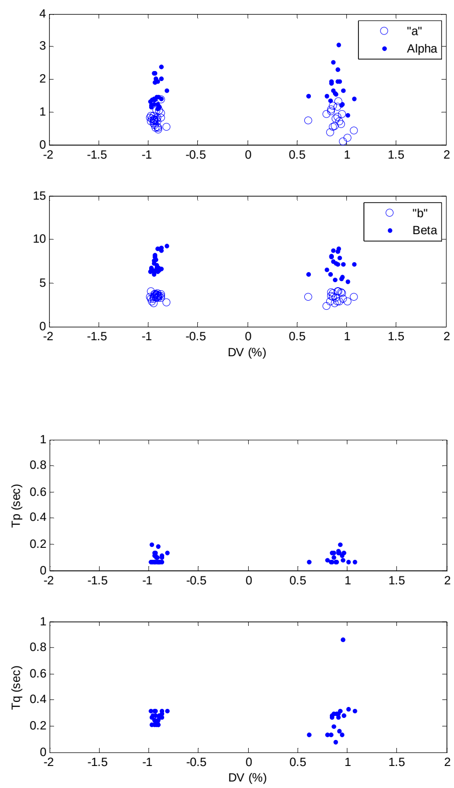

Transformer P1.1 – Commercial and Residential

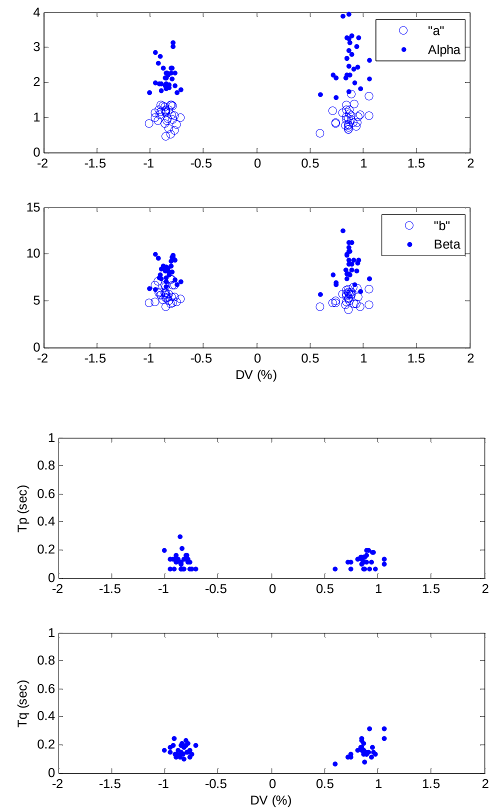

Transformer P1.2 – Commercial and Residential

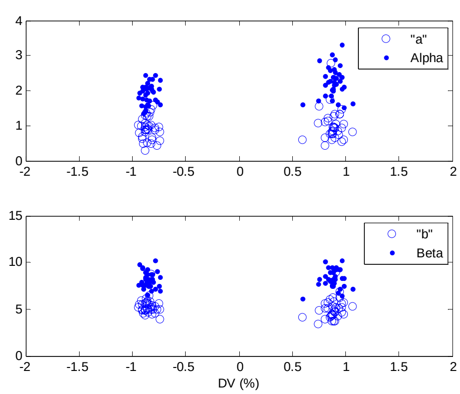

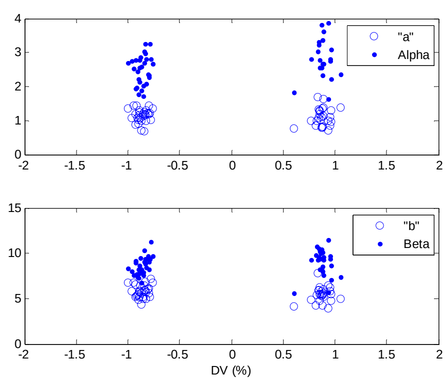

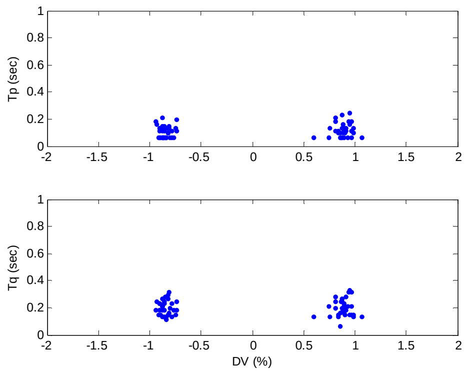

Transformer P2.7 – Mostly Residential

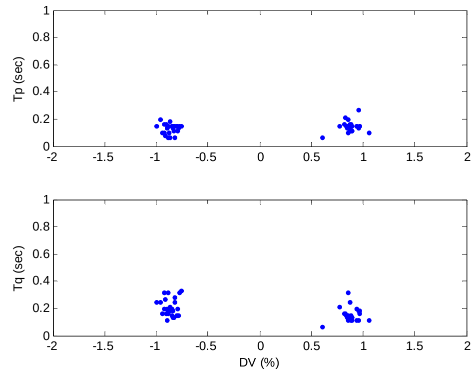

Transformer P2.8 – Mostly Residential

Figure E.6. Load parameters vs. voltage step change - Substation Two

3. Substation Three

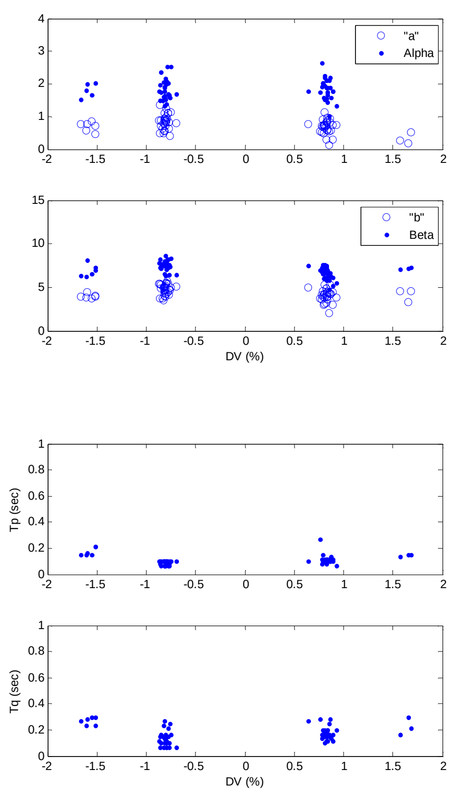

Transformer J3.1 – Mostly Commercial

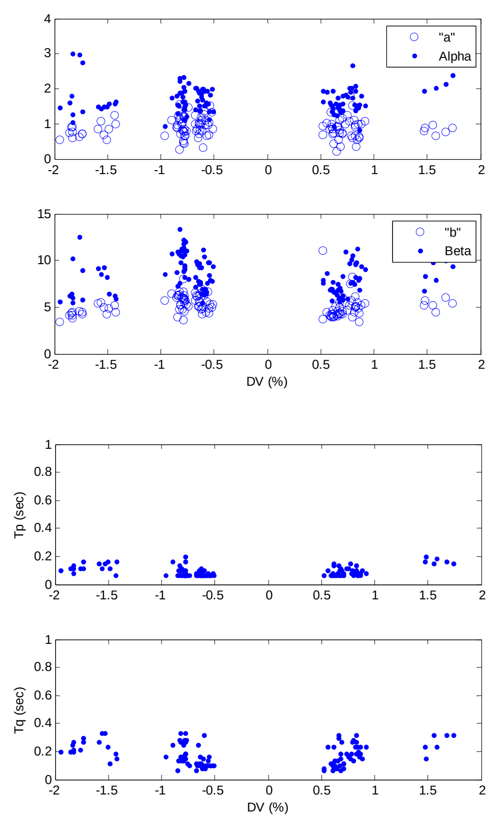

Transformer J3.3 – Mostly Commercial

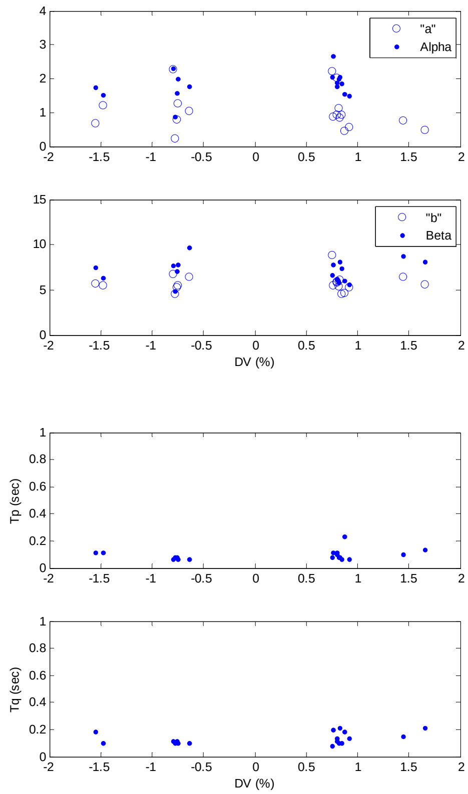

Transformer J3.8 – Mostly Commercial

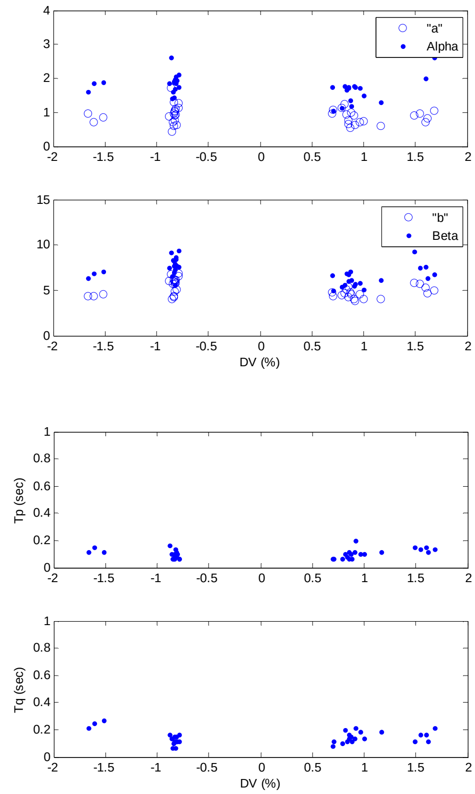

Transformer J4.2 – Mostly Commercial

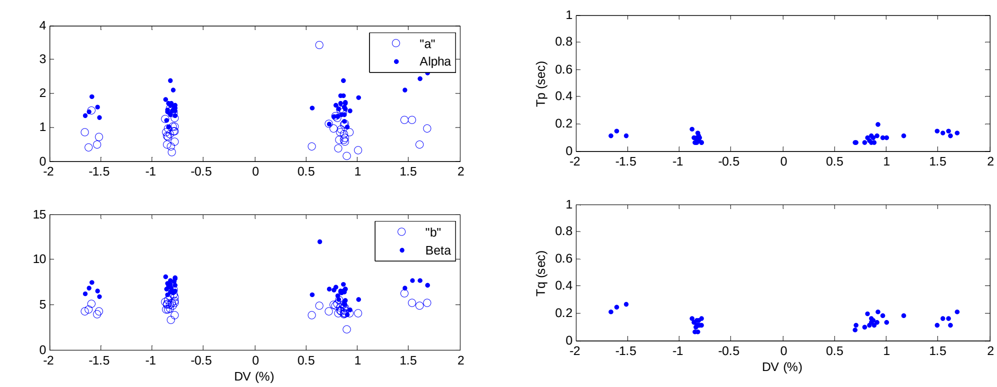

Transformer J4.7 – Mostly Commercial

Figure E.7. Load parameters vs. voltage step change - Substation Three

4. Substation Four

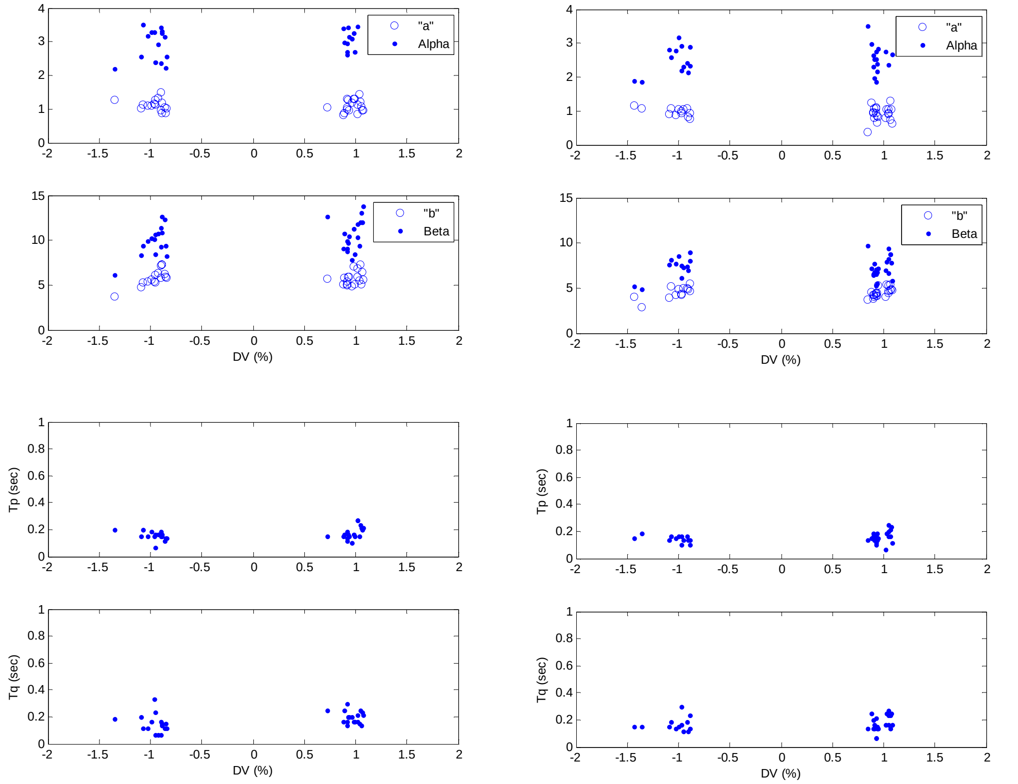

Transformer C1.2 – Mostly Residential Transformer C2.8 – Commercial and Residential

Figure E.8. Load parameters vs. voltage step change - Substation Four

E.5 Load parameters as Affected by Pre-Tap Values of Loads

In this section the load model parameters are plotted versus the pre-tap voltage, active and reactive power.

1. Substation One

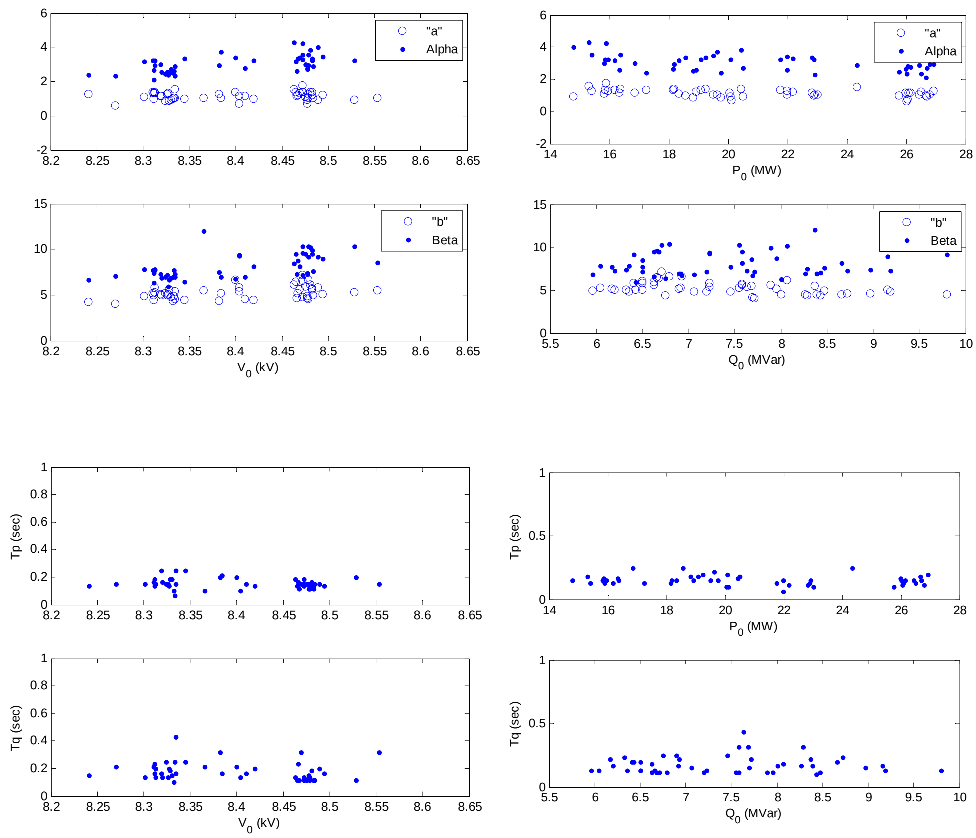

Transformer M1.1 – Commercial and Residential

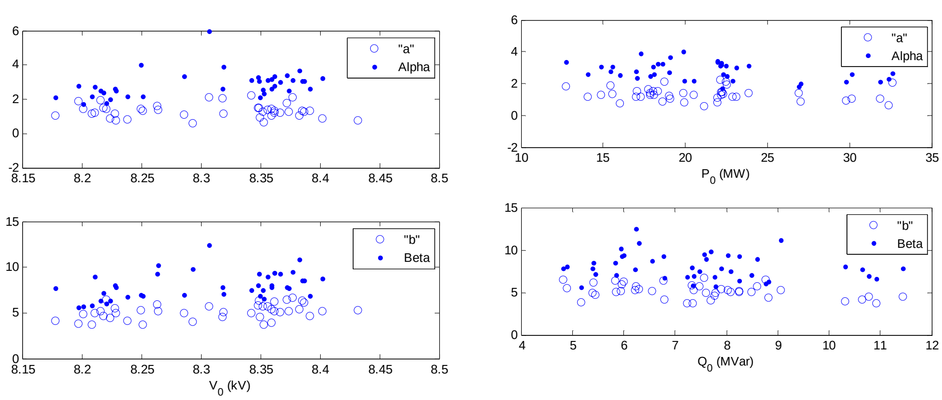

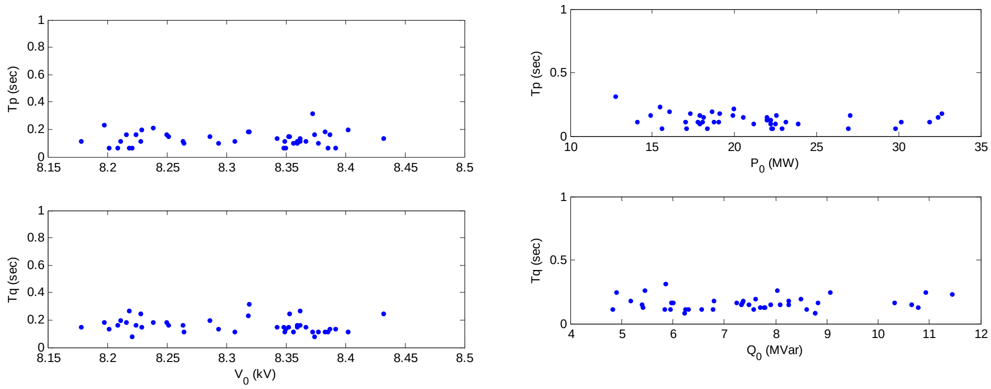

Transformer M2.1 – Commercial and Residential

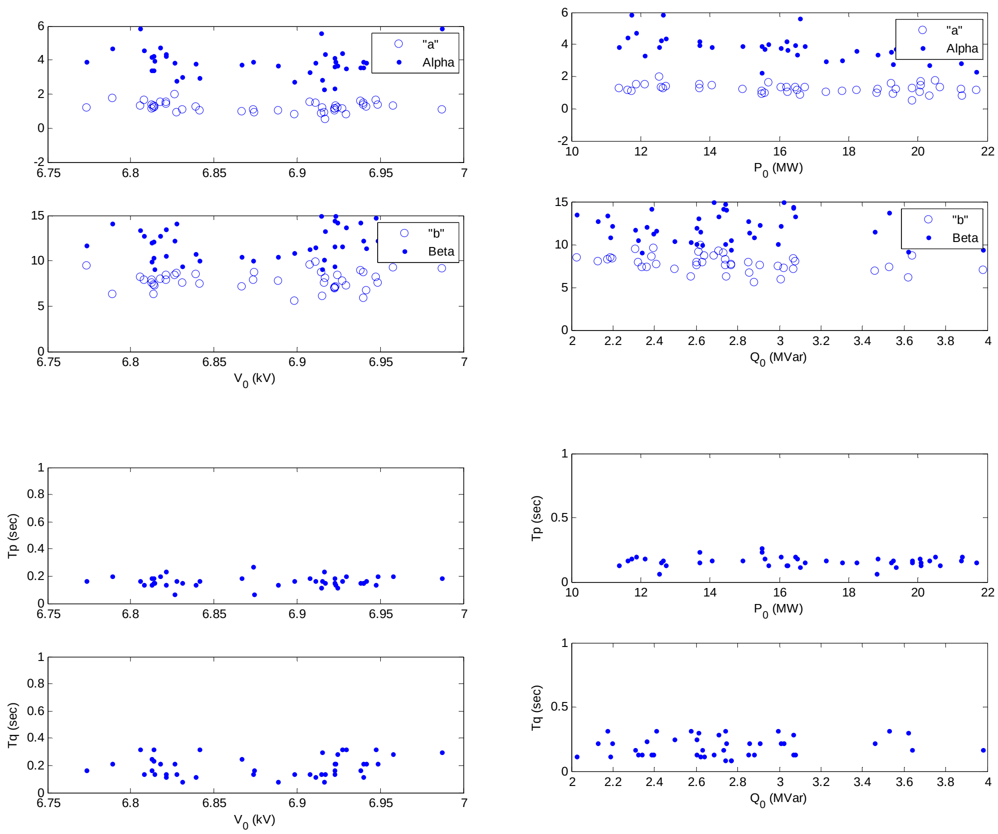

Transformer M3.1 – Commercial and Residential

Figure E.9. Load parameters vs. pre-tap values of loads - Substation One

2. Substation Two

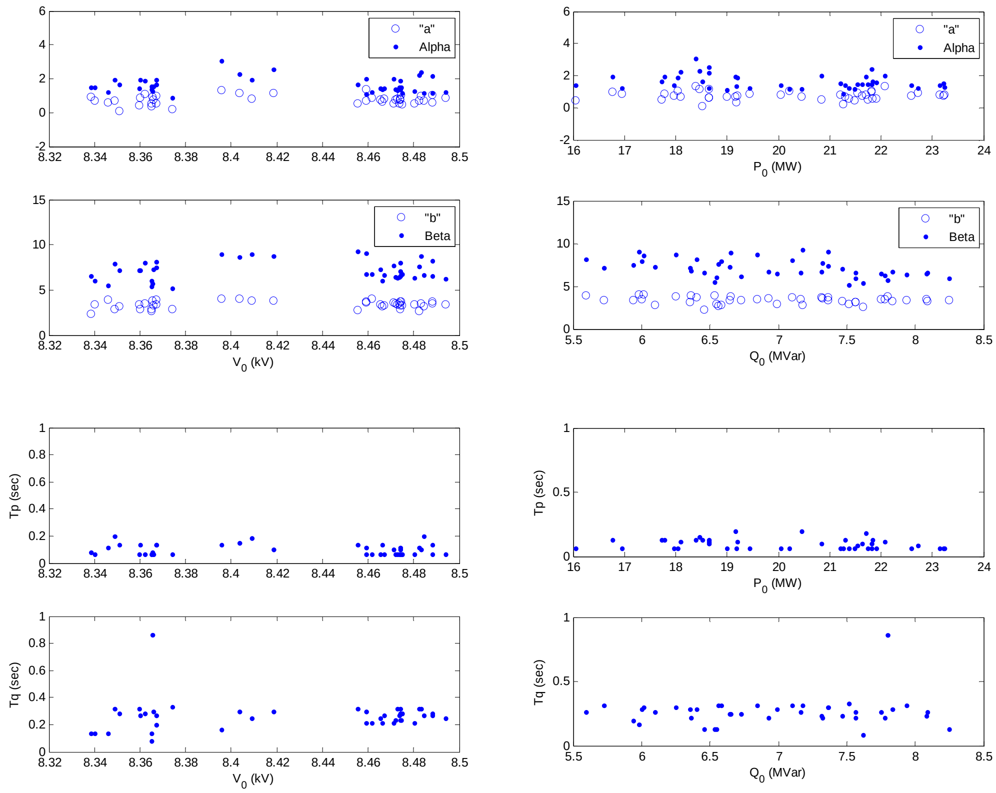

Transformer P1.1 – Commercial and Residential

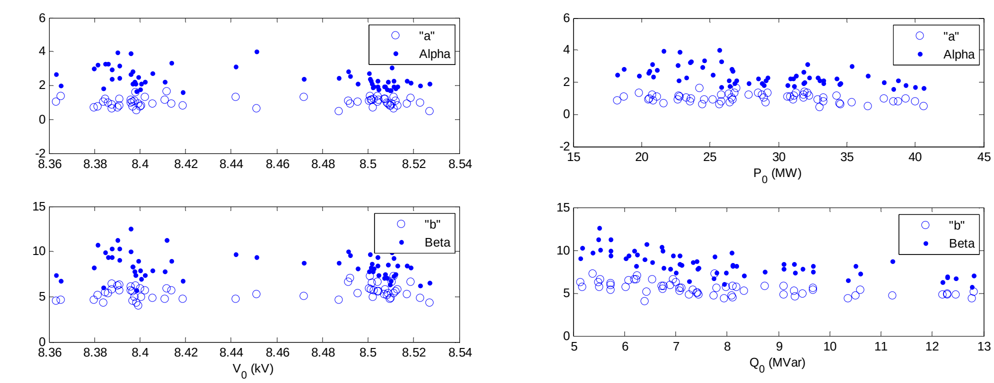

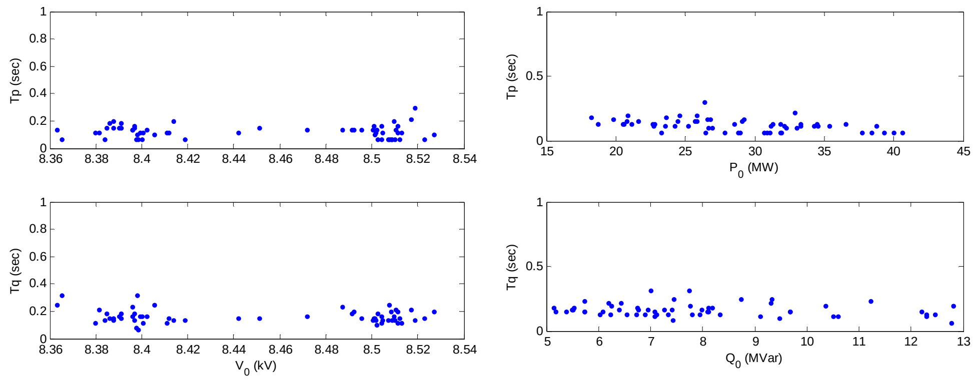

Transformer P1.2 – Mostly Residential

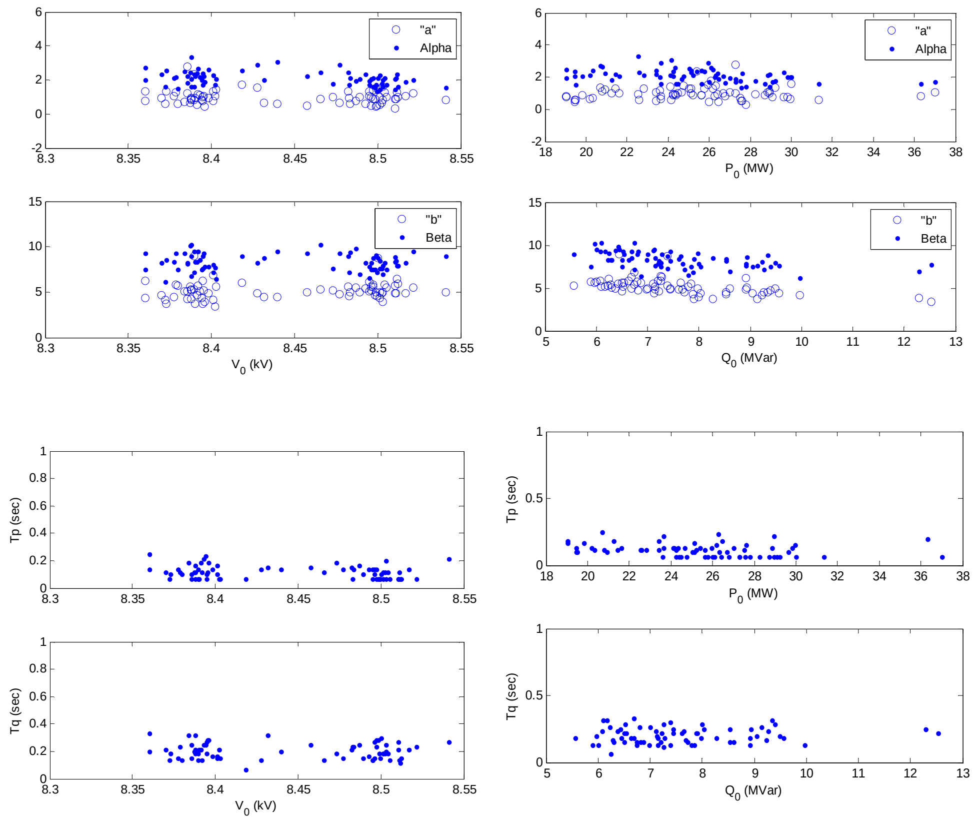

Transformer P2.7 – Mostly Residential

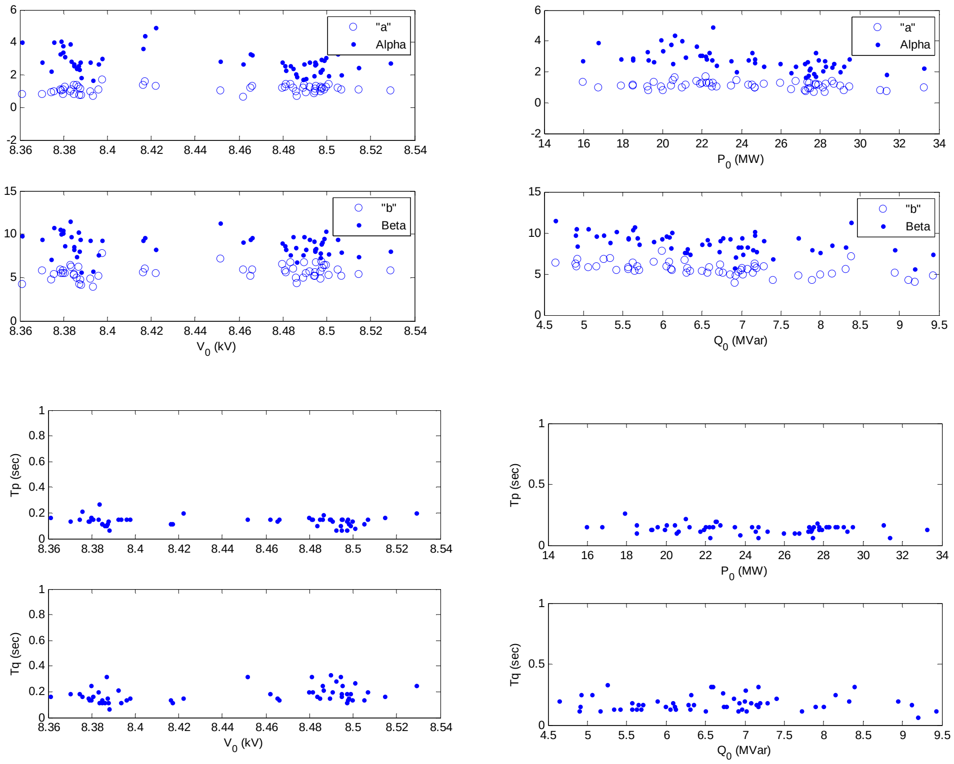

Transformer P2.8 – Mostly Residential

Figure E.10. Load parameters vs. pre-tap values of loads - Substation Two

3. Substation Three

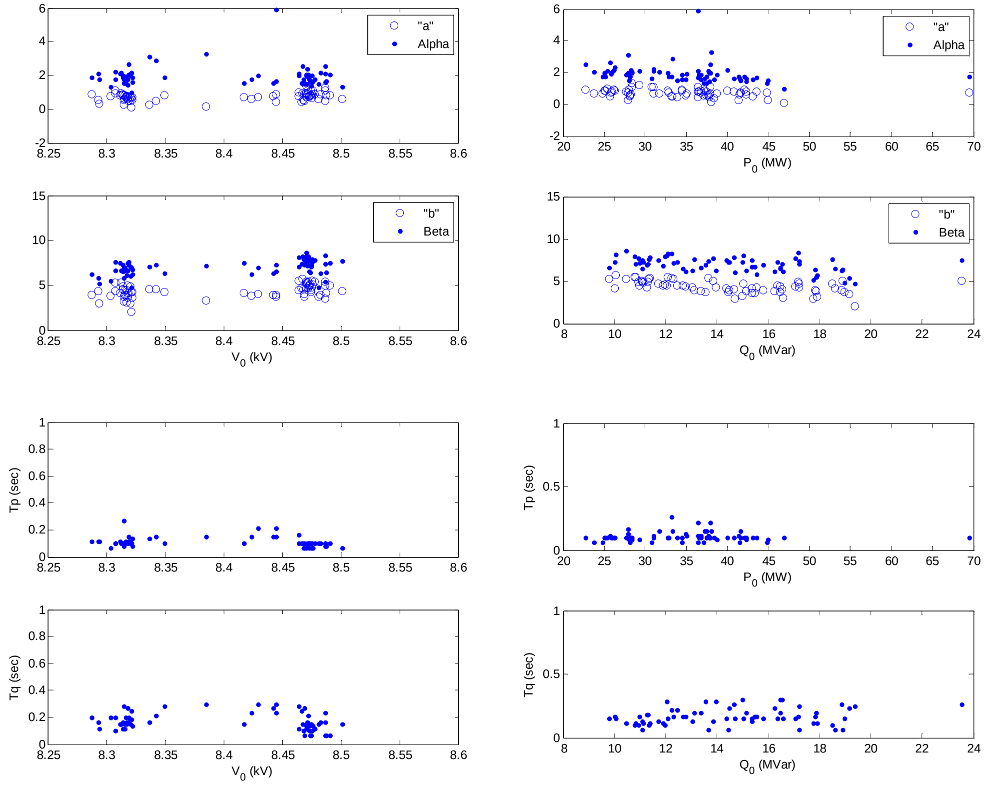

Transformer J3.1 – Mostly Commercial

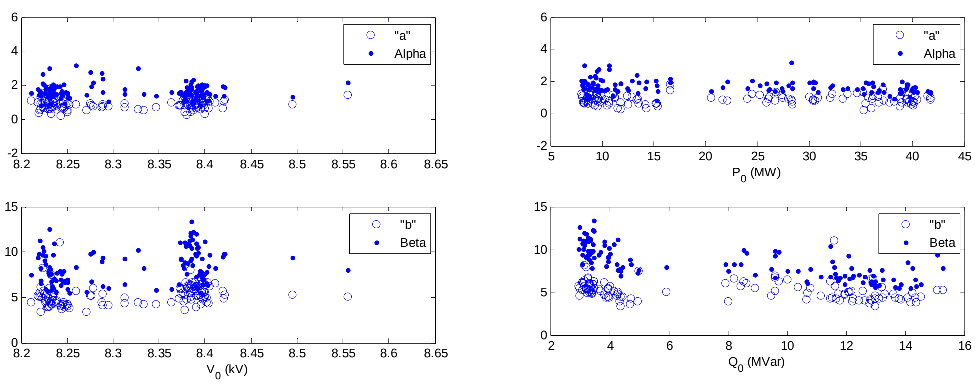

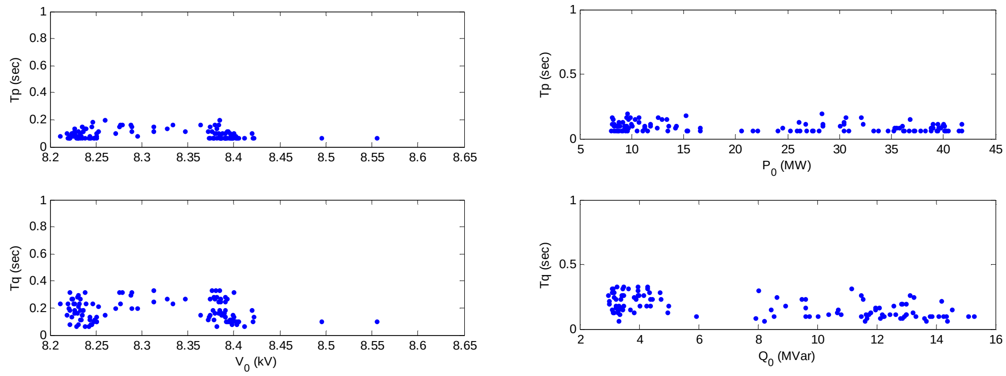

Transformer J3.3 – Mostly Commercial

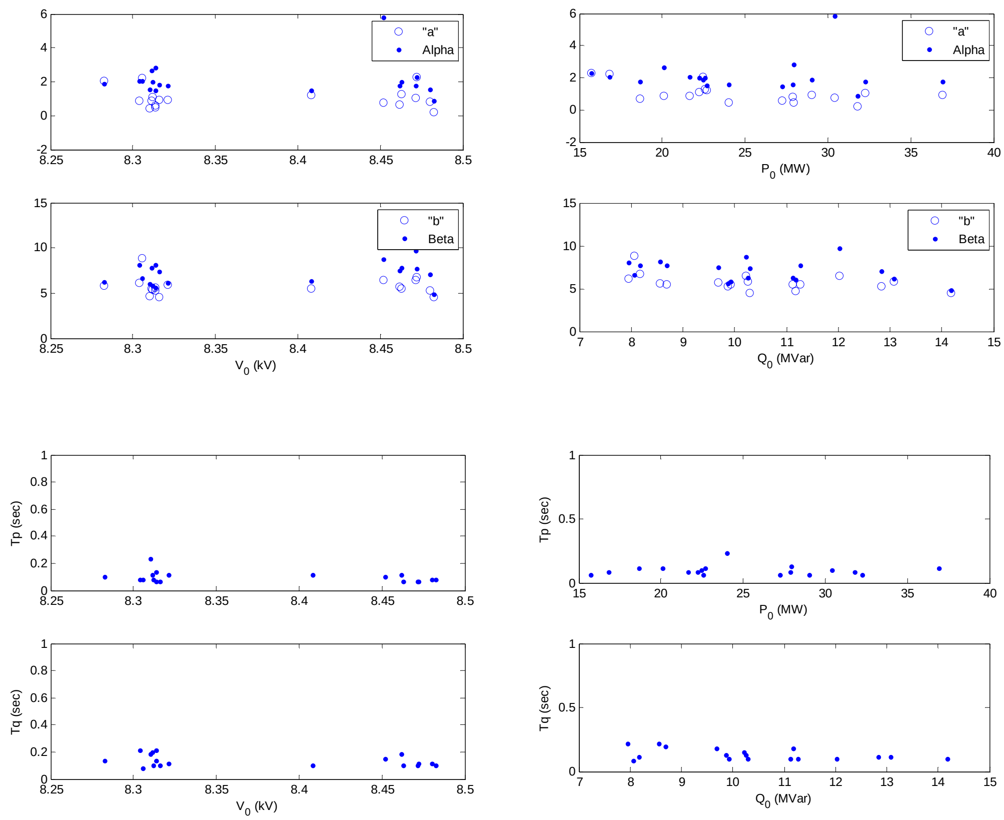

Transformer J3.8 – Mostly Commercial

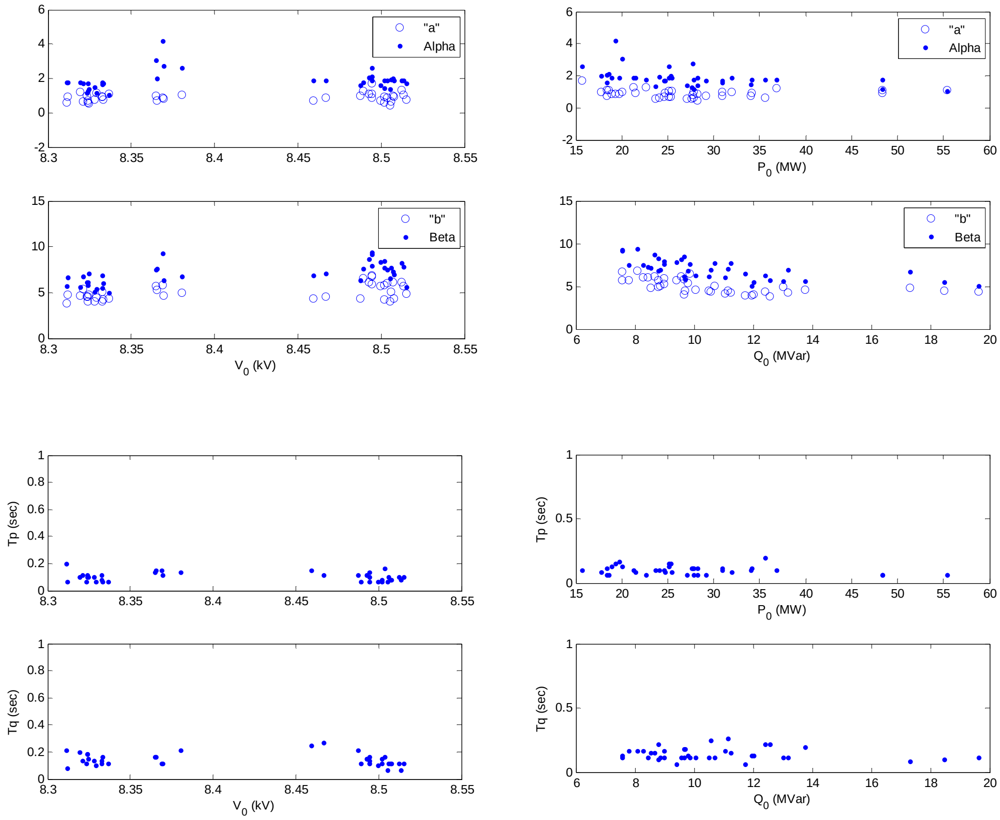

Transformer J4.2 – Mostly Commercial

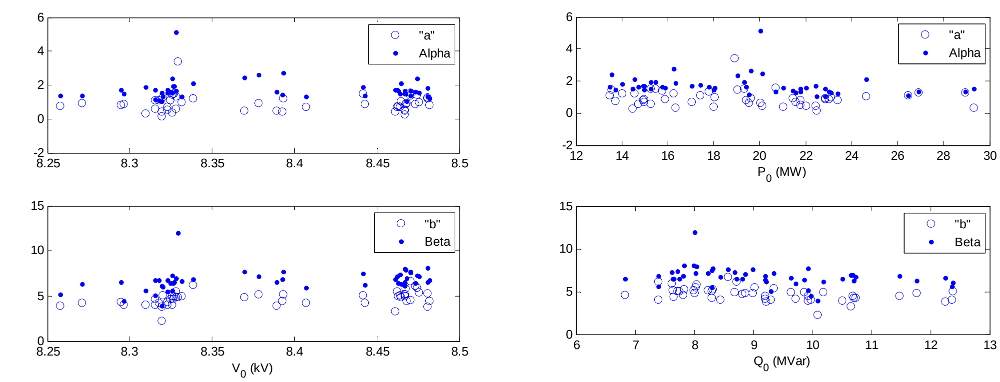

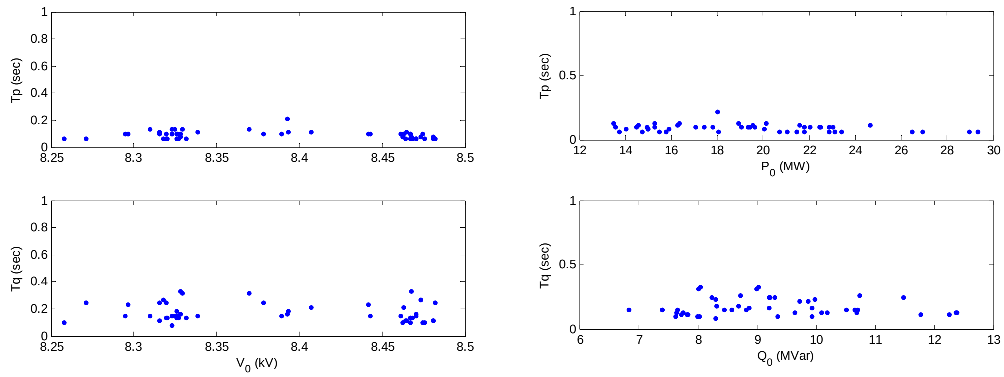

Transformer J4.7 – Mostly Commercial

Figure E.11. Load parameters vs. pre-tap values of loads - Substation Three

4. Substation Four

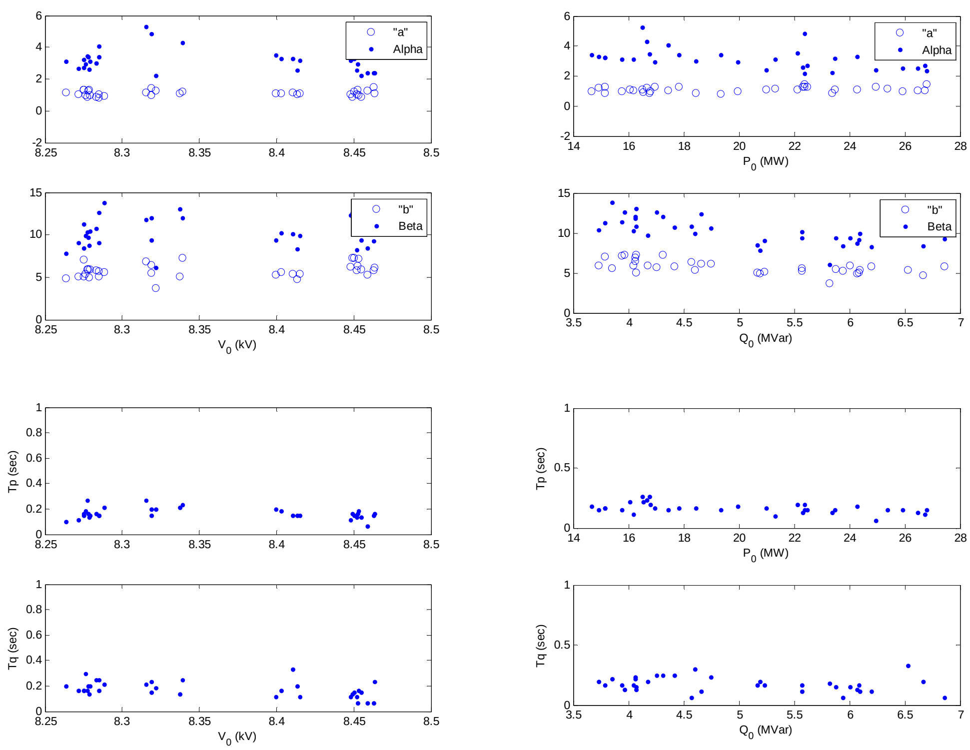

Transformer C1.2 – Mostly Residential

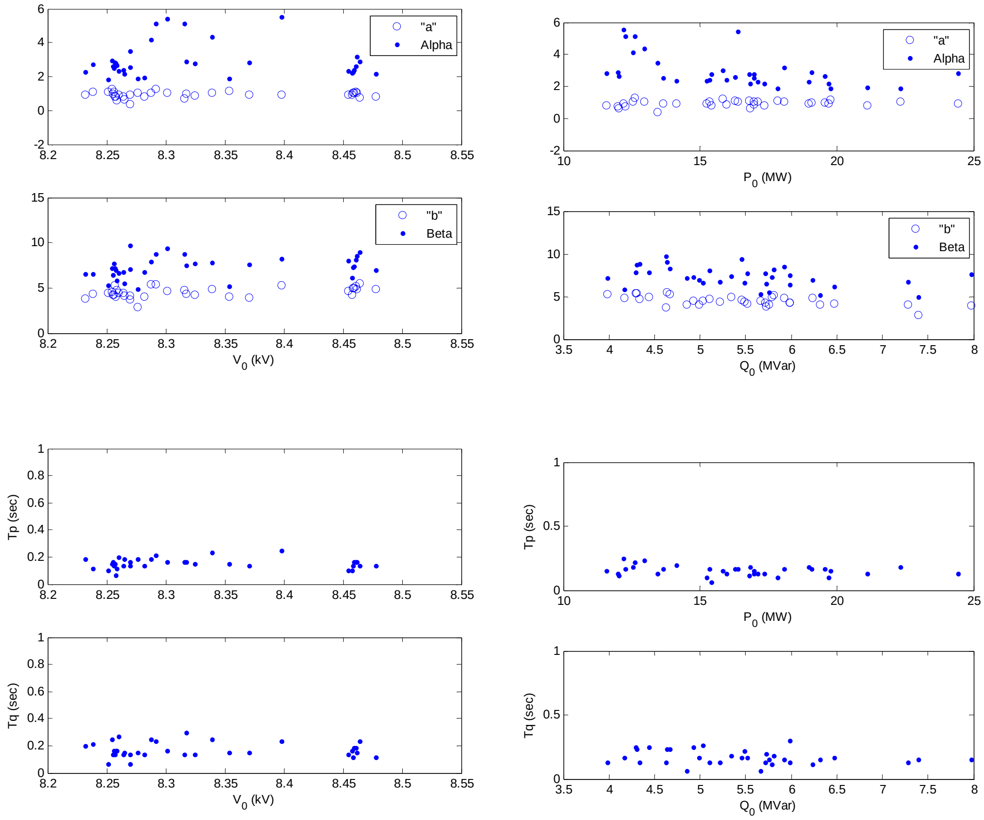

Transformer C2.8 – Mostly Residential

Figure E.12. Load parameters vs. pre-tap values of loads - Substation Four